Aus dem
CharitéCentrum für Grundlagenmedizin CC 2
Institut für Biochemie
Direktorin: Prof. Dr. Britta Eickholt

Habilitationsschrift

Modellierung des Leberstoffwechsels

zur Erlangung der Lehrbefähigung
für das Fach Biochemie

vorgelegt dem Fakultätsrat der Medizinischen Fakultät
Charité-Universitätsmedizin Berlin

von

Dr. rer. nat. Nikolaus Berndt

Eingereicht:	**Mai 2019**
Dekan:	**Prof. Dr. med. Axel R. Pries**
1. Gutachter/in:	**Prof. Dr. Hannes Link, Marburg**
2. Gutachter/in:	**Prof. Dr. Ursula Kummer, Heidelberg**

Inhalt

Abkürzungen

ADP	Adenosindiphosphat
AMP	Adenosinmonophosphat
ATP	Adenosintriphosphat
cAMP	cyclisches Adenosinmonophosphat
CT	Computertomographie
DGAT1/2	Diacylglycerol-O-Acyltransferase 1/2
FBA	Fluss-Bilanz-Analysen
FBP1/2	Fructose-1,6/2,6-bisphosphatase
GK	Glucokinase
HCC	hepatozelluläres Karzinom
NAFLD	*non-alcoholic fatty liver disease*
NASH	*non-alcoholic steatohepatitis*
PC	Pyruvatcarboxylase
PEP(CK)	Phosphoenolpyruvat(-Carboxykinase)
PFK1/2	Phosphofructokinase 1/2
PK	Pyruvatkinase
RSP	*regulatory surface proteins*
STU	*sinusoidal tissue unit*
VLDL	*very low density lipoprotein*

1. Einleitung

1.1 Systembiologie

Es ist das Hauptziel der Systembiologie komplexe biologische Systeme zu verstehen. Dieses Verstehen äußert sich in der Fähigkeit, die Eigenschaften eines biologischen Systems aus den Eigenschaften seiner Konstituenten zu rekonstruieren. Insbesondere möchte man in der Lage sein, die Reaktion eines biologischen Systems auf Veränderungen in den internen und/oder externen Bedingungen vorherzusagen [1]. Das Ziel der computerorientierten Systembiologie ist die Entwicklung verlässlicher Computermodelle, welche die molekularen Prozesse adäquat beschreiben, die den komplexen zellulären Eigenschaften wie Funktionalität, Wachstum, Replikation, Altern oder Adaptation zugrunde liegen. Der Metabolismus beschreibt die Eigenschaft von Zellen, verschiedene chemische Stoffe aus ihrer Umgebung aufzunehmen und diese in Energie (z.B. in der Form von energiereichen chemischen Verbindungen oder elektrischen Potentialen) sowie einer Vielzahl organischer Komponenten zu überführen und somit den Selbsterhalt, die Replikation sowie die zelluläre Funktionalität zu gewährleisten. Die metabolischen Prozesse wiederum hängen von verschiedenen Regulationsmechanismen und komplizierten Signalnetzwerken ab, die Umwelteinflüsse und intrinsische Signale in eine adäquate metabolische Reaktion umsetzen sollen. Um den Stoffwechsel zu verstehen, ist es daher notwendig, die verschiedenen regulatorischen Ebenen zu erfassen.

1.2 Rolle von Modellen in der Systembiologie

Die Modellierung metabolischer Systeme besteht in der Konstruktion mathematischer Repräsentationen, die es erlauben, Größen wie den Stoffaustausch mit der Umgebung sowie die Erzeugung und den Verbrauch von Metaboliten zu beschreiben. Abhängig vom Aufwand, Informationsgehalt und Fragestellung gibt es verschiede Techniken der metabolischen Modellierung, die sich in der Komplexität der Modelle, der Detailliertheit der benötigten Information, der Prädiktionsfähigkeit sowie in der Qualität der Modellvorhersagen unterscheiden.

Die einfachste Form der Modellierung besteht in der Verknüpfung verschiedener Beobachtungen. Dafür ist nichts weiter vonnöten, als verschiede Beobachtungen miteinander zu korrelieren – genau das, was mit statistischen Modellen versucht wird. Diese Art der Modellierung ist sehr einfach durchzuführen und ermöglicht, Hinweise auf mögliche Gesetzmäßigkeiten zu bekommen, ohne jedoch selber kausale Zusammenhänge herzustellen. Der große Vorteil besteht in ihrer universellen Anwendbarkeit, da jenseits der beobachteten Größen keinerlei Information notwendig ist. Allerdings versteht man vom untersuchten System auch nichts im eigentlichen Sinne. Diese Art von Modellen liefert lediglich statistische Zusammenhänge, aber keine Kausalitäten oder mechanistische Erklärungen.

Ein intrinsischer Zusammenhang zwischen Input und Output in metabolischen Modellen wird erst durch metabolische Netzwerke hergestellt. Ein metabolisches Netzwerk beschreibt die chemische Umwandlung verschiedener Stoffe ineinander, wodurch mögliche Zusammenhänge zwischen den Konstituenten des Systems stark eingeschränkt werden. Ein metabolisches Netzwerk besteht aus Reaktionen, ihren Katalysatoren und den chemischen Verbindungen, die mit Hilfe der Enzyme ineinander umgewandelt werden. Es gibt vor, welcher

Stoff mit Hilfe gegebener Enzyme und Kofaktoren ineinander transformiert werden können. Es beschreibt nicht, mit welchen Raten diese Umwandlungen tatsächlich stattfinden, es legt aber fest ob eine Umwandlung prinzipiell möglich ist oder nicht. Metabolische Netzwerke ermöglichen damit ein genaueres Verständnis des Metabolismus, da sie potentielle kausale Verknüpfungen beschreiben. Für die Konstruktion metabolischer Netzwerke benötigt man Informationen, in welchem Verhältnis die Enzyme ihre jeweiligen Substrate in ihre jeweiligen Produkte umsetzen. Dies wird für jedes Enzym durch eine Reaktionsgleichung beschrieben. Die Gesamtheit der Reaktionsgleichungen eines Systems bildet die stöchiometrische Matrix. Die Zuordnung in Substrat und Produkt ist dabei nicht eindeutig, da bei reversiblen Reaktionen Produkt und Substrat von der Reaktionsrichtung abhängen. Die Reaktionsrichtung wiederum hängt von der Thermodynamik der jeweiligen Reaktion ab und ist keine Eigenschaft eines Enzyms. Reaktionen verlaufen immer in Richtung zunehmender Entropie/Enthalpie. In welche Richtung die Entropie/Enthalpie zunimmt, hängt dabei im Wesentlichen von den Konzentrationen der beteiligten Substrate und Produkte ab (was auch den pH-Wert umfasst, wenn bei der Reaktion Protonen freigesetzt oder fixiert werden). Metabolische Netzwerke erlauben auch, die Kompartimentierung der Zelle in räumlich voneinander getrennte Bereiche zu berücksichtigen, indem man Subnetzwerke bildet, die einem bestimmten Teil der Zelle zugeordnet sind. Sie sind nützliche Werkzeuge, um unser Wissen auf Konsistenz zu überprüfen. Man kann mit ihrer Hilfe untersuchen, ob es chemische Wege zwischen verschieden Stoffen gibt und ob die uns bekannten Enzyme diese Wege adäquat beschreiben oder aber ob das Netzwerk Lücken aufweist. Metabolische Netzwerke erlauben allerdings nicht, Umsatzraten von Stoffen, metabolische Flüsse oder Konzentrationen von Metaboliten zu bestimmen. Um das zu tun, ist es notwendig, die Regulation der beteiligten Enzyme genau zu verstehen.

Der Metabolismus von Zellen enthält unzählige komplexe Feedback- und Feedforward-Mechanismen, die eine koordinierte Regulation verschiedener zellulärer Prozesse unter veränderten Bedingungen und Anforderungen ermöglichen und somit das zelluläre Überleben und die zelluläre Funktion in einem breiten Spektrum an Bedingungen aufrechterhalten können. Beispielsweise können Zellen je nach Verfügbarkeit zwischen der Metabolisierung von Zuckern, Fetten und Aminosäuren wechseln, um so die zelluläre Versorgung mit Adenosintriphosphat (ATP) unabhängig vom Nahrungsangebot zu gewährleisten. Die benötigten Informationen über die Regulation müssen für jedes Enzym einzeln experimentell gesammelt werden. Glücklicherweise gab es in der Geschichte der biochemischen und physiologischen Forschung einen längeren Zeitraum, in dem die kinetischen Eigenschaften und regulativen Besonderheiten von tausenden metabolischen Enzymen untersucht wurden. Daher ist der Metabolismus besser untersucht als viele andere zelluläre Systeme (wie z.B. die Genregulation oder Signalwege). Diese Forschung ermöglicht es, mittels kinetischer Modelle den Metabolismus besser zu verstehen. Bisher waren solche kinetischen metabolischen Modelle allerdings auf kleine Teilsysteme beschränkt, wobei die Glykolyse sicher der am häufigsten modellierte und am besten verstandene Stoffwechselweg ist.

1.3 Von der Zelle zum Gewebe und Organ

Fälschlicherweise wird in der Regel die metabolische Kapazität der Zellen mit ihrer metabolischen Aktivität gleichgesetzt. Neben der enzymatischen Ausstattung der einzelnen Zellen und ihrer Regulation spielt allerdings ihre Versorgung eine entscheidende Rolle, da alle

metabolischen Ausgangsstoffe und Abfallprodukte die Zelle auch erreichen bzw. verlassen müssen. Daher ist es notwendig, die Versorgung von Zellen miteinzubeziehen, wenn man ihre metabolische Leistung richtig beurteilen möchte. Die Versorgung ist sehr einfach, wenn man einzelne Zellen betrachtet. In komplizierten Zellverbänden wie Geweben spielt allerdings die Anordnung der Zellen und der sie versorgenden Gefäße eine entscheidende Rolle. Hinzukommen Parameter wie die Geometrie der Blutgefäße, Durchblutungsraten, Druckverhältnisse, Austauschkapazitäten von Metaboliten zwischen Blut und Interstitialraum bzw. Interstitialraum und Zelle. Diese Größen können entweder feste Eigenschaften des Gewebes sein oder ihrerseits gezielt reguliert werden (z.B. Perfusionsdruck). Um den Metabolismus in komplexen Zellverbänden und Gewebe zu verstehen, ist es demnach nicht ausreichend, den Metabolismus der einzelnen Zelle abzubilden, vielmehr ist es notwendig, das Zusammenspiel vieler Zellen gleichzeitig darzustellen. Das ist insbesondere erforderlich, wenn die metabolische Versorgung in einem Gewebe nicht einheitlich, sondern heterogen ist. Außerdem erfolgt die Versorgung von Zellen innerhalb eines Gewebes nicht unabhängig voneinander. So ist beispielsweise bei Zellen, die durch das gleiche Blutgefäß versorgt werden, wichtig, welche Zelle das Blut zuerst passiert. Alle nachgeschalteten Zellen werden eine veränderte Plasmazusammensetzung bekommen, die von der Stoffwechselaktivität (Aufnahme und Abgabe) der vor ihr liegenden Zellen abhängt. Die metabolische Leistung eines Gewebes hängt daher neben der zellulären Regulation des Stoffwechsels außerdem von der Interaktion der einzelnen Gewebekonstituenten und ihrer jeweiligen Anordnung und Regulation ab.

1.4 Metabolismus der Leber

Die Leber ist das Stoffwechsel-aktivste Organ in Vertebraten. Zu ihren zentralen Aufgaben gehört die Bereitstellung von wichtigen Nährstoffen für die systemische Versorgung des Körpers. Darunter fallen Kohlenhydrate für die Energieversorgung, Lipoproteine für die Bereitstellung von Triglyzeriden, Cholesterinester für die Energieversorgung und Biosynthesen sowie Aminosäuren für die Energiegewinnung, Proteinsynthese und Entgiftung (z.B. die Glutaminsynthese für die Ammoniakfixierung). Zusätzlich spielt sie eine entscheidende Rolle bei der Entsorgung von metabolischen Abfallprodukten wie Ammoniak oder überschüssigem Cholesterol, bei der Metabolisierung von Medikamenten und der Entgiftung von Xenobiotika. Eine weitere Aufgabe der Leber besteht in der Bereitstellung wichtiger Proteine. Sie synthetisiert Akute-Phase-Proteine für Immunabwehr sowie Albumin für Stofftransport und Osmoregulation. Außerdem produziert sie Galle, die sowohl für Verdauung von Fetten als auch für Abtransport von Abfallprodukten notwendig ist. All diese Aufgaben müssen miteinander koordiniert und bedarfsgerecht reguliert werden. Dafür muss die Leber ihren Stoffwechsel ständig an sich verändernde innere und äußere Bedingungen anpassen, um sowohl ihr eigenes Überleben zu gewährleisten, als auch die ihr zugewiesene Funktion innerhalb des Körpers zu erfüllen.

Die Regulation des zellulären Stoffwechsels findet auf verschiedenen Zeitskalen statt. Die Kurzzeitregulation umfasst die schnelle Änderung von Enzymaktivitäten bei konstanten Proteinmengen innerhalb von Sekunden oder Minuten. Zusätzlich passt die Zelle innerhalb von Stunden oder Tagen ihre Proteinmengen mittels Genexpression an länger persistierende Bedingungen an. Durch Methylierung der zellulären DNA besteht sogar die Möglichkeit Genexpressionsmuster zu vererben, obwohl noch nicht klar ist, wie wichtig dieser Prozess

wirklich ist [2]. Kurzzeitige Aktivitätsänderungen können durch viele verschiede Mechanismen erreicht werden, wie reversible Bindung eines Enzyms an Membranen (wie z.B. die Glutaminase [3]), Bindung von regulatorischen Einheiten und Lokalisationsänderung (z.B. Glucokinase [4]), chemische Modifikation der betroffenen Enzyme (z.B. Phosphofructo-kinase 2 (PFK2) [5]) oder einfach Veränderungen in den Metabolitkonzentrationen. Diese Aktivitätsänderungen sind oftmals das Resultat intrazellulärer Feedback- oder Feedforward-Mechanismen, die den funktionellen und metabolischen Zustand der Zelle wiederspiegeln. Ein Beispiel für einen Feedforward-Mechanismus ist das Glucokinase regulierende Protein, welches die Glucokinase bei steigender intrazellulärer Glukosekonzentration aktiviert und somit die Metabolisierung von Glukose fördert [6]. Die beteiligten Regelkreise können auch komplizierter sein, wie das Beispiel der Adenosinmonophosphat (AMP)-abhängigen Kinase zeigt. AMP ist das wichtigste intrazelluläre Signal für Energiemangel und wird von der Adenylatkinase bei fallendem ATP-Spiegel hergestellt [7]. Nach ihrer Aktivierung inaktiviert die AMP-abhängige Kinase durch Interkonversion metabolische Schlüsselenzyme wie PFK2 und Pyruvatkinase (PK) im Glukosestoffwechsel oder Acetyl-Coenzym A-Carboxylase im Fettstoffwechsel [8]. Sie aktiviert zusätzlich andere Signalkaskaden, die ihrerseits wiederum den Stoffwechsel regulieren (z.B. die Glykogen-Synthetase-Kinase, die unter anderem den Glykogen- und den Fettabbau steuert [9]). Insgesamt führt die Aktivierung der AMP-abhängigen Kinase zu einem verstärkten Abbau von Fettsäuren, Glukose und Glykogen und zum Abschalten von energieintensiven Prozessen wie der Fettsäuresynthese und somit zu einem Anstieg von ATP, Abfall von AMP und ihrer eigenen Deaktivierung.

Die wichtigste Kurzzeitregulation von Enzymen basiert auf Veränderungen in den Metabolit-konzentrationen, was sowohl die Regulation durch Änderungen in den Substraten und Kofaktoren als auch die allosterische Regulation von metabolischen Enzymen umfasst. Ein Enzym wird allosterisch reguliert, wenn seine Aktivität von Metaboliten abhängt, die durch das Enzym nicht selber chemisch verändert werden (also keine Substrate des Enzyms sind). Dafür besitzen Enzyme neben ihren katalytischen Zentren, an denen die chemische Modifikation der Substrate stattfindet, zusätzlich allosterische Bindungsstellen, an die die allosterischen Regulatoren binden. Die Bindung eines allosterischen Regulators führt zu Konformationsänderungen des Enzyms, so dass sich die kinetischen Eigenschaften und somit die Enzymaktivität ändern. Die allosterischen Regulatoren bilden oftmals sehr spezifische Feedbackmechanismen innerhalb der Zelle, die als Kontrollstellen für die Regulation des Stoffwechsels wichtig sind. Ein gutes Beispiel ist die Phosphofructokinase1 (PFK1). Ihre Aktivität hängt allosterisch von ATP und AMP ab und reagiert damit direkt auf den Energiezustand der Zelle [10, 11]. Ein weiterer, sehr spezifischer allosterischer Regulator der PFK1 ist Fruktose-2,6-bisphosphat. Es wird abhängig von den Hormonen Insulin und Glukagon hergestellt und signalisiert somit nicht den internen Zustand der Zelle, sondern den systemischen Bedarf [12]. Außerdem signalisiert Zitrat [11], das Endprodukt der aeroben Glykolyse, den funktionellen Zustand der Glykolyse als Ganzes.

Neben den intrazellulären Signalen gibt es auch extrazelluläre Signalgeber, die der Leber den Zustand des systemischen Stoffwechsels anzeigen. Die wichtigsten Mediatoren für die Leberzelle sind die beiden pankreatischen Hormone Insulin und Glukagon. Beide Hormone werden vom Pankreas glukoseabhängig in die Pfortader sezerniert und von dort zur Leber transportiert. Glukagon bindet an den β-adrenergen Rezeptor, der sich an der Oberfläche der Hepatozyten befindet. Das führt zur Aktivierung der Adenylatzyklase, die ATP in den Botenstoff cAMP (cyclisches AMP) umwandelt. Der cAMP-Spiegel reguliert direkt die Aktivität der Proteinkinase A (cAMP-abhängige Kinase), die ihrerseits, ähnlich wie die AMP-abhängige

Kinase, über Phosphorylierung von Enzymen und Aktivierung weitere Signalkaskaden des hepatischen Stoffwechsels reguliert. Im Ergebnis aktiviert Glukagon die Glykoneogenese und Glykogenolyse, hemmt die Fettsäuresynthese, aktiviert den Triglyzeridabbau und steigert die Bildung und Freisetzung von Lipoproteinen. Der direkte Gegenspieler von Glukagon ist Insulin. Insulin bindet an den Insulinrezeptor, der daraufhin dimerisiert und aktiviert wird. Der aktivierte Insulinrezeptor bindet und phosphoryliert das Insulinrezeptorsubstrat und setzt damit eine Signalkaskade in Gang, die über Phosphoinositid-3-Kinase- und Proteinkinase B-Aktivierung schließlich zur Aktivierung der Phosphodiesterase führt, die cAMP abbaut und somit die Signalwirkung von Glukagon unterbindet. Als Antagonist zu Glukagon steigert Insulin daher die Glykolyse und Glykogensynthese, aktiviert die Fettsäuresynthese sowie die Speicherung von Triglyzeriden und hemmt die Lipopoteinfreisetzung.

> *„Es gibt viele weitere Regulationsmechanismen in metabolischen Systemen. Prinzipiell hängt die Aktivität der einzelnen Enzyme von den lokalen Konzentrationen der Metabolite und der Enzyme ab, aber es gibt auch eine Menge an Umwelteinflüssen und strukturellen Faktoren, die die Aktivität beeinflussen. Die räumliche Trennung von metabolischen Aktivitäten in verschieden Kompartimenten erlaubt es der Zelle, durch den kontrollierten Austausch von Ionen und Metaboliten besondere Mikroumgebungen zu schaffen, die spezielle metabolische Funktionen erleichtern oder überhaupt erst ermöglichen. Mitochondrien z.B. erzeugen einen Protonengradienten und ein Membranpotential über die innere Mitochondrienmembran, die eine ATP-Generierung ermöglichen [13]. Metabolite können auch direkt zwischen Enzymen weitergereicht werden (diese bilden dann sogenannte Metabolone). Das ermöglicht die Aktivierung von Stoffwechselwegen in der Zelle, ohne dass die metabolischen Zwischenprodukte verloren gehen können. Beispielsweise können die glykolytischen Enzyme in Arabidopsis Thaliana mit den Mitochondrien assoziieren und damit direkt die mitochondriale Respiration antreiben [14]. Diese Verbindung kann so stark sein, dass verschiedene Enzyme dadurch faktisch ein einziges Enzym bilden. Das ist wahrscheinlich der Ursprung verschiedener Enzymkomplexe wie der Pyruvatdehydrogenase oder Komplex I der Atmungskette. Die räumliche Struktur kann auch großen Einfluss auf den zellulären Stoffwechsel haben. So werden z.B. räumliche Gradienten von Metaboliten für den intrazellulären Stofftransport genutzt. Das in Mitochondrien erzeugte ATP muss beispielsweise zu den Hauptverbrauchern wie der Natrium-Kalium-ATPase an der Plasmamembran gelangen. Dies geschieht durch Diffusion entlang des intrazellulären ATP-Gradienten zwischen Mitochondrium und Plasmamembran. Dieser Mechanismus wird durch die Kreatinkinase verstärkt [15].“* (Übersetzung durch den Autor aus [16])

Die Kreatinkinase katalysiert die reversible Übertragung vom hochenergetischen Phosphat zwischen ATP und Kreatin und befindet sich sowohl an der Mitochondrienmembran als auch an der Plasmamembran. Das Phosphorylierungspotential ist in den Mitochondrien aufgrund der mitochondrialen ATP-Synthese hoch, so dass dort Phosphat von ATP auf Kreatin übertragen wird. An der Plasmamembran hingegen ist die ATP-Konzentration aufgrund des lokalen Verbrauchs niedrig und die Kreatinkinase überträgt Phosphat von Kreatinphosphat auf ADP (Adenosindiphosphat). Da Kreatinphosphat kleiner ist als ATP, ist seine Diffusionsgeschwindigkeit innerhalb der Zelle deutlich höher. Es beschleunigt somit den Gradientenabhängigen ATP-Transport und ermöglicht dadurch, größere Zellen homogener mit ATP zu versorgen [16].

1.5 Struktur der Leber

Um ihre Aufgaben zu erfüllen, weist die Leber eine einzigartige anatomische Struktur auf. Die Gesamtleber ist aus verschiedenen Leberlappen zusammengesetzt, welche wiederum aus ca. 1 Million kleinster funktioneller Einheiten, den Leberazini, bestehen. Ein Leberazinus besteht aus einem zentralen Blutgefäß, dem Sinusoid, das die Leberarterie mit der Zentralvene verbindet. Das Blut fließt von der Leberarterie zur Zentralvene und passiert die Hepatozyten, die sich aufgereiht entlang des Sinusoids befinden. Zwischen Blutgefäß und Hepatozyten befindet sich der Disse-Raum, der den Stoffaustausch zwischen Hepatozyten und Plasma kontrolliert. Er wird auf der einen Seite von den Endothelzellen des Blutgefäßes und auf der anderen Seite von der basolateralen Plasmamembran der Hepatozyten begrenzt. Die sinusoidalen Endothelzellen bilden dabei Poren, die sogenannte Fenestrierung, deren Größe bestimmen, welche Stoffe in den Disse-Raum gelangen können [17]. Auf der Seite der Hepatozyten bilden die basolateralen Membranen Ausstülpungen, um eine große Kontaktfläche zu ermöglichen und damit einen besseren Austausch von Stoffen zwischen Disse-Raum und Hepatozyten zu gewährleisten.

Der Stoffaustausch hängt wesentlich von der Mikrostruktur und der Perfusion der Leber ab. Das lineare Arrangement der Hepatozyten entlang des Sinusoids und der kontinuierliche Austausch von Metaboliten entlang des Sinusoids sorgen dafür, dass sich die Plasmakonzentrationen von Metaboliten und Hormonen zwischen der portalen Region (Gebiet um die Portalvene) und der zentralen Region (Gebiet um die Zentralvene) deutlich unterscheiden. Diese unterschiedlichen Plasmakonzentrationen führen zu unterschiedlichen Proteinausstattungen in den verschiedenen Leberregionen. Dieses Phänomen ist als Leberzonierung bekannt. Dadurch kommt es innerhalb der Leber zu einer heterogenen Verteilung von metabolischen Kapazitäten, die für die Gesamtleistung des Organs äußerst bedeutend sein kann. Während einige Stoffwechselleistungen kontinuierlich zwischen portaler und zentraler Region variieren, wie z.B. der Glukosemetabolismus, der sich von vorwiegender Glykoneogenese in der portalen Region zu vorwiegender Glykolyse in der zentralen Region verändert [18, 19], sind andere Stoffwechselwege ausschließlich in einer Leberregion zu finden, wie z.B. die Glutaminsynthese, die nur in den perizentralen Hepatozyten vorkommt [20].

1.6 Pathologische Veränderungen der Leber

NAFLD (*non-alcoholic fatty liver disease*) und NASH (*non-alcoholic steatohepatitis*) sind weitverbreitete Lebererkrankungen, die ein weites Spektrum an Veränderungen von exzessiver Fetteinlagerung (Steatosis), Entzündung (Steatohepatitis), Fibrose, Zirrhose bis hin zum hepatozellulären Karzinom (HCC) umfassen [21]. NAFLD ähnelt alkoholischen Fettlebererkrankungen und zeichnet sich durch eine makrovesikuläre Verfettung in mindestens 5% der Hepatozyten aus. Sie kommt allerdings in Patienten mit nur mäßigen oder ohne Alkoholkonsum vor und kann auch ohne anderen erkennbaren Grund (wie Medikamenteneinnahme) auftreten [22]. Die Haupteigenschaft einer NASH sind exzessive Fetteinlagerungen zusammen mit Entzündungen und morphologischen Schäden.

NAFLD und NASH sind oft mit Insulinresistenz, systemischen Bluthochdruck und anderen Symptomen des metabolischen Syndroms assoziiert [23] und NAFLD wird heute als die erste hepatische Manifestation des metabolischen Syndroms angesehen [24]. Das metabolische

Syndrom mit seinen Kennzeichen von Fettleibigkeit, Insulinresistenz und Dyslipedämie ist eine unspezifische Stoffwechselstörung epidemischen Ausmaßes, die bereits in sehr jungen Patienten beginnt [25]. Es geht mit stark erhöhten Risiken für verschiedene Erkrankungen wie Typ-2-Diabetes, kardiovaskuläre Erkrankungen, Schlaganfälle oder Herzinfarkte einher [26]. Umgekehrt trägt die Leber als zentrales Stoffwechselorgan maßgeblich zum Fortschreiten des metabolischen Syndroms bei und NAFLD und NASH gehen oftmals mit der Entwicklung von weiteren Leber-und kardiovaskulären Erkrankungen einher.

Schätzungsweise 20-30% der westlichen Bevölkerung leiden an NAFLD, wobei der Anteil in Fettleibigen mehr als 60% beträgt [21]. Außerdem ist NAFLD heutzutage bereits die weitverbreitetste Lebererkrankung bei Kindern und Jugendlichen in der industrialisierten Welt. In einer Autopsiestudie mit 742 Kindern wiesen 9,6% aller Untersuchten eine NAFLD aus, während der Anteil in der Gruppe der Fettleibigen auf 42% stieg und 23% der Kinder mit einer Fettleber Anzeichen einer NASH zeigten [27].

Leberzirrhose und HCC sind die Endpunkte dieser Leberpathologie. Vor ihrer vollständigen klinischen Manifestation, geht diesen lebensbedrohlichen Erkrankungen oftmals eine lange Phase struktureller Veränderungen des Leberparenchyms, das nur zu unspezifischen und schwer zuordenbaren klinischen Auffälligkeiten führt, voraus. Symptome die mit NAFLD und NASH assoziiert sind, reichen von unspezifischen leichten Bauchschmerzen bis Müdigkeit. Das erste klare Symptom ist oftmals akutes Leberversagen, das zur Beeinträchtigung anderer Organe wie der Niere (durch Veränderung des Blutvolumens), der Lungen (unzureichende Immunabwehr) oder des Gehirns (Enzephalopathie) führen kann. Das liegt daran, dass die Leber ein hoch anpassungsfähiges Organ ist, das durch adaptive Prozesse trotz erheblicher Veränderungen in ihren inneren und äußeren Bedingungen ihre Leistung weitgehend aufrechterhalten kann. Heutzutage ist Leberversagen in Folge einer NASH der dritthäufigste Grund für eine Lebertransplantation in den Vereinigten Staaten [28].

Die meisten Menschen mit NASH fühlen sich gut und wissen nicht, dass eine schwerwiegende Lebererkrankung mit irreversiblen strukturellen Veränderungen wie Narbenbildung innerhalb der Leber vorliegt. Der Goldstandard der Diagnose ist die Leberbiopsie. Histologische Parameter wie der Grad an Steatose, Entzündung, Zellgröße (*ballooning*), Fibrose, Pigmentierung von Markrophagen, Glykogen-Anreicherung in Zellkernen, Mega-mitochondrien, acidophile Körper und Mallory-Körper sind die Marker für die Klassifikation und Einteilung der Schwere der Erkrankung [29]. In einer groß angelegten Studie mit 285 Erwachsenen mit chronischer Hepatitis C hatten 171 Patienten einen histologisch bestätigten Fibrosegrad 2-4 (Fibrose) und 114 Grad 5 oder 6 (Zirrhose), ohne dass eine klinische Auffälligkeit vorlag [30]. Es wird allgemein angenommen, dass die Funktionseinschränkungen der Leber mit den histologischen Befunden korrelieren. Allerdings weisen verschiedene Studien eine klare Diskrepanz zwischen histologischen und klinischen Daten auf, was die Frage aufwirft, was tatsächlich ein geeigneter Parameter für die Leberfunktion bei NAFLD sein könnte [31].

Alternativ zur Leberbiopsie wird die Leberfunktion und der Leberschaden durch die Analyse der Konzentration von verschiedenen Metaboliten im Blutplasma vollzogen. Die Konzentration der Aminotransferasen ALAT und ASAT im Blut wir für die Abschätzung des Grades von Leberschädigung benutzt, weil man davon ausgeht, dass sie beim Sterben von Hepatozyten ins Blut gelangen. Leberfunktionseinschränkungen werden durch das Ansteigen von Bilirubin in Plasma diagnostiziert, welches die Leber normallerweise schnell abbaut. Andere Marker sind der Abfall von Proteinen, die hauptsächlich in der Leber synthetisiert

werden wie z.B. Albumin, oder die Beeinträchtigung anderer Organe in Folge eines Leberversagens wie z.B. das Auftreten von Enzephalopathien durch eine verminderte Ammoniakentgiftung durch die Leber. In einer anderen großangelegten Studie an 16.390 übergewichtigen europäischen Kindern und Jugendlichen wiesen 11% erhöhte Leber-transaminasewerte auf [32].

Morphologische Eigenschaften wie Grad und Art der Fetteinlagerung, Form der Mitochondrien und allgemeine Parameter wie der Body-Mass-Index, Alter und Ko-morbiditäten werden heutzutage auch benutzt, um den Krankheitsverlauf zu bewerten [31]. Funktionale Parameter werden in verschiedenen Scoring-Systemen wie dem Child-Pugh- oder dem MELD-Score benutzt, um zu einer prognostischen Einschätzung zu kommen. Beide Systeme versuchen, Leberversagen bei starken Beeinträchtigungen vorherzusagen. Sie sind allerdings nur begrenzt einsetzbar und viele Einwände hinsichtlich ihrer Methodik, Signifikanz und fehlender Objektivität bei der Bewertung von klinischen Parametern wurden vorgebracht.

Leider gibt es bisher keine Möglichkeit, den Krankheitsverlauf für einzelne Patienten vorherzusagen. Eine Studie an 52 Patienten über drei Jahre zeigte, dass es eine Progression von der Steatose zu schwereren Lebererkrankungen wie NASH gibt. Manche Patienten zeigten aber auch eine Regression von NASH zu Borderline-NASH und ein Patient entwickelte sich sogar wieder zurück zu einer normalen Leber. Während 27% der Patienten ein Fortschreiten der Fibrose zeigten und 48% ihren jeweiligen Grad an Fibrose beibehielten, zeigten 25% einen Rückgang der Fibrose [33]. Das macht deutlich, dass der Fortgang der Krankheit heterogen ist.

Insgesamt gibt es keine zufriedenstellende Einschätzung für den Grad einer Lebererkrankung und die sich daraus ergebenden funktionalen Einschränkungen. Dieser Mangel an funktionalem Verständnis ist sicher auch ein Grund dafür, dass es bis heute keine effektive Behandlung von NAFLD gibt [34]. Es wird generell empfohlen abzunehmen und die physische Aktivität zu erhöhen, da die betroffenen Patienten meist übergewichtig sind. Während das in bestimmten Subgruppen sicherlich erfolgreich ist, ist der langfristige Erfolg aber aufgrund einer später wieder erfolgenden Gewichtszunahme eher gering. Der antisteatotische Effekt von veränderten Ernährungsgewohnheiten wurde allerdings in kleineren Gruppen und an Einzelfällen nachgewiesen [35].

1.7 Modellierung des Leberstoffwechsels

Grundsätzlich ist es nicht realistisch, alle denkbaren Regulationsebenen in mathematischen Modellen abzubilden. Daher besteht eine wichtige Herausforderung für die Modellierung darin, die Regulationsmechanismen zu identifizieren, die für das Systemverständnis und die korrekte Abbildung des modellierten Systems wichtig sind.

Bisher ist die Modellierung des Leberstoffwechsel hauptsächlich auf große stöchiometrische Netzwerke mit Fluss-Bilanz-Analysen (FBA) oder kleine mechanistische kinetische Modelle beschränkt (z.B. [36, 37]). Weiterhin spielen traditionell pharmakokinetische Modelle eine große Rolle in der Vorhersage für die Aufnahme, Verteilung, Metabolisierung und Ausscheidung von synthetischen und natürlichen Substanzen im Menschen (ADME - "*absorption, distribution, metabolism, and excretion*"). Das sind im wesentlichem Muli-kompartimentmodelle, in denen die verschiedenen Organe des Körpers (inklusive der Leber als zentrales Organ der Entgiftung) einfach als Quelle oder Senke der untersuchten Substanzen

betrachtet werden. Die Aufnahme und Abgabe für jedes Kompartiment wird dabei jeweils durch einen einzigen Parameter beschrieben. Diese Modelle werden dafür verwendet, um Messungen in Leberfunktionstests in einen quantitativen Score zu übersetzen. Neuere Modelle versuchen auch, biochemische und biophysikalische Eigenschaften (wie Sättigungskinetiken von Transportproteinen) zu berücksichtigen. Ein Beispiel hierfür ist ein PBPK-(*physiologically based pharmacokinetic*)-Modell [38], das ein FBA-Modell des Lebermetabolismus [36] benutzt, um Hyperurikämie-Therapie, Ammoniakentgiftung und Acetaminophen-induzierte Vergiftung zu untersuchen.

Kinetische Modelle bemühen sich um eine möglichst akkurate Beschreibung der einzelnen metabolischen Enzyme, was ein umfangreiches Wissen voraussetzt. Da außerdem die möglichen intrinsischen Abhängigkeiten und wechselseitigen Einflussnahmen mit der Anzahl der beschriebenen Enzyme und Metaboliten stark zunehmen, sind kinetische Modelle meist auf kleine Netzwerke beschränkt. FBA-Modelle verzichten auf diese Art von detaillierter Beschreibung, modellieren dafür aber viele verschiedene Stoffwechselwege gleichzeitig.

1.8 Aufbau und Ziel der vorliegenden Arbeit

Die Leberfunktion ist das Ergebnis des Wechselspiels aus metabolischer Umgebung, der Mikroarchitektur, des Blutflusses und der Nährstoff- sowie Hormonzusammensetzung des Plasmas. Sie hängt von der Proteinausstattung der einzelnen Hepatozyten ebenso ab, wie ihrer räumlichen Anordnung entlang des Sinusoids (der Zonierung) und Veränderungen in jeder dieser Komponenten führt zu Anpassungen in den anderen Komponenten.

Ziel dieser Arbeit ist es, verschiedene sich ergänzende mathematische Modelle des Lebermetabolismus vorzustellen, die zu einem besseren Verständnis der Funktionalität der Leber führen. Metabolisch ist die Leber eines der bestuntersuchtesten Organe, was die Möglichkeit eröffnet, die Vernetzung von FBA-Modellen mit der Detailtreue kinetischer Modelle zu verknüpfen.

Die nachfolgenden Arbeiten beschäftigen sich mit verschiedenen Aspekten des Lebermetabolismus. Die Komplexität und Qualität der Modelle hängt dabei von der jeweiligen Fragestellung und den verfügbaren Informationen ab. Während einige Modelle molekular aufgelöst sind und auf der detaillierten Charakterisierung jedes einzelnen beteiligten Enzyms basieren, müssen sich andere mit einer prinzipiellen Beschreibung von phänomenologischen Zusammenhängen begnügen, da entweder die zugrundeliegende Netzwerkstruktur unbekannt ist oder die benötigte kinetische Charakterisierung der Enzyme nur unvollständig erfolgt ist. Je nach Fragestellung wird außerdem die Leberarchitektur, der Blutfluss und die Genregulation miteinbezogen.

Die erste Arbeit [39] beschäftigt sich mit dem Glukosestoffwechsel der Leber (2.1), die zweite Arbeit [40] beschäftigt sich mit dem Einfluss der hepatischen Ultrastruktur auf den Glukosemetabolismus (2.2), die dritte Arbeit [41] handelt von der Adaptation des hepatischen Glukosestoffwechsels an veränderte Bedingungen (2.3), in der der vierten Arbeit [42] geht es um die hepatische Einlagerung und Freisetzung von Triglyzeriden (2.5) und in der fünften Arbeit [43] geht es um den Zentralstoffwechsel der Leber (2.4), bei dem erstmals die Vernetzung von FBA-Modellen mit der detailtreue eines kinetischen Modells verknüpft wird.

Es wird gezeigt, wie kinetische Modelle in der Lage sind, aus Informationen über molekulare Eigenschaften ihrer Konstituenten zu Aussagen über das Verhalten des gesamten Systems zu kommen. Alle Arbeiten stellen einen engen Bezug zu pathologischen Veränderungen her und leisten damit einen wichtigen Beitrag zum Verstehen von Krankheiten wie Fettleber, Diabetes, Leberzirrhose und HCC. Weiterhin wird vorgeführt, wie Modelle genutzt werden können, um scheinbar widersprüchliche Ergebnisse zu verstehen, tatsächliche Widersprüche aufzudecken und zu Erkenntnissen zu gelangen, die auf experimentellen Wegen entweder nur sehr aufwendig und teuer oder gar nicht zu erreichen sind. Alle Modelle legen großen Wert auf experimentellen Input. Man kann mit Fug und Recht sagen, dass diese Arbeit ohne die Jahrzehnte dauernde aufwendige Arbeit unzähliger Biochemiker nicht möglich gewesen wäre.

2. Eigene Arbeiten

2.1 *The relative importance of kinetic mechanisms and variable enzyme abundances for the regulation of hepatic glucose metabolism - insights from mathematical modeling* [39]

Dieses Kapitel basiert auf [39] (DOI: 10.1186/s12915-016-0237-6).

Einleitung: Es ist eine der wichtigsten Aufgaben der Leber, die Glukosehomöostase im Plasma aufrechtzuerhalten. Um das zu gewährleisten, besitzt die Leber diverse Kurz- und Langzeit Mechanismen, die es ihr ermöglichen, ihren Glukoseaustausch mit dem Plasma an die Ernährungssituation und den systemischen Bedarf anzupassen.

Fragestellung: Ziel der Arbeit war es, die verschiedenen Ebenen der Kurzzeitregulation, bestehend aus Substratregulation, allosterischer Regulation, hormoneller Regulation und Langzeitregulation zu modellieren und die Bedeutung der verschiedenen Regulationsmechanismen für die effiziente Kontrolle des Blutzuckerspiegels durch die Leber zu untersuchen.

Methoden: Es wurde ein kinetisches Modell des hepatischen Glukosemetabolismus erstellt, das basierend auf enzymkinetischen Messungen für alle beteiligten Enzyme detaillierte Leberspezifische Ratengleichungen aufstellt. Die Ratengleichungen berücksichtigen die Thermodynamik (Reversibilität) der Reaktion sowie ihre kinetischen Eigenschaften. Neben Substrataffinitäten wurden inhibitorische und aktivierende allosterische Regulatoren sowie Änderungen der enzymkinetischen Parameter aufgrund von reversibler Phosphorylierung (Interkonversion) berücksichtigt. Da der Phosphorylierungsgrad über Hormone vermittelt wird (hauptsächlich Insulin und Glukagon), wurde das kinetische Modell mit einem effektiven Modell der Hormonantwort des Körpers auf den Blutzuckerspiegel sowie einem effektiven Modell der Leberantwort auf den Plasmahormonspiegel ergänzt.

Resultat: Das Modell beschreibt den Glukoseaustauschfluss der Leber in Abhängigkeit der Proteinmengen, des Blutzuckerspiegels (Ernährungszustand) und des Plasmahormonspiegels. Es zeigt, wie die Leber durch Änderungen der Enzymmengen und des internen metabolischen Zustandes ihren Glukoseaustausch an verschiedene physiologische und pathologische Bedingungen anpasst. Insbesondere wurden die metabolischen Veränderungen während des Hungerns und Fastens sowie die Adaptation an den diabetischen Zustand untersucht. Es wurde gezeigt, dass die allosterische und hormonelle Kurzzeitregulation für die Adaptation genauso wichtig ist wie die langzeitige Veränderung der Proteinmengen. Ein wichtiges Ergebnis war außerdem, dass die Kontrolle des Glukoseaustauschflusses der Leber auf wenige Schlüsselenzyme verteilt ist, wobei die regulatorisch wichtigen Enzyme sich mit den unterschiedlichen Bedingungen verändern. In verschiedenen metabolischen Zuständen können Enzyme, die entgegengesetzte Reaktionen katalysieren, regulatorisch wichtig sein. Weiterhin wurde gezeigt, dass die diabetische Leber (unabhängig vom tatsächlichen Ernährungszustand) als eine stark gefastete Leber betrachtet werden kann.

Diskussion: Die relative Wichtigkeit der verschiedenen Regulationsebenen ist für jedes Enzym unterschiedlich und hängt zusätzlich noch sehr von dem physiologischen Zustand der Zelle ab. Grundsätzlich werden aber alle Regulationsmechanismen gleichzeitig benutzt. Bei normalen Blutzuckerspiegeln hat die Proteinmenge den größten Einfluss (ca. 50%), während im

gefasteten Zustand die hormonelle Regulation durch Interkonversion die größte Auswirkung hat (ebenfalls ca. 50%). Die allosterischen Regulation ist mit jeweils etwa 25% an der Gesamtregulation beteiligt. Außerdem ist die Kontrolle in den verschiedenen Bedingungen auf unterschiedliche Enzyme verteilt.

Das Modell ermöglicht die systematische Einordnung des bekannten stückhaften Wissens über die regulative Bedeutung einzelner Enzyme. Die effektive Kontrolle des Blutzuckerspiegels muss nicht notwendigerweise mit einer optimalen Nutzung bezüglich der Energieeffizienz einhergehen. Innerhalb der Glykolyse/Glukoneogenese gibt es vier verschiedene Substratzyklen, in denen potentiell Energie verschwendet werden kann. Substratzyklen treten immer dann auf, wenn biochemische Reaktionen gleichzeitig in entgegengesetzten Richtungen verlaufen. Da nur eine Richtung thermodynamisch begünstigt sein kann, muss für die Reaktion in die andere Richtung Energie aufgewendet werden, die somit verloren geht. Trotz des Energieverlustes können Substratzyklen sinnvoll sein, z.B. weil durch sie der Nettofluss sehr viel sensibler auf kleine Änderungen in der Reaktion einer der beiden Richtungen reagieren kann. Der erste Substratzyklus tritt in dem Reaktionspaar Glucokinase (GK) und Glucose-6-Phosphatase auf. Beide Enzyme unterliegen nicht der hormonellen Kontrolle, aber GK wird stark von allosterischen Regulatoren kontrolliert. Unsere Analysen zeigen, dass beide Enzyme eine starke Kontrolle auf den Glukosefluss ausüben. Der Substratzyklus wird dadurch minimiert, dass beide Enzyme in unterschiedlichen zellulären Kompartimenten aktiv sind (Zytosol und endoplasmatische Retikulum). Ein zweiter Substratzyklus tritt zwischen Fructose-6-phosphat und Fructose-1,6-bisphosphat auf. Er wird durch PFK1 und Fructose-1,6-bisphosphatase (FBP1) katalysiert, von denen nur FBP1 interkonvertierbar ist. Obwohl die direkte hormonelle Kontrolle dieses Enzyms eher klein ausfällt, ist die hormonelle Kontrolle in diesem Zyklus entscheidend, da die Konzentration von Fructose-2,6-bisphosphat, dem stärksten allosterischen Regulator der PFK1 und der FBP1, vom Phosphorylierungszustand des bifunktionalen Tandemenzyms PFK2/FBP2 abhängt. Ein dritter Substratzyklus verläuft zwischen Phosphoenolpyruvat (PEP) und Pyruvat. Dieser Substratzyklus ist komplizierter als die anderen, da es keine direkte Umkehrreaktion zur PK gibt. Im Umgehungsweg vom Pyruvat zum PEP spielen Pyruvatcarboxylase (PC) und PEP-Carboxykinase (PEPCK) die entscheidende Rolle. Während PK hormonell reguliert wird, entfällt die hormonelle Kontrolle bei PEPCK und PC. Unsere Analyse zeigt, dass weder PEPCK noch PC stark allosterisch reguliert werden und auch die Kontrollkoeffizienten bezüglich ihrer Proteinmenge klein sind. Das heißt, dass die Energie, die für die Glukoneogenese aufgewendet wird, sich auch unter Bedingungen, unter denen keine Glukoneogenese stattfindet, nicht vermindert. Die hormonelle Kontrolle der PK sorgt allerdings dafür, dass in Zeiten der Nahrungskarenz die Gegenreaktion zum Erliegen kommt. Der Substratzyklus ist also immer dann besonders ausgeprägt, wenn genug Glukose zur Verfügung steht, und wird in Zeiten der Nahrungskarenz klein. Der vierte Substratzyklus verläuft zwischen der Glykogensynthase und der Glykogenphosphorylase. Beide Enzyme teilen sich die Kontrolle über den Glykogenspeicher und unterliegen reziproker hormoneller Kontrolle. Die vier auftretenden Substratzyklen werden also auf vier verschiede Arten kontrolliert: direkte reziproke hormonelle Kontrolle (Glykogensynthase und -phosphorylase), indirekte reziproke hormonelle Kontrolle über einen gemeinsamen Regulator (PFK1 und FBP1), räumliche Trennung in verscheide Kompartimente (GK und Glucose-6-Phosphatase) sowie hormonelle Inaktivierung eines Zweiges der Reaktion bei Nahrungskarenz (PK und PC/PEPCK).

Bulik et al. BMC Biology (2016) 14:15
DOI 10.1186/s12915-016-0237-6

BMC Biology

RESEARCH ARTICLE Open Access

The relative importance of kinetic mechanisms and variable enzyme abundances for the regulation of hepatic glucose metabolism – insights from mathematical modeling

Sascha Bulik, Hermann-Georg Holzhütter* and Nikolaus Berndt

Abstract

Background: Adaptation of the cellular metabolism to varying external conditions is brought about by regulated changes in the activity of enzymes and transporters. Hormone-dependent reversible enzyme phosphorylation and concentration changes of reactants and allosteric effectors are the major types of rapid kinetic enzyme regulation, whereas on longer time scales changes in protein abundance may also become operative. Here, we used a comprehensive mathematical model of the hepatic glucose metabolism of rat hepatocytes to decipher the relative importance of different regulatory modes and their mutual interdependencies in the hepatic control of plasma glucose homeostasis.

Results: Model simulations reveal significant differences in the capability of liver metabolism to counteract variations of plasma glucose in different physiological settings (starvation, *ad libitum* nutrient supply, diabetes). Changes in enzyme abundances adjust the metabolic output to the anticipated physiological demand but may turn into a regulatory disadvantage if sudden unexpected changes of the external conditions occur. Allosteric and hormonal control of enzyme activities allow the liver to assume a broad range of metabolic states and may even fully reverse flux changes resulting from changes of enzyme abundances alone. Metabolic control analysis reveals that control of the hepatic glucose metabolism is mainly exerted by enzymes alone, which are differently controlled by alterations in enzyme abundance, reversible phosphorylation, and allosteric effects.

Conclusion: In hepatic glucose metabolism, regulation of enzyme activities by changes of reactants, allosteric effects, and reversible phosphorylation is equally important as changes in protein abundance of key regulatory enzymes.

Keywords: Diabetes, Enzyme abundance, Glucose metabolism, Hormonal enzyme regulation, Kinetic enzyme regulation, Liver, Reversible phosphorylation

Background

An important feature of cellular metabolic networks is their ability to adjust the functional output to largely varying external conditions such as changes in nutrient supply, enforced synthesis of macromolecules during the growth phase, varying hormone levels, or presence of toxins. This adjustment is achieved by diverse regulatory mechanisms tuning the activities of enzymes and transporters in a concerted fashion. The simplest mechanism operative for virtually all reactions in the network consists in changes of the enzymatic turnover rate owing to concentration changes of substrates and products as long as these concentrations remain below the saturation level. Further, during the natural evolution of living systems, two basic regulatory mechanisms have been established to regulate the activity of enzymes and transporters in a metabolic network.

One such mechanism is to vary the amount of an enzyme, which linearly relates to the enzyme's maximal

* Correspondence: hergo@charite.de
Charité – Universitätsmedizin Berlin, Institute of Biochemistry, Computational Systems Biochemistry Group, Charitéplatz 1, 10117 Berlin, Germany

catalytic capacity. Enzyme abundances can be regulated at the level of gene transcription, mRNA translation or protein degradation. In the rat liver, significant changes of enzyme amounts in the carbohydrate metabolism occur between 5 and 100 hours during a starvation-refeeding cycle [1, 2].

A second fundamental regulatory concept, usually termed kinetic regulation, consists of changes in the specific activity of enzymes due to conformational changes of the protein structure. This allows a rapid adaptation of the network to varying external and internal conditions within a few seconds. Conformational changes can be brought about by covalent or non-covalent binding of specific ligands (organic and inorganic metabolites, proteins, metal ions) or by partial proteolysis. The predominant concepts of kinetic regulation are allostery and reversible chemical modification. Allostery designates the modulation of enzyme kinetic properties by non-covalent binding of an effector molecule at the protein's allosteric site, i.e. a site other than the binding site for the substrates and products. Reversible chemical modification encompasses the temporary covalent attachment of a molecule to and detachment from the enzyme protein. In a given metabolic system, not all enzymes are equally important for the regulation of the systemic behavior. Rather, only specific key enzymes carry the burden of the regulatory control.

High-throughput technologies enabling the cell-wide monitoring of RNA and protein levels have revealed high variability in the abundance of transcripts and protein amounts of metabolic enzymes, both among individual cells and among cells exposed to different physiological settings. This finding has promoted the current prevailing view that metabolic regulation is basically achieved by variable gene expression. For example, 90 % of contemporary scientific publications containing the keyword 'metabolic regulation' deal with variable gene expression of metabolic enzymes. This raises the question of whether metabolic regulation can really be inferred from changes in the expression profile of enzymes and transporters. Serious doubts in this simplifying concept emerge from several studies demonstrating that changes of pathway fluxes commonly displayed poor or even lacking correlation with changes of enzyme abundances [3, 4]. The need for inclusion of all modes of enzyme control in the regulation of cellular metabolism has already been pointed out by the time-dependent regulation analysis of Westerhoff et al. [5]. However, to date, such an analysis for a physiologically meaningful metabolic network is lacking. To this end, herein, we use a detailed kinetic model of hepatic glucose metabolism to quantify how variable protein abundances, changes of reactant concentrations, allosteric regulation, and reversible phosphorylation of metabolic enzymes contribute to the metabolic capacity of rat liver to assure the homeostasis of plasma glucose levels in different physiological settings including fasting, ad libitum feeding, and diabetes. The model takes into account allosteric effects as well as hormonal regulation of key metabolic enzymes by insulin and glucagon and thus allows a detailed recapitulation of kinetic regulation of the hepatic glucose metabolism. Experimentally determined enzyme abundances were used to scale the maximal rates of the respective enzymes. The model was parameterized and calibrated for rat hepatocytes because experimental information on uptake and release rates of glucose, enzyme-kinetic parameters, and condition-dependent differences in enzyme abundance is more extensive for rats than for humans.

In this work, we address two interrelated questions. First, what is the relative importance of different modes of enzyme regulation for the dynamic behavior of hepatic glucose metabolism? In other words, how would the regulation of the metabolic system change if one mode of regulation was lacking. Addressing this question we argue, from an evolutionary perspective, that owing to continuous mutational alterations of protein structures and natural selection, increasingly sophisticated mechanisms of enzyme regulation have been established. For example, allosteric regulation requires the enzyme protein to possess specific binding sites for potential effector molecules. Such binding sites will not have been present for primordial enzymes. A feasible computational method to study how the occurrence of different regulatory modes may have improved the regulation of a metabolic system is to compare the dynamic behavior of the system in the presence and absence of a specific regulatory mode. We performed this analysis by simulating the response of the net hepatic glucose uptake to varying external concentrations of plasma glucose by freezing those terms of the kinetic rate equations belonging to a given mode of regulation. The second question addressed in this work relates to the sensitivity of network fluxes against changes in the regulatory properties of individual enzymes. This is a question of practical importance for the design of drugs affecting the activity of selected target enzymes with the aim to change the dynamical behavior of the network into a desired direction. Here, it is important to know which regulatory mode of the target enzyme is best suited for such intervention. As the network response depends on the strength of the parameter change as well as on the external conditions, we restricted our analysis to selected stationary metabolic states of the liver and to small parameter changes allowing the application of sensitivity measures used in metabolic control theory.

Methods

Metabolic reactions

The mathematical model of hepatic glucose metabolism encompasses the reactions of the pathways of glycolysis, gluconeogenesis, and glycogen turnover (Fig. 1). For all

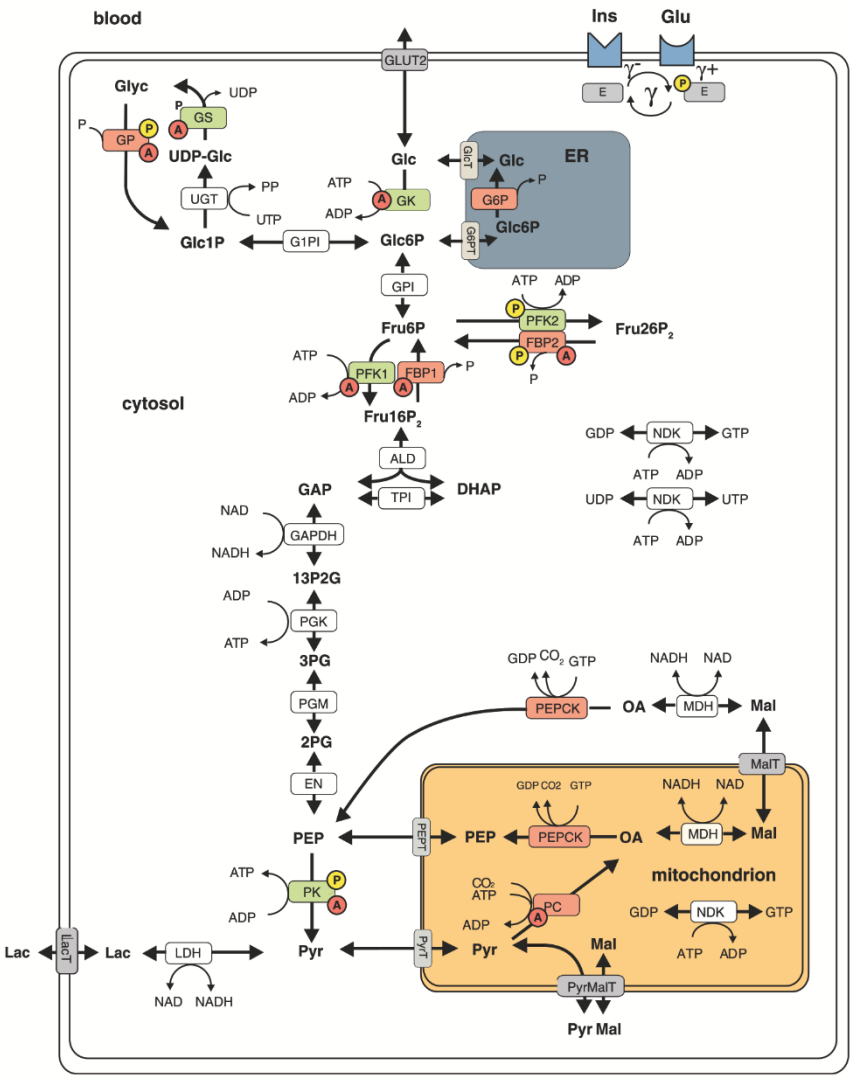

Fig. 1 Schematic representation of the model of rat hepatocyte carbohydrate metabolism. The model contains enzymes involved in glycolysis, glyconeogenesis, and glycogen synthesis and utilization (ALD, EN, FBP1, FBP2, GAPDH, GK, GP, G6P, GPI, G1PI, GS, LDH, NDK, MDH, PC, PEPCK, PFK1, PFK2, PGK, PGM, PK, TPI, UGT) and transporters (ER < - > cytosol: GlcT, G6PT; mito < - > cytosol: MalT, PEPT, PyrMalT, PyrT; external space < - > cytosol: GLUT2, LacT). Enzymes (E) that are phosphorylated or dephosphorylated (γ) in response to insulin (Ins) and glucagon stimulus are marked by a yellow P, allosteric modification of enzymes is marked by a red A. The model contains the metabolites: DHAP, Fru6P, Fru16P_2, Fru26P_2, GAP, Glc, Glc1P, Glc6P, Glyc, Lac, Mal, OA, P, PEP, 13P2G, 2PG, 3PG, PP, Pyr, and UDP-Glc. The cofactors NAD, its reduced form NADH, ADP, and ATP are not treated as dynamic variables. GDP and GTP as well as UTP and UDP are generated from ATP and ADP by NDK. The physiological metabolic processes consuming Pyr in the hepatocyte during glycolysis are comprised into Lac formation and export. The rate equations are given in the Additional file 1. ADP, Adenosine diphosphate; ALD, Aldolase; EN, Enolase; ATP, Adenosine triphosphate; DHAP, Dihydroxyacetone phosphate; ER, Endoplasmic reticulum; FBP1, Fructose-1,6-bisphosphatase; FBP2, Fructose-2,6-bisphosphatase; Fru26P_2, Fructose 2,6-bisphospate; GAP, Glyceraldehyde 3-phosphate; GAPDH, Glyceraldehyde 3-phosphate dehydrogenase; GDP, Guanosine diphosphate; GK, Glucokinase; GlcT, Glucose transporter; GLUT2, Glucose transporter 2; Glyc, Glycogen; G1PI, Glucose-1-phosphate isomerase; G6P, Glucose-6-phosphate phosphatase; GPI, Glucose-6-phosphate isomerase; GTP, Guanosine triphosphate; LacT, Lactate transporter; LDH, Lactate dehydrogenase; MDH, Malate dehydrogenase; mito, Mitochondrion; NAD, Nicotinamide adenine dinucleotide; NDK, Nucleoside-diphosphate kinase; P, Orthophosphate; PP, Pyrophosphate; Pyr, Pyruvate; PyrMalT, Pyruvate/malate antiporter; PC, Pyruvate carboxylase; PEPCK, Phosphoenolpyruvate carboxykinase; PEPT, Phosphoenolpyruvate transporter; PFK1/2, Phosphofructokinase-1/2; PGK, Phosphoglycerate kinase; PGM, Phosphoglycerate mutase; PK, Pyruvate kinase; PyrT, Pyruvate transporter; TPI, Triose-phosphate isomerase; UDP-Glc, uridine diphosphate glucose; UGT, Uridine diphospho-glucuronosyltransferase; UTP, Uridine triphosphate; 2PG, 2-phosphoglycerate; 3PG, 3-phosphoglycerate; 13P2G, 1,3-bisphosphoglycerate

reactions, detailed liver-specific enzymatic rate equations have been established based on literature data (Additional file 1). Enzymatic rate equations describe the relationship between the reaction rate (i.e. amount of substrate converted into product per time unit) and the concentration of substrates, products, and allosteric effectors (activators or inhibitors). A list of fixed parameters is given in Additional Table S2 (Additional file 1). The overall rate law of enzymes regulated by reversible phosphorylation was composed as weighted linear combination of two rate laws, one holding for the phosphorylated form of the enzyme and the other holding for the dephosphorylated form. The weighting factor represents the relative fraction of the phosphorylated form and is related to the concentration of the hormones insulin and glucagon by empirical transfer and signal functions (Figs. 2 and 3, and Signaling transfer functions in Additional file 1). Parameterization of rate laws was carried out for rat hepatocytes.

In all model simulations, we have chosen the exchange flux of glucose with the external space as the crucial target flux determining the capacity of the metabolic network to counteract changes in the plasma concentration of glucose. Numerical values for kinetic parameters of the enzymes were extrapolated from values determined in in vitro enzyme assays. However, numerical values for the maximal enzyme activities (V_{max}) in vivo are unknown. The V_{max} values of enzymes depend on the (varying) expression level of the enzyme protein as well as effectors acting inside the cell but being (yet) unknown. Thus, there was no other option than to estimate these parameters by minimizing the difference between model predictions and experimental data. In order to use the model for predicting the impact of changes in the expression (= protein) level of enzymes elicited by changes in the physiological status (fed, fasted, normal, diabetic) of the rat it is compulsory to estimate the V_{max} values for only one of these states (serving as reference state) and to relate the V_{max} values for all other states to the V_{max} values of the reference state by the ratio of enzyme abundances, thereby exploiting the fact that the V_{max} value is a linear function of enzyme abundance. We have chosen the fed state as the reference case. With V_{max}^{fed} denoting the V_{max} value of an enzyme in the reference state, the V_{max} value of this enzyme in the fasted and diabetic state is put to $V_{max}^{fasted} = \alpha_{fasted} V_{max}^{ref}$ and $V_{max}^{d} = \alpha_{d} V_{max}^{ref}$ where the scaling factors α_{fasted} and α_{d} are given by the ratio of mean enzyme abundances $\langle E \rangle$ shown in Fig. 4:

$$\alpha_{fasted} = {}^{\langle E \rangle_{fasted}}/_{\langle E \rangle_{fed}} \quad and \quad \alpha_{d} = {}^{\langle E \rangle_{d}}/_{\langle E \rangle_{fed}}$$

We additionally defined a fourth physiological state, the so-called normal state, referring to a situation where the rat is kept under limited but energetically balanced food supply. As for the normal state no experimental data on enzyme abundances are available in the literature we made the assumption that the V_{max} values in the normal state can be reasonably well approximated by the V_{max} values in the fed and fasted state:

$$\alpha_{normal} = \frac{1}{2}(\alpha_{fasted} + \alpha_{fed}) \tag{6}$$

With these settings, the only adjustable parameters to be estimated are the values of V_{max}^{fed} for the (fed) reference state.

Relationship between plasma levels of glucose and the hormones insulin and glucagon

The phosphorylation state of enzymes controlled by reversible phosphorylation is determined by the insulin and glucagon concentrations within the liver sinusoids. Both

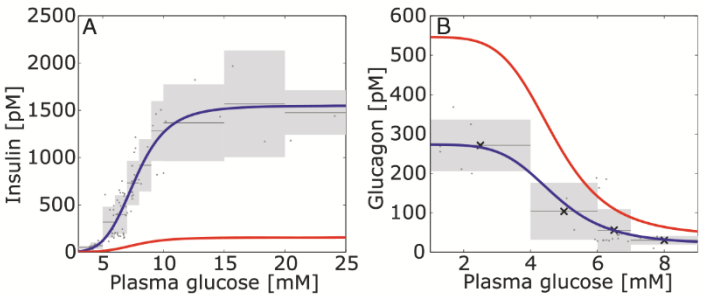

Fig. 2 Glucose-hormone-transfer (GHT) functions. The GHT functions describe the dependence of plasma insulin (**a**) and plasma glucagon (**b**) on plasma glucose levels. Experimentally determined plasma concentrations of glucose and hormone (grey dots) from various sources (insulin: [59–61], glucagon: [42, 62–65]) were pooled (black lines – mean values, light grey boxes – standard deviations). The additional Tables S3 and S4 summarize the used values (Additional file 1). A Hill-type function was used to fit the data by least-square minimization yielding the normal GHT function (blue line). The red line depicts diabetic GHT function. For details of the used fit functions see Additional file 1

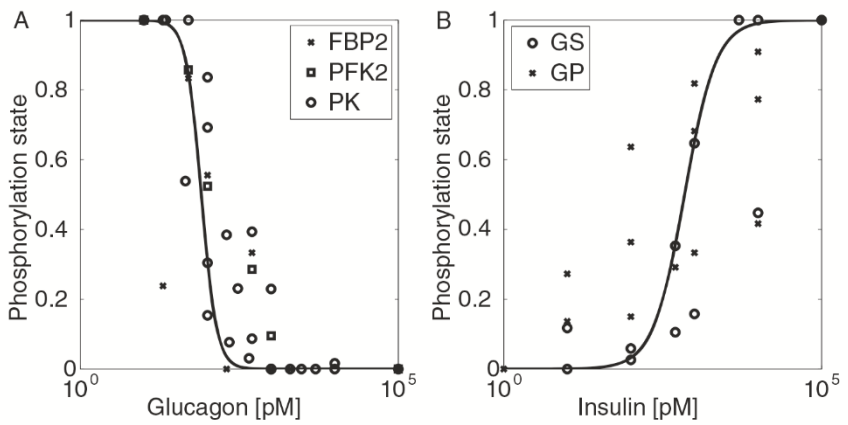

Fig. 3 Phosphorylation states of enzymes as function of glucagon (**a**) or insulin (**b**) concentrations. Bold lines depict the function γ (Additional file 1) used to relate the level of insulin and glucagon to the phosphorylated form of enzymes regulated by reversible phosphorylation. Experimental data are from various sources [66–73]. Additional Tables S5 and S6 summarize the used values (Additional file 1)

hormones are secreted by the pancreas into the portal vein. The secretion rate is mainly controlled by the glucose concentration of the blood. An increase of glucose concentration stimulates the release of insulin from beta cells and reduces the release of glucagon from alpha cells in the pancreatic islets of Langerhans. Similarly to Koenig et al. [6], we established an empirical GHT function, which describes the relationship between the plasma level of glucose and of insulin and glucagon. To this end, we fitted a sigmoid function of Hill-type to a large data set of experimentally determined glucose-insulin and glucose-glucagon relations determined in the rat (Fig. 2).

Relationship between plasma hormone level and phosphorylation state of enzymes

On the short-term, insulin and glucagon control the phosphorylation state of key regulatory enzymes by glucagon-stimulated enzyme phosphorylation and insulin-mediated inhibition of enzyme phosphorylation. We constructed an empirical signal function to describe the relationship between hormone levels and the relative share (γ) of the phosphorylated enzyme in the total enzyme pool (Fig. 3). We assumed that, at saturating concentrations of the hormone (set to 10^5 pM), the phosphorylated fraction of the enzyme tends to γ = 1 (glucagon) or γ = 0 (insulin), respectively.

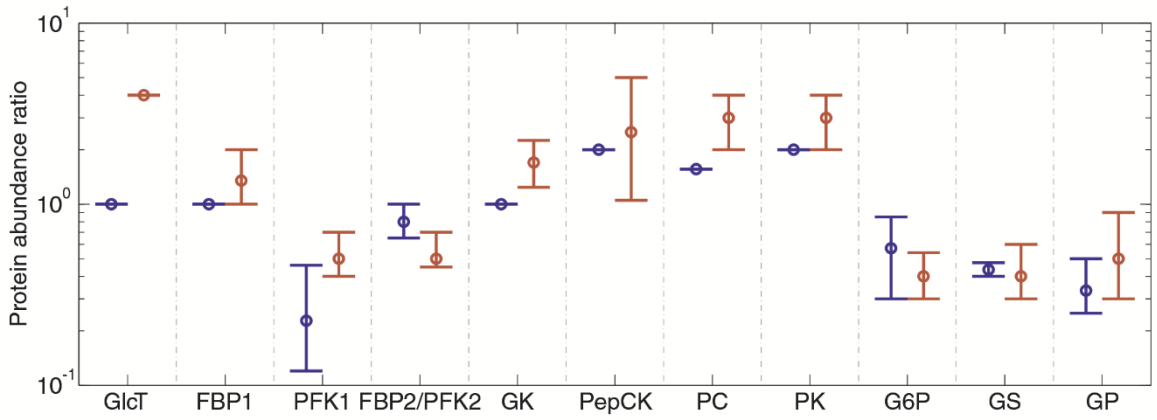

Fig. 4 Experimentally determined variations in the abundance of key metabolic enzymes. The circles denote the average ratio between measured protein abundances in hepatocytes from fasted versus fed hepatocytes (blue) and diabetic versus normal hepatocytes (red). Vertical lines indicate the range of reported values. Experimental data are from various sources [2, 7, 19–38]

Experimentally determined variations of enzyme abundances

Long-term alterations on the average values of plasma glucose and hormone concentrations induce changes in the abundance of key metabolic enzymes in the liver. Such adaptation occurs under extreme physiological and pathological settings like starvation or diabetes. Figure 4 shows the range of reported ratios of enzyme abundances, which were experimentally determined in fed and fasted hepatocytes and in 'normal' hepatocytes (for which the enzyme abundances were set to the mean values of abundances from fasted and fed hepatocytes) and diabetic hepatocytes. For example, the abundance of the glycolytic enzyme pyruvate kinase was found in different publications to be between two- and four-fold higher in diabetic hepatocytes compared with normal hepatocytes. We used the mean of the reported ranges for the fold-change of enzyme abundances depicted in Fig. 4 to scale the maximal enzyme activities when we parameterized the model for different physiological settings.

Software

Computations were performed with MATLAB Release 2009a, The MathWorks, Inc., Natick, Massachusetts, United States. The SBML version of the model is supplied as Additional file 2.

Results

Validation of the model

We checked the validity of the kinetic model by comparing simulated glucose exchange fluxes, metabolite concentrations and filling states of the glycogen store with experimental data. Throughout the paper, we use the term glucose exchange flux to designate the glucose transport flux from the external space into the cell (= glucose net uptake), i.e. negative flux values indicate net release of glucose from the cell to the external space. The literature data used for the parametrization and validation of the model were obtained from liver tissue or hepatocytes of rats that have adopted different physiological states owing to either nutritional, genetic, or chemical interventions. The fed state designates a situation where rats are routinely fed ad libitum, i.e. food is available at all times in unlimited quantities. These animals are thus moderately obese and display elevated plasma glucose levels compared to rats in the normal state kept under well-controlled feeding. The fasted state is attained after 24 hours of complete food deprivation and is characterized by low plasma glucose levels. The diabetic state refers to a situation in which the animals exhibit an impaired glucose-insulin and glucose-glucagon relationship (for details see below). Finally, in the normal state, the rats have limited access to food without any signs of malnutrition. For the sake of convenience, livers or hepatocytes from fasted, fed, diabetic, and normal rats will be referred to as fasted, fed, diabetic, and normal livers/hepatocytes in the following sections.

The gene expression and, thus, the protein abundance of metabolic enzymes differs in these different physiological states. Figure 4 depicts ratios of enzyme abundances gathered from different literature sources. These ratios were used to put the maximal enzyme activities of different physiological states into a linear relation, thereby using the enzyme abundances in the fed state as reference. The relative maximal activities are given in Table 1. Using protein abundances for scaling maximal enzyme activities exploits the fact that the maximal activity of an enzyme is a linear function of the enzyme abundance with the turnover number (number of catalytic events per time unit) serving as a proportionality factor. For details of the procedure used to fix the numerical values of these scaling factors see Methods.

Hepatic glucose production (HGP) from lactate

In this simulation, we compared rates of gluconeogenesis (also referred to as hepatic glucose production, HGP) from lactate with experimental data obtained in perfused fasted livers (Fig. 5). We set the maximal enzyme activities to fasting conditions (Table 1) and varied the external concentration of lactate as done in various

Table 1 Relative maximal enzyme activities for the normal, fasted, and diabetic rat liver. The numbers represent relative maximal enzyme activities with respect to those of the fed state (= reference state). They are based on the experimentally observed protein abundance ratios shown in Fig. 1. For the absolute values of maximal enzyme activities in the fed (reference) state see section model parameters in Additional file 1. Where there is no range given, only the given fixed ratio was used

Enzyme	Normal liver	Fasted liver		Diabetic liver	
	mean	mean	range	mean	range
FBP1	1.00	1.00	–	4.00	–
FBP2	0.66	0.43	0.4–0.475	0.26	0.20–0.40
GK	0.48	0.23	0.12–0.46	0.24	0.19–0.33
GlcT	1.00	1.00	–	1.35	1.00–2.00
GP	0.89	0.80	0.65–1.0	0.45	0.40–0.63
G6P	1.41	2.00	–	3.54	1.48–7.07
GS	1.00	1.00	–	1.70	1.24–2.25
PC	1.25	1.56	–	3.75	2.50–5.00
PEPCK	1.41	2.00	–	4.24	2.83–5.66
PFK1	0.76	0.57	0.3–0.85	0.30	0.23–0.41
PFK2	0.66	0.43	0.4–0.475	0.26	0.20–0.40
PK	0.58	0.33	0.25–0.5	0.29	0.17–0.52

FBP1 Fructose-1,6-bisphosphatase, *FBP2* Fructose-2,6-bisphosphatase, *GK* Glucokinase, *GlcT* Glucose transporter, *G6P* Glucose-6-phosphate phosphatase, *GP* Glycogen phosphorylase, *GS* Glycogen synthase, *PC* Pyruvate carboxylase, *PEPCK* Phosphoenolpyruvate carboxykinase, *PFK1/2* Phosphofructokinase-1/2, *PK* Pyruvate kinase

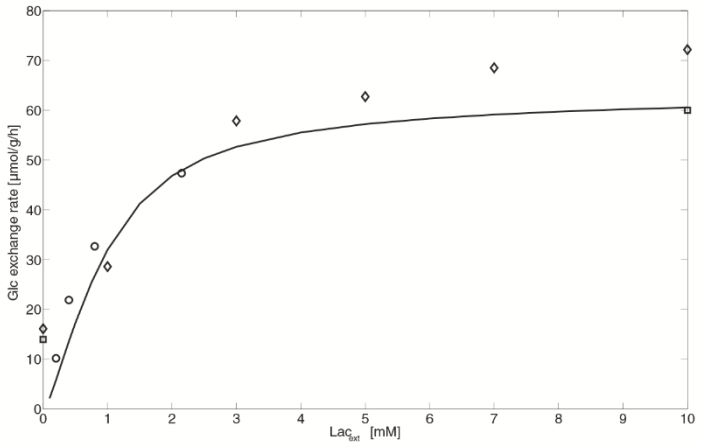

Fig. 5 Gluconeogenesis from lactate. The solid line depicts the simulated stationary hepatic glucose exchange flux for fasted hepatocytes as function of the external lactate concentration (Lac_{ext}), which was varied between 0–10 mM. Data points represent experimental data taken from [39–41] with different shapes for each experiment

experiments. As the perfusion medium used in the experiments was devoid of glucose and hormones, we put these concentrations to zero. The integration time was chosen long enough to reach a stationary steady state. In agreement with the data, for lactate concentrations larger than 5 mM, the glucose exchange flux starts to become saturated to finally reach a maximum of approximately 60–70 μmol/g/L (= maximal net glucose production rate).

Transition between HGP and hepatic glucose utilization (HGU) in vivo

In a second simulation, we varied the plasma glucose level between 3–12 mM and calculated the stationary glucose exchange flux of the fasted, normal, and fed liver in vivo. The relative enzyme abundances for the normal, fasted, and diabetic state relative to those of the fed (reference) state are given in Table 1. The plasma level of the hormones insulin and glucagon associated with a given value of plasma glucose was obtained by means of glucose-hormone transfer (GHT) functions (see Methods, Fig. 2). The external lactate concentration was put to the average physiological value of 1 mM. Again, we let the simulations run long enough to obtain a metabolic steady state. Figure 6 shows simulated and experimentally determined glucose exchange fluxes for normal, fasted, and fed livers in dependence of plasma glucose levels in vivo. Note that the experimental data in Fig. 6 merely indicate the expected range of glucose exchange fluxes because a clear assignment of these data to the specific state of the laboratory rat was not extractable from the literature sources. The simulated curves suggest that the glucose output of the liver is shifted to higher values in the fasted state compared with the fed state. In what follows, we define the glucose set point by the plasma glucose level at which the glucose exchange flux is zero, i.e. the liver neither utilizes nor produces glucose. This glucose set point is shifted from about 6.5 mM of the fed liver to about 9 mM of the fasted liver.

Hepatic glycogen storage during a starvation-refeeding cycle

Thus far we considered stationary fluxes under various external conditions. Stationarity implies that the intrahepatic glycogen store also adopts a steady state where rates of glycogenolysis and glycogen synthesis are equal and thus do not contribute to the glucose exchange flux. However, in vivo, the plasma concentrations of glucose and hormones are continuously changing thus preventing the attainment of a steady state. Therefore, in a third simulation, we investigated the time-dependent variation of the glycogen pool during a starvation-refeeding cycle, which starts at time t = 0 with a fasted liver that is completely emptied in glycogen after 48 hours of starvation (plasma glucose concentration set to 4 mM). The corresponding glucagon and insulin concentrations were calculated from the GHT functions shown in Fig. 2. Figure 7 shows the simulated time-dependent filling state of the hepatic glycogen store together with experimental data during 20-h refeeding (plasma glucose concentration set to 8 mM) and subsequent fasting over a 32-h period. During the fasting period starting at t = 20 h, depletion of the glycogen store contributes to net glucose production.

Conversion of imported glucose to glycogen

In the feeding phase, hepatocytes take up plasma glucose that is either used to replenish their glycogen store or to form pyruvate via glycolysis. To check the relative share

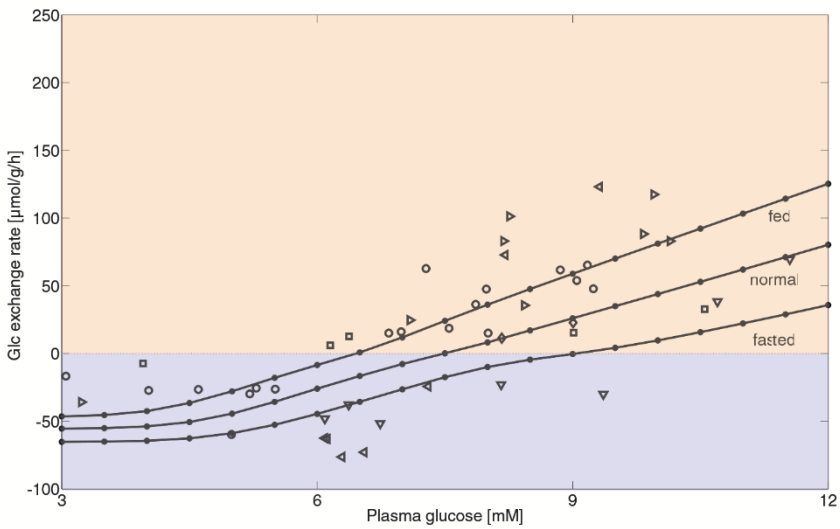

Fig. 6 Glucose exchange flux in vivo in dependence of plasma glucose levels. The solid lines depict stationary hepatic glucose exchange rates for fasted, normal, and fed hepatocytes in dependence from the plasma glucose concentration. Data points represent experimental data taken from [6, 42–44] with different shapes for each experiment

of these two alternative modes of glucose utilization we simulated an oral glucose tolerance test applied to fasted rats [7]. Figure 8 shows the average fluxes of glucose uptake and glycogen synthesis during the first 60 minutes. The absolute values of measured and computed flux rates as well as the flux ratios are in good concordance, indicating that more than 90 % of the glucose taken up by the fasted liver is used to replenish the glycogen store.

Range of intracellular metabolite levels

Finally, we compared the intracellular metabolite concentrations in fed, normal, and fasted hepatocytes with reported tissue concentrations. To this end, we varied plasma glucose concentration within the physiological range of 3–12 mM and calculated the concentration range of all cellular metabolites occurring in the model. Lactate was fixed at 1 mM while glucagon and insulin concentrations were determined by means of the GHT functions (Fig. 2). Figure 9 demonstrates the good agreement between the computed ranges of intracellular metabolite concentrations for fasted and fed hepatocytes and ranges of reported experimental values.

Model applications

The impact of variable protein abundance on glucose exchange fluxes in different conditions

The liver switches from glucose production to glucose utilization depending on the plasma glucose level and the two main hormones insulin and glucagon. Depending on

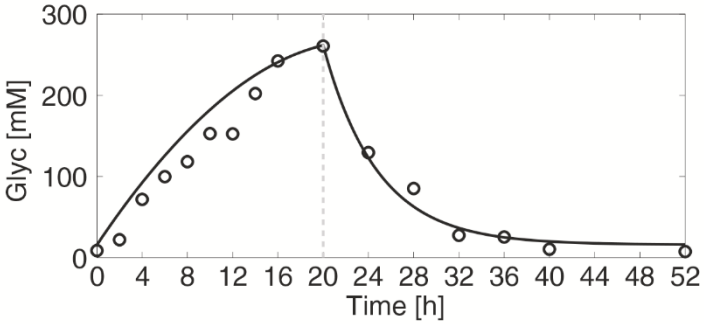

Fig. 7 Hepatic glycogen storage. The solid line depicts the time course of intrahepatic glycogen content (Glyc) during refeeding and fasting of initially fasted hepatocytes. Open circles represent experimental data [45], where 48-h fasted rats were fed ad libitum for 20 h before they were fasted again. The broken vertical line indicates the transition from refeeding to fasting conditions

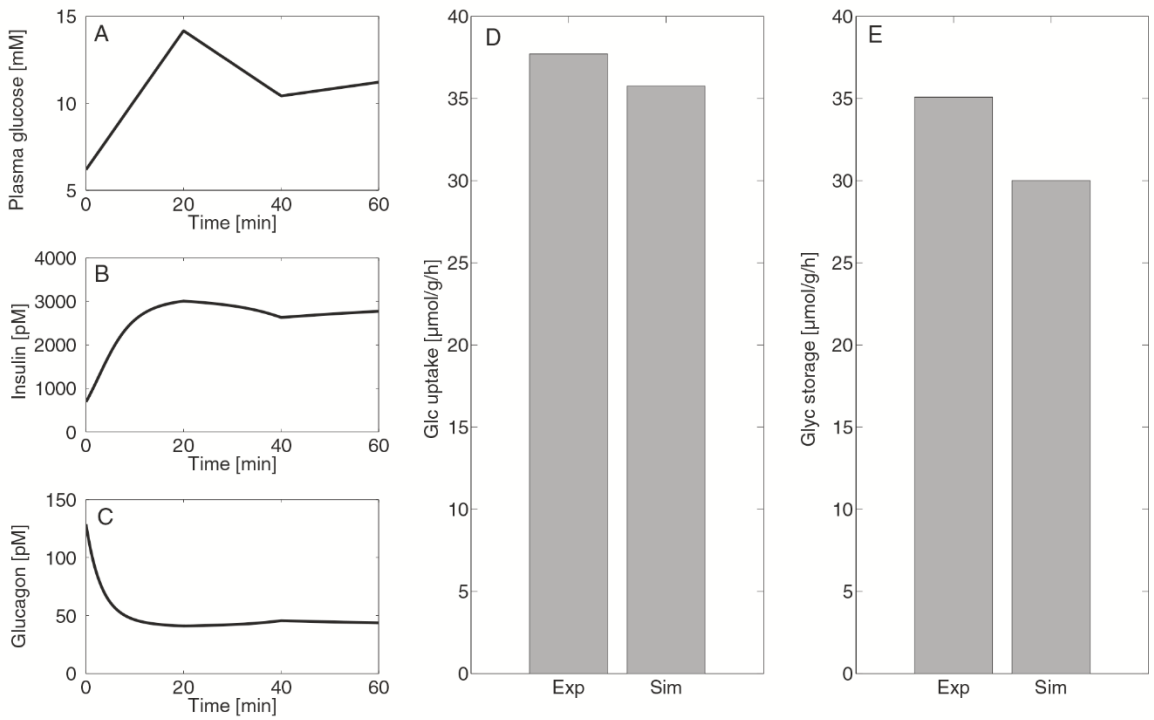

Fig. 8 Glycogen production during the first hour of an oral glucose tolerance test. Experimental data (Exp) and the glucose profile (**a**) used as model input are taken from Niewoehner and Nuttall [6]. Insulin (**b**) and glucagon concentrations (**c**) were computed by means of the GHT function (Fig. 2). The bars depict the glucose exchange flux (= net glucose uptake) (**d**) and the cellular flux of glucose into the glycogen store (**e**) in units of glucose moieties for the first hour of an oral glucose tolerance test

the timing of nutrient uptake this switch may occur several times during a day and is mainly controlled by hormone-dependent reversible phosphorylation of key regulatory enzymes. If changes of the external conditions persist over several days or even longer time periods, regulation of protein abundance represents a further mechanism of metabolic adjustment. To reveal the physiological implications of metabolic adaptation through variable abundance of metabolic enzymes we calculated the glucose exchange flux of the liver over a broad range of blood plasma glucose concentrations. Lactate concentration was set to 1 mM, the intrahepatic filling state of the glycogen store was put to fixed values between 0 and 100 %, and insulin and glucagon values were determined by the GHT functions (Fig. 2).

Figure 10 depicts stationary exchange fluxes in response to varying plasma glucose levels at various filling states of the glycogen store. In the fasted liver, the glucose set point at which the glucose exchange flux is zero (indicated by bold black lines) lies between 8.0 and 9.2 mM depending on the filling state of the glycogen store. For the normal and fed liver, the set point is increasingly shifted to lower values lying between 6.7 and 7.7 mM and between 5.9 and 6.6 mM, respectively. These computations clearly demonstrate the impact of variable enzyme abundance on the capability of the liver to utilize or produce glucose at given plasma glucose levels – fasting shifts the range of glucose exchange rates into the direction of glucose production and decreases the capacity for glucose uptake. In contrast, fed hepatocytes possess about equal capacities for glucose production and glucose uptake.

Putting the filling state of the glycogen store to 100 % and the blood plasma glucose concentration to 3 mM and, conversely, putting the filling state of the glycogen store to zero and the blood plasma glucose concentration to 10 mM, the maximal observable rates of the glucose exchange flux predicted by the model were approximately between −70 µmol/g/h and +80 µmol/g/h for the fed hepatocyte and approximately between −120 µmol/g/h and +20 µmol/g/h for the fasted hepatocyte.

The impact of diabetes type 2 on the hepatic glucose exchange flux

The diabetic liver is not only characterized by changes in the abundance of metabolic enzymes (Table 1) but also by alterations in the glucose-hormone relationships (see GHT

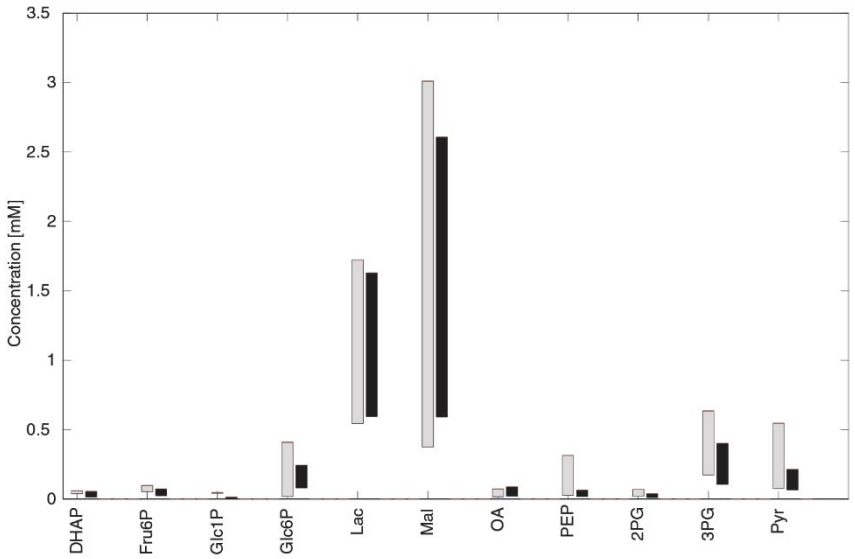

Fig. 9 Simulated and measured concentration ranges of metabolites. Experimentally determined concentration ranges of metabolites (gray) are shown together with simulated concentration ranges (black) for the fed, normal, and fasted liver. Simulated concentration ranges were obtained as steady state concentrations when plasma glucose concentration was varied between 3–12 mM with constant plasma lactate (1 mM). Experimental data are from various experimental sources [46–54]. Experimental concentration values given in μmol/g wet weight were converted into mM by dividing these by the factor 0.46 and corrected for the liver density of 1.067 g/mL [55]. DHAP, Dihydroxyacetone phosphate; Fru6P, Fructose 6-phosphate; Glc1P, Glucose 1-phosphate; Glc6P, Glucose 6-phosphate; Mal, Malate; OA, Oxaloacetate; PEP, Phosphoenolpyruvate; 2PG, 2-Phosphoglycerate; 3PG, 3-Phosphoglycerate; Pyr, Pyruvate

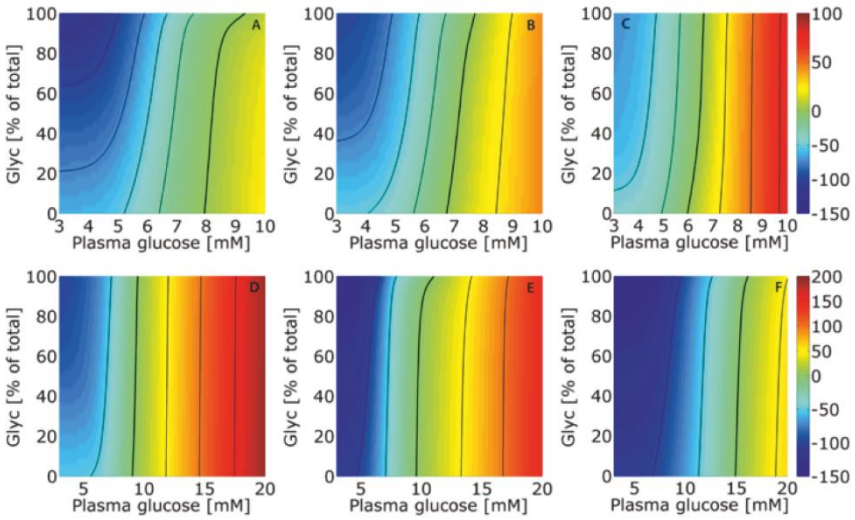

Fig. 10 Stationary glucose exchange fluxes in dependence of plasma glucose and glycogen store. Plasma glucose was varied between 3 and 10 mM and filling state of glycogen storage was variably fixed to values between 0 and 100 %. The color encodes the steady state flux rates of glucose exchange of fasted (**a**), normal (**b**), fed (**c**), and diabetic hepatocytes (**d**–**f**). Green colors indicate small values of the glucose exchange flux around the set point where the net glucose exchange is zero (marked by bold black lines). Warm colors indicate net glucose uptake and cool colors indicate net glucose release. The legend is given on the right-hand axis in units of μmol/h/g tissue. Thin black isoclines connect equal exchange fluxes (in steps of 25 μmol/h/g tissue). Note that the set point values at 6.5 mM (fed), 7.5 mM (normal), and 9 mM (fasted) at half-filling of the glycogen store are identical with those in Fig. 6, where the glycogen contribution is zero due to the condition of stationarity. For the diabetic liver, the calculations were performed for three different scenarios: (**d**) no change of enzyme abundances compared with the normal state but impaired glucose-hormone relationship (see red curves of the GHT function in Fig. 2); (**e**) altered protein abundances (see Table 1 for scaling factors) but normal GHT function; and (**f**) combined effect of altered glucose-hormone relationship and protein abundances

functions represented by the red curves in Fig. 2). Portal insulin was found to be reduced to about 10 %, while portal glucagon was increased to almost 200 % of normal concentrations [8]. In order to quantify the impact of either of these changes on the glucose exchange flux we performed three different simulations where changes in either the glucose-hormone response, the enzyme abundances, or both were taken into account.

We simulated the glucose exchange flux of the diabetic liver over a wide range of plasma glucose concentrations spanning from approximately 3 mM (observed during hypoglycemic crises) to approximately 20 mM (a commonly observed level in untreated diabetic rats [9]). Lactate concentration was set to 1 mM. Insulin and glucagon values were either computed by the normal or diabetic GHT (represented by the blue or red curves in Fig. 2, respectively).

Taking into account alterations of the glucose-hormone profiles only (Fig. 10d) our model predicts a shift of the set point to the right, i.e. an increase of the capability of the liver to function as glucose producer. This right-shift is even more pronounced if only changes in protein abundances are taken into account (Fig. 10e). The combined effect of altered hormonal control and altered enzyme abundances results in an additional right-shift of the set point such that the diabetic liver works as a glucose producer up to plasma glucose levels of 15 mM (Fig. 10f).

The importance of variable enzyme abundances for the adaptation of the liver to different physiological settings is summarized in Fig. 11 showing the calculated maximal range of glucose exchange rates at variations of the plasma glucose level between 3 and 10 mM, with and without adaptation of enzyme abundances and altered glucose-hormone relationship. These ranges were estimated by setting the filling of the glycogen store to 0 or 100 % at 3 mM and 10 mM plasma glucose, respectively.

Diurnal metabolic profiles of fasted, fed, and diabetic hepatocytes

We used the model to investigate the response of the liver to diurnal variations of the plasma glucose level in different physiological settings. Measured plasma glucose profiles monitored over 24 hours were used as model input. Since the diurnal plasma glucose levels differ significantly between the fasted, fed, and diabetic conditions, we used representative profiles for each condition. The associated hormone profiles were again calculated by means of the GHT function (Fig. 2). To estimate the impact of random individual variations in enzyme abundances on the simulation results we repeated the simulations 50 times with protein abundance ratios randomly sampled from the experimentally determined ranges (Table 1).

Figures 12 and 13 show simulated diurnal variations of the glucose exchange flux for the fed and fasted state. At rich nutrient supply (fed state), the liver acts either as glucose producer or utilizer depending on the actual plasma glucose level (Fig. 12d). Over one day, glycogen decreases by approximately 50 %, but is fully replenished, resulting in no net glycogen utilization (Fig. 12e). Integrated over 1 day, the net glucose exchange rate of the liver is close to zero. In contrast, at fasting conditions, the model simulation predicts the liver to act persistently as glucose producer (Fig. 13d). Moreover, the hepatic glycogen store remains low over the whole day as it cannot be substantially replenished in phases of elevated plasma glucose (Fig. 13e).

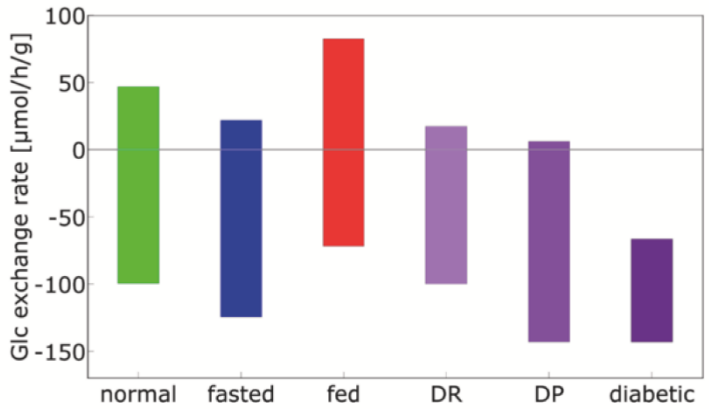

Fig. 11 Maximal ranges of the glucose exchange fluxes. Plasma glucose was varied between 3 and 10 mM. Normal: protein abundance of normal hepatocytes; fasted: protein abundance of fasted hepatocytes; fed: protein abundance of fed hepatocytes; DR: diabetic GHT function, protein abundance of normal hepatocytes; DP: protein abundance of diabetic hepatocytes; diabetic: diabetic GHT function and protein abundance of diabetic hepatocytes

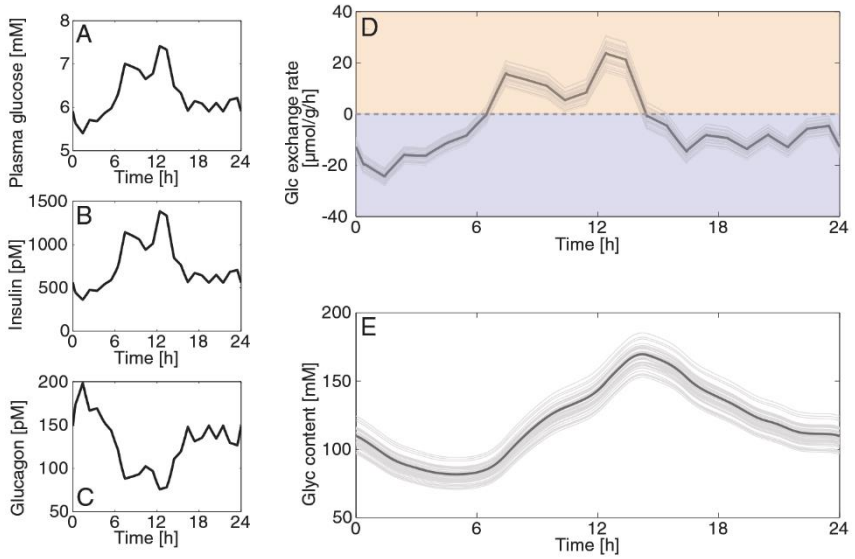

Fig. 12 Diurnal variations of the glucose exchange flux and glycogen in the fed state. (**a**) Measured diurnal profiles of plasma glucose for fed hepatocytes taken from [56] and used as model input. (**b**, **c**) Diurnal profiles of insulin and glucagon calculated from the plasma glucose profile in (**a**) by means of the GHT function. (**d**) Simulated diurnal glucose exchange flux. (**e**) Simulated diurnal glycogen content in fed hepatocytes. The simulation was repeated 50 times with uniformly sampled protein abundances from the observed range for each enzyme (Table 1)

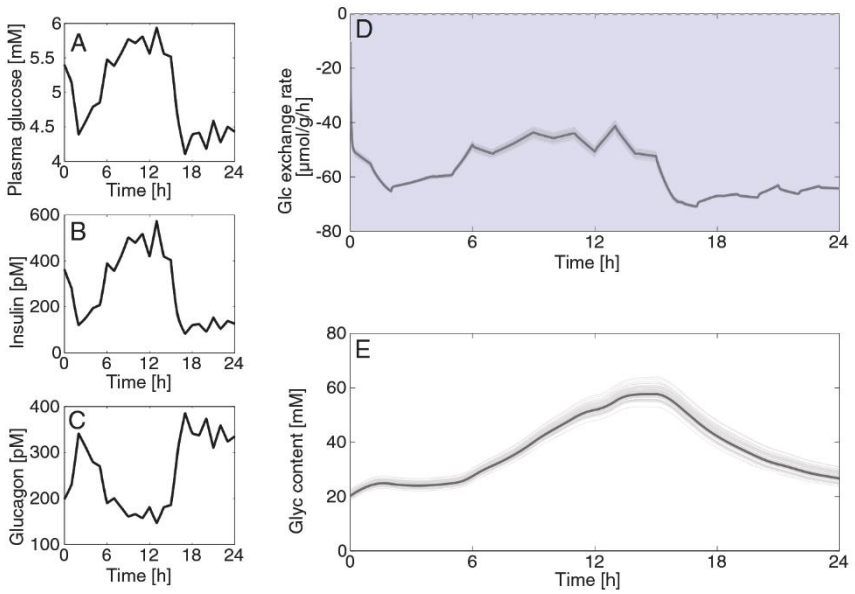

Fig. 13 Diurnal variations of the glucose exchange flux and glycogen in the fasted state. (**a**) Measured diurnal profiles of plasma glucose for fasted hepatocytes taken from [56] and used as model input. (**b**, **c**) Diurnal profiles of insulin and glucagon calculated from the plasma glucose profile in (**a**) by means of the GHT function. (**d**) Simulated diurnal glucose exchange flux. (**e**) Simulated diurnal glycogen content in fasted hepatocytes. The simulation was repeated 50 times with uniformly sampled protein abundances from the observed range for each enzyme (Table 1)

For the simulation of the diurnal glucose exchange flux of the diabetic liver (Fig. 14) we tested three different scenarios regarding the abundance of glycogen synthase and glycogen phosphorylase as the respective literature findings are controversial (see legend of Fig. 14). Here, glucose plasma levels are extraordinarily high, but insulin levels are still low due to impaired beta cell function, while glucagon levels are elevated. Although the plasma glucose remains persistently above 14 mM, there is a time window between 2 and 5 h where the liver acts as glucose producer. This is the result of the remarkable right-shift of the glucose set point (Fig. 10f). Glycogen levels range between almost filled and almost empty depending on enzyme abundance of glycogen synthase and glycogen phosphorylase.

The thin grey curves in Figs. 12, 13 and 14 illustrate how the diurnal profile of the glucose exchange flux is affected by variations of enzyme abundances around their mean. In these simulations, the enzyme abundances were randomly sampled within the reported ranges given in Table 1. The simulations reveal large differences in the impact of individual variations of enzyme abundances on the deviation of diurnal profile of the hepatic glucose exchange flux from the average. Whereas these deviations remain moderate for fed and fasted hepatocytes, they are substantially higher in diabetic hepatocytes because of large variations of enzyme abundances in this condition (see red bars in Fig. 4).

Adaptation of the cellular enzyme endowment to long-term fed or fasted conditions shifts the metabolic output of the liver towards a better response to the 'anticipated' physiological state. However, this beneficial effect may turn to a regulatory disadvantage if the 'anticipated' external situation suddenly changes. This is illustrated in Fig. 15, showing the response of the glucose exchange flux to a perturbation of the typical plasma glucose profile for fasting conditions by a pulse-like increase of glucose as it may occur after intake of a glucose-rich meal. In the fasted state (liver metabolism shaped to deliver glucose to the plasma), the capability of the liver to rapidly and efficiently clear an excess of plasma glucose by increased glucose uptake and channeling into the glycogen pool is significantly lower than the capability of a liver which is adapted to persistent conditions of rich nutrient supply.

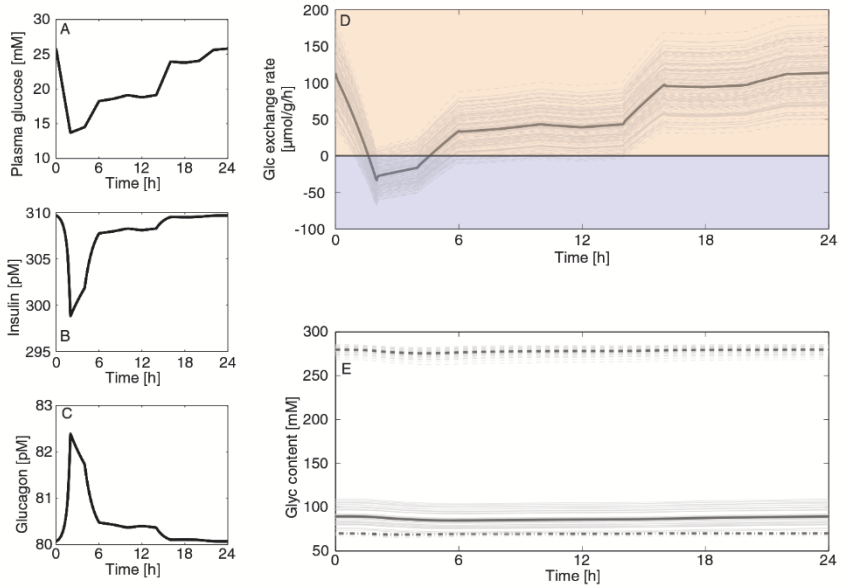

Fig. 14 Diurnal variations of HGP/HGU and glycogen in the diabetic state. (**a**) Measured diurnal profiles of plasma glucose for diabetic hepatocytes taken from [8] and used as model input. (**b**, **c**) Diurnal profiles of insulin and glucagon calculated from the plasma glucose profile in (**a**) by means of the GHT function (Fig. 2, red curve). (**d**) Simulated diurnal glucose exchange flux. (**e**) Simulated diurnal glycogen content in diabetic hepatocytes. The simulation was repeated 50 times with uniformly sampled protein abundances from the observed range for each enzyme (Table 1). Due to conflicting experimental data regarding the amount of glycogen synthase (GS) and glycogen phosphorylase (GP) in diabetic hepatocytes, we set up three different scenarios: increased activity of GS by 70 % and diminished activity of GP by 50 % [29] (top trace – solid line); increased activity of GS by 70 % and decreased activity of GP by 50 % and reduced total glycogen storage capacity to 75 % [57] (bottom trace – dashed line); and decreased GS activity by 50 % and unchanged GP activity [58] (middle trace – dash-dotted line)

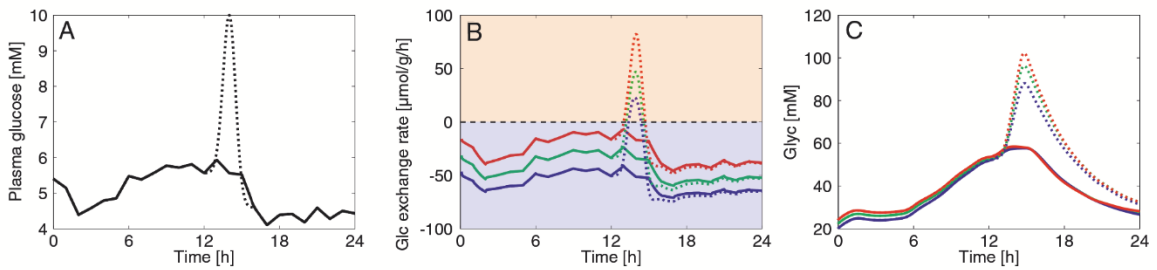

Fig. 15 Different capabilities of fasted and fed hepatocytes to cope with transient hyperglycemic conditions. The figure depicts glucose exchange flux (**b**) and glycogen content (**c**) of fasted (blue), normal (green), and fed (red) hepatocytes in response to the 24-h glucose profile of fasted rats (**a**). The dotted lines refer to a situation where a transient glucose bolus (between 12 and 16 h) was added, driving the plasma glucose to a peak value of 10 mM. While the fasted hepatocyte has the highest glucose release rates in the unperturbed case it is clearly less efficient than the normal and fed hepatocyte to take up large amounts of glucose under sudden hyperglycemic conditions

The impact of varying enzyme abundances, reversible phosphorylation and allosteric regulation on the long-term regulation of hepatic glucose metabolism

The central homeostatic function of the liver in the regulation of systemic glucose metabolism consists of efficiently counteracting deviations of plasma glucose from the normal level. This is reflected in the diurnal changes of the glucose exchange flux shown in Figs. 12, 13 and 14 mirroring, in an inverse manner, the variations of plasma glucose. Thus, a physiologically meaningful measure for the relative importance of various modes of metabolic regulation for plasma glucose homeostasis is the change of the diurnal profile of the glucose exchange flux that would result if changes of enzyme abundances, allosteric effects, and hormonal regulation were not present. As the reference state for such comparisons we have chosen the normal state, which refers to a situation where the rat is neither fasted nor fed ad libitum. Such a nutritional regime should better reflect the typical situation of a wild rat than extreme laboratory feeding regimes. The maximal enzyme capacities of the normal state are chosen as arithmetic mean of the maximal capacities in the fed and fasted state (Table 1). Technically, the absence of a specific regulatory mode was accomplished by freezing, in the kinetic rate equations, those terms belonging to a selected mode of regulation to their values adopted at the glucose set point of the normal state at which the glucose exchange flux is zero. Owing to this setting, the full model and the reduced models (lacking one mode of regulation) yield the same stationary state at the set point. Choosing the set point as the common point of reference for all model variants takes into account the fact that the homeostatic function of the liver with respect to plasma glucose consists in preventing larger deviations from the set point despite larger changes in plasma glucose.

For the comparison of the full model with the regulation-depleted models we used the following distance measure:

$$\Delta = \int_0^{24h} \left| v_{ex}^{normal} - v_{ex}^{(-)} \right| dt \Big/ \int_0^{24h} \left| v_{ex}^{normal} \right| dt \qquad (1)$$

Here, v_{ex}^{normal} denotes the glucose exchange flux in the presence of all modes of metabolic regulation and $v_{ex}^{(-)}$ is the glucose exchange flux if one mode of regulation is dropped in the model simulations (for more details see legend of Fig. 16). From the values of Δ summarized in Table 2 and the corresponding diurnal profiles of the glucose exchange flux shown in Fig. 16 follows that all three modes of regulation have a significant impact on the response of the hepatic glucose exchange flux to variations of plasma glucose. Whereas the impact of the fast regulatory modes (reversible phosphorylation and allosteric regulation) is almost equal in the fed and fasted state, the change of enzyme abundances results in the essential mechanism in adapting the hepatic glucose metabolism to the fed state.

Flux control coefficients, enzyme elasticities, and regulator strengths

Flux control coefficients In the previous section, we studied the global impact of different modes of enzyme regulation on the metabolic response of the liver to varying plasma glucose concentrations. In this section, we use the model to study how individual enzymes are controlled by different modes of regulation and how they contribute to the overall regulation of the hepatic glucose exchange flux. The established method to address such questions is the Metabolic Control Analysis (MCA) [10]. In this concept, the regulatory importance of any reaction is quantified by its so-called flux control

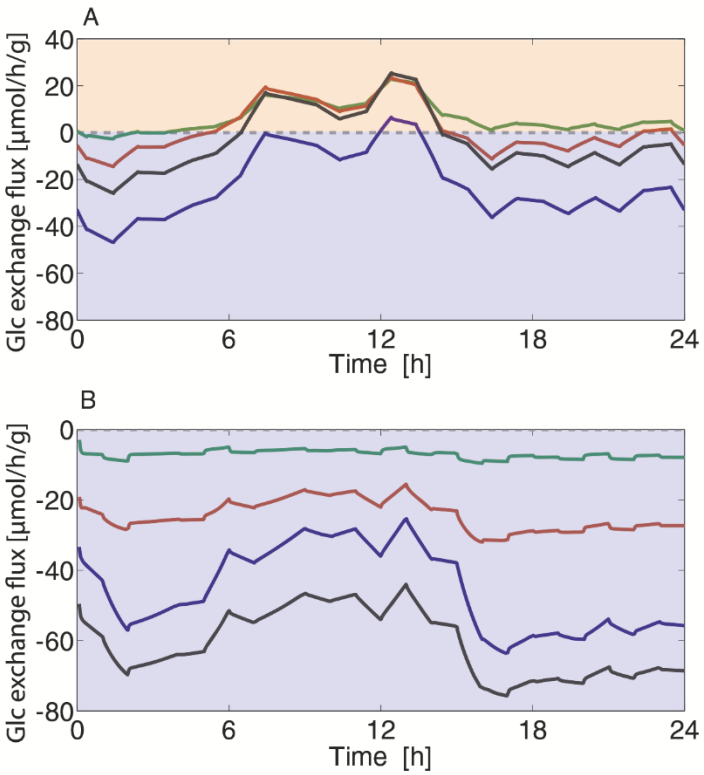

Fig. 16 Influence of different levels of metabolic control on diurnal glucose exchange rates. Black curves: Full control – enzyme abundances are adapted to the fed (**a**) and fasted (**b**) state (Table 1) with full allosteric and hormonal control. Blue curves: No change of enzyme abundance – enzyme abundances of fed and fasted livers are the same as in the normal liver; full allosteric and hormonal control. Green curves: Lacking hormonal control – enzyme abundances are adapted to the fed (**a**) and fasted (**b**) state with full allosteric control. The value of the function γ controlling the ration between the phosphorylated and non-phosphorylated form of all enzymes is put to the constant value of 0.32, which holds at the reference case (= set point of the normal hepatocyte). Red curves: No allosteric regulation – enzyme abundances were adapted to the fed (**a**) and fasted (**b**) state, with full hormonal control. The saturation terms for allosteric effectors in the enzymatic rate equations were fixed to the values achieved in the reference state

coefficient, defined as the relative change of the target flux of interest (in our case the glucose exchange flux, v_{ex}) elicited by an infinitely small relative change in the flux (v_i) of a single reaction:

$$C_i = \frac{v_i}{v_{ex}} \frac{\partial v_{ex}}{\partial v_i} \quad (2)$$

According to the summation theorem, the flux control coefficients add up to unity. We calculated the control coefficients of the system for two extreme complementary physiological states, fasted hepatocytes at a hypoglycemic plasma glucose level of 4 mM and fed hepatocytes at a hyperglycemic plasma glucose level of 10 mM (Table 3).

Table 2 Average curve difference Δ

Scenario	Difference of diurnal HGP/HGU profile	
	Fasted	Fed
No change of enzyme abundance	0.25	1.54
No allosteric effectors	0.60	0.47
No interconversion	0.89	0.88

The control analysis revealed that the glucose exchange flux is under control of only seven enzymes (out of 32) exhibiting C_i values larger than 0.1 in at least one of the two physiological conditions studied (Table 3). Importantly, these key regulatory enzymes are known to change their abundance in response to altered external conditions. Moreover, each of these key regulatory enzymes is relevant in only one extreme physiological setting. In the fasted, hypoglycemic state, the glucose exchange flux is controlled by only two reactions catalyzed by pyruvate carboxylase and lactate transporter, which on the other hand exert no control in the fed, hyperglycemic state. Conversely, the hepatic glucose exchange flux in

Table 3 Control coefficients in the fasted and fed state. 0.00 means –0.005 < value <0.005

Enzyme	Fasted state		Fed state		Enzyme	Fasted state		Fed state	
	4 mM glucose [a]	10 mM glucose [b]	4 mM glucose [b]	10 mM glucose [a]		4 mM glucose [a]	10 mM glucose [b]	4 mM glucose [b]	10 mM glucose [a]
ALD	**0.00**	0.00	0.00	**0.00**	MDH_{mito}	**0.00**	0.00	0.00	**0.00**
EN	**0.00**	0.00	0.00	**0.00**	NDK_{UTP}	**0.00**	0.00	0.00	**0.00**
FBP1	**0.01**	–0.03	0.04	**0.00**	NDK_{GTP}	**0.00**	0.00	0.00	**0.00**
FBP2	**0.00**	–2.01	0.12	**–0.18**	$NDK_{mito(GTP)}$	**0.00**	0.00	0.00	**0.00**
GAPDH	**0.00**	0.00	0.00	**0.00**	PC	**0.66**	–0.25	0.60	**–0.01**
GK	**0.00**	2.87	–0.05	**0.56**	PEPCK	**0.00**	0.00	0.00	**0.00**
GlcT	**0.00**	0.27	0.04	**0.54**	$PEPCK_{mito}$	**0.00**	0.00	0.00	**0.00**
$GlcT_{ER}$	**0.00**	0.00	0.00	**0.00**	PEPT	**0.00**	0.00	0.00	**0.00**
GP	**–0.04**	0.11	–0.08	**0.00**	PFK1	**0.00**	0.22	0.00	**0.01**
G6P	**0.06**	–2.34	0.30	**–0.12**	PFK2	**0.00**	2.01	–0.12	**0.18**
GPI	**0.00**	0.00	0.00	**0.00**	PGK	**0.00**	0.00	0.00	**0.00**
$G6PT_{ER}$	**0.00**	0.00	0.00	**0.00**	PGM	**0.00**	0.00	0.00	**0.00**
GS	**0.04**	–0.15	0.06	**0.00**	PK	**–0.01**	0.28	–0.06	**0.01**
LacT	**0.28**	0.01	0.14	**0.00**	PyrT	**0.00**	0.00	0.00	**0.00**
LDH	**0.00**	0.00	0.00	**0.00**	PyrMalT	**0.00**	0.00	0.00	**0.00**
MDH	**0.00**	0.00	0.00	**0.00**	TPI	**0.00**	0.00	0.00	**0.00**

For the numerical calculation of the control coefficients the amounts of the catalyzing enzymes were varied by 5 % (0.5 % yielded similar results). The sum of all control coefficients is equal to unity (summation theorem) within the limit of numerical accuracy

[a] In bold font are the control coefficients for the physiological states (i.e. fasted protein profile and 4 mM plasma glucose and low glycogen store and fed protein profile and 10 mM blood glucose and high glycogen store)

[b] In normal font are the control coefficients for the two states with the respective other protein profile. The reference flux values are –64 μmol/g/h for fasted hepatocytes and 81 μmol/g/h for fed hepatocytes

ALD Aldolase, *EN* Enolase, *ER* Endoplasmic reticulum, *FBP1* Fructose-1,6-bisphosphatase, *FBP2* Fructose-2,6-bisphosphatase, *GAPDH* Glyceraldehyde 3-phosphate dehydrogenase, *GK* Glucokinase, *GlcT* Glucose transporter, *G6P* Glucose-6-phosphate phosphatase, *GPI* Glucose-6-phosphate isomerase, *G6PT* Glucose-6-phosphate transporter, *GTP* Guanosine triphosphate, *GS* Glycogen synthetase, *LacT* Lactate transporter, *LDH* Lactate dehydrogenase, *MDH* Malate dehydrogenase, *mito* Mitochondrion, *NDK* Nucleoside-diphosphate kinase, *PyrMalT* Pyruvate/malate antiporter, *PC* Pyruvate carboxylase, *PEPCK* Phosphoenolpyruvate carboxykinase, *PEPT* Phosphoenolpyruvate transporter, *PFK1/2* Phosphofructokinase-1/2, *PGK* Phosphoglycerate kinase, *PGM* Phosphoglycerate mutase, *PK* Pyruvate kinase, *PyrT* Pyruvate transporter, *TPI* Triose-phosphate isomerase, *UTP* Uridine triphosphate

the fed, hyperglycemic state is controlled by fructose-2,6-bisphosphatase (FBP2), glucokinase (GK), glucose transporter, glucose-6-phosphate phosphatase, and phosphofructokinase-2 (PFK2), which exert no control in the complementary physiological setting.

Figure 17 illustrates, for hepatocytes adapted to either fed or fasted conditions, the variation of the flux control coefficients of the relevant regulatory enzymes over one day. In the fed state, the variations are larger than in the fasted one and assume, in theory, infinitely large values at time points where the plasma glucose level approaches the set point at which the glucose exchange flux (appearing in the denominator of Equation 2) tends to zero during the switch from net glucose utilization to net glucose uptake and vice versa.

The flux control coefficient of a reaction is independent from the specific regulatory mechanism underlying the (small) change of the reaction rate. However, (small) relative changes of different kinetic parameters p_{ik} of the i-th enzyme may have largely different influence on the glucose exchange flux, which in the frame of MCA is expressed by the so-called response coefficient R_{ik}, as follows:

$$R_{ik} = \frac{p_{ik}}{v_{ex}}\frac{\partial v_{ex}}{\partial p_{ik}} = \left[\frac{v_i}{v_{ex}}\frac{\partial v_{ex}}{\partial v_i}\right]\left[\frac{p_{ik}}{v_i}\frac{\partial v_i}{\partial p_{ik}}\right] = C_i\,\pi_{ik} \qquad (3)$$

According to Equation 3, the response coefficient R_{ik} is given as product of the flux control coefficient C_i and the so-called π-elasticity coefficient π_{ik}

$$\pi_{ik} = \frac{p_k}{v_i}\frac{\partial v_i}{\partial p_k} \qquad (4)$$

quantifying the relative impact of the kinetic parameter p_{ik} on flux v_i [11]. Note that the π-elasticity coefficient π_{ik} has to be distinguished from the common elasticity coefficient

$$\varepsilon_{ik} = \frac{E_k}{v_i}\frac{\partial v_i}{\partial E_k} \qquad (5)$$

expressing the relative variation of the velocity v_i of the isolated enzyme caused by relative variations in the

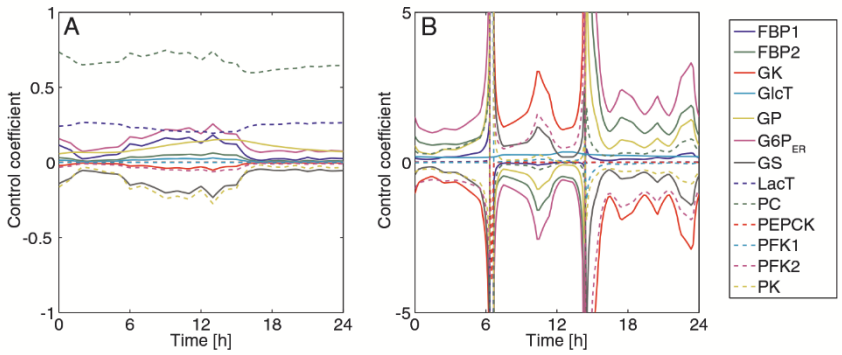

Fig. 17 Control coefficients of regulatory enzymes. The control coefficients of the key regulatory enzymes are shown for the diurnal glucose profiles of the fasted (**a**) and fed (**b**) liver (see Figs. 12 and 13)

concentration of effector E_k. Both coefficients are closely related because, in the rate equation, the dependence of the rate v_i from the effector E_k is usually a function of the term $X_k = \frac{E_k}{p_k}$ with p_k having the meaning of a binding constant of E_k. In this case, it follows immediately from Equation 4 and Equation 5 that $\varepsilon_{ik} = -\pi_{ik}$, i.e. a large value of the π-elasticity coefficient implies a large value of the common elasticity coefficient and vice versa. We thus used π-elasticities to characterize the controllability of key regulatory enzymes by their effectors.

π-Elasticity coefficients In our model, the enzyme-kinetic parameters p_{ik} fall into four categories: (1) the maximal enzyme activity (V_{max}) being a linear function of the enzyme abundance E_i, (2) the binding constants for reactants (substrates and products), (3) the binding constants for allosteric effectors, and (4) the signal function γ determining the phosphorylation state of the enzyme and being itself a non-linear multi-parametric function of the plasma level of insulin and glucagon (see Additional file 1 and Methods, Fig. 3). By definition, the π-elasticity coefficient of an enzyme with respect to the enzyme's abundance E_i is unity, i.e. the response coefficient with respect to E_i equals the flux control coefficient. For a better comparison of individual elasticity coefficients we calculated relative elasticity coefficients by relating the absolute value of an elasticity coefficient for a given enzyme to the sum of absolute values of all elasticity coefficients, i.e. the relative elasticity coefficients of an enzyme add up to unity. Figure 18 depicts the magnitude of the relative π-elasticity coefficients of the most important regulatory enzymes for the two complementary states, fasted hepatocytes at 4 mM plasma glucose and fed hepatocytes at 10 mM plasma glucose, considered in the previous sections. The complete list of elasticity coefficients is given in Additional Table S1 (Additional file 1).

Notably, with the exception of the glucose transporter, the kinetic effects caused by changes in the concentration of ligands and effectors prove to have a significant share in the total control of the key regulatory enzymes of hepatic glucose metabolism. For example, GK, which has a strong control of the glucose exchange flux in the fed state, exhibits a remarkable sensitivity against changes of its substrate glucose. GK activity is mainly regulated by a binding protein so that changes in the respective binding (Michaelis) constant have a large impact on the glucose exchange flux, especially at high plasma glucose levels. The physiological implications of the result of the control analysis are discussed below.

Discussion

General considerations

In this work, we used a detailed kinetic model of the hepatic glucose metabolism to investigate the contribution of the liver to the homeostasis of blood glucose under physiological and pathological conditions. We validated the model by comparing model simulations with a variety of experimental data on glucose exchange fluxes, metabolite concentrations and filling/emptying of the intrahepatic glycogen store. Our central goal was to dissect the relative importance of individual enzyme-regulatory mechanisms for the adequate response of the liver to varying plasma glucose levels. The general finding of this analysis is that changes in the hormone-induced phosphorylation state of key regulatory enzymes as well as changes in the concentration of allosteric effectors are at least of the same importance as changes in the enzyme abundance for the adjustment

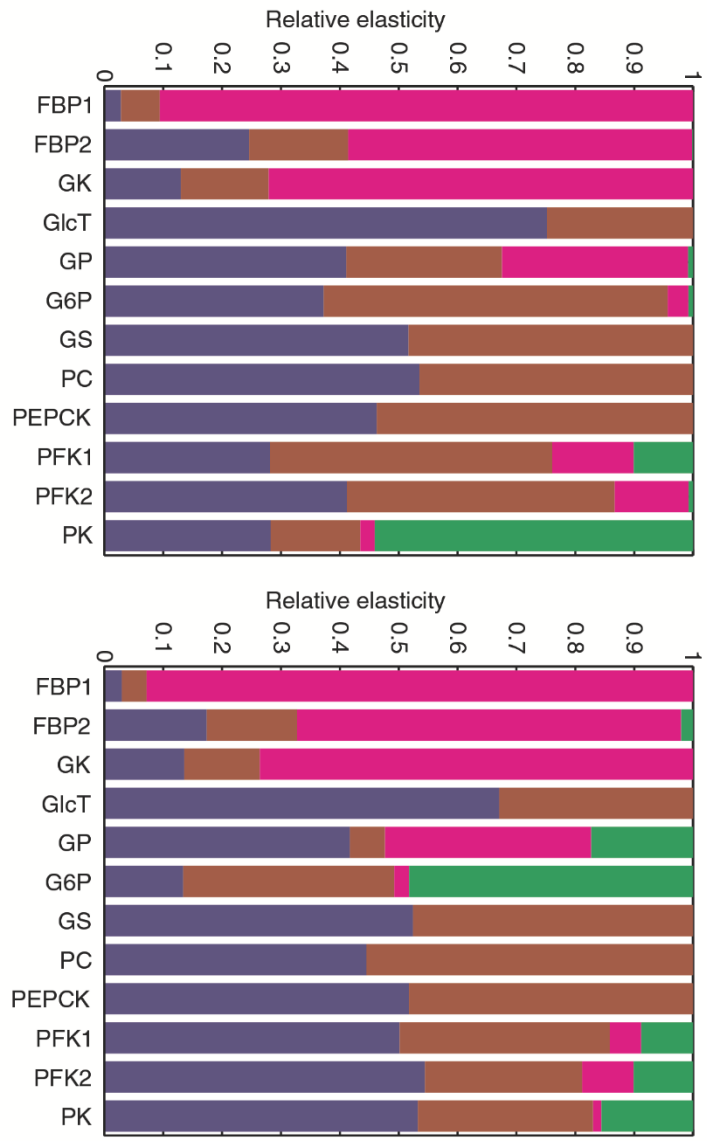

Fig. 18 Relative enzyme π-elasticity coefficients. The π-elasticity coefficients (defined in Equation 4) with respect to protein abundance (blue), reactants (brown), allosteric effectors (pink), and reversible phosphorylation (green) for fasted hepatocytes at 4 mM plasma glucose (**a**) and fed hepatocytes at 10 mM plasma glucose (**b**). The elasticity coefficients for each enzyme were normalized to their absolute sum. For the reference flux values see legend of Table 3

of the metabolic output to the metabolic demand defined by the external conditions. The strong influence of regulators beyond changes in protein abundance is presumably the main reason for the poor correlation usually observed between metabolic fluxes and abundance of the associated catalyzing enzymes.

The need for a concerted action of different modes of enzyme regulation can be reasoned by considering that even extremely high challenges to the adaptation of the cellular metabolism (e.g. during periods of starvation or overnutrition, exposure to toxic agents, inflammation or proliferation) are never constant over time but fluctuating, and thus cannot be met by just increasing or decreasing the abundance of enzymes. Therefore, it is fair to claim that any theoretical concept aiming at a better understanding of the regulation of metabolic networks has to take into account regulation of enzyme activities beyond the gene expression level.

Functional consequences of changes in protein abundance during the transition between fasted and fed nutritional states and in diabetes

First, we analyzed how changes in the abundance of key metabolic enzymes reported for the rat liver under fasted and fed nutritional conditions influence the metabolic output at various physiological conditions. Changes in the abundance of key regulatory enzymes of the glycolytic and gluconeogenic pathways were found to entail significant differences in the relationship between plasma glucose levels and the hepatic glucose exchange fluxes – the 'fasted' liver becomes a stronger glucose producer, whereas the 'fed' liver becomes a stronger glucose utilizer. This adaptation is achieved by changes in enzyme abundance and is of advantage for the homeostasis of plasma glucose as long as the anticipated physiological situation persists. It may, however, turn to a disadvantage if a sudden (unexpected) change occurs. A liver adapted to fasting for 1–2 days is less prepared to respond to a sudden strong increase of plasma glucose than a liver experiencing continuously elevated plasma glucose levels (Fig. 15). A well-known clinical complication occurring during refeeding in strongly malnourished patients is glucose intolerance [12], a type of metabolic dysregulation that typically occurs in early stages of diabetes type 2. In line with this observation, the relation between plasma glucose levels and hepatic glucose exchange rates predicted by the model are very similar in fasting conditions and diabetes (Fig. 10), i.e. gluconeogenesis is increased and the glycolytic capacity reduced.

Diurnal glucose production and utilization by the liver

The rates of HGP and HGU depend on the plasma level of nutrients and hormones that are permanently changing during the time course of the day. Taking measured diurnal plasma profiles as input, the kinetic model allows the simulation of diurnal changes of HGP and HGU and the filling state of glycogen (Figs. 12, 13 and 14). These simulations show that, in the fed nutritional state, the liver is able to switch between HGP and HGU. During the day time, the liver works predominantly as a glucose utilizer and during the night it is a glucose producer. Depending on the timing of food intake and the duration and intensity of physical exercise, the individual metabolic profiles may significantly differ from the generic profile used as input for our simulations. In contrast to the fed state, during long-term starvation, the liver is predicted to constantly work as a glucose producer to ensure that plasma glucose levels remain sufficiently high to fuel obligate glucose consumers such as the brain and erythrocytes. In the diabetic case, alterations in enzyme abundance of the glycolytic and gluconeogenetic enzymes together with impaired glucose hormone responses lead to a pathological shift towards gluconeogenesis (Fig. 11). The good concordance between the shift of the set point and the observed plasma glucose levels underpins the importance of the liver in determining plasma glucose levels. These fundamental differences in the basal metabolic states of the liver are also reflected in the filling states of glycogen. In the fed nutritional state, glycogen is degraded during HGP and replenished during HGU, glycogen store filling thereby varying between 50 % and 80 % of the total storage capacity. In the fasted state, the overall filling state of the glycogen store is much lower and varies between 10 % and 25 % only.

Assessing the relative importance of variable enzyme abundance and kinetic regulation of enzyme activities for the regulation of hepatic glucose exchange rates

To investigate the relative importance of the different regulation modes of enzyme activities we simulated the glucose exchange flux of the liver for different nutritional states (Fig. 16 and Table 2). In the fed state, the strongest regulatory influence is exerted by the changes of enzyme abundances, whereas in the fasted state, reversible phosphorylation has the largest impact. An important finding is that the short-term metabolic adaptation of the liver can be largely attributed to hormonal regulation as the glucose exchange fluxes become almost constant when we fix the phosphorylation state of the interconvertible enzymes. Nevertheless, the impact of allosteric regulation is substantial both in the fasted and the fed state, accounting for approximately 50 % of flux changes brought about by reversible phosphorylation in the fasted and fed state, respectively. It has to be noted that the role of allosteric regulation is certainly underestimated in our model as the concentration values of important cofactors (adenosine tri-/di-/monophosphate, nicotinamide adenine dinucleotide, and its reduced form NADH) and of allosterically important metabolites of the citric acid cycle (e.g. citrate inhibition of the phosphofructokinase) were not taken into account.

Metabolic control analysis (MCA)

To dissect the importance of individual enzymes for hepatic glucose exchange rates under different conditions we used the MCA concept. Calculation of flux control coefficients for the 'fed' and 'fasted' states revealed that enzymes carrying significant control are those showing significant changes of their abundance under different physiological conditions. Furthermore, the flux control is shared between different groups of enzymes in different conditions – enzymes being important in the glycolytic phase of liver metabolism are different from the ones central during gluconeogenesis (Table 3). Importantly, the control coefficients for the

glucose exchange flux exhibit significant fluctuation over one day and diverge (by definition) when the glucose exchange flux is zero (Fig. 17).

We also calculated π-elasticity coefficients to quantify the relative share of reversible phosphorylation and concentration changes of reactants and allosteric effectors in the regulation of individual enzymes of hepatic glucose metabolism (Fig. 18). This analysis revealed a large variability in the relative contribution of the three fast regulatory modes to the control of regulatory enzymes and hence the control of glucose exchange flux.

Direct experimental validation of the computed elasticities in vivo is unfeasible because this would require monitoring of the glucose exchange flux of the liver at clamped plasma levels of glucose and hormones in response to the gradual variation of an effector specifically influencing one kinetic parameter of the target enzyme under study. As a surrogate, we checked whether the predicted elasticities are concordant with observed changes in plasma glucose levels induced by targeting a single key regulatory enzyme either by drugs or genetic interventions.

GK

The maximal control that can be exerted by GK is low in the fasted-hypoglycemic state but becomes large in the fed-hyperglycemic state. Experimentally, glucosamine-induced inhibition of GK caused only marginal reduction of glucose uptake in euglycemia, whereas in hyperglycemia a significant reduction of the net hepatic glucose uptake of about 40 % was observed [13], confirming our simulation results. Clinically, the regulatory importance of GK in hyperglycemia is used to target this enzyme in diabetes type 2 [14, 15].

Glycogen phosphorylase (GP)

Torres et al. [16] investigated the effects of a GP inhibitor (GP_I) and metformin on hepatic glucose in presence of basal and four-fold increased levels of plasma glucagon in 18-h fasted conscious dogs. In euglycemic conditions, no change in the net hepatic glucose balance and plasma glucose was observed in the presence of GP_I. However, after glucagon stimulation, the presence of GP_I significantly diminished the glucose output. Both findings confirm the predicted relatively high control of the GP in hypoglycemic conditions as well as the large share of allosteric regulation of this enzyme.

Phosphofructokinase-1 (PFK1)

To our knowledge, a rate-limiting role of this enzyme in the liver is not reported. In several non-hepatic tissues, PFK1 exerts only insignificant control of glycolytic flux [17], which agrees with the predicted very small values of control coefficients in both the hypo- and hyperglycemic cases.

PFK2/FBP2

The enzyme PFK2/FBP2 exerts control of the glucose exchange flux mainly by changes in its phosphorylation state, whereas changes in the abundance of this enzyme have no impact of the glucose exchange flux. The reason for the latter is the bifuncionality of this enzyme – the phosphorylated enzyme (PFK2) acts as a kinase catalyzing the formation of fructose 2,6-bisphosphate ($Fru26P_2$), an efficient allosteric activator of PFK1, whereas the non-phosphorylated enzyme (FBP2) acts as a phosphatase catalyzing the degradation of $Fru26P_2$ to fructose 6-phosphate (Fru6P). These two opposite reactions create a futile cycle $Fru6P \rightarrow Fru26P_2 \rightarrow Fru6P$ that consumes one molecule of ATP. Obviously, unequal modulation of these opposite activities cannot be achieved by changes of protein abundance because any change in enzyme amount influences both activities to the same extent and thus leaves the net flux unchanged. However, reversible phosphorylation enhances FBP2-activity and in parallel diminishes the PFK2-activity of this enzyme, resulting in a high sensitivity of the glucose exchange flux to changes in the phosphorylation state of the PFK2/FBP2.

Phosphoenolpyruvate carboxykinase (PEPCK)

Metabolic control of liver gluconeogenesis was quantified in groups of mice with varying PEPCK protein content. Surprisingly, livers with a 90 % reduction in PEPCK content showed only a 40 % reduction in gluconeogenic flux, indicating a lower than expected capacity for PEPCK protein content to control gluconeogenesis (estimated control coefficient of about 0.18) [18]. This is in good agreement with our theoretical predictions. She et al. [18] concluded that the liver PEPCK functions more as an integrator of hepatic energy metabolism than as a determinant of gluconeogenesis.

Knowledge of the flux control exerted by a specific enzyme and of the regulatory mechanisms that contribute to its control is valuable information for the design of new drugs. For example, our analysis revealed that changing the protein abundance of the bifunctional enzyme PFK2/FBP2 should have no influence on the stationary glucose exchange flux of hepatocytes. Hence, drugs targeting this enzyme as non-competitive inhibitors can be expected to have little impact on the modulation of the hepatic glucose exchange flux. However, our analysis suggests that drugs specifically targeting only the phosphorylated enzyme (phosphatase) or non-phosphorylated enzyme (kinase) have a strong impact on the glucose exchange flux. These theoretical findings are supported by the fact that cancer cells express a specific phosphatase (TIGAR) that catalyzes the degradation of the glycolytic activator

$Fru26P_2$ in order to suppress glycolysis and to redirect the glucose flux through the oxidative pentose phosphate pathway. Flux control by PFK2/FBP2 may serve as a good example of why up or down regulation of the abundance of an enzyme does not necessarily imply corresponding flux changes as is assumed in numerous publications dealing with the potential metabolic consequences of varying protein abundances.

Conclusions

In summary, our work underlines the utility of kinetic modeling for the integration of experimental data from proteomics, metabolomics, and flux measurements, and for a wide range of physiological conditions into a unifying computational framework. Unraveling the role of different metabolic enzymes and different modes of enzyme regulation in the control of the hepatic glucose flux, the presented model may guide the design of novel drugs that reduce excessive glucose production of the liver in diabetic patients.

Additional files

Additional file 1: Supplementary information for this publication is available in Additional file 1. (PDF 952 kb)

Additional file 2: The SBML version of the model is supplied as Additional file 2. (XML 83 kb)

Abbreviations

FBP2: Fructose-2,6-bisphosphatase; $Fru26P_2$: Fructose 2,6-bisphosphate; Fru6P: Fructose 6-phosphate; GHT: Glucose hormone transfer; GK: Glucokinase; GP: Glycogen phosphorylase; GP_i: Glycogen phosphorylase inhibitor; GPI: Glucose-6-phosphate isomerase; GS: Glycogen synthetase; HGP: Hepatic glucose production; HGU: Hepatic glucose utilization; MCA: Metabolic control analysis; PEPCK: Phosphoenolpyruvate carboxykinase; PEPT: Phosphoenolpyruvate transporter; PFK1/2: Phosphofructokinase-1/2.

Competing interests

The authors declare that they have no competing interests.

Authors' contributions

NB, HH, SB developed the concept and wrote the manuscript. NB developed the model. SB performed the calculations. All authors read and approved the final manuscript.

Acknowledgements

Sascha Bulik was funded by the German Systems Biology Program "Virtual Liver", grant no. 0315741, "LiSyM", grant no. 31 L0057 and the e:Bio (Module I) project "HepatomaSys", grant no. 0316172A, all sponsored by the German Federal Ministry of Education and Research (BMBF).

Received: 16 December 2015 Accepted: 16 February 2016
Published online: 02 March 2016

References

1. Hopgood MF, Ballard FJ. Synthesis and degradation of phosphoenolpyruvate carboxylase in rat liver and adipose tissue. Changes during a starvation-re-feeding cycle. Biochem J. 1973;134(2):445–53.
2. Weinberg MB, Utter MF. Effect of streptozotocin-induced diabetes mellitus on the turnover of rat liver pyruvate carboxylase and pyruvate dehydrogenase. Biochem J. 1980;188(3):601–8.
3. ter Kuile BH, Westerhoff HV. Transcriptome meets metabolome: hierarchical and metabolic regulation of the glycolytic pathway. FEBS Lett. 2001;500(3):169–71.
4. Vogt AM, Poolman M, Ackermann C, Yildiz M, Schoels W, Fell DA, et al. Regulation of glycolytic flux in ischemic preconditioning. A study employing metabolic control analysis. J Biol Chem. 2002;277(27):24411–9.
5. Bruggeman FJ, de Haan J, Hardin H, Bouwman J, Rossell S, van Eunen K, et al. Time-dependent hierarchical regulation analysis: deciphering cellular adaptation. Syst Biol (Stevenage). 2006;153(5):318–22.
6. Konig M, Bulik S, Holzhutter HG. Quantifying the contribution of the liver to glucose homeostasis: a detailed kinetic model of human hepatic glucose metabolism. PLoS Comput Biol. 2012;8(6):e1002577.
7. Niewoehner CB, Nuttall FQ. Relationship of hepatic glucose uptake to intrahepatic glucose concentration in fasted rats after glucose load. Diabetes. 1988;37(11):1559–66.
8. Miethke H, Wittig B, Nath A, Zierz S, Jungermann K. Metabolic zonation in liver of diabetic rats. Zonal distribution of phosphoenolpyruvate carboxykinase, pyruvate kinase, glucose-6-phosphatase and succinate dehydrogenase. Biol Chem Hoppe Seyler. 1985;366(5):493–501.
9. Rasch R. Control of blood glucose levels in the streptozotocin diabetic rat using a long-acting heat-treated insulin. Diabetologia. 1979;16(3):185–90.
10. Burns JA, Cornishbowden A, Groen AK, Heinrich R, Kacser H, Porteous JW, et al. Control analysis of metabolic systems. Trends Biochem Sci. 1985;10(1):16.
11. Heinrich R, Rapoport TA. A linear steady-state treatment of enzymatic chains. General properties, control and effector strength. Eur J Biochem. 1974;42(1):89–95.
12. Obeid OA, Hachem DH, Ayoub JJ. Refeeding and metabolic syndromes: two sides of the same coin. Nutr Diabetes. 2014;4:e120.
13. Barzilai N, Hawkins M, Angelov I, Hu M, Rossetti L. Glucosamine-induced inhibition of liver glucokinase impairs the ability of hyperglycemia to suppress endogenous glucose production. Diabetes. 1996;45(10):1329–35.
14. Agius L. Targeting hepatic glucokinase in type 2 diabetes: weighing the benefits and risks. Diabetes. 2009;58(1):18–20.
15. Grimsby J, Sarabu R, Corbett WL, Haynes NE, Bizzarro FT, Coffey JW, et al. Allosteric activators of glucokinase: potential role in diabetes therapy. Science. 2003;301(5631):370–3.
16. Torres TP, Sasaki N, Donahue EP, Lacy B, Printz RL, Cherrington AD, et al. Impact of a glycogen phosphorylase inhibitor and metformin on basal and glucagon-stimulated hepatic glucose flux in conscious dogs. J Pharmacol Exp Ther. 2011;337(3):610–20.
17. Urbano AM, Gillham H, Groner Y, Brindle KM. Effects of overexpression of the liver subunit of 6-phosphofructo-1-kinase on the metabolism of a cultured mammalian cell line. Biochem J. 2000;352(Pt 3):921–7.
18. She P, Shiota M, Shelton KD, Chalkley R, Postic C, Magnuson MA. Phosphoenolpyruvate carboxykinase is necessary for the integration of hepatic energy metabolism. Mol Cell Biol. 2000;20(17):6508–17.
19. la Fleur SE, Kalsbeek A, Wortel J, Fekkes ML, Buijs RM. A daily rhythm in glucose tolerance: a role for the suprachiasmatic nucleus. Diabetes. 2001;50(6):1237–43.
20. Frangioudakis G, Gyte AC, Loxham SJ, Poucher SM. The intravenous glucose tolerance test in cannulated Wistar rats: a robust method for the in vivo assessment of glucose-stimulated insulin secretion. J Pharmacol Toxicol Methods. 2008;57(2):106–13.
21. Hara E, Saito M. Diurnal changes in plasma glucose and insulin responses to oral glucose load in rats. Am J Physiol. 1980;238(5):E463–6.
22. Balks HJ, Jungermann K. Regulation of peripheral insulin/glucagon levels by rat liver. Eur J Biochem. 1984;141(3):645–50.
23. Diaz B, Blazquez E. Effect of pinealectomy on plasma glucose, insulin and glucagon levels in the rat. Horm Metab Res. 1986;18(4):225–9.
24. Patel DG. Lack of glucagon response to hypoglycemia in long-term experimental diabetic rats. Diabetes. 1983;32(1):55–60.
25. Wan CK, Giacca A, Matsuhisa M, El-Bahrani B, Lam L, Rodgers C, et al. Increased responses of glucagon and glucose production to hypoglycemia with intraperitoneal versus subcutaneous insulin treatment. Metabolism. 2000;49(8):984–9.
26. Zhou H, Tran PO, Yang S, Zhang T, LeRoy E, Oseid E, et al. Regulation of alpha-cell function by the beta-cell during hypoglycemia in Wistar rats: the 'switch-off' hypothesis. Diabetes. 2004;53(6):1482–7.
27. Feliu JE, Hue L, Hers HG. Hormonal control of pyruvate kinase activity and of gluconeogenesis in isolated hepatocytes. Proc Natl Acad Sci U S A. 1976;73(8):2762–6.
28. Claus TH, El-Maghrabi MR, Pilkis SJ. Modulation of the phosphorylation state of rat liver pyruvate kinase by allosteric effectors and insulin. J Biol Chem. 1979;254(16):7855–64.

29. Pilkis S, Schlumpf J, Pilkis J, Claus TH. Regulation of phosphofructokinase activity by glucagon in isolated rat hepatocytes. Biochem Biophys Res Commun. 1979;88(3):960–7.
30. Schudt C. Regulation of glycogen synthesis in rat-hepatocyte cultures by glucose, insulin and glucocorticoids. Eur J Biochem. 1979;97(1):155–60.
31. El-Maghrabi MR, Claus TH, Pilkis J, Fox E, Pilkis SJ. Regulation of rat liver fructose 2,6-bisphosphatase. J Biol Chem. 1982;257(13):7603–7.
32. Bartrons R, Hue L, Van Schaftingen E, Hers HG. Hormonal control of fructose 2,6-bisphosphate concentration in isolated rat hepatocytes. Biochem J. 1983;214(3):829–37.
33. Hartmann H, Probst I, Jungermann K, Creutzfeldt W. Inhibition of glycogenolysis and glycogen phosphorylase by insulin and proinsulin in rat hepatocyte cultures. Diabetes. 1987;36(5):551–5.
34. Syed NA, Khandelwal RL. Reciprocal regulation of glycogen phosphorylase and glycogen synthase by insulin involving phosphatidylinositol-3 kinase and protein phosphatase-1 in HepG2 cells. Mol Cell Biochem. 2000;211(1–2):123–36.
35. Bahnak BR, Gold AH. Effects of alloxan diabetes on the turnover of rat liver glycogen synthase. Comparison with liver phosphorylase. J Biol Chem. 1982; 257(15):8775–80.
36. Ballard FJ, Hopgood MF. Phosphopyruvate carboxylase induction by L-tryptophan. Effects on synthesis and degradation of the enzyme. Biochem J. 1973;136(2):259–64.
37. Bock KW, Frohling W, Remmer H. Influence of fasting and hemin on microsomal cytochromes and enzymes. Biochem Pharmacol. 1973;22(13):1557–64.
38. Chang AY, Schneider DI. Hepatic enzyme activities in streptozotocin-diabetic rats before and after insulin treatment. Diabetes. 1971;20(2):71–7.
39. Cladaras C, Cottam GL. Turnover of liver pyruvate kinase. Arch Biochem Biophys. 1980;200(2):426–33.
40. Colosia AD, Marker AJ, Lange AJ, el-Maghrabi MR, Granner DK, Tauler A, et al. Induction of rat liver 6-phosphofructo-2-kinase/fructose-2,6-bisphosphatase mRNA by refeeding and insulin. J Biol Chem. 1988;263(35):18669–77.
41. Crepin KM, Darville MI, Hue L, Rousseau GG. Starvation or diabetes decreases the content but not the mRNA of 6-phosphofructo-2-kinase in rat liver. FEBS Lett. 1988;227(2):136–40.
42. Dipietro DL, Weinhouse S. Hepatic glucokinase in the fed, fasted, and alloxan-diabetic rat. J Biol Chem. 1960;235:2542–5.
43. Donofrio JC, Thompson RS, Reinhart GD, Veneziale CM. Quantification of liver and kidney phosphofructokinase by radioimmunoassay in fed, starved and alloxan-diabetic rats. Biochem J. 1984;224(2):541–7.
44. Dunaway Jr GA, Weber G. Effects of hormonal and nutritional changes on rates of synthesis and degradation of hepatic phosphofructokinase isozymes. Arch Biochem Biophys. 1974;162(2):629–37.
45. Gannon MC, Nuttall FQ. Effect of feeding, fasting, and diabetes on liver glycogen synthase activity, protein, and mRNA in rats. Diabetologia. 1997;40(7):758–63.
46. Giffin BF, Drake RL, Morris RE, Cardell RR. Hepatic lobular patterns of phosphoenolpyruvate carboxykinase, glycogen synthase, and glycogen phosphorylase in fasted and fed rats. J Histochem Cytochem. 1993;41(12):1849–62.
47. Miralpeix M, Carballo E, Bartrons R, Crepin K, Hue L, Rousseau GG. Oral administration of vanadate to diabetic rats restores liver 6-phosphofructo-2-kinase content and mRNA. Diabetologia. 1992;35(3):243–8.
48. Neely P, El-Maghrabi MR, Pilkis SJ, Claus TH. Effect of diabetes, insulin, starvation, and refeeding on the level of rat hepatic fructose 2,6-bisphosphate. Diabetes. 1981;30(12):1062–4.
49. Raju J, Gupta D, Rao AR, Baquer NZ. Effect of antidiabetic compounds on glyoxalase I activity in experimental diabetic rat liver. Indian J Exp Biol. 1999; 37(2):193–5.
50. Slieker LJ, Sundell KL, Heath WF, Osborne HE, Bue J, Manetta J, et al. Glucose transporter levels in tissues of spontaneously diabetic Zucker fa/fa rat (ZDF/drt) and viable yellow mouse (Avy/a). Diabetes. 1992;41(2):187–93.
51. Thorens B, Flier JS, Lodish HF, Kahn BB. Differential regulation of two glucose transporters in rat liver by fasting and refeeding and by diabetes and insulin treatment. Diabetes. 1990;39(6):712–9.
52. Van Schaftingen E, Hers HG. The role of fructose 2,6-bisphosphate in the long-term control of phosphofructokinase in rat liver. Biochem Biophys Res Commun. 1983;113(2):548–54.
53. Zalitis JG, Pitot HC. The synthesis and degradation of rat liver and kidney fructose bisphosphatase in vivo. Arch Biochem Biophys. 1979;194(2):620–31.
54. Manna P, Jain SK. Decreased hepatic phosphatidylinositol-3,4,5-triphosphate (PIP3) levels and impaired glucose homeostasis in type 1 and type 2 diabetic rats. Cell Physiol Biochem. 2012;30(6):1363–70.
55. Exton JH, Park CR. Control of gluconeogenesis in the perfused liver of normal and adrenalectomized rats. J Biol Chem. 1965;240:955–7.
56. Exton JH, Park CR. Control of gluconeogenesis in liver. II. Effects of glucagon, catecholamines, and adenosine 3',5'-monophosphate on gluconeogenesis in the perfused rat liver. J Biol Chem. 1968;243(16):4189–96.
57. Scholz R, Hansen W, Thurman RG. Interaction of mixed-function oxidation with biosynthetic processes. 1. Inhibition of gluconeogenesis by aminopyrine in perfused rat liver. Eur J Biochem. 1973;38(1):64–72.
58. Holness MJ, Palmer TN, Worrall EB, Sugden MC. Hepatic carbon flux after re-feeding in the glycogen-storage-disease (gsd/gsd) rat. Biochem J. 1987; 248(3):969–72.
59. Holness MJ, MacLennan PA, Palmer TN, Sugden MC. The disposition of carbohydrate between glycogenesis, lipogenesis and oxidation in liver during the starved-to-fed transition. Biochem J. 1988;252(2):325–30.
60. Friedmann B, Goodman Jr EH, Weinhouse S. Effects of glucose feeding, cortisol, and insulin on liver glycogen synthesis in the rat. Endocrinology. 1967;81(3):486–96.
61. Aw TY, Andersson BS, Jones DP. Mitochondrial transmembrane ion distribution during anoxia. Am J Physiol. 1987;252(4 Pt 1):C356–61.
62. Bellamy D. The endogenous citric acid-cycle intermediates and amino acids of mitochondria. Biochem J. 1962;82:218–24.
63. Gardner LB, Liu Z, Barrett EJ. The role of glucose-6-phosphatase in the action of insulin on hepatic glucose production in the rat. Diabetes. 1993;42(11):1614–20.
64. MacDonald MJ, Fahien LA, Buss JD, Hasan NM, Fallon MJ, Kendrick MA. Citrate oscillates in liver and pancreatic beta cell mitochondria and in INS-1 insulinoma cells. J Biol Chem. 2003;278(51):51894–900.
65. Parrilla R. The effect of starvation in the rat on metabolite concentrations in blood, liver and skeletal muscle. Pflugers Arch. 1978;374(1):9–14.
66. Siess EA, Brocks DG, Wieland OH. Distribution of metabolites between the cytosolic and mitochondrial compartments of hepatocytes isolated from fed rats. Hoppe Seylers Z Physiol Chem. 1978;359(7):785–98.
67. Siess EA, Kientsch-Engel RI, Wieland OH. Concentration of free oxaloacetate in the mitochondrial compartment of isolated liver cells. Biochem J. 1984; 218(1):171–6.
68. Tischler ME, Hecht P, Williamson JR. Determination of mitochondrial/cytosolic metabolite gradients in isolated rat liver cells by cell disruption. Arch Biochem Biophys. 1977;181(1):278–93.
69. Veech RL, Veloso D, Mehlman MA. Thiamin deficiency: liver metabolite levels and redox and phosphorylation states in thiamin-deficient rats. J Nutr. 1973;103(2):267–72.
70. Bolender RP, Weibel ER. A morphometric study of the removal of phenobarbital-induced membranes from hepatocytes after cessation of treatment. J Cell Biol. 1973;56(3):746–61.
71. La Fleur SE, Kalsbeek A, Wortel J, Buijs RM. A suprachiasmatic nucleus generated rhythm in basal glucose concentrations. J Neuroendocrinol. 1999; 11(8):643–52.
72. Van de Werve G, Sestoft L, Folke M, Kristensen LO. The onset of liver glycogen synthesis in fasted-refed rats. Effects of streptozocin diabetes and of peripheral insulin replacement. Diabetes. 1984;33(10):944–9.
73. Ferrannini E, Lanfranchi A, Rohner-Jeanrenaud F, Manfredini G, Van de Werve G. Influence of long-term diabetes on liver glycogen metabolism in the rat. Metabolism. 1990;39(10):1082–8.

2.2 *A multiscale modelling approach to assess the impact of metabolic zonation and microperfusion on the hepatic carbohydrate metabolism* [40]

Dieses Kapitel basiert auf [40] (DOI: 10.1371/journal.pcbi.1006005).

Einleitung: Im vorigen Kapitel wurde für den Glukosestoffwechsel gezeigt, wie die metabolische Kapazität und die Kurzzeitregulation der Enzyme die metabolische Leistung der Leber bestimmt. Bei dieser Analyse wurde jedoch nur das metabolische Netzwerk betrachtet, ohne die einzigartige Feinstruktur der Leber zu berücksichtigen. Die Leber ist aus einer Vielzahl strukturell gleichartiger funktioneller Einheiten, den Leberazini, aufgebaut. Ein Leberazinus besteht aus Hepatozyten entlang eines zentralen Blutgefäßes (Sinusoid), mit fenestriertem Epithel, das den Blutraum vom Interstitzialraum abgrenzt. Der lineare Aufbau des Sinusoids führt dabei dazu, dass sich die Plasmametabolitkonzentrationen entlang des Sinusoids stark verändern und dass die metabolische Ausstattung von Hepatozyten von ihrer Position innerhalb des Sinusoids abhängt. Diese Heterogenität von Leberzellen entlang eines Sinusoids wird als Leberzonierung bezeichnet. Die metabolische Leistungsfähigkeit der Leber hängt außerdem möglicherweise vom Stoffaustausch zwischen Hepatozyten und Blut und damit von der Feinstruktur der Leber ab. Je größer die Fenestrierung und je kleiner der Disse-Raum ist, desto schneller ist der Stoffaustausch zwischen Leber und Blut und umso direkter kann die Leber auf Veränderungen in der Zusammensetzung der Plasmametabolite reagieren.

Fragestellung: Das Ziel dieser Arbeit war es, den Einfluss der Feinstruktur, der metabolischen Zonierung und des Blutflusses auf den hepatischen Glukosestoffwechsel zu untersuchen.

Methode: Das kinetische Modell des hepatischen Glukosestoffwechsels wurde in ein Modell des Leberazinus eingebettet, das die hepatische Feinstruktur und die metabolische Zonierung berücksichtigt. Das Modell beschreibt neben dem hepatischen Glukose- und Glykogenmetabolismus in den einzelnen Hepatozyten den sinusoidalen Blutfluss und den Stoffaustausch zwischen Kapillare, Disse-Raum und Hepatozyten.

Resultat: Als erstes wurde der metabolische Phänotyp der Hepatozyten in den verschiedenen Leberzonen untersucht. Es wurde gezeigt, dass periportale Hepatozyten eine höhere Kapazität für Glukoneogenese haben, währen Hepatozyten der zentralen Zone eher einem glykolytischen Phänotyp entsprechen. Danach wurde der Blutfluss und Stoffaustausch innerhalb eines Azinus simuliert und der Einfluss der Varianz der strukturellen Parameter auf den Glukoseaustausch untersucht. Die Abhängigkeit der arterio-venösen Glukosedifferenz von der portalen Glukosekonzentration zeigte, dass die physiologischen Varianzen in den strukturellen und metabolischen Parametern zu Veränderungen von bis zu 25% in der arterio-venösen Differenz von Glukose führen können. Durch Sensitivitätsanalyse wurde dann gezeigt, dass es keine klare Hierarchie in der regulatorischen Bedeutung der Veränderungen der strukturellen Parameter, metabolischen Enzymkapazitäten und der Zonierung gibt, sondern dass alle ähnlich wichtig für die Leberfunktion sind. Zum Schluss wurde noch mit Hilfe von Computertomographie- (CT)-basierten Perfusionsmessungen ein Funktiogramm der Leber erstellt.

Diskusion: Die kleinste funktionale Einheit der Leber ist die sinusoidale Einheit (STU = *sinusoidal tissue unit*) bestehend aus einem zentralem Blutgefäß umgeben von linear aufgereihten Hepatozyten. Da die metabolische Ausstattung der Hepatozyten sich abhängig von ihrer Position im Sinusoid verändert (metabolische Zonierung), haben wir als erstes den

funktionalen Effekt von Veränderungen in den Proteinmengen der Schlüsselenzyme in den verschiedenen Zonen der Leber auf den Glukoseaustausch untersucht.

Unsere Analyse zeigt, dass die Reaktion der Hepatozyten in der jeweiligen Zone im Vergleich zur Gesamtleber systematisch verschoben ist. Dabei wird der periportale Hepatozyt zu einem sehr starken Glukoseproduzenten, während der perizentrale Hepatozyt vermehrt Glukose aufnimmt. Bei physiologischen Blutzuckerspiegeln kann das zu einem intrasinusoidalen Zyklus führen, bei dem ATP alleine dadurch verbraucht wird, dass Glukose in den periportalen Hepatozyten erzeugt wird, die dann in den perizentralen Heaptozyten wieder verbraucht wird. Weiterhin gibt es in der Leber einen starken Sauerstoffgradienten von der portalen zur zentralen Zone. Durch Verbrauch innerhalb des Sinusoids reduziert sich der pO_2 von ~90 mmHg in der portalen Zone auf ~40 mmHg in der zentralen Zone [44, 45]. Der Sättigungsgrad der Atmungskette reduziert sich dabei allerdings lediglich von 97% auf 93%, so dass ein Ausfall der oxidativen Phosphorylierung ausgeschlossen werden kann. Es ist eher anzunehmen, dass die in der periportalen Zone vorliegende Kapazität zur Glukoneogenese den normalen physiologischen Bedarf übersteigt, und die perizentrale Zone ihrerseits dafür sorgt, dass der Blutzuckerspiegel nicht zu hoch ansteigt. Die portale Zone hat also eher die Aufgabe die Hypoglykämie zu verhindern, während die perizentrale Zone der Hyperglykämie entgegenwirkt. Damit hält die Leber den Blutzuckerspiegel in engen physiologischen Grenzen. Ähnlich wie bei den intrazellulären Substratzyklen ist unter normalen physiologischen Bedingungen genug Energie vorhanden, um sich diese Verschwendung zu leisten. Dafür ermöglicht die hohe Reservekapazität der Leber bei stark abfallenden Glukosespiegel, beispielsweise bei starker Anstrengung, die systemische Versorgung mit Glukose sicherzustellen.

Mithilfe des Modells kann auch die Rolle der Leber als Glukosehomöostat des Körpers sehr anschaulich gezeigt werden. Die durchschnittliche STU transformiert eine Glukose-konzentration zwischen 3-15 mM in der Pfortader in eine Glukosekonzentration von 6-10 mM in der Zentralvene. Aufgrund der starken Nichtlinearität der beteiligten Prozesse ist die Glukosekonzentration in der Zentralvene dabei keine monotone Funktion der Glukosekonzentration in der Pfortader. Bei sehr niedrigen Glukosewerten in der Pfortader ist die Glukoneogenese der Leber so hoch, dass hyper-physiologische Glukosekonzentrationen in der Zentralvene auftreten, um damit bei Glukosemangel die systemische Glukoseversorgung aufrecht zu erhalten. Die Stärke dieses Effekts hängt allerdings sehr von der Länge der STU und ihrer strukturellen Eigenschaften ab.

Um den Einfluss der strukturellen Parameter abzuschätzen und mit dem Einfluss der enzymatischen Parameter zu vergleichen, wurde die metabolische Kontrollanalyse verwendet. Das führte zu zwei wichtigen Erkenntnissen. Erstens sind die strukturellen Parameter ähnlich wichtig wie die metabolischen Parameter. Das heißt, dass die strukturellen Eigenschaften der Leber einen vergleichbar großen Einfluss auf die Leberleistung haben wie die enzymatische Ausstattung. Zweitens, bleibt der Einfluss der verschiedenen Parameter auf die Leberfunktion stark vom betrachteten metabolischen Zustand abhängig. Z.B. hat die Länge des Sinusoids einen großen Einfluss auf den Glukoseaustausch bei hohen (>10 mM) und niedrigen (<5 mM) Plasmaglukosekonzentrationen, ist im mittleren physiologischen Bereich aber von untergeordneter Bedeutung. Ähnlich verhält es sich mit den metabolischen Enzymen, wo z.B. die PC einen großen Einfluss auf den Glukoseaustausch der STU bei niedrigen Plasmaglukosewerten hat, bei hohen Glukosewerten aber ohne regulatorischen Einfluss ist.

Das hier vorgestellte Modell der STU ermöglicht die Berechnung der Gesamtleberfunktion aus strukturellen Parametern (die aus Leberbiopsien gewonnen werden können) zusammen mit regionalen Perfusionsmessungen der Leber (die man aus einem Perfusions-CT bekommt). Eine Anwendung auf reale Patientendaten zeigt, dass die funktionalen Unterschiede von verschiedenen Regionen innerhalb der Leber kleiner sind als die Unterschiede in der Perfusion der verschiedenen Regionen. Trotzdem liegt der Unterschied zwischen verschiedenen Regionen immer noch zwischen 25-42%. Das heißt, dass die Leber auf Gewebeebene zwar in der Lage ist, Heterogenitäten teilweise auszugleichen, sie aber weit davon entfernt ist, ein funktional homogenes Organ zu sein.

PLOS COMPUTATIONAL BIOLOGY

RESEARCH ARTICLE

A multiscale modelling approach to assess the impact of metabolic zonation and microperfusion on the hepatic carbohydrate metabolism

Nikolaus Berndt[1]*, Marius Stefan Horger[2], Sascha Bulik[1,3☯], Hermann-Georg Holzhütter[1☯]

1 Computational Biochemistry Group, Institute of Biochemistry, Charite—University Medicine Berlin, Charitéplatz 1, Berlin, **2** Department of Diagnostic and Interventional Radiology, Eberhard-Karls-University Tubingen, Tuebingen, Germany, **3** German Federal Institute for Risk Assessment, Junior Research Group Supply-Chain-Models, Max-Dohrn-Straße 8–10, Berlin, Germany

☯ These authors contributed equally to this work.
* nikolaus.berndt@charite.de

Citation: Berndt N, Horger MS, Bulik S, Holzhütter H-G (2018) A multiscale modelling approach to assess the impact of metabolic zonation and microperfusion on the hepatic carbohydrate metabolism. PLoS Comput Biol 14(2): e1006005. https://doi.org/10.1371/journal.pcbi.1006005

Editor: Daniel A. Beard, University of Michigan, UNITED STATES

Received: November 20, 2017

Accepted: January 26, 2018

Published: February 15, 2018

Data Availability Statement: All relevant data are within the paper and its Supporting Information files.

Funding: SB was funded by the German Systems Biology Program "Virtual Liver", grant no. 0315741, "LiSyM", grant no. 31 L0057 and the e:Bio (Module I) project "HepatomaSys", grant no. 0316172A, all sponsored by the German Federal Ministry of Education and Research (BMBF). The funders had no role in study design, data collection

Abstract

The capacity of the liver to convert the metabolic input received from the incoming portal and arterial blood into the metabolic output of the outgoing venous blood has three major determinants: The intra-hepatic blood flow, the transport of metabolites between blood vessels (sinusoids) and hepatocytes and the metabolic capacity of hepatocytes. These determinants are not constant across the organ: Even in the normal organ, but much more pronounced in the fibrotic and cirrhotic liver, regional variability of the capillary blood pressure, tissue architecture and the expression level of metabolic enzymes (zonation) have been reported. Understanding how this variability may affect the regional metabolic capacity of the liver is important for the interpretation of functional liver tests and planning of pharmacological and surgical interventions. Here we present a mathematical model of the sinusoidal tissue unit (STU) that is composed of a single sinusoid surrounded by the space of Disse and a monolayer of hepatocytes. The total metabolic output of the liver (arterio-venous glucose difference) is obtained by integration across the metabolic output of a representative number of STUs. Application of the model to the hepatic glucose metabolism provided the following insights: (i) At portal glucose concentrations between 6–8 mM, an intra-sinusoidal glucose cycle may occur which is constituted by glucose producing periportal hepatocytes and glucose consuming pericentral hepatocytes, (ii) Regional variability of hepatic blood flow is higher than the corresponding regional variability of the metabolic output, (iii) a spatially resolved metabolic functiogram of the liver is constructed. Variations of tissue parameters are equally important as variations of enzyme activities for the control of the arterio-venous glucose difference.

and analysis, decision to publish, or preparation of the manuscript.

Competing interests: The authors declare that they have no competing interests.

Author summary

Glucose homeostasis is one of the central liver functions. The liver extracts glucose from the blood when plasma glucose levels are high and produces glucose when plasma glucose levels are low. To fulfill this function the liver is organized in smallest functional units, the sinusoidal tissue units (STUs). These STUs consist of a single sinusoid surrounded by linear arranged hepatocytes. Liver zonation describes the spatial separation of metabolic pathways along the STUs. As blood flows through the sinusoid the plasma nutrient and hormone composition changes and in conjunction with the heterogeneous endowment of metabolic enzymes this leads to big differences in the metabolic performance of hepatocytes depending on their position within the sinusoid. This makes liver zonation and blood flow two central determinants for the functional output of the liver. In this work we present a tissue model of hepatic carbohydrate metabolism that combines liver zonation and microperfusion within the STU. We show that structural properties, enzymatic properties and regional bloodflow are equally important for the understanding of liver functionality. With our work we provide a true multi-scale model bridging the scale from the cellular to the tissue level.

Introduction

In mammals, the liver is the central organ for the control of plasma glucose. To restrict variations of plasma glucose to the range between 3 mM (after exercise or moderate fast [1]) and 10 mM (after meal ingestion, [2]), liver metabolism may switch between glucose production (gluconeogenesis and glycogenolysis) and glucose consumption. At the cellular level, this switch is accomplished by the interplay of multiple regulatory mechanisms including long term alterations in the abundance of metabolic enzymes, alterations in kinetic properties of key regulatory enzymes due to external hormonal regulation, alterations in enzymatic activity in response to internal substrate availability and allosteric regulation.

The majority of metabolic functions of the liver are confined to hepatocytes. These cells form tightly connected cell layers that are separated from the liver capillaries (sinusoids) by the space of Disse [3]. The transport of plasma metabolites from the lumen of sinusoids through the space of Disse into the cytosol of hepatocytes and vice versa connects the cellular metabolism with the blood plasma. Thus, blood flow is a crucial determinant of the liver's overall metabolic output [4].

The importance to include blood perfusion and the tissue architecture into a quantitative estimate of liver metabolism has been stressed in an earlier modeling work of Chalhoub und Belovich [5]. However, this simple truth is routinely neglected in experimental and modeling studies where the metabolic capacity of the hepatocyte (assessed in cell cultures) is wrongly equated with the metabolic capacity of the organ.

To better understand the role of blood perfusion and tissue structure for the metabolic performance of the liver, we have developed a multi-scale tissue model of the so-called sinusoidal tissue unit (STU). We define a single STU by an ensemble of a single sinusoid, the accompanying space of Disse and the adjacent layers of hepatocytes. The sinusoids form the microvascular bed linking the hepatic portal vein and artery with the hepatic central vein. The exchange of substances between the blood, the space of Disse and the hepatocytes leads to a progressive alteration of plasma composition along the STU, continuously changing from the portal region (where the blood from the liver artery and portal vein mix) to the central region connected to the liver vein.

Importantly, hepatocytes at different spatial positions of the STU display a differential endowment with metabolic enzymes. Higher amounts of the glycolytic enzymes glucokinase (GK), PFK2/FBP2, phosphofructokinase 1 (PFK1), pyruvate kinase (PK) are found in the pericentral region, while higher enzyme levels of the gluconeogenetic enzymes glucose-6-phosphate phosphatase (G6PP), fructose1,6bisphosphatase (FBP1), mitochondrial pyruvate carboxylase (PCmito) and PEPCK are found in the periportal region [6–21]. Consistent with such a heterogeneous distribution of enzyme activities, the glycogen content of periportal and percentral hepatocytes may largely differ [22]. These findings point to a zonated carbohydrate metabolism in the liver: Periportal hepatocytes are more engaged in glucose production, while pericentral hepatocytes are generally more engaged in glucose utilization [9, 10].

In a previous work [23], we constructed a detailed kinetic model of liver glucose metabolism and examined the relative importance of the different modes of enzyme regulation for the dynamic behavior of hepatic glucose metabolism. However, the influence of tissue architecture and blood flow on the ability of the liver to function as glucose homeostat were not considered in this model. It is obvious that the unique sinusoidal structure allows an efficient nutrient exchange, but how alterations in this architecture impacts on liver function is largely unknown. Therefore, in this paper we combined our previously published model of the hepatocyte carbohydrate metabolism with a model of sinusoidal blood flow that comprises some important structural and functional tissue parameters as the thickness of sinusoids, width and number of endothelial fenestrae, thickness of the space of Disse, volume of hepatocytes and diffusion coefficients of organic molecules in the various compartments of the STU. We accounted for heterogeneous enzyme expression by constructing distinct metabolic models for the periportal and pericentral hepatocyte. The model was used to investigate the relative impact of metabolic zonation, tissue architecture and microperfusion on the hepatic carbohydrate metabolism.

Methods

Description of the mathematical model

Glucose metabolism of single hepatocytes. The reaction scheme for the glucose metabolism of a single hepatocyte is depicted in Fig 1A. It comprises the pathways for glycolysis, gluconeogenesis, glycogen synthesis and degradation and the three cellular compartments of cytosol, endoplasmic reticulum and mitochondrion (see Fig 1A). The time-dependent variations of metabolite concentrations are governed by ordinary differential equations. The rate laws for enzymes and membrane transporters were either taken from the literature or constructed on the basis of published experimental data. The rate equations for the metabolic enzymes explicitly take into account substrate regulation, allosteric regulation as well as activity changes due to reversible phosphorylation in response to insulin and glucagon signalling. Model input comprises extracellular nutrient and hormone concentrations as well as cellular protein abundance. The detailed rate laws describing the metabolic part of the model are given in S1 Supplement. The model is based on a previously published model of hepatic carbohydrate metabolism [23].

Parameterization of the metabolic model. The kinetic parameters of metabolic enzymes were taken from the literature. For each parameter, the experimental source is cited in supplements 1 and 2. If for an enzyme-kinetic parameter more than a single measurement was available, we used one representative value that fits with the majority of the reported values and that—whenever possible—was obtained in an enzyme assay that reported consistent values for other kinetic parameters. Mathematical terms in the rate law related to allosteric enzyme effectors which are not included in the model were neglected. Their average contribution is thus

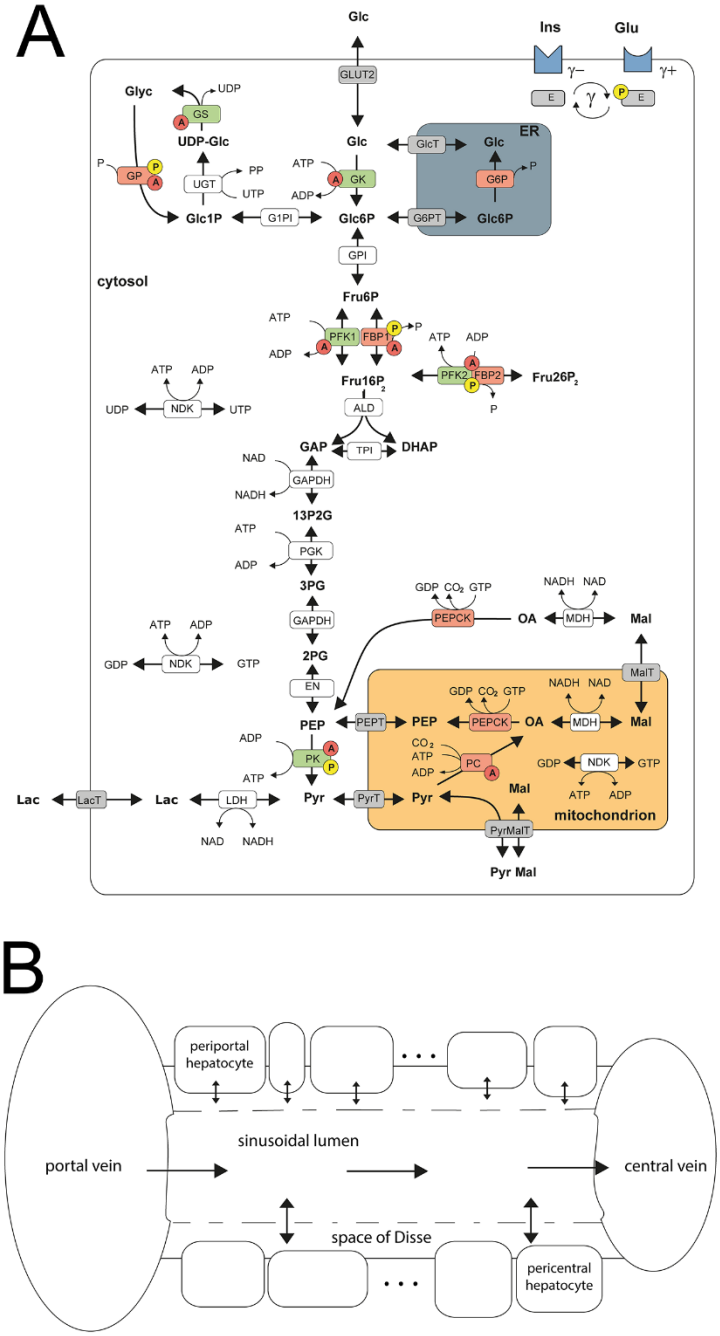

Fig 1. *Schematic model representation* (A) model of carbohydrate metabolism describing glycolysis, glyconeogenesis and glycogen synthesis and utilization. The model describes the enzymes Glucokinase (GK), Glucose-6-phosphate isomerase (GPI), Phosphofructokinase 1 (PFK1), Aldolase (ALD), Triosephosphate isomerase (TPI), Glyceraldehydephosphate

dehydrogenase (GAPDH), Phosphoglycerate kinase (PGK), Phosphoglycerate mutase (PGM), Enolase (EN), Pyruvate kinase (PK) Lactate dehydrogenase (LDH), Glucose-6-phosphate phosphatase (G6P), Phosphofructokinase 2 (PFK2), Fructose-2,6-bisphosphatase (FBP2), Fructose-1,6-bisphosphatase (FBP1), Phosphoenolpyruvate carboxykinase (PEPCK), Pyruvate carboxylase (PC), Nucleoside-diphosphate kinase (NDK), Malate dehydrogenase (MDH), Pyrophosphatase (PPASE), Glucose-1-phosphate isomerase (P1PI), Glycuronosyltransferase (UGT), Glycogen phosphorylase (GP), Glycogen synthase (GS) and transporters (ER <-> cytosol: Glucose-6-phosphate transporter (Glc6PT), Glucose transporter (GlcT); mitochondrion <-> cytosol: Pyruvate transporter (PYRT), Phosphoenolpyruvate transporter (PEPT), Malate transporter (MALT); extern <-> cytosol: Glucose transporter 2 (GLUT2), Lactate transporter (LACT). Enzymes that are phosphorylated or dephosphorylated in response to insulin (Ins) and glucagon (Glu) stimulus are marked by a yellow P, allosteric modification of enzymes is marked by a red A. The model contains the metabolites: glucose (Glc), glucose-6-phosphate (Glc6P), fructose-6-phosphate (Fru6P), fructose-1,6-bisphosphate ($Fru16P_2$), glyceraldehydephosphate (GraP), dihydroxyacetonephosphate (DHAP), 1,3-bisphosphoglycerate (13P2G), 3-phosphoglycerate (3PG), 2-phosphoglycerate (2PG), phosphoenolpyruvate (PEP), pyruvate (Pyr), lactate (Lac), malate (Mal), oxaloacetate (OA), glucose-1-phosphate (Glc1P), UDP-glucose (UDP-glc), glycogen, fructose-2,6-bisphosphate ($Fru26P_2$). The cofactors NADH, NAD, ATP, ADP, phosphate, UTP and UDP are not treated as dynamic variables. All physiological metabolites produced or consumed in the hepatocyte during glycolysis and gluconeogenesis are comprised into lactate. Reproduced from [23], adapted from [67]. (B) sinusoidal unit describing blood flow, nutrient and hormone distribution within the sinusoids. The model encompasses the blood vessel, the adjacent space of Disse and the surrounding hepatocyte cell layer. It is described by morphological parameters (blood vessel radius, thickness of the space of Disse, hepatocyte thickness, hepatocyte number, sinusoid length, degree of fenestration) and systemic parameters (central and portal vein hydrostatic pressure, plasma and lympgh oncotic pressure, diffusion coefficients).

https://doi.org/10.1371/journal.pcbi.1006005.g001

indirectly contained in the fitted Vmax values. The only free adjustable parameters of the model are the maximal enzyme activities (Vmax) which depend on the expression level of the enzyme protein and numerous other factors (cellular milieu, ligands not included into the model or even unknown). Vmax values were determined by adjusting simulated steady-state and time-dependent metabolite profiles and flux distributions to experimental data obtained with isolated hepatocytes in culture or the perfused liver (details are given in [23]).

Blood perfusion and tissue transport. The tissue transport of water, nutrients and blood is described by a compartment model. within the sinusoid by a compartment model. The STU is dissected into N discrete adjacent domains where N is the number of hepatocytes. Each domain subdivides into three compartments representing a single hepatocyte and the spatially associated part of the sinusoid and the space of Disse. Within the 3N compartments the concentrations of metabolites and hormones are constant. The exchange of metabolites and hormones between adjacent compartments are given by the following elementary processes: (i) Pressure-dependent directional convective flow of blood within the sinusoid from the periportal to pericentral pole, (ii) diffusion within the sinusoid, (iii) pressure-dependent directional convective flow from the sinusoid lumen to the space of Disse, (iv) diffusional exchange between the sinusoid lumen and space of Disse, (v) pressure-dependent directional convective transport of fluid in the space of Disse, (vi) diffusion within the space of Disse, (vii) active transport of metabolites between the space of Disse and the cytosol of hepatocytes.

Lateral blood flow in the vessel compartment is described by the Hagen-Poiseuille law for fluid flow through a cylinder. Water flow in the space of Disse is described by the Hagen-Poiseuille law for a hollow cylinder. Exchange of water between the vessel and the space of Disse is driven by hydrostatic and oncotic pressure difference between the blood vessel and the space of disse. The blood-born substances considered in our model are the metabolites glucose and lactate, the hormones insulin and glucagon and the indicator substances erythrocytes, albumin and water. The mathematical description of the tissue model and a complete list of all tissue parameters is given in S2 Supplement.

Hormonal regulation of metabolism. Hormonal regulation of metabolic fluxes is on the short term brought about by changes in the ratio of the phosphorylated and de-phosphorylated form of interconvertible metabolic enzymes. The phosphorylation states of the key regulatory

enzymes of hepatic carbohydrate metabolism are controlled by the concentrations of the hormones insulin and glucagon. Insulin and glucagon concentrations in the plasma are determined by the glucose-dependent secretion rates of these hormones from the pancreas (ß- and α cells, respectively) and their plasma clearance. We used the same empirical functions developed in [23] to relate the plasma level of glucose to the plasma level of insulin and glucagon (= glucose-hormone transfer function, GHT) and to relate the plasma concentration of the hormones to the phosphorylation state of hormone sensitive enzymes (= hormone-phosphorylation transfer function, HPT).

Plasma concentrations of insulin and glucagon are usually determined in peripheral blood samples. However, pancreatic hormones released in the portal vein are cleared during their passage through the liver and the body which results in a gap between reported plasma concentrations and the true intra-hepatic hormone concentrations Comparison of measured hormone concentrations in the portal vein, central vein and systemic circulation revealed that the extra-hepatic body clearance accounts for about 50% of total hormone clearance [24]. We took this fact into account by setting the concentration values of insulin and glucagon in the incoming portal blood to the two-fold value of their plasma values.

Hepatic hormone clearance occurs preferentially through binding of the hormones to their respective receptors and subsequent internalization. We thus linearly scaled the rate of hormone clearance to the signaling strength of the hormone. A detailed description of the functions and their construction is given in S3 Supplement.

Main limitations and simplifications of the model.

1. The main gluconeogenetic precursors lactate, external and internal amino acids and glycerol are lumped together into one generic precursor "lactate"
2. ATP producing and utilizing processes are not included, the adenine nucleotides ATP, ADP and AMP, the uridine nucleotides UTP and UDP and inorganic phosphate Pi are kept constant at their normal values. The same holds for the pyridine nucleotides NAD and NADH.
3. The contribution of monosaccharides other than glucose (fructose, galactose) to the hepatic carbohydrate metabolism is not considered.
4. Coupling of oxaloacetate (OA) with reactions of the citric acid cycle (formation by the malate dehydrogenase, utilization by the citrate synthase) is not included
5. Branching of the glycolytic triose phosphates (DHAP) to the lipid precursor glycerol phosphate is neglected
6. The representation of the sinusoid as a straight tube aligned by a single layer of linearly arranged cells is certainly a gross simplification of the true microanatomy of the liver.

Model simulations. With 20 hepatocytes per STU, the model is given by a system of 889 first-order differential equations which was numerically integrated by using the ODE15S solver of the MatLab package, Release R2011b, The MathWorks, Inc., Natick, Massachusetts, United States. The numerical simulation yielded stable solutions at variable number of cells (15–25) and variable parameter values.

For the interested reader, an SBML file of the cellular metabolic model is available from the authors.

CT perfusion of the liver

CT data acquisition. The perfusion CT study was performed using a multi-slice scanner (SOMATOM Definition AS and Definition Flash Siemens Healthcare, Forchheim, Germany).

The CT protocol consisted of a non-enhanced abdominal low-dose CT (40 mAs; 100 kV; SL, 5.0 mm; collimation, 128 0.6 mm; tube rotation time, 0.5 s; pitch, 0.6), which was obtained to localize the liver porta. Subsequently, a scan range of 6.9 cm z-axis coverage was planned over the involved liver, followed by a VPCT using an adaptive spiral scanning technique in shuttle mode. Perfusion parameters were: 80 kV; 100/ 120 mAs (for patients</>70 kg, respectively); collimation, 64 0.6 mm with z-flying focal spot; and 26 CT-whole coverages of the liver volume within a total scan time of 40 s. The mean radiation exposure for liver perfusion measurements was 7.5 mSv. Contrast medium was administered by using a dual-head pump injector (Stellant, Medtron, Saarbruecken, Germany). For this purpose, 50 mL Ultravist 370 (Bayer Vital, Leverkusen, Germany) were injected in all patients irrespective of patients' weight at a flow rate of 5 mL/s in an antecubital vein followed by a saline flush of 50 mL NaCl at 5 mL/s. All images were transferred to an external workstation (Multi-Modality Workplace, Siemens, Erlangen, Germany) for analysis. An abdominal scan in portal vein phase was also obtained.

CT data analysis. All data sets were transferred to a dedicated workstation (Syngo MMWP, VE 36A, Siemens Healthcare, Forchheim, Germany) and quantitative data evaluation was performed with a commercial software (Syngo Volume Perfusion CT Body (Siemens Healthcare, Forchheim, Germany).

CT perfusion analysis software is based on the maximum slope model using time density curves (TDC) to determine perfusion. Calculation of arterial liver perfusion (ALP) and portal venous perfusion (PVP) according to the dual blood supply of the liver by hepatic artery and portal vein is done by using the time of peak splenic enhancement as a separation point of arterial and portal-venous phase by drawing region of interest (ROI) in portal vein and spleen respectively. Arterial TDC for ALP is calculated dividing maximum arterial slope by maximum aortic enhancement. Portal-venous TDC for PVP is calculated dividing maximum portal-venous slope by maximum portal-vein enhancement. Hepatic Perfusion index (HPI) in % represents ALP divided by the sum of ALP and PVP.

Automated motion correction and noise reduction of the datasets were applied by using an integrated motion correction algorithm with non-rigid deformable registration for anatomic alignment. Regions of interest (ROI) were placed in the abdominal aorta, portal vein, and spleen. For the HCC lesions quantitative perfusion parameters BF, BV, ALP, PVP and hepatic perfusion index (HPI) were obtained. Additionally, arterial liver perfusion (ALP), portal venous perfusion (PVP) and hepatic perfusion index (HPI) were registered also in the non-involved liver parenchyma at more sites including the right and left liver lobes. This was done drawing a Volume of interest (VOI); an automatic pixel based recognition algorithm allowed for encompassing whole tumor volume along the z-axis. Subsequently, a separate VOI was drawn encompassing the maximum perfused site within the tumor which was visually determined using the ALP-color coded map. BF, ALP and PVP is indicated as ml per 100ml of tissue per minute, BV is indicated as ml per 100ml of tissue and HPI is indicated in percent.

All data generated or analyzed during this study are included in this published article.

Results

Zonation of carbohydrate metabolism: Periportal and pericentral hepatocytes

The various hepatocytes lining the sinusoids display a heterogeneous endowment with metabolic enzymes. Fig 2C shows the reported ratios of enzyme abundances in periportal and pericentral hepatocytes. For example, the abundance of the glycolytic enzyme pyruvate kinase (PK) was found up to 3-fold higher in hepatocytes isolated from the pericentral region compared to cells isolated from the periportal region. For the calibration of the model, it was

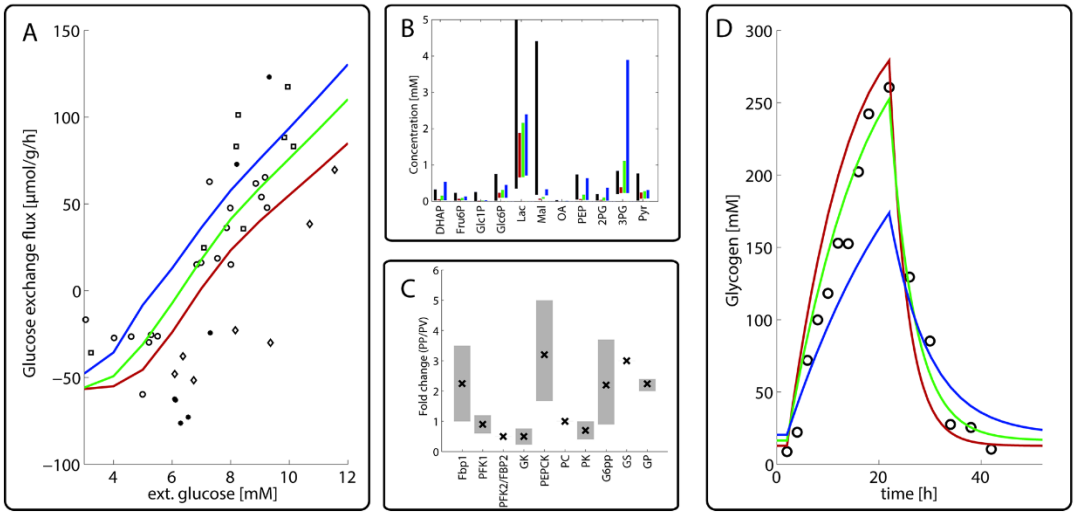

Fig 2. *Metabolic features of the periportal (PPH), pericentral (PCH) and mean (MH) hepatocyte* (A) Simulated glucose exchange fluxes of the PPH (red), MH (green) and PCH (blue). Positive values of the glucose exchange flux correspond to net glucose uptake, negative values correspond to net glucose release. External glucose was varied between 3 and 12 mM. Experimental data were taken from [24, 26–28]. (B) Reported (black) concentration ranges of selected metabolites and simulated concentration values for the PPH (red), MH (green) and PCH (blue). Note that the experimental concentration values were obtained in liver homogenates or cultures of isolated hepatocytes and thus represent average values across different types of hepatocytes. Data were taken from various experimental sources [29–37]. (C) Average ratio of measured protein abundances in hepatocytes stemming preferentially from the periportal and pericentral region. Vertical lines indicate standard deviations. The circles indicate abundance ratios used to calibrate the model for the PPH and PCH. Experimental data are from various sources [6–21]. (D) Simulated glycogen concentration in PPH (red), MH (green) and PCH (blue) during a starvation-refeeding experiment. The initial state at t = 0 was obtained by simulating as 24h fasting period with a plasma glucose level of 4 mM. At t = 0 the plasma glucose level was elevated to 10 mM for 24 hours and then again reduced to 4 mM. Experimental data were taken from [25].

https://doi.org/10.1371/journal.pcbi.1006005.g002

necessary to define a 'mean hepatocyte' (MH) which best represents metabolic parameters determined for the whole organ. To this end we put the maximal enzyme activities (V_{max} values) of the MH to the arithmetic mean of the V_{max} values of the hepatocytes that are spatially closest to the portal and central pole (in the following referred to as periportal and pericentral hepatocytes, PPH and PCH). The ratios of the V_{max} values of the PPH and PCH were put to the measured ratios of protein abundances. All V_{max}-values are given in S1 Supplement.

For the enzyme endowment of the individual hepatocytes lying between the PPH and PCH we assumed that the protein abundances of the key regulatory enzymes (see Fig 2C) change linearly from the portal to the central region, i.e. the protein abundance of the enzyme in the i-th hepatocyte is given by the relation

$$E(i) = E_{pp} + \frac{i-1}{N-1}(E_{PC} - E_{pp}) = E_{pp}\left(1 + \frac{i-1}{N-1}[\alpha - 1]\right)$$

where i numbers the spatial position of the hepatocyte along the sinusoid (i = 1 labels the hepatocyte closest to the portal pole, i = N labels the hepatocyte closest to the central pole), E_{PP} and E_{PC} are the enzyme abundances of the enzyme in the first and the last cell and $\alpha = {}^{E_{PC}}/_{E_{pp}}$ is the ratio of enzyme abundances in periportal and pericentral cells. We assume that the metabolism of the whole liver can be best represented by the metabolism of a 'mean' hepatocyte at position i = N/2 which is endowed with the mean protein abundance (E_{PP}+ E_{PC})/2. Hence, the Vmax values of the enzymes in this cell, V_{max} (N/2), were chosen such that that the best concordance between simulated metabolite concentrations and fluxes and measured values in the

whole organ was achieved. Once a numerical value for V_{max} (N/2) is known, the V_{max} values of the enzyme in the other cells can be calculated from the relation

$$\frac{V_{max}(i)}{V_{max}(\frac{N}{2})} = \frac{E(i)}{E(\frac{N}{2})}$$

because the maximal enzyme activity of an enzyme is up to a constant factor (the turnover rate constant) proportional to the protein abundance.

First we simulated the glucose exchange flux for the PPH, PCH and MH at plasma glucose concentrations in the physiological range between 3 mM and 12 mM (Fig 2A) and compared them to the experimentally determined whole liver glucose exchange fluxes (see [23]) for details). The feasibility of the calculated metabolic states was checked by the good concordance of calculated and experimentally determined ranges of metabolite concentrations (Fig 2B). The simulations show that the PPH has a higher capacity for gluconeogenesis, while the PCH has a higher capacity for glycolysis for each plasma glucose concentration. The set-point, i.e. the plasma glucose concentration at which net glucose exchange flux of the liver equals zero, is shifted from 7.0 mM for the PPH to 5.4 mM for the PCH. Notably, we found a similar set-point shift between hepatocytes in the fasted and fed state for the liver ([23]).

Next we simulated the dynamic changes of intrahepatic glycogen during a starvation-refeeding cycle (Fig 2D). Experimental data of the temporal glycogen content were taken from [25] where fasted rats were fed ad libitum for 20 hours and subsequently starved. We started the simulation with a pre-fasted liver (plasma glucose concentration of 4 mM). Interestingly, both the PPH and the PCH display smaller variations of the glycogen pool compared to the MH.

Simulation of indicator dilution curves

For the calibration of the blood flow model we compared calculated time courses of various indicators with the experimental data obtained by the indicator dilution technique in an in situ perfused phenobarbital-treated rat liver [34] (Fig 3A–3C). A soluble indicator substance is injected into the portal vein and the temporal concentration change in the central vein (= indicator dilution curve) is measured. Depending on blood flow velocity, diffusional exchange rates and the accessible distribution space, different indicators give rise to different dilution curves. Indicators used for model calibration were red blood cells (RBC), albumin and water. Since RBCs are larger than the size of the fenestrae, they are confined to the vascular compartment. Albumin is small enough to penetrate the fenestrae and to enter the space of Disse, but the endocytotic uptake rate of albumin into hepatocytes is negligible within the short time window (1–2 minutes). Water can enter the space of Disse and the cellular compartment.

From the average length of sinusoids ($\approx$ 300 μm) and the mean blood flow velocity one can estimate that the transition time of red blood cells trough a liver sinusoid is about 1 second. However, the experimentally determined dilution curve for red blood cells has a width of about 40 seconds. This delay is due to the time required by the red cells to be transported from the injection site to the sinusoids and from the sinusoids to the collecting veins. To take this into account, we approximated the temporal plasma profile of all indicators by the mean dilution curve of the red cells.

To take into account random variations in tissue structure and blood pressure, we simulated indicator dilution curves for a multitude of liver sinusoids while randomly sampling the trans-sinusoidal pressure difference Δp and the structural parameters vessel diameter and thickness of the space of Disse from the respective observed distributions (see Fig 3D–3F). The largest variability of the indicator dilution curves was obtained for labeled water where the

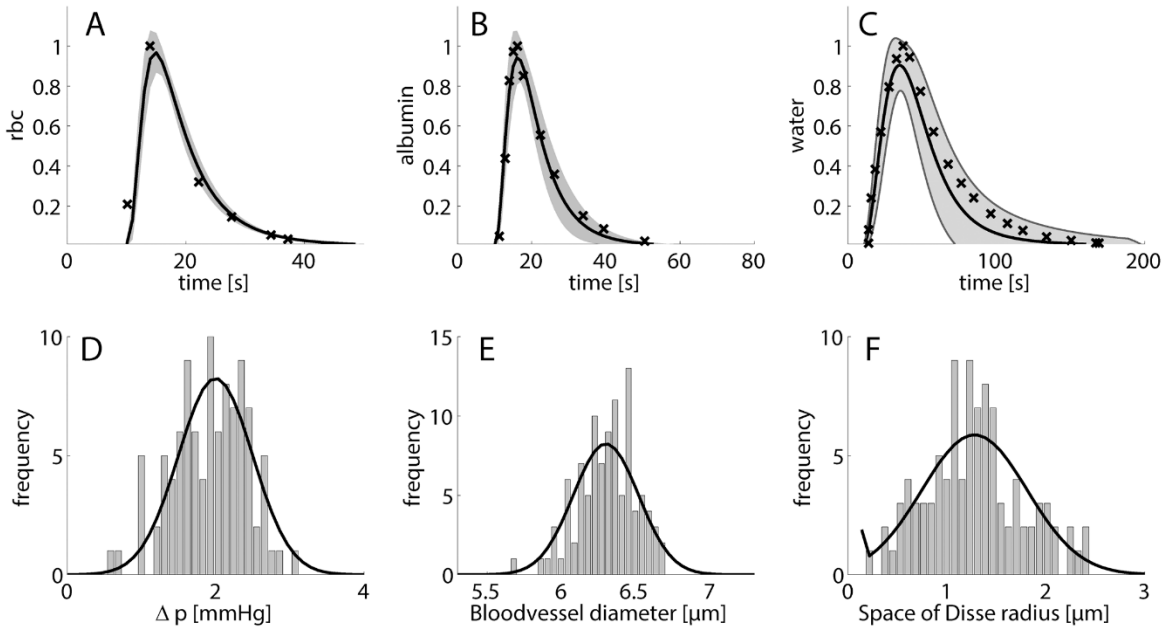

Fig 3. ***Effect of variations of tissue parameter on indicator dilution curves*** **Simulations were run 100 times with random structural parameter sampling.** Sampled parameters include portal-central pressure difference, blood vessel diameter, thickness of space of Disse, hepatocyte radius, cell number along the sinusoid, degree of fenestration. (A) indicator dilution curve for labeled red blood cells; (B) indicator dilution curve for labeled albumin; (C) indicator dilution curve for labeled water. Crosses depict experimental data taken from [38], black line represents the mean of 100 simulations, gray shaded areas represent standard deviations. Parameter distribution for portal-central pressure difference (D), blood vessel diameter (E) and thickness of space of Disse (F). Data taken from [39–41].

https://doi.org/10.1371/journal.pcbi.1006005.g003

half-life decay time varied between 50–70 seconds. The smallest variability resulted for the dilution curves of red cells.

Hepatic glucose exchange and hormone clearance at the tissue scale

During the passage of blood through the liver, the plasma concentrations of glucose and hormones are continuously changing. We simulated the intra-sinusoidal alterations in plasma glucose and hormone concentrations at different fixed portal glucose concentrations in the physiological range of 3–15 mM. The corresponding portal hormone concentrations were calculated by means of the glucose-hormone transfer (GHT) function (see S3 Supplement). The concentration of plasma lactate, which in our model represents all gluconeogenetic precursor substrates, was kept at 2 mM. Simulations were run until a steady state was reached.

The simulations were repeated 100 times with randomly and independently sampled structural, morphological and metabolic parameters. Structural and morphological parameters were drawn from their measured distributions (Fig 3D–3F), while protein abundances were sampled from equal distributions reflecting the variability of the periportal to pericentral protein ratios (Fig 2C).

A convenient measure to assess the contribution of the liver to the homeostasis of the plasma glucose is the portovenous glucose concentration difference. The mean and variance of the computed and the clearance of the hormones insulin and glucagon are shown in Fig 4. In agreement with the experimental data, the model simulations predict that the liver acts as

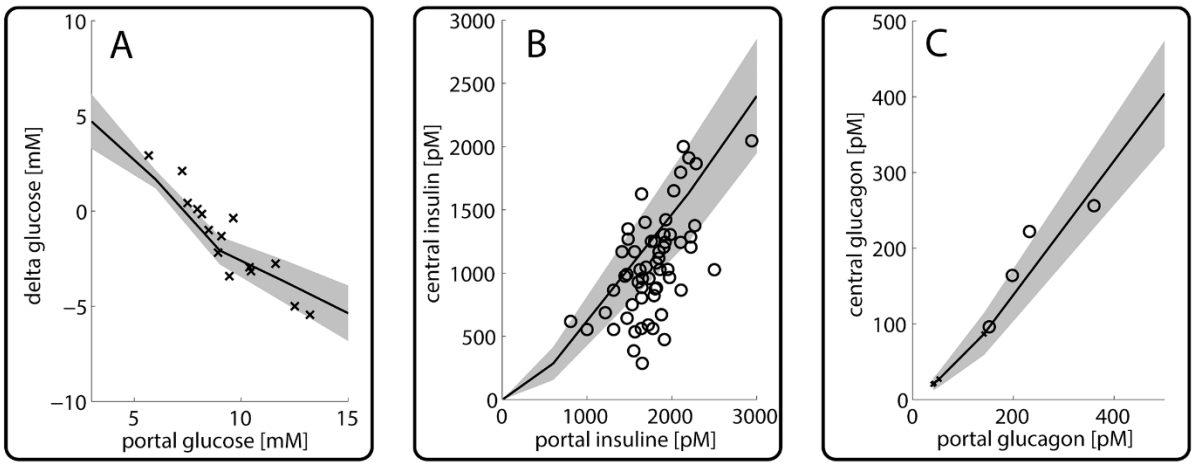

Fig 4. *Hepatic porto-venous glucose and hormone concentrations differences* (A) Porto-venous concentration difference of plasma glucose concentration as function of the portal glucose concentration. Experimental data from [42]. (B) Insulin concentration in the central vein in dependence of portal insulin concentration. Experimental data from [24]. (C) Glucagon concentration in the central vein in dependence of portal glucagon concentration. Experimental data from [43].

https://doi.org/10.1371/journal.pcbi.1006005.g004

glucose producer for portal plasma glucose concentrations below 8 mM, whereas it turns to a glucose consumer for portal glucose concentrations higher than 8mM. The hormone extraction curves in Fig 4B and 4C show that during one passage a fraction of 20–40% glucagon and 30–80% of insulin can be removed by the liver. These values are also in good agreement with experimental findings [20].

Interestingly, the set-point for the STU lies at approximately 7.5 mM and is therefore even higher than the set-points of the isolated periportal and pericentral hepatocyte (see Fig 2A). While the set-points for the individual hepatocytes were calculated with the GHTF given in appendix 3, the relation between plasma glucose and plasma hormones changes along the portal-central axis as glucose is exchanged (either taken up or produced) and hormones are gradually cleared. Therefore the actual relation between glucose and hormones (and thereby the position of the set-point) changes from cell to cell and eventually determines the set point of the STU as a whole.

The grey-shaded areas in Fig 4 indicate the range of variability in the arteriovenous glucose difference for a single STU as caused by random variations of tissue parameters. In the fibrotic and cirrhotic liver, striking structural changes are an enlargement of hepatocytes ([44]) and a decrease in the effective length of sinusoids (mainly due to sinusoidal capillarization ([45]). We thus simulated how the metabolic input-output relation of a single STU is affected by the length of the sinusoid (see Fig 5). This analysis revealed that the length of the sinusoid has severe consequences for the functional output. The longer the sinusoidal length–and thereby the contact time for the exchange of glucose–the higher the alteration in plasma glucose concentration. At high glucose levels a longer sinusoid clears more glucose form the blood (red lines), while at low glucose levels a longer sinusoid produces more glucose (blue lines). If the plasma glucose is close to the set point, the sinusoidal length is not a major determinant for glucose exchange (green lines).

We further analyzed the distribution of glucose within the various compartments of the STU and the contribution of individual hepatocytes to the net glucose balance. Depending on the portal glucose concentration, the glucose concentration along the sinusoid decreases or

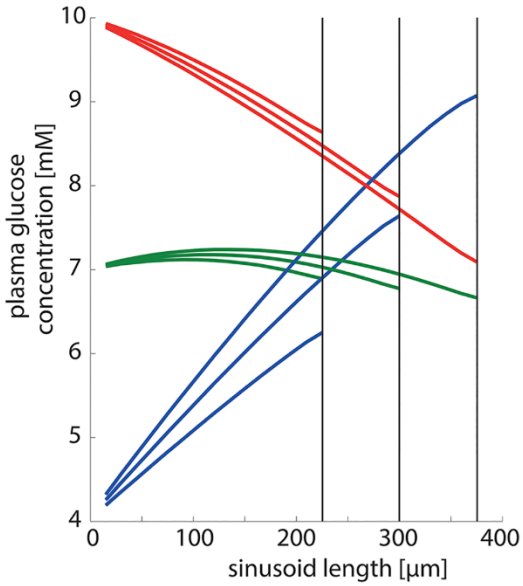

Fig 5. Effect of sinusoidal length on STU functionality. Sinusoidal length was 375 μm /300 μm/ 225 μm corresponding to 25/20/15 hepatocytes. Portal plasma glucose concentrations were 10 mM (red lines), 7 mM (green lines) and 4 mM (blue lines) corresponding to fed, normal and fasted state.

https://doi.org/10.1371/journal.pcbi.1006005.g005

increases in a nonlinear manner (Fig 6A). Intriguingly, for portal glucose concentrations in the range between 6 and 8 mM, upstream hepatocytes in the region around the portal field act as glucose producer (= positive glucose exchange flux) whereas downstream hepatocytes closer to the central pole act a glucose consumers (Fig 6B). This gives rise to an intra-sinusoidal glucose cycle where the glucose produced by the upstream hepatocytes are reutilized by the downstream hepatocytes.

As shown in Fig 6C, the glucose concentration gradient between the space of Disse and the sinusoidal lumen is largest at high portal glucose concentrations. But even in this situation the gradient remains below 1 mM. Thus, diffusion through endothelial fenestrae is sufficiently fast to prevent larger concentration gradients. Somewhat larger concentrations differences of up to 2 mM may occur between the space of Disse and the cytosol of hepatocytes (Fig 6D).

Zonated glycogen variations during a starvation-refeeding cycle

Next, we simulated the impact of a starvation-refeeding cycle on the dynamic changes of the glycogen content in the individual hepatocytes of the STU (Fig 7). As for the single cell case (Fig 2D), the simulation started with a pre-fasted liver (portal plasma glucose concentration of 4 mM) where the glycogen stores of all cell are almost completely emptied. During the feeding phase, the portal glucose concentration is increased to 8 mM, before it is reset to 4 mM during the fasting period. Simulations were repeated 100 times, again randomly and independently varying structural and morphological parameters as well as metabolic enzyme abundances from their respective distributions (see Fig 3, Fig 2 and S1 Supplement).

The amplitude of variations of the cellular glycogen content decrease from PPH to the PCH. In the PPH, the synthesis and degradation of glycogen PPH occurs with a significantly

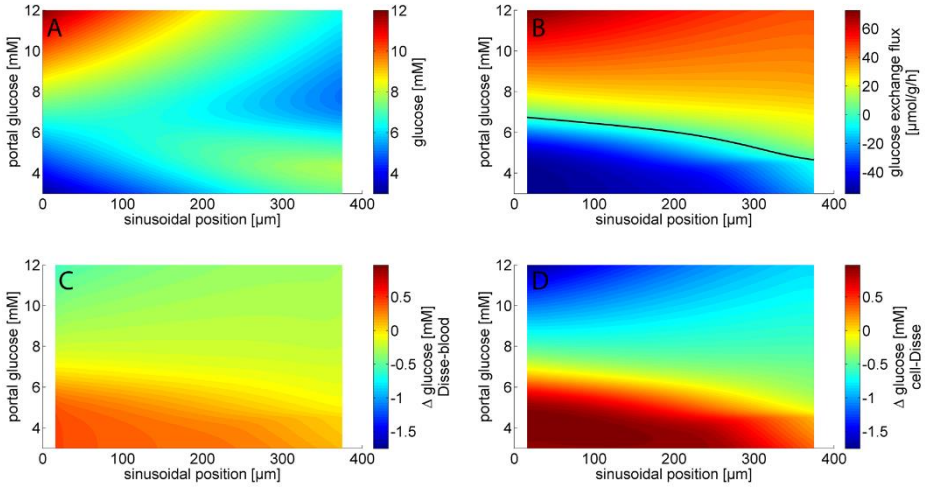

Fig 6. Glucose distribution at different spatial positions within the STU. Mean values from 100 simulations with randomly sampled STUs are shown. The STU is made up by 22 hepatocytes arranged along a sinusoid with a length of 200 μm. Portal glucose concentrations were varied between 3 and 12 mM. The continuous lines were created by linear interpolation between the discrete values (one value per compartment) obtained in the model simulation. (A) Glucose concentration; (B) Glucose exchange fluxes; (C) Glucose concentration differences between the space of Disse and the sinusoid glucose gradient; (D) Glucose concentration differences between the space of Disse and hepatocytes.

https://doi.org/10.1371/journal.pcbi.1006005.g006

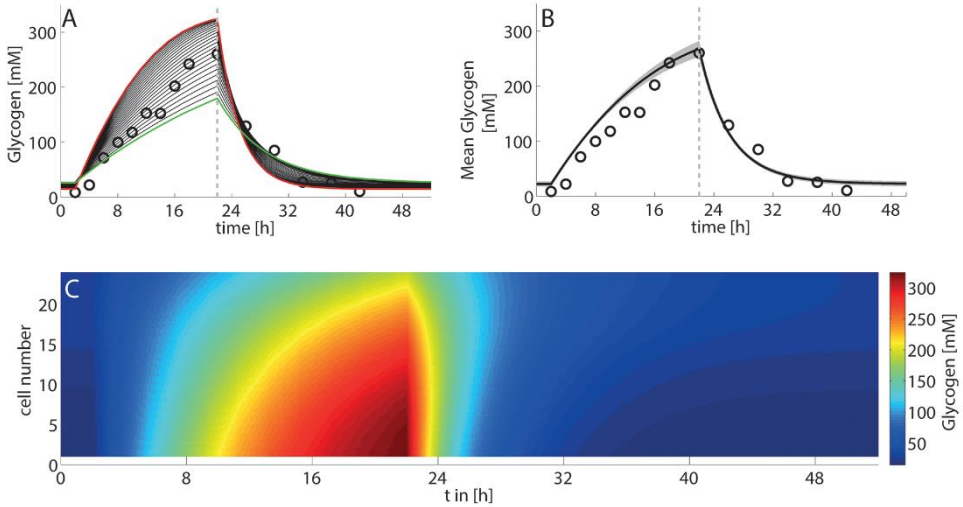

Fig 7. *Variations of the cellular glycogen content during a 48h fasting-refeeding cycle* (A) Simulated glycogen content of individual hepatocytes along the liver sinusoid. Red line–PPH (cell#1), green line–PCH (cell#22). Experimental data (open circles) were taken from [25]. (B) Simulated mean hepatic glycogen content (black line) and standard deviation (grey-shaded area) in response to parameter variation (100 trials with random parameter sampling based on the parameter distribution functions shown in Fig 3D–3F). (C) Simulated distribution of glycogen content across individual hepatocytes over time.

https://doi.org/10.1371/journal.pcbi.1006005.g007

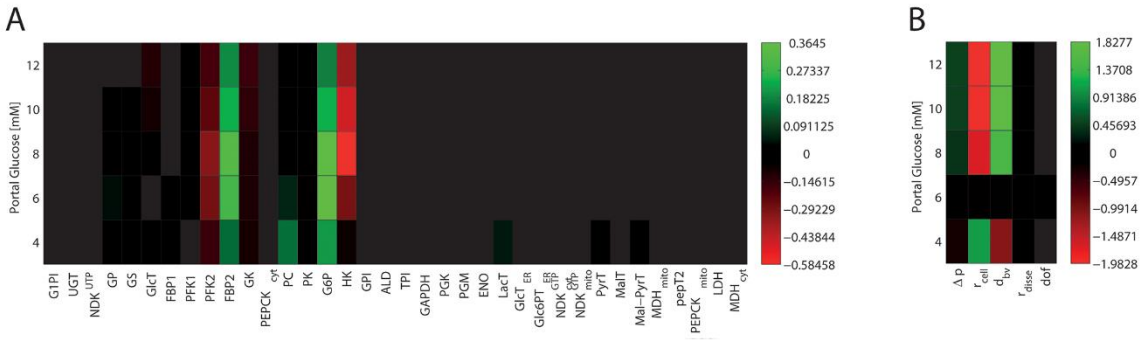

Fig 8. *Sensitivities* for metabolic enzymes (A) as well as structural and systemic parameters (B) with respect to central glucose concentration for different plasma glucose concentrations.

https://doi.org/10.1371/journal.pcbi.1006005.g008

higher rate compared to the PCH. This implicates for hepatocytes of the periportal zone a higher glycogen content under euglycemic conditions but lower glycogen content in hypoglycaemia.

Sensitivity analysis of the porto-venous glucose difference

To check the relative influence of metabolic parameters and tissue parameters on the performance of the STU, we carried out a sensitivity analysis of the model (Fig 8). The sensitivity S (p) was quantified by the change of the hepatic arteriovenous glucose difference ΔGlu_{PV} elicited by a small (= 5%) change of the model parameter p (enzyme activity, tissue parameter, capillary blood pressure), i.e.

$$S(p) = \frac{p}{\delta p}\frac{\delta\, \Delta v_{PV}}{\Delta v_{PV}} = \frac{1}{\varepsilon}[\Delta v_{PV}(p + \varepsilon p) - \Delta v_{PV}(p - \varepsilon p)]$$

with $\varepsilon = 0.05$.

The relative impact of individual metabolic enzymes is dependent on the metabolic state (fasted, fed), similar as found in [23] for the single hepatocyte. In contrast, the influence of structural parameters is less dependent on the metabolic state. The size of hepatocytes and the diameter of the sinusoids turned out to have the largest impact on ΔGlu_{PV}. Intriguingly, the sensitivity analysis shows that variations of the tissue architecture have an equally important influence of the metabolic performance of the liver than variations of protein abundances.

Regional metabolic differences due to inhomogeneous blood perfusion of the liver

The blood flow within different regions of the liver may vary up to a factor of three (see e.g. [46, 47]). We used our model to study the metabolic consequences of such variations of the regional blood flow. Blood flow was measures by perfusion CT (see Methods).

Fig 9 shows the CT—perfusion data and the corresponding model-based regional glucose production or utilization rate of a normal human liver. The blood flow through the sinusoid of the STU representing a small volume of liver was obtained by dividing the blood flow assessed by the perfusion CT through number of sinusoids $1.5 \cdot 10^9$ (sinusoids per 100 ml liver volume, see legend to Fig 9).

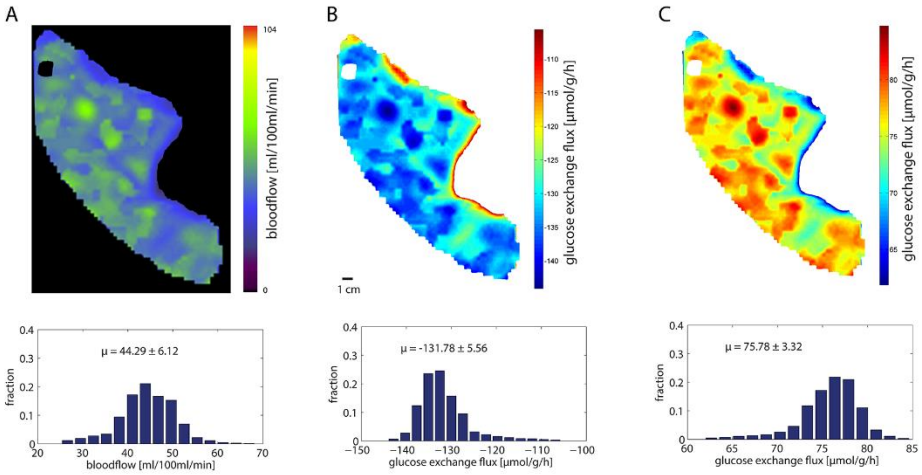

Fig 9. ***Influence of the regional blood flow on the regional glucose uptake/production rate of the human liver*** **A Regional distribution of blood flow in a normal human liver assessed by perfusion CT.** The histogram below shows the fractional distribution of blood flow values. The mean blood flow amounts to µ = 44.3 ml/100ml/min. *B* Simulated regional glucose exchange flux at a glucose plasma concentration of 4 mM (hypoglycemic condition) using the regional blood flow values shown in A as model input for the tissue model. The measured blood flow in a volume element of 100 ml was treated as the integral blood flow through $1.5 \cdot 10^9$ sinusoids. This estimate was based on an average liver volume of 1.5 liter, an average number of 1.5 million lobules and an average number of 1000 sinusoids per lobule. The histogram below shows the fractional distribution of glucose exchange flux values. Note that negative flux values indicate glucose release. The mean glucose production rate of the liver amounts to µ = -131,8 µmol/g/h. C Simulated regional glucose exchange flux at a high glucose plasma concentration of 10 mM (hyperglycemic condition) using the regional blood flow values shown in A as model input for the tissue model. The mean glucose uptake rate of the liver amounts to µ = 75.8 µmol/g/h.

https://doi.org/10.1371/journal.pcbi.1006005.g009

The average liver perfusion rate in this example was 44.3 ml/100ml/min with a standard variance of 6.1 ml/100ml/min. The computed regional glucose production rates (hypoglycemic case: portal glucose concentration set to 4 mM) and glucose uptake rates (hyperglycemic case: portal glucose concentration set to 10 mM) add up to a whole liver uptake rate of—131.8 µmol/g/h and production rate of 75.8 µmol/g/h, respectively. Interestingly, the variance of the glucose exchange fluxes is smaller than the variance of the blood flow values (compare the histograms in Fig 9A with those in Fig 9B and 9C). This is a consequence of the reciprocal relationship between blood flow rate and the exchangeable fraction of metabolites between blood and tissue. A decrease of the regional blood flow reduces the venous output volume but on the other hand increases in the leaving blood the concentrations of metabolites secreted by hepatocytes and increases the concentration of metabolites cleared by hepatocytes owing to the increased time span available for the exchange of blood metabolites with the tissue. Hence the mass output (= flow volume x concentration) is moderately buffered against changes of the blood perfusion rate.

Discussion

Tissue level models are becoming an emerging tool for enabling clinical translational research [48]. In this work, we developed a multi-scale model of the sinusoidal tissue unit of the liver defined by a single sinusoid that is surrounded by the space of Disse and adjacent monolayers of hepatocytes. We used the model to investigate how the metabolic performance of the liver to ensure homeostasis of the systemic glucose metabolism is affected by zonated expression of

metabolic enzymes, blood perfusion of the organ and metabolic coupling of hepatocytes via gradients of metabolites and hormones in the capillary blood stream.

Up to now only few models of liver metabolism exist which explicitly take into account the heterogenous intraacinar expression of metabolic enzymes and the metabolic implications of nutrient and hormone gradients along the portal-central axis. Ohno et al. [49] studied how the heterogenous expression of enzymes of the urea cycle and the glutamine synthetase may impact on the overall hepatic detoxification of ammonia. Their model subdivides the space between periportal blood entry and pericentral blood exit into 6 compartments. Compartment models with a similar architecture have been constructed for pharmacological applications, i.e. understanding the molecular basis for differential uptake and metabolization of xenobiotics in different zones [50, 51]. The most advanced zonated metabolic model of the liver has been published by Ashworth et al. [52]. They also used an 8- compartment model of the sinusoidal unit but on top included into their model 3 additional compartments representing the release of insulin from the pancreas and the exchange of glucose and fatty acids between the circulation and extra-hepatic tissues. The focus of this model was on the zonated lipid hyper-accumulation in case of non-alcoholic steatosis (NAFLD) caused by insulin resistance. A much simpler skeleton model addressing also the intriguing question of dispersed hepatic lipid accumulation has been recently proposed by Schleicher et al. [53]. Based on a 3-compartment model of the sinusoid they found that even in the absence of zonated enzyme expression the gradient of oxygen and fatty acids along the sinusoid may cause a zonated accumulation of lipid. In agreement with findings of the more advanced model of (Ashworth) their model suggests the zone-specific differences in the kinetic properties of the fatty acid uptake into hepatocytes are a key factor controlling the predominant accumulation of lipid in the pericentral region.

In the first part of this study, we analyzed how changes in the abundance of key metabolic enzymes reported for different zones of the liver acinus may affect the glucose exchange flux of the hepatocyte. As shown in Fig 2, zone-dependent expression of key regulatory enzymes of the glycolytic and gluconeogenetic pathway gives rise to significant differences in the relationship between plasma glucose level and the glucose exchange flux and glycogen turnover. Our calculations reveal a shift of the glucose-response curves for the periportal and pericentral hepatocyte in that periportal hepatocytes are stronger glucose producers whereas pericentral hepatocytes are more engaged in glucose utilization.

The signaling pathways responsible for the differential expression of metabolic enzymes in hepatocytes that are resident in different local positions of the sinusoid still remain unclear. Initially, the oxygen gradient was considered to be the most important driving force [54, 55]. Furthermore, the fact that incubation of isolated hepatocytes with high concentrations of either insulin or glucagon invokes a metabolic phenotype that resembles that of an periportal or pericentral hepatocyte [16] points to an important role of these hormones in the regulation of zonated gene expression. More recently, the Wnt/β-catenin developmental pathway has been shown to play a key role in the functional heterogeneity between periportal and pericentral mouse hepatocytes [56]. The Wnt pathway induces the genetic program of the pericentral hepatocyte and represses the genetic program of the periportal hepatocyte. On the contrary, the MAPK/ERK pathway seems to act in a reciprocal manner to counterbalance Wnt signaling and favors a periportal genetic program [57]. Also, a cross-talk between the transcription factor Hnf4a(alpha) and Wnt signaling has been proposed as a potential mechanism of liver zonation [58]. Comparing the protein ratios between periportal and pericentral hepatocytes to adaptive changes occurring in livers under extreme physiological settings like starvation, overnutrition or diabetes (see [23]) it becomes evident that the protein ratios between perioportal and pericentral hepatocytes are similar to the protein ratios observed between fed and starved

or normal and diabetic liver. This indicates that the same mechnisms ensuring adaptation of the whole organ to variable nutrient and hormone challenges are responsible for liver zonation.

Heterogeneity occurs among liver lobules regarding their enzymatic endowment as well as in their geometric parameters (such as sinusoidal length and width, width of the space of Disse and degree of fenestration) and systemic parameters (such as central and portal vein hydrostatic pressures or plasma and lymph oncotic pressure). To assess the functional variability introduced by variances in these parameters, we conducted a multitude of simulations by randomly and independently varying structural, morphological and metabolic parameters. The simulations in Fig 4 show that on the microscopic scale, variability of metabolic and tissue parameters may cause variations of ΔGlu_{PV} of about 25%.

Interestingly the set-point for the STU lies at approximately 7.5 mM and is therefore higher than the set-point for the periportal and pericentral hepatocyte alone. While the set-points for the individual hepatocytes were calculated with the GHTF given in appendix 3, the relation between plasma glucose and plasma hormones changes along the sinusoid as glucose is exchanged (either taken up or produced) and hormones are degraded. Therefore the actual relation between glucose and hormones (and thereby the position of the set-point) for a cell within the STU (and the STU itself) does depend on the metabolic activity of the preceding cells resulting in the observed shift.

To better understand the influence of individual model parameters on the capability of the liver to act as an glucose homeostat, we calculated the sensitivity of ΔGlu_{PV} with respect to variations of each model parameter. This analysis revealed two important peculiarities in the control of the hepatic glucose metabolism. First, the impact of variances in the expression of metabolic enzymes on ΔGlu_{PV} is highly dependent on the metabolic state of the liver. For example, the enzyme pyruvate carboxylase exerts considerable control on ΔGlu_{PV} at low plasma glucose concentrations, but is unimportant at high glucose concentrations. This is in agreement with findings in [23], where we investigated the influence of metabolic enzymes under various pathological and physiological metabolic states. Second, the sensitivity of ΔGlu_{PV} towards variations of cell size, blood vessel diameter and pressure gradients are comparable to the largest sensitivity with respect to variations of enzyme activities, and this holds for every metabolic state studied (fasted, fed). Hence, alterations of tissue parameters as, for example, volume expansion of hepatocytes in the fatty liver, increased collagen density in the space of Disse in the fibrotic liver or arterioportal shunting of sinusoids in the cirrhotic liver, can be expected to have profound effects on the metabolic performance of the affected liver region. How such effects are possibly compensated by other healthy regions of the liver remains to be elucidated.

The model allows interesting insights into the intra-sinusoidal glucose distribution which is not directly accessible to experimentation. The average STU is able to transfer incoming plasma glucose concentrations over a wide physiological range of 3–15 mM to a narrow interval of 6–10 mM pericentral glucose concentration. This reflects the enormous capacity of the liver to regulate plasma glucose concentration over a wide range of physiological situations. The glucose output of the liver must not be confused with measured plasma glucose concentrations which normally lie around 5 mM to 6 mM. The difference arises from the glucose clearance by extrahepatic tissues, mainly muscle and brain. Importantly, the glucose gradient between the cells and the space of Disse is twice as large as between the space of Disse and the blood. Hence the exchange of glucose between the sinusoid and the space of Disse through endothelial fenestrae does not appear to be a rate limiting step. This is also reflected by the almost vanishing sensitivities against changes of the diameter of the fenestrae.

Relating our model simulations of the glycogen metabolism to experimental data it has to be noted that strikingly different glycogen distributions in the liver have been reported in the literature depending on the species (mice, rat, dog, human), assay (isolated hepatocytes, perfused liver, in vivo measurements), method of glycogen quantification (PAS staining, isotopomer analysis) and day-time of sampling. For example, Bartels et al. ([59]) found glycogen repletion in the perfused liver of fasted rats to be exclusively localized to PCH whereas an isotopomer analysis based on administration of [U-^{13}C] glucose provided no evidence for zone-dependent differences in the glycogen repletion of 24h fasted conscious rats [60]. This makes it difficult to compare or simulations of the intra-acinar glycogen dynamics with experimental data. Both findings are in contradiction to our simulation which suggests a larger span and more rapid changes of glycogen in PPH compared with PCH (see Fig 2). However, this prediction is in perfect agreement with observations in [61] according to which glycogen withdrawal begins in zone 1, then spreads gradually to zone 3 and disappears after 12 hours if mice are fasted from 10.00 a.m. onwards. Intriguingly, the depletion pattern changes if fasting starts at midnight or at 10 p.m. In this case the glycogen is withdrawn evenly throughout the lobule. The authors speculated that circadian rhythms in the glycogen metabolism may account for these day-time dependent differences in the pattern of starvation-induced glycogen dynamics. Indeed, in Clock mutant mice the circadian oscillation of both the hepatic glycogen content and the circadian mRNA and protein expression of glycogen synthase 2 was severely dampened [62]. Moreover, the existence of a circadian rhythm of pancreatic insulin secretion in humans has been established [63]. We like to mention that shifting the HGR curve to higher or lower insulin secretion also shifts the glycogen distribution within the STU. Freinkel et al. ([64]) reported significantly higher insulin-to-glucose ratios in the morning than in the afternoon. Lambert and Hoet ([65]), studying seven obese and three non-obese females, found serum insulin levels to be higher during the night, when the subjects were not eating.

Our simulations shed some light on a novel mechanism which could be involved in the rapid adjustment of hepatic glucose metabolism to sudden changes of plasma glucose. As can be seen in Fig 6B, at portal glucose concentrations between 6 mM to 8 mM, glucose is produced in periportal hepatocytes and at the same time utilized in the pericentral hepatocytes. Such an intra-organ subdivision into glucose-producing and glucose-utilizing tissue regions is present in the kidney where the epithelial cells of the proximal tubule produce glucose along the gluconeogenetic pathways whereby glutamine serves as the major carbon source. The glucose-enriched blood reaches the cells of the distal tubule which utilize glucose in the glycolytic pathway for the production of ATP because oxidative phosphorylation is strongly limited by the low oxygen pressure in the distal region of the nephron. A similar function of the hepatic self-supply with respect to glucose seems not very likely because the oxygen gradient in the sinusoidal blood stream is only moderately changing from about 60 mmHg at the portal site to about 40 mmHg at the central site of the mice liver [66]. In the liver, the glucose cycle might establish a regulatory mechanism that allows a rapid increase of the glucose output by abruptly reducing the intra-hepatic glucose consumption. Hyperglycemia does not constitute an immediate threat for the organism as the adverse effects like protein glycosylation, diabetes, cardiovascular diseases, nephropathies or impaired vision develop over time periods of years. Contrary, short term hypoglycemia can have severe consequences. As the brain functionality relies almost exclusively on glucose as energy delivering substrate, even short hypoglycemic episodes of some minutes are accompanied by impaired vision, dizziness, unconsciousness or even death. To prevent the occurrence of hypoglycemic crisis, the liver produces in the periportal region more glucose than normally required for the plasma glucose homeostasis and extracts the surplus glucose in the pericentral region. By just reducing the intra-hepatic glucose consumption the glucose output could be rapidly elevated.

Finally, as first step towards a model-based construction of metabolic liver 'functiogram', we have used the model to convert the regional blood flow of the liver into regional glucose production- and utilization rates in hypo- and hyperglycemia, respectively. Interestingly, the metabolic heterogeneity appears to be smaller than the perfusion heterogeneity although there is still 25% - 42% variability in regional glucose exchange rates. The next step will be to apply our approach to unravel the regional metabolic capacity of steatotic, inflammatory, fibrotic and cirrhotic livers. This will require the re-parametrization of the tissue model with histological parameters of the diseased tissue and proteomics-based protein levels of metabolic enzymes. In combination with transient elastography and perfusion CT, such an *in silico* approach will provide a 3D *metabolic functiogram* of the liver of individual patients that provides valuable information on the available metabolic reserve capacity in distinct liver regions.

Conclusions

In summary, we presented a model of sinusoidal glucose metabolism by extending a previously established model of hepatic glucose metabolism to include liver zonation. We developed a realistic sinusoidal blood flow model taking morphological and systemic parameters into account thereby bridging the scale from the cellular to the tissue level. Taking into account variations in the tissue parameters as well as variations in the enzyme abundance we assessed the variability of sinusoidal glucose input-output relationship occurring among different livers sinusoids thereby assessing inter-organ variability. Swelling, cirrhosis and restriction of blood flow contribute to progression of liver disease thus allowing for interesting future uses of the model as a valuable tool to analyze liver functionality especially under disease conditions.

Supporting information

S1 Supplement. Mathematical description of the metabolic model.
(DOCX)

S2 Supplement. Mathematical description of the blood flow model.
(DOCX)

S3 Supplement. Mathematical description of the hormone signaling model.
(DOCX)

Author Contributions

Conceptualization: Nikolaus Berndt, Sascha Bulik, Hermann-Georg Holzhütter.

Data curation: Marius Stefan Horger, Sascha Bulik.

Investigation: Nikolaus Berndt.

Methodology: Nikolaus Berndt, Sascha Bulik, Hermann-Georg Holzhütter.

Writing – original draft: Nikolaus Berndt, Hermann-Georg Holzhütter.

Writing – review & editing: Marius Stefan Horger, Sascha Bulik, Hermann-Georg Holzhütter.

References

1. Rizza R.A., et al., Control of blood sugar in insulin-dependent diabetes: comparison of an artificial endocrine pancreas, continuous subcutaneous insulin infusion, and intensified conventional insulin therapy. N Engl J Med, 1980. 303(23): p. 1313–8. https://doi.org/10.1056/NEJM198012043032301 PMID: 7001229

2. Wahren J., Felig P., and Hagenfeldt L., Physical exercise and fuel homeostasis in diabetes mellitus. Diabetologia, 1978. 14(4): p. 213–22. PMID: 640298
3. Saxena R., Theise N.D., and Crawford J.M., Microanatomy of the human liver-exploring the hidden interfaces. Hepatology, 1999. 30(6): p. 1339–46. https://doi.org/10.1002/hep.510300607 PMID: 10573509
4. Lautt W.W., Relationship between hepatic blood flow and overall metabolism: the hepatic arterial buffer response. Fed Proc, 1983. 42(6): p. 1662–6. PMID: 6832383
5. Chalhoub E., et al., A distributed model of carbohydrate transport and metabolism in the liver during rest and high-intensity exercise. Ann Biomed Eng, 2007. 35(3): p. 474–91. https://doi.org/10.1007/s10439-006-9217-2 PMID: 17151925
6. Chen K.S. and Katz J., Zonation of glycogen and glucose syntheses, but not glycolysis, in rat liver. Biochem J, 1988. 255(1): p. 99–104. PMID: 3143359
7. Evans J.L., Quistorff B., and Witters L.A., Zonation of hepatic lipogenic enzymes identified by dual-digitonin-pulse perfusion. Biochem J, 1989. 259(3): p. 821–9. PMID: 2567158
8. Frederiks W.M., Marx F., and van Noorden C.J., Homogeneous distribution of phosphofructokinase in the rat liver acinus: a quantitative histochemical study. Hepatology, 1991. 14(4 Pt 1): p. 634–9. PMID: 1833303
9. Jungermann K. and Katz N., Functional hepatocellular heterogeneity. Hepatology, 1982. 2(3): p. 385–95. PMID: 7042508
10. Jungermann K. and Katz N., Functional specialization of different hepatocyte populations. Physiol Rev, 1989. 69(3): p. 708–64. https://doi.org/10.1152/physrev.1989.69.3.708 PMID: 2664826
11. Katz N., et al., Heterogeneous reciprocal localization of fructose-1,6-bisphosphatase and of glucokinase in microdissected periportal and perivenous rat liver tissue. FEBS Lett, 1977. 83(2): p. 272–6. PMID: 201494
12. Katz N., et al., Heterogeneous distribution of glucose-6-phosphatase in microdissected periportal and perivenous rat liver tissue. FEBS Lett, 1977. 76(2): p. 226–30. PMID: 193728
13. Miethke H., et al., Metabolic zonation in liver of diabetic rats. Zonal distribution of phosphoenolpyruvate carboxykinase, pyruvate kinase, glucose-6-phosphatase and succinate dehydrogenase. Biol Chem Hoppe Seyler, 1985. 366(5): p. 493–501. PMID: 2988584
14. Minchenko O., Opentanova I., and Caro J., Hypoxic regulation of the 6-phosphofructo-2-kinase/fructose-2,6-bisphosphatase gene family (PFKFB-1-4) expression in vivo. FEBS Lett, 2003. 554(3): p. 264–70. PMID: 14623077
15. Morselt A.F., et al., Mechanism of damage to liver cells after chronic exposure to low doses of cadmium chloride. Arch Toxicol Suppl, 1987. 11: p. 213–5. PMID: 2820354
16. Probst I., Schwartz P., and Jungermann K., Induction in primary culture of 'gluconeogenic' and 'glycolytic' hepatocytes resembling periportal and perivenous cells. Eur J Biochem, 1982. 126(2): p. 271–8. PMID: 6751822
17. Quistorff B., Gluconeogenesis in periportal and perivenous hepatocytes of rat liver, isolated by a new high-yield digitonin/collagenase perfusion technique. Biochem J, 1985. 229(1): p. 221–6. PMID: 2994630
18. Teutsch H.F. and Lowry O.H., Sex specific regional differences in hepatic glucokinase activity. Biochem Biophys Res Commun, 1982. 106(2): p. 533–8. PMID: 7104008
19. Trus M., et al., Hexokinase and glucokinase distribution in the liver lobule. J Histochem Cytochem, 1980. 28(6): p. 579–81. https://doi.org/10.1177/28.6.7391551 PMID: 7391551
20. Wals P.A., Palacin M., and Katz J., The zonation of liver and the distribution of fructose 2,6-bisphosphate in rat liver. J Biol Chem, 1988. 263(10): p. 4876–81. PMID: 2895107
21. Wolfle D. and Jungermann K., Long-term effects of physiological oxygen concentrations on glycolysis and gluconeogenesis in hepatocyte cultures. Eur J Biochem, 1985. 151(2): p. 299–303. PMID: 4029136
22. Jungermann K., Zonation of Metabolism and Gene-Expression in Liver. Histochemistry and Cell Biology, 1995. 103(2): p. 81–91. PMID: 7634156
23. Bulik S., Holzhutter H.G., and Berndt N., The relative importance of kinetic mechanisms and variable enzyme abundances for the regulation of hepatic glucose metabolism—insights from mathematical modeling. BMC Biol, 2016. 14: p. 15. https://doi.org/10.1186/s12915-016-0237-6 PMID: 26935066
24. Balks H.J. and Jungermann K., Regulation of Peripheral Insulin Glucagon-Levels by Rat-Liver. European Journal of Biochemistry, 1984. 141(3): p. 645–650. PMID: 6378634

25. Friedmann B., Goodman E.H. Jr., and Weinhouse S., Effects of glucose feeding, cortisol, and insulin on liver glycogen synthesis in the rat. Endocrinology, 1967. 81(3): p. 486–96. https://doi.org/10.1210/endo-81-3-486 PMID: 4291802

26. Holness M.J., et al., The disposition of carbohydrate between glycogenesis, lipogenesis and oxidation in liver during the starved-to-fed transition. Biochem J, 1988. 252(2): p. 325–30. PMID: 3415654

27. Holness M.J., et al., Hepatic carbon flux after re-feeding in the glycogen-storage-disease (gsd/gsd) rat. Biochem J, 1987. 248(3): p. 969–72. PMID: 3481265

28. Niewoehner C.B. and Nuttall F.Q., Relationship of hepatic glucose uptake to intrahepatic glucose concentration in fasted rats after glucose load. Diabetes, 1988. 37(11): p. 1559–66. PMID: 3181645

29. Aw T.Y., Andersson B.S., and Jones D.P., Mitochondrial transmembrane ion distribution during anoxia. Am J Physiol, 1987. 252(4 Pt 1): p. C356–61. https://doi.org/10.1152/ajpcell.1987.252.4.C356 PMID: 3565556

30. Bellamy D., The endogenous citric acid-cycle intermediates and amino acids of mitochondria. Biochem J, 1962. 82: p. 218–24. PMID: 13866863

31. Gardner L.B., Liu Z., and Barrett E.J., The role of glucose-6-phosphatase in the action of insulin on hepatic glucose production in the rat. Diabetes, 1993. 42(11): p. 1614–20. PMID: 8405703

32. MacDonald M.J., et al., Citrate oscillates in liver and pancreatic beta cell mitochondria and in INS-1 insulinoma cells. J Biol Chem, 2003. 278(51): p. 51894–900. https://doi.org/10.1074/jbc.M309038200 PMID: 14522964

33. Parrilla R., The effect of starvation in the rat on metabolite concentrations in blood, liver and skeletal muscle. Pflugers Arch, 1978. 374(1): p. 9–14. PMID: 567336

34. Siess E.A., Brocks D.G., and Wieland O.H., Distribution of metabolites between the cytosolic and mitochondrial compartments of hepatocytes isolated from fed rats. Hoppe Seylers Z Physiol Chem, 1978. 359(7): p. 785–98. PMID: 680639

35. Siess E.A., Kientsch-Engel R.I., and Wieland O.H., Concentration of free oxaloacetate in the mitochondrial compartment of isolated liver cells. Biochem J, 1984. 218(1): p. 171–6. PMID: 6424654

36. Tischler M.E., Hecht P., and Williamson J.R., Determination of mitochondrial/cytosolic metabolite gradients in isolated rat liver cells by cell disruption. Arch Biochem Biophys, 1977. 181(1): p. 278–93. PMID: 18107

37. Veech R.L., Veloso D., and Mehlman M.A., Thiamin deficiency: liver metabolite levels and redox and phosphorylation states in thiamin-deficient rats. J Nutr, 1973. 103(2): p. 267–72. PMID: 4346216

38. Varin F. and Huet P.M., Hepatic microcirculation in the perfused cirrhotic rat liver. J Clin Invest, 1985. 76(5): p. 1904–12. https://doi.org/10.1172/JCI112186 PMID: 4056057

39. Hung D.Y., et al., Quantitative evaluation of altered hepatic spaces and membrane transport in fibrotic rat liver. Hepatology, 2002. 36(5): p. 1180–9. https://doi.org/10.1053/jhep.2002.36820 PMID: 12395328

40. Armonis A., Patch D., and Burroughs A., Hepatic venous pressure measurement: an old test as a new prognostic marker in cirrhosis? Hepatology, 1997. 25(1): p. 245–8. https://doi.org/10.1053/jhep.1997.v25.ajhep0250245 PMID: 8985299

41. Koo A. and Liang I.Y., Microvascular filling pattern in rat liver sinusoids during vagal stimulation. J Physiol, 1979. 295: p. 191–9. PMID: 521923

42. Huang M.T. and Veech R.L., Role of the Direct and Indirect Pathways for Glycogen-Synthesis in Rat-Liver in the Postprandial State. Journal of Clinical Investigation, 1988. 81(3): p. 872–878. https://doi.org/10.1172/JCI113397 PMID: 3343346

43. Herold K.C. and Jaspan J.B., Hepatic glucagon clearance during insulin induced hypoglycemia. Horm Metab Res, 1986. 18(7): p. 431–5. https://doi.org/10.1055/s-2007-1012339 PMID: 3527924

44. Blendis L.M., et al., The role of hepatocyte enlargement in hepatic pressure in cirrhotic and noncirrhotic alcoholic liver disease. Hepatology, 1982. 2(5): p. 539–46. PMID: 7118067

45. Reichen J., et al., Determinants of hepatic function in liver cirrhosis in the rat. Multivariate analysis. J Clin Invest, 1988. 82(6): p. 2069–76. https://doi.org/10.1172/JCI113828 PMID: 3198765

46. Kim S.H., Kamaya A., and Willmann J.K., CT perfusion of the liver: principles and applications in oncology. Radiology, 2014. 272(2): p. 322–44. https://doi.org/10.1148/radiol.14130091 PMID: 25058132

47. Sherriff S.B., Smart R.C., and Taylor I., Clinical-Study of Liver Blood-Flow in Man Measured by Xe-133 Clearance after Portal-Vein Injection. Gut, 1977. 18(12): p. 1027–1031. PMID: 606629

48. Lerapetritou M.G., et al., Tissue-level modeling of xenobiotic metabolism in liver: An emerging tool for enabling clinical translational research. Clin Transl Sci, 2009. 2(3): p. 228–37. https://doi.org/10.1111/j.1752-8062.2009.00092.x PMID: 20443896

49. Ohno H., et al., Construction of a biological tissue model based on a single-cell model: a computer simulation of metabolic heterogeneity in the liver lobule. Artif Life, 2008. 14(1): p. 3–28. https://doi.org/10.1162/artl.2008.14.1.3 PMID: 18171128

50. Pang K.S., Weiss M., and Macheras P., Advanced pharmacokinetic models based on organ clearance, circulatory, and fractal concepts. AAPS J, 2007. 9(2): p. E268–83. https://doi.org/10.1208/aapsj0902030 PMID: 17907768

51. Anissimov Y.G. and Roberts M.S., A compartmental model of hepatic disposition kinetics: 1. Model development and application to linear kinetics. J Pharmacokinet Pharmacodyn, 2002. 29(2): p. 131–56. PMID: 12361240

52. Ashworth W.B., Davies N.A., and Bogle I.D., A Computational Model of Hepatic Energy Metabolism: Understanding Zonated Damage and Steatosis in NAFLD. PLoS Comput Biol, 2016. 12(9): p. e1005105. https://doi.org/10.1371/journal.pcbi.1005105 PMID: 27632189

53. Schleicher J., et al., Zonation of hepatic fat accumulation: insights from mathematical modelling of nutrient gradients and fatty acid uptake. J R Soc Interface, 2017. 14(133).

54. Jungermann K. and Kietzmann T., Role of oxygen in the zonation of carbohydrate metabolism and gene expression in liver. Kidney Int, 1997. 51(2): p. 402–12. PMID: 9027713

55. Jungermann K. and Kietzmann T., Oxygen: modulator of metabolic zonation and disease of the liver. Hepatology, 2000. 31(2): p. 255–60. https://doi.org/10.1002/hep.510310201 PMID: 10655244

56. Torre C., Perret C., and Colnot S., Molecular determinants of liver zonation. Prog Mol Biol Transl Sci, 2010. 97: p. 127–50. https://doi.org/10.1016/B978-0-12-385233-5.00005-2 PMID: 21074732

57. Hijmans B.S., et al., Zonation of glucose and fatty acid metabolism in the liver: mechanism and metabolic consequences. Biochimie, 2014. 96: p. 121–9. https://doi.org/10.1016/j.biochi.2013.06.007 PMID: 23792151

58. Colletti M., et al., Convergence of Wnt signaling on the HNF4alpha-driven transcription in controlling liver zonation. Gastroenterology, 2009. 137(2): p. 660–72. https://doi.org/10.1053/j.gastro.2009.05.038 PMID: 19454287

59. Bartels H., Vogt B., and Jungermann K., Glycogen synthesis from pyruvate in the periportal and from glucose in the perivenous zone in perfused livers from fasted rats. FEBS Lett, 1987. 221(2): p. 277–83. PMID: 3622767

60. Cline G.W. and Shulman G.I., Mass and positional isotopomer analysis of glucose metabolism in periportal and pericentral hepatocytes. J Biol Chem, 1995. 270(47): p. 28062–7. PMID: 7499292

61. Kanamura S., Asada-Kubota M., and Kanai K., The pattern of glycogen withdrawal within the liver acinus during fasting. Anat Embryol (Berl), 1980. 160(2): p. 145–51.

62. Doi R., Oishi K., and Ishida N., CLOCK regulates circadian rhythms of hepatic glycogen synthesis through transcriptional activation of Gys2. J Biol Chem, 2010. 285(29): p. 22114–21. https://doi.org/10.1074/jbc.M110.110361 PMID: 20430893

63. Boden G., et al., Evidence for a circadian rhythm of insulin secretion. Am J Physiol, 1996. 271(2 Pt 1): p. E246–52. https://doi.org/10.1152/ajpendo.1996.271.2.E246 PMID: 8770017

64. Freinkel N., Mager M., and Vinnick L., Cyclicity in the interrelationships between plasma insulin and glucose during starvation in normal young men. J Lab Clin Med, 1968. 71(1): p. 171–8. PMID: 5635005

65. Lambert A.E. and Hoet J.J., Diurnal pattern of plasma insulin concentration in the human. Diabetologia, 1966. 2(1): p. 69–72. PMID: 6005292

66. Tsukada K. and Suematsu M., Visualization and analysis of blood flow and oxygen consumption in hepatic microcirculation: application to an acute hepatitis model. J Vis Exp, 2012(66): p. e3996. https://doi.org/10.3791/3996 PMID: 22895109

67. König M, Bulik S, Holzhütter H-G (2012) Quantifying the Contribution of the Liver to Glucose Homeostasis: A Detailed Kinetic Model of Human Hepatic Glucose Metabolism. PLoS Comput Biol 8(6): e1002577. https://doi.org/10.1371/journal.pcbi.1002577

2.3 *Dynamic Metabolic Zonation of the Hepatic Glucose Metabolism Is Accomplished by Sinusoidal Plasma Gradients of Nutrients and Hormones* [41]

Dieses Kapitel basiert auf [41] (DOI: 10.3389/fphys.2018.01786).

Einleitung: Die Leber muss den Blutzuckerspiegel unabhängig vom Nahrungsangebot und vom systemischen Verbrauch in engen Grenzen halten (normalerweise zwischen 3 mM und 10 mM). Dafür muss sie ihren Stoffwechsel ständig an sich veränderte Bedingungen anpassen, wofür ihr verschiedene Mechanismen zur Verfügung stehen. Die Kurzzeitregulation erlaubt die optimale Nutzung der vorhandenen Proteine, während die Langzeitadaptation in der Anpassung der Proteinmengen an persistierende veränderte Bedingungen besteht. Diese Regulation der Proteinmenge kann durch Anpassung der Genexpression, Transkription, mRNA-Translation und/oder des Proteinabbaus erfolgen. Die Anpassung findet nicht nur beim Übergang zwischen verschiedenen Nahrungsregimen (z.B. Hungern/Fasten) statt, sondern auch bei der Anpassung an pathologische Zustände wie Diabetes. Zusätzlich gibt es auch Unterschiede in der Proteinausstattung zwischen den verschiedenen Zonen einer normalen Leber (siehe Abschnitt 2.2), die von der Entfernung der Zone zur arteriellen Blutzufuhr innerhalb der Leber abhängen. Das arterielle Blut aus der Portalvene hat hohe Insulin- und Glukagonkonzentrationen, die entlang des Sinusoids immer weiter abnehmen, da die Hepatozyten sie aus dem Blut entfernen. Gleiches gilt für Sauerstoff und viele weitere Nährstoffe, so dass sich die Plasmazusammensetzung in den verschiedenen Zonen der Leber deutlich unterscheidet. Insulin und Glukagon wirken durch die Aktivierung verschiedener Signalwege, die sowohl die Kurzzeitregulation steuern als auch auf verschiede Transkriptions-faktoren wirken. Somit ist es plausibel anzunehmen, dass die lokale Konzentration verschiedener Effektoren ausschlaggebend für die Proteinausstattung der Leber ist.

Fragestellung: Ziel dieser Arbeit war es, die bestehenden Modelle des hepatischen Glukosestoffwechsels um die adaptive Genexpression zu erweitern und somit zu einem selbstkonsistenten Modell der Glykolyse zu gelangen, mit dessen Hilfe die Anpassung des hepatischen Glukosestoffwechsels an verschiedene physiologische und pathologische Zustände beschrieben werden kann.

Methode: Das Modell des hepatischen Glukosestoffwechsels wurde mit einem neu entwickelten Modell des Proteinumsatzes ergänzt, welches die Synthese und den Abbau der regulativ wichtigen Enzyme in Abhängigkeit der lokalen Plasmakonzentration von Glukose, Sauerstoff, Insulin und Glukagon beschreibt. Die individuellen Ratengleichungen stellen dabei effektive Transferfunktionen dar, die experimentell bestimmte Zusammenhänge zwischen den Effektorkonzentrationen und den Synthese- und Abbauraten der einzelnen Enzyme beschreiben.

Resultat: Mit diesem Modell des Proteinumsatzes konnte sowohl die Zonierung der Leber als auch die Adaptation der Leber beim Hungern/Fasten sowie bei diabetischen Bedingungen erklärt werden. Das zeigt, dass die Zonierung eine Folge der intra-siunsoidalen Gradienten von Hormonen und Nährstoffen ist und dass die Mechanismen, die es der Leber ermöglichen, ihren Proteingehalt an den Bedarf und das Angebot an Nährstoffen anzupassen, auch für die Zonierung verantwortlich sind. Es zeigt auch, dass Glukose, Sauerstoff, Insulin und Glukagon

die wichtigsten dynamischen Modulatoren sind und dass andere bekannte Effektoren für die hier betrachteten Adaptationen nur eine untergeordnete Rolle spielen.

Diskusion: Das Modell beschreibt die experimentell bestimmten Proteinlevel in verschiedenen Zonen der Leber, die Adaptation der Leber an verschiede Ernährungszustände sowie metbolische Veränderungen bei Diabetes. Das Modell kann aus sich selbst heraus die variable Genexpression metabolischer Enzyme mit einer kleinen Zahl von externen Effektoren (Glukose, Sauerstoff, Insulin und Glukagon) erklären. Es beschreibt die Adaptation der Leber an verschiedene physiologische und pathologische Zustände (Hungern/Fasten, gesund/ diabetisch) sowie die metabolische Zonierung innerhalb der Leber.

> *„Daraus ergeben sich wichtige Erkenntnisse: (1) Die Zonierung des Kohlenhydratstoffwechsels der Leber ergibt sich aus der Kontrolle der Schlüsselenzyme des hepatischen Glukosestoffwechsels durch Effektoren, die einen Gradienten innerhalb des Sinusoids aufweisen. (2) Die gleichen Mechanismen, die die dynamische Adaptation des Organs an verschiedene physiologische Situationen ermöglichen, führen auch zur Zonierung des hepatischen Glukosemetabolismus. (3) Die vier in diesem Modell betrachteten Modulatoren sind ausreichend, um die Adaptation des hepatischen Glukosemetabolismus zu beschreiben. (4) Phänomenologische Transferfunktionen, die direkt Modulatoren mit dem Proteinabbau und der Synthese verknüpfen, sind eine vielversprechende Möglichkeit, um variable Genexpression zu berücksichtigen, auch wenn das zugrundeliegende genregulatorische Netzwerk nicht bekannt ist.“* (Übersetzung durch den Autor aus [41])

Wenn auch in ihren molekularen Wechselwirkungen unverstanden, so sind auf phänomenologischer Ebene doch viele wichtige Effektoren der Genregulation bekannt. Schon früh wurde entdeckt, dass man durch Hormonzugabe zu isolierten Hepatozytenkulturen deren Phänotyp in Richtung perizentral oder periportal ändern kann [46]. Später wurde der Sauerstoffgradient als wichtiger Faktor für die Zonierung und Adaptation der Leber entdeckt [45, 47, 48]. Neuere Arbeiten zeigen eine ganze Reihe weiterer an der Zonierung beteiligter Signalwege. So spielt der Wnt/β-Catenin-Signalweg, dem auch eine zentrale Bedeutung in der Entwicklung der Leber zukommt, eine wichtige Rolle in der metabolischen Heterogenität von periportalen und perizentralen Hepatozyten [49], indem er das genetische Programm der zentralen Hepatozyten begünstigt und das der periportalen Hepatozyten unterdrückt. Dementgegen induziert der Ras/MAPK/ERK-Signalweg [50] eher den periportalen Phänotyp. Auch andere Effektoren wie HNF4α [51] oder Schilddrüsenhormone [52] sind an der Zonierung beteiligt. Das Modell ermöglicht es, die relative Bedeutung dieser Effektoren bei der Adaptation der Leber einzuschätzen.

Außerdem ermöglicht das Modell, Veränderungen der Proteinmengen bei normaler Ernährung zu untersuchen. Die täglichen Schwankungen bei Proteinen des Glukosestoffwechsels liegen da bei moderaten 10-20%, was deutlich weniger ist als bei Schlüsselenzymen anderer Stoffwechselwege [53, 54]. Im Vergleich zu den täglichen Schwankungen in den Enzymmengen sind die Veränderungen während der Adaptation an veränderte Ernährungszustände allerdings deutlich größer. Die Simulationen zeigen, dass diese Umstellung auch nach mehreren Tagen noch nicht abgeschlossen ist und wesentlich dazu beiträgt, den Glukoseaustausch der Leber an veränderte Ernährungssituationen anzupassen (siehe auch 2.1).

Das Modell liefert auch eine gute Erklärung für die starke Ähnlichkeit des metabolischen Phänotyps der gefasteten Leber, der diabetischen Leber und den Hepatozyten der peri-

portalen Zone, da es erlaubt, die zugrundeliegenden gemeinsamen Mechanismen zu identifizieren. Unter all diesen Bedingungen ist die Wirkung von Glukagon, welches für die vermehrte Expression glukoneogenetischer Enzyme sorgt, stark erhöht. Im gefasteten Zustand liegt das am niedrigen Blutzucker, der zu einer erhöhten Sekretion von Glukagon aus dem Pankreas führt. Die Sekretion von Glukagon ist auch im diabetischen Zustand stark erhöht, obwohl die Glukosekonzentration sehr hoch ist. In der periportalen Zone wiederum ist die Konzentration von Glukagon hoch, da noch kein Glukagon aus der Zirkulation entfernt wurde. Im Gegensatz dazu ist in der perizentralen Zone die Glukagonkonzentration sehr viel niedriger, da die Leber selbst einen Großteil des zirkulierenden Glukagons aus dem Plasma entfernt. Das Modell kann auch für medizinische Fragestellungen relevant sein. Beispielsweise kann man damit den Einfluss einer Insulintherapie auf den Glukoseaustausch einer diabetischen Leber untersuchen.

frontiers in Physiology

ORIGINAL RESEARCH
published: 12 December 2018
doi: 10.3389/fphys.2018.01786

Dynamic Metabolic Zonation of the Hepatic Glucose Metabolism Is Accomplished by Sinusoidal Plasma Gradients of Nutrients and Hormones

Nikolaus Berndt[1,2] *and Hermann-Georg Holzhütter*[1]*

[1] *Computational Biochemistry Group, Institute of Biochemistry, Charite—University Medicine Berlin, Berlin, Germany,*
[2] *Institute for Computational and Imaging Science in Cardiovascular Medicine, Charite—University Medicine Berlin, Berlin, Germany*

Being the central metabolic organ of vertebrates, the liver possesses the largest repertoire of metabolic enzymes among all tissues and organs. Almost all metabolic pathways are resident in the parenchymal cell, hepatocyte, but the pathway capacities may largely differ depending on the localization of hepatocytes within the liver acinus-a phenomenon that is commonly referred to as metabolic zonation. Metabolic zonation is rather dynamic since gene expression patterns of metabolic enzymes may change in response to nutrition, drugs, hormones and pathological states of the liver (e.g., fibrosis and inflammation). This fact has to be ultimately taken into account in mathematical models aiming at the prediction of metabolic liver functions in different physiological and pathological settings. Here we present a spatially resolved kinetic tissue model of hepatic glucose metabolism which includes zone-specific temporal changes of enzyme abundances which are driven by concentration gradients of nutrients, hormones and oxygen along the hepatic sinusoids. As key modulators of enzyme expression we included oxygen, glucose and the hormones insulin and glucagon which also control enzyme activities by cAMP-dependent reversible phosphorylation. Starting with an initially non-zonated model using plasma profiles under fed, fasted and diabetic conditions, zonal patterns of glycolytic and gluconeogenetic enzymes as well as glucose uptake and release rates are created as an emergent property. We show that mechanisms controlling the adaptation of enzyme abundances to varying external conditions necessarily lead to the zonation of hepatic carbohydrate metabolism. To the best of our knowledge, this is the first kinetic tissue model which takes into account in a semi-mechanistic way all relevant levels of enzyme regulation.

Keywords: metabolism, metabolic zonation, kinetic model, multiscale model, gene expression

OPEN ACCESS

Edited by:
Steven Dooley,
Universitätsmedizin Mannheim, Medizinische Fakultät Mannheim, Universität Heidelberg, Germany

Reviewed by:
Adil Mardinoglu,
Chalmers University of Technology, Sweden
Rolf Gebhardt,
Leipzig University, Germany

***Correspondence:**
Hermann-Georg Holzhütter
hergo@charite.de

Specialty section:
This article was submitted to Gastrointestinal Sciences, a section of the journal Frontiers in Physiology

Received: *16 August 2018*
Accepted: *28 November 2018*
Published: *12 December 2018*

Citation:
Berndt N and Holzhütter H-G (2018) Dynamic Metabolic Zonation of the Hepatic Glucose Metabolism Is Accomplished by Sinusoidal Plasma Gradients of Nutrients and Hormones. Front. Physiol. 9:1786. doi: 10.3389/fphys.2018.01786

INTRODUCTION

The tightly controlled switch between hepatic uptake and release of glucose keeps the plasma glucose concentrations within a range between 4 and 10 mM despite largely varying carbohydrate intake and utilization. This homeostatic function of the liver with respect to plasma glucose is achieved by several enzyme-regulatory mechanisms acting on different time scales. On the

short term, hormone-dependent reversible enzyme phosphorylation and changes of reaction rates elicited by concentration changes of reaction substrates/products and allosteric modulators enable a metabolic response within seconds or minutes. Recurrent activation of these fast regulatory modes is typically accompanied by slow changes in the abundance of metabolic enzymes on a time scale of hours to days (Hopgood et al., 1973; Weinberg and Utter, 1980). Both the fast and slow mode of enzyme regulation are important for the regulation of the glucose exchange flux between hepatocytes and blood plasma (Bulik et al., 2016), Owing to concentration gradients of oxygen, metabolites, hormones, and morphogens along the hepatic capillaries (sinusoids) the expression of metabolic enzymes may differ in various zones of the liver acinus. For example, the oxygen pressure decreases by 50% along the porto-central axis of the acinus (Jungermann and Kietzmann, 2000). This goes in line with the number and structure of mitochondria (Schmucker et al., 1978) and glycolytic capacities in the periportal and pericentral zone (Braeuning et al., 2006). Hepatocytes close to the portal pole (zone 1) experiencing the highest concentration of oxygen pressure are predestined for strong ATP-demanding anabolic pathways like gluconeogenesis and urea synthesis. Contrary, hepatocytes close to the venous pole of the acinus (zone 3) experience the lowest oxygen concentrations and thus possess a high glycolytic capacity, a typical feature of cells working under conditions of permanent oxygen deprivation. The heterogeneous allocation of gluconeogenetic and glycolytic capacities to different hepatocytes along the porto-central axis may even result in a situation where a certain fraction of glucose produced by periportal cells is used to fuel the glycolysis of pericentral cells (Berndt et al., 2018).

Several blood-born factors have been identified as regulators of zone-dependent gene expression of metabolic enzymes. Oxygen, glucose, the hormones glucagon and insulin, the morphogens Wnt and hedgehog and the growth factor HGF belong to the best studied factors. The various factors appear to act in a hierarchical fashion whereby the gradients of morphogens and growth factors create a basic expression pattern that is further modulated by nutrition-related factors such as oxygen, glucose, fatty acids and the hormones insulin and glucagon. In this work, we will focus on the latter group of modifiers, i.e., we restrict our model to the metabolic response of the liver to nutritional challenges and oxygen availability.

Metabolic adaptation of hepatocytes to varying oxygen pressures is mainly controlled by hypoxia-inducible transcription factors (HIFs), heterodimeric complexes consisting of a constitutively expressed β-subunit and an oxygen-sensitive α-subunit. In the liver, HIF-1α regulates primarily glycolytic genes whereas HIF-2α is known to primarily regulate genes involved in cell proliferation and iron metabolism (Ramakrishnan and Shah, 2017). In line with the falling oxygen pressure along the porto-central axis, HIFαs were found with higher levels in the less aerobic pericentral zone (Kietzmann et al., 2001). Besides oxygen, the pancreatic hormones insulin and glucagon are important drivers of zone-dependent differences in enzyme activities. The regulatory role of these hormones is 2-fold. They control the cellular cAMP level in an antagonistic manner and thus exert opposite effects on the reversible phosphorylation of key regulatory enzymes of glycolysis and gluconeogenesis as PFK2, PK, and PEPCK. The hepatic clearance of the two hormones by endocytic uptake into hepatocytes creates a concentration gradient along the porto-central axis which entails zone-dependent differences in the phosphorylation level of interconvertible enzymes. With respect to gene expression of metabolic enzymes, insulin and glucagon also control the efficiency of several transcription factors as ChREBP, SREBP-1c, CREB, and Foxo (Han et al., 2016). Both actions of glucagon and insulin are tightly interrelated and function in part through the same mechanisms. For example, the cAMP-activated protein kinase A (PKA) is responsible for phosphorylation of interconvertible enzymes such as FBPFK2 and PK, as well as for the phosphorylation of the transcription factors ChREBP and CREP (Uyeda and Repa, 2006). cAMP is produced by glucagon-induced activation of the adenylate cyclase and degraded by insulin-stimulated cAMP phosphodiesterase. Consequently, the protein level of key regulatory enzymes reflects the integral hormone levels over longer time periods.

In this work we included dynamic changes in the abundance of metabolic enzymes into our previously developed multi-scale tissue model of hepatic glucose metabolism (Berndt et al., 2018). The rates of protein synthesis and degradation were modeled by phenomenological rate equations which were parameterized by using experimentally determined protein levels at varying concentrations of oxygen, glucose, insulin, and glucagon. The central aims of our work were (i) to provide a proof of principle for integrating in a self-consistent manner the temporal gene expression of enzymes into kinetic models of cellular metabolism, (ii) to lend further support to the concept of post-differentiation patterning according to which metabolic zonation is driven by gradients of oxygen, nutrients and hormones in the capillary blood and (iii) to present a modeling approach that obviates the requirement to measure the cellular abundance of metabolic enzymes (e.g., by quantitative proteomics) in different physical states of the liver, a procedure burdened with many problems as, for example, invasive tissue sampling and protein quantification in cells separated from different zones.

MODEL DESCRIPTION

The model combines a mathematical model of the sinusoidal tissue unit (STU) (Berndt et al., 2018) with a kinetic model of the protein turnover of key regulatory enzymes.

Compartment Model of Metabolite and Hormone Transport in the Sinusoidal Tissue Unit (STU)

Structurally, the STU is defined by a single sinusoid, the adjacent space of Disse and a monolayer of hepatocytes flanking the space of Disse (see **Figure 1A**). Functionally, the model describes the exchange of oxygen, metabolites and hormones between the sinusoidal blood, the space of Disse and the hepatocytes and the glucose metabolism within hepatocytes. The transport of metabolite and hormones within the STU is driven by diffusion

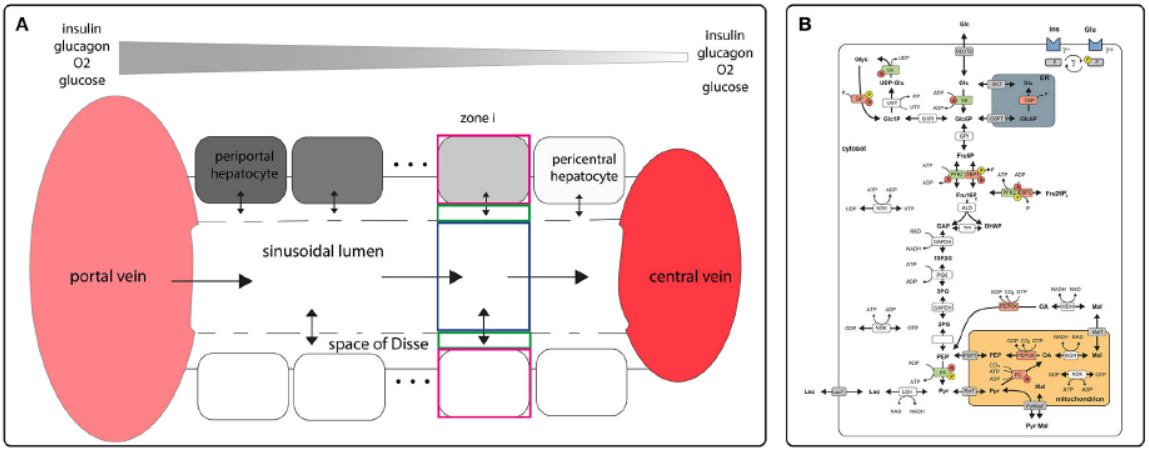

FIGURE 1 | Schematic model representation **(A)** sinusoidal blood flow model describing blood flow, nutrient and hormone distribution within the sinusoids. The model encompasses a single sinusoid, the adjacent space of Disse and the surrounding layer of hepatocytes. It is described by morphological parameters (blood vessel radius, thickness of the space of Disse, hepatocyte thickness, hepatocyte number, sinusoid length, degree of fenestration), and systemic parameters (central and portal vein hydrostatic pressure, plasma and lymph oncotic pressure, diffusion coefficients); **(B)** model of carbohydrate metabolism encompassing glycolysis, glyconeogenesis and glycogen synthesis and utilization. These pathways comprise the enzymes Glucokinase (GK), Glucose-6-phosphate isomerase (GPI), Phosphofructokinase 1 (PFK1), Aldolase (ALD), Triosephosphate isomerase (TPI), Glyceraldehydephosphate dehydrogenase (GAPDH), Phosphoglycerate kinase (PGK), Phosphoglycerate mutase (PGM), Enolase (EN), Pyruvate kinase (PK) Lactate dehydrogenase (LDH), Glucose-6-phosphate phosphatase (G6P), Phosphofructokinase 2 (PFK2), Fructose-2,6-bisphosphatase (FBP2), Fructose-1,6-bisphosphatase (FBP1), Phosphoenolpyruvate carboxykinase (PEPCK), Pyruvate carboxylase (PC), Nucleoside-diphosphate kinase (NDK), Malate dehydrogenase (MDH), Pyrophosphatase (PPASE), Glucose-1-phosphate isomerase (P1PI), Glycuronosyltransferase (UGT), Glycogen phosphorylase (GP), Glycogen synthase (GS) and transporters (ER <-> cytosol: Glucose-6-phosphate transporter (Glc6PT), Glucose transporter (GlcT); mitochondrion <-> cytosol: Pyruvate transporter (PYRT), Phosphoenolpyruvate transporter (PEPT), Malate transporter (MALT); extern <-> cytosol: Glucose transporter 2 (GLUT2), Lactate transporter (LACT). Enzymes that are phosphorylated or dephosphorylated in response to insulin (Ins) and glucagon (Glu) stimulus are marked by a yellow P, allosteric modification of enzymes is marked by a red A. The model contains the metabolites: glucose (Glc), glucose-6-phosphate (Glc6P), fructose-6-phosphate (Fru6P), fructose-1,6-bisphosphate ($Fru16P_2$), glyceraldehydephosphate (GraP), dihydroxyacetonephosphate (DHAP), 1,3-bisphosphoglycerate (13P2G), 3-phosphoglycerate (3PG), 2-phosphoglycerate (2PG), phosphoenolpyruvate (PEP), pyruvate (Pyr), lactate (Lac), malate (Mal), oxaloacetate (OA), glucose-1-phosphate (Glc1P), UDP-glucose (UDP-glc), glycogen, fructose-2,6-bisphosphate ($Fru26P_2$). The cofactors NADH, NAD, ATP, ADP, UTP and UDP are not treated as dynamic variables. All physiological metabolites produced or consumed in the hepatocyte during glycolysis and gluconeogenesis are comprised into lactate. Figures adapted from Berndt et al. (2018).

and directional transport along the flow of water and blood. Lateral blood flow in the vessel is described by Hagen-Poiseuille law for fluid flow through a cylinder, water flow in the space of Disse is described by Hagen-Poiseuille law for fluid flow in a hollow cylinder. Exchange of water between the vessel and the space of Disse is driven by hydrostatic and oncotic pressure difference between the blood vessel and the space of Disse.

Conceptually, the STU was divided into N_H zones, where N_H is the number of hepatocytes along the porto-central axis. Each zone is made up of the sinusoid volume, the space of Disse and the hepatocyte (**Figure 1A**). Within one zone, the concentration of metabolites and hormones is given by a single value. The mathematical description of the STU model and a complete list of parameters used can be found in Berndt et al. (2018).

Kinetic Model of Hepatocyte Glucose Metabolism

The reaction scheme for the glucose metabolism of a single hepatocyte is depicted in **Figure 1B**. It consists of the pathways for glycolysis, glyconeogenesis, glycogen synthesis and degradation. The time-dependent variation of metabolite concentrations is given by first-order differential equations. The liver specific enzymatic rate laws take into account substrate regulation, allosteric regulation and hormonal regulation by hormone-dependent reversible phosphorylation (Bulik et al., 2016).

Kinetic Model of Hormonal Signaling

The pancreatic hormones glucagon and insulin are released into the portal vein in response to the plasma glucose concentration and are partially cleared during their passage through the liver. Hence, there is a difference between their plasma concentrations determined in peripheral blood samples and effective intra-hepatic concentrations. This difference was taken into account by setting the concentration values of insulin and glucagon in the periportal blood to the 2-fold of their plasma values (Balks and Jungermann, 1984). The rate of intra-hepatic hormone clearance via receptor binding and subsequent endocytosis was put proportional to the binding and signaling strength of the hormone. We used empirical transfer functions to describe the relationship between glucose and hormone concentrations in the plasma and the relationship between and the phosphorylation

state of interconvertible enzymes as described in Bulik et al. (2016). A detailed description of the functions and their construction can be found in Berndt et al. (2018).

Kinetic Model of Protein Turnover

The temporal change of the protein level P^{ENZ} of a metabolic enzyme (ENZ) is given by the difference between the rates of protein synthesis $v_{syn}^{ENZ}(E)$ and protein degradation $v_{deg}^{ENZ}(E)$:

$$\frac{d}{dt}P^{ENZ} = v^{ENZ}(E) = v_{syn}^{ENZ}(E) - v_{deg}^{ENZ}(E) \quad (1)$$

The right-hand side of equation (1), $v^{ENZ}(E)$, represents the turnover rate of the enzyme protein. It is controlled by modulators affecting either the synthesis or the degradation or both. Note that the enzyme level P^{ENZ} scales linearly with the maximal rate of the enzyme. The rate equations of protein synthesis and degradation both depend on the momentary concentration of at least one of the four modulators E_i, $i = 1$ (insulin), $i = 2$ (glucagon), $i = 3$ (glucose), $i = 4$ (oxygen) considered in the model. The general structure of the rate equation for the protein synthesis of enzyme ENZ reads.

$$v_{syn}^{ENZ} = k_{syn}^{ENZ} \prod_{i=1}^{4} (k_i^{ENZ} \pm f_i^{ENZ}) \quad (2)$$

where k_i^{ENZ} is a constant determining the basal synthesis rate and f_i is a nonlinear function of the i-th modulator. The "+" sign holds if E_i is an activator (inductor) of protein synthesis, the (–) sign holds If E_i is an inhibitor (repressor) . If E_i has not been reported so far to exert an effect on the protein synthesis of enzyme ENZ it holds $k_i^{ENZ} = 1$ and $f_i^{ENZ} = 0$ Numerical values for the rate constants k_{syn}^{enz} and k_{deg}^{enz} were fixed in such a manner that for a normal 24 h plasma profile (see below) the zone- and time averaged protein levels coincided with the stationary protein levels as reported in Bulik et al. (2016). Numerical values of all other kinetic parameters were obtained by adjusting the rate equations to experimentally determined protein levels at varying concentrations of the four possible modulators (see **Supplement 1**). **Table 1** depicts the rate equations for the synthesis and degradation of those enzymes of hepatic glucose metabolism possessing in the model timely variable protein levels.

In order to quantify the sensitivity of the turnover rate $v^{ENZ}(E)$ of a protein against small changes of an modulator E, we used the sensitivity (elasticity) coefficient as defined in metabolic control analysis:

$$SV^{ENZ} = \frac{E}{v^{ENZ}(E)} \frac{\partial v^{ENZ}(E)}{\partial E} \quad (3)$$

Figure 2 depicts the sensitivity coefficients for the turnover rates of the nine enzyme proteins with variable expression level as function of the four modulators oxygen (I), glucagon (II), insulin (III) and glucose (IV). Except for the sensitivities of the PEPCK and G6PP turnover with respect to glucagon and glucose, respectively, the extremum of all other sensitivity characteristics lies within the reported physiological range of the related modulators (green-shaded areas in **Figure 2**). The sensitivity of G6PP turnover with respect to glucose becomes important in the diabetic case, where glucose levels can exceed 20 mM (see below).

RESULTS

Dynamic Metabolic Zonation in a Well-Fed State of the Rat

First, we used the model to simulate the temporal variation of enzyme abundances, metabolite concentrations and fluxes within the various zones along the porto-central axis of the STU. The simulation was initiated with identical abundance of enzymes along the sinusoid which we set to the stationary mean protein abundance used in Bulik et al. (2016). We used as model input the diurnal glucose profile reported for the healthy normal liver of a fed rat (La Fleur et al., 1999) and carried out the numerical integration of the model over several 24 h cycles until there was no change in the 24 h enzyme and metabolite profiles.

Even with identical enzyme abundances across all hepatocytes, there occurs a progressive decline of hormone plasma levels from the portal to the central pole due to the ongoing hormone uptake by hepatocytes in each zone. Moreover, oxygen uptake in one zone diminishes the available oxygen pressure seen by the cells in the adjacent zone toward the pericentral pole. As oxygen is not part of the model, we assumed a linear decrease in oxygen partial pressure from 90 mmHG in the periportal zone to 35 mm HG in the pericentral zone (Jungermann and Kietzmann, 2000; Allen et al., 2005). These initial gradients of hormones, glucose and oxygen feed back to the level of metabolic enzymes so that finally zone-dependent patterns of both enzyme abundances and metabolic variables (see **Figures 3**, **4**) are generated.

Figures 3A–C depicts the timely variation of glucose, insulin, glucagon in various sinusoidal compartments. Intriguingly, the highest glucose concentrations in the very portal zone (see red curve in **Figure 3A**) are paralleled by the lowest glucose concentrations in the very central zone (green curve). This seemingly paradoxical situation is due to the fact that the high level of insulin and low level of glucagon strongly increase the glucose uptake capacity of hepatocytes such that the otherwise strong zone-dependent differences in the glucose exchange flux (see **Figure 3E**) almost disappear. The simulation also reveals large zone-dependent differences in the cellular dynamics of glycogen (**Figure 3D**). The variation of the glycogen content in portal cells is much more pronounced than in central cells.

The time-dependent variation in the protein levels of key glycolytic and gluconeogenetic enzymes in different zones are depicted in **Figure 4**. The uniform overall shape of the curves reflects essentially the daily variation of the plasma glucose level. Generally, the daily fluctuations of enzyme levels around their 24 h mean hardly exceed 10%. Thus, as long as the liver is repeatedly confronted with the same 24 h plasma profile of metabolites and hormones, timely variations of protein levels should have only a marginal impact on the hepatic control of the plasma glucose level.

TABLE 1 | Synthesis and degradation rates of the regulatory enzymes of hepatic carbohydrate.

Enzyme name	v_{syn}^{ENZ}	v_{deg}^{ENZ}	References
Glucose transporter	$k_{syn}^{glcT} \cdot \left(k_1 + k_2 \frac{glc_{ext}}{glc_{ext}+K_{glc_{ext}}}\right)$ $k_{syn}^{glcT} = 6.1 \cdot 10^{-3}$ $k_1 = 0.8$ $k_2 = 6$ $K_{glc_{ext}} = 15\ mM$	k_{deg}^{glcT} $k_{deg}^{glcT} = \frac{\ln(2)}{40}$	Postic et al., 1993; Weinstein et al., 1994
Glucokinase	$k_{syn}^{gk} \cdot \left(k_1 - k_2 \frac{o_2^n}{o_2^n+K_{o_2}^n}\right) \cdot \left(k_3 \frac{ins}{ins+K_{ins}}\right)$ $k_{syn}^{glcT} = 6.5 \cdot 10^{-3}$ $k_1 = 2$ $k_2 = 1$ $K_{o_2} = 80\ mmHG$ $n = 15$ $k_3 = 10$ $K_{ins} = 500\ pM$	k_{deg}^{gk} $k_{deg}^{gk} = \frac{\ln(2)}{15}$	Dice and Goldberg, 1975; Sibrowski et al., 1981, 1982; Iynedjian et al., 1989; Kietzmann et al., 1997
Glucose-6-phosphatase	$k_{syn}^{g6p} \cdot \left(k_1 - k_2 \frac{glucagon^{n1}}{glucagon^{n1}+K_{glucagon}^n}\right) \cdot \left(k_3 + k_4 \cdot k_{eff} \frac{glc_{ext}^{n2}}{glc_{ext}^{n2}+K_{glc_{ext}}^{n2}}\right)$ $k_{syn}^{g6p} = 1.16 \cdot 10^{-2}$ $k_1 = 1$ $k_2 = 0.8$ $n1 = 3$ $K_{glucagon} = 100\ pM$ $k_3 = 1$ $k_4 = 15$ $k_{eff} = 0.3$ $K_{glc_{ext}} = 17\ mM$ $n2 = 20$	k_{deg}^{g6p} $k_{deg}^{g6p} = \frac{\ln(2)}{48}$	Leskes et al., 1971; Argaud et al., 1996; Massillon, 2001
Phosphofructokinase 1	k_{syn}^{pfk1} $k_{syn}^{pfk1} = 7.8 \cdot 10^{-3}$	k_{deg}^{pfk1} $k_{deg}^{pfk1} = \frac{\ln(2)}{22+k_2 \cdot \frac{ins^n}{ins^n+K_{ins}^n}}$ $k_2 = 80\ h$ $K_{ins} = 100\ pM$ $n = 1.5$	Dunaway and Weber, 1974; Dunaway et al., 1978
Fructosebis-phosphatase 1	$k_{syn}^{fbp1} \cdot \left(k_1 + k_2 \cdot \frac{glu^n}{glu^n+K_{glu}^n}\right)$ $k_{syn}^{fbp1} = 2.99 \cdot 10^{-2}$ $k_1 = 0.25$ $k_2 = 1$ $K_{glu} = 100\ pM$ $n = 3$	k_{deg}^{fbp1} $k_{deg}^{g6p} = \frac{\ln(2)}{40}$	Dice and Goldberg, 1975; Zalitis and Pitot, 1979; el-Maghrabi et al., 1991
Phosphofructo-kinase 2/Fructosebis-phosphatase 2	$k_{syn}^{pk} \cdot \left(k_1 - k_2 \cdot \frac{o_2^n}{o_2^n+K_{o_2}^n}\right) \cdot \left(k_3 - k_4 \frac{glu}{glu+K_{glu}}\right)$ $k_{syn}^{pfk2} = 1.1 \cdot 10^{-2}$ $k_1 = 2$ $k_2 = 1$ $K_{o_2} = 75\ mmHG$ $n = 10$ $k_3 = 1$ $k_4 = 1$ $K_{glu} = 80\ pM$	k_{deg}^{pfk2} $k_{deg}^{g6p} = \frac{\ln(2)}{69}$	Dunaway and Weber, 1974; Dunaway et al., 1978; Rosa et al., 1993; Minchenko et al., 2003
Pyruvate kinase	$k_{syn}^{pk} \cdot \left(k_1 - k_2 \cdot \frac{o_2^n}{o_2^n+K_{o_2}^n}\right) \cdot \left(k_3 - k_4 \frac{glu}{glu+K_{glu}}\right) \cdot \left(k_5 + k_6 \frac{ins^{n2}}{ins^{n2}+K_{ins}^{n2}}\right)$ $k_{syn}^{pk} = 1.06 \cdot 10^{-2}$ $k_1 = 3.2$ $k_2 = 1$ $K_{o_2} = 75\ mmHG$ $n = 10$ $k_3 = 1$ $k_4 = 0.5$ $K_{glu} = 150\ pM$ $k_5 = 0.2$ $k_6 = 1$ $K_{ins} = 500\ pM$ $n2 = 2$	k_{deg}^{pk} $k_{deg}^{pk} = \frac{\ln(2)}{69}$	Hopkirk and Bloxham, 1979, 1980; Noguchi et al., 1985; Wölfle and Jungermann, 1985
Pyruvate carboxylase	$k_{syn}^{pc} \cdot \left(k_1 + k_2 \cdot \frac{glu}{glu+K_{glu}}\right)$ $k_{syn}^{pc} = 1.47 \cdot 10^{-2}$ $k_1 = 0.1$ $k_2 = 1$ $K_{glu} = 150\ pM$	k_{deg}^{pc} $k_{deg}^{pc} = \frac{\ln(2)}{110}$	Weinberg and Utter, 1979, 1980
Phosphoenol-pyruvate Carboxykinase	$k_{syn}^{pepck} \cdot \left(k_1 + k_2 \cdot \frac{o_2^{n1}}{o_2^{n1}+K_{o_2}^{n1}}\right) \cdot \left(k_3 + k_4 \frac{glu^{n2}}{glu^{n2}+K_{glu}^{n2}}\right) \cdot \left(k_5 - k_6 \frac{ins}{ins+K_{ins}}\right)$ $k_{syn}^{pepck} = 3.43 \cdot 10^{-2}$ $k_1 = 0.5$ $k_2 = 2$ $K_{o_2} = 75\ mmHG$ $n1 = 10$ $k_3 = 1$ $k_4 = 3$ $n2 = 0.5$ $K_{glu} = 0.2\ pM$ $k_5 = 1$ $k_6 = 0.8$ $K_{ins} = 100\ pM$	k_{deg}^{pepck} $k_{deg}^{pepck} = \frac{\ln(2)}{13}$	Nauck et al., 1981; Christ et al., 1988; Gabbay et al., 1996

In contrast to the modest time-dependent variations of protein levels, the computed zone-dependent differences of enzyme levels display a large scatter. The maximal differences between the enzyme endowment of hepatocytes closest to the portal and central pole lie between 0.1 [e.g., glucose transporter (glcT) and phosphofructokinase 1 (pfk1)] and 4.5 [phosphoenolpyruvate kinase (pepck)]. For the validation of these computational predictions, we calculated the 24 h-average protein levels of the first (most portal) and last (most central) hepatocyte and compared the ratio of the computed average protein levels with experimental data (see first columns for each enzyme in **Figure 5**). We further compared the ratio of 24 h- and zone-averaged mean protein levels between a fed and fasted rat and a diabetic and normal rat.

This analysis provided a good concordance between theoretical and experimental results. The only exception is the pyruvate carboxylase, a key regulatory enzyme of gluconeogenesis, were portal to central gradients could not be univocally explained by the reported oxygen dependency. Oxygen dependency accounts only for about 35% percent of the observed zonation (see **Table 1** and **Supplement 1**).

Dynamic Metabolic Zonation of the Liver During Adaptation to Fasting

Next, we studied how the zonation of metabolic enzymes is affected if the liver has to cope with a fundamentally different nutritional regime. To this end, we simulated the zone-dependent dynamic changes of protein levels and metabolites during the transition from a fed state of the rat to a fasting state. The simulation started with the stable 24 h zonated enzyme profile that is established if the liver experiences recurrently the same plasma profile of a fed rat (see above). At time $t = 24$ h, the

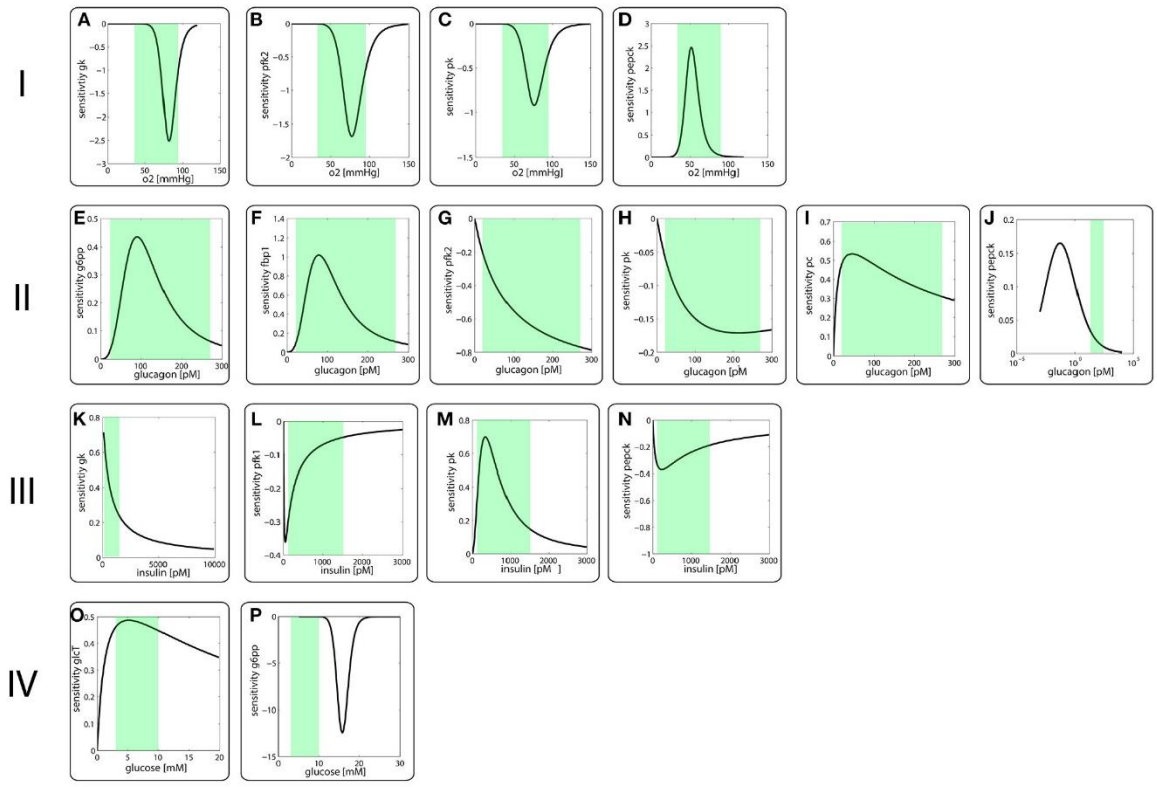

FIGURE 2 | Sensitivity coefficients of protein turnover rates defined in equation (3) as function of modulator concentrations.
I Sensitivity of protein turnover rates with respect to oxygen of **(A)** GK, **(B)** FBPFK2, **(C)** PK, **(D)** PEPCK
II Sensitivity of protein turnover rates with respect to **(E)** G6PP, **(F)** FBP1, **(G)** FBPFK2, **(H)** PK, **(I)** PC, **(J)** PEPCK
III Sensitivity of protein turnover rates with respect to **(K)** GK, **(L)** PFK1, **(M)** PK, **(N)** PEPCK
IV Sensitivity of protein turnover rates with respect to **(O)** GlcT, **(P)** G6PP
The green-shades areas indicate the reported physiological concentration range of the respective modulator.

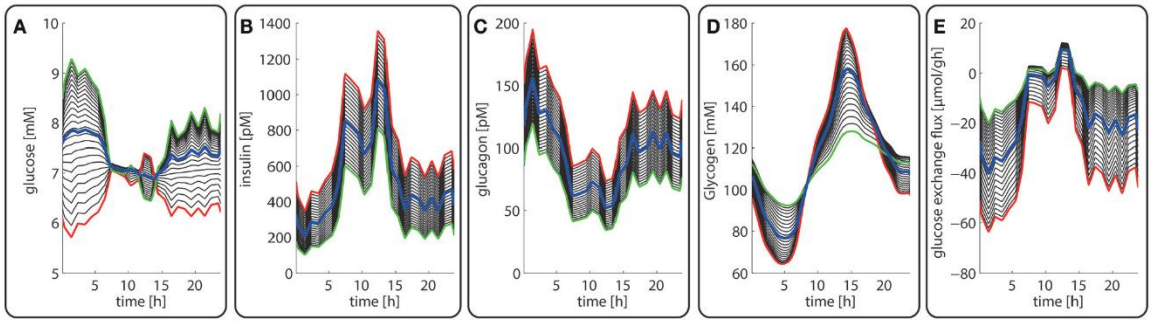

FIGURE 3 | Diurnal variations in the plasma levels of glucose **(A)**, insulin **(B)**, glucagon **(C)**, cellular glycogen **(D)** and the glucose exchange flux **(E)** in different zones along the porto-central axis. The different curves refer to different spatial positions of hepatocytes, counted from periportal (red curve) to percentral (green curve). The bold blue line refers to the means values of the shown variable. Note that the red curves (= most portal cell) for the hormones and glucose are identical with their plasma profiles.

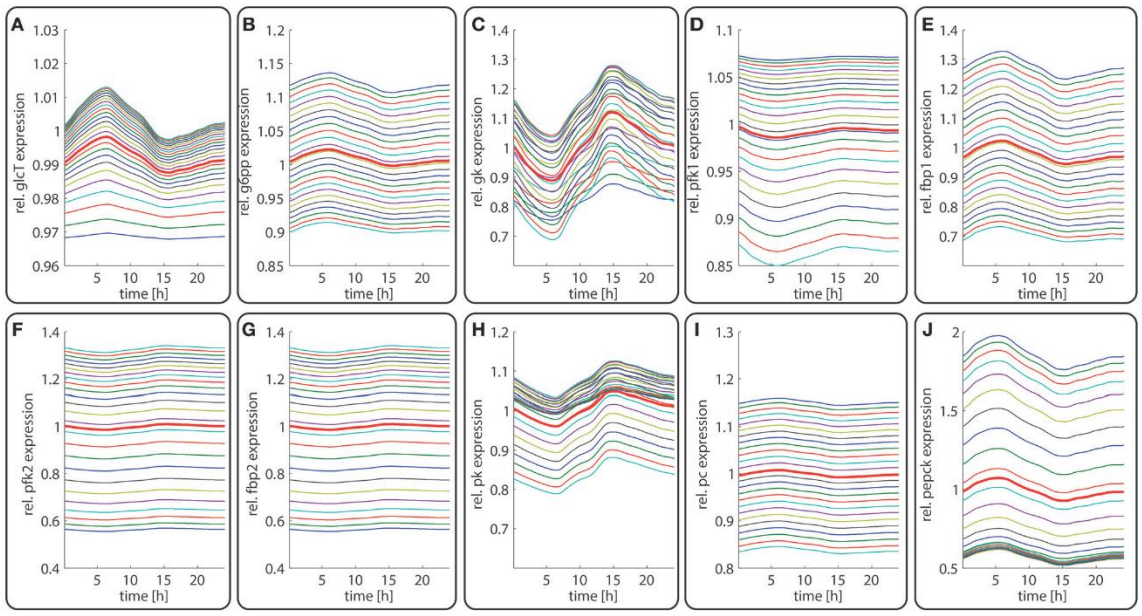

FIGURE 4 | Diurnal variations in the relative abundance of glycolytic and gluconeogenetic enzymes within hepatocytes along the porto-central axis of a well-fed rat. The curves illustrate the relative deviation of protein abundances from the overall spatial and 24h- mean (=24 h mean of the bold red curve). From the top to the bottom, the different curves refer to the spatial position of the hepatocyte counted from periportal to percentral. The bold red line refers to the average protein abundance across all cells. **(A)** GlcT, **(B)** G6PP, **(C)** GK, **(D)** PFK1, **(E)** FBPPFK1, **(F)** PFK2, **(G)** FBPPFK2, **(H)** PK, **(I)** PC, **(J)** PEPCK.

plasma profile of the fed rate was replaced by plasma profile of a fasted rat (La Fleur et al., 1999). The latter was only available for a time range of 24 h of fasting. After about 16 h of fasting, stable values of plasma metabolites were reached. Therefore, we used for time points $t > 48$ h (i.e., >24 h of fasting) for the model input a plasma profile that was composed of 6 repetitions of the last part (16–24 h) of the 24 h fasting plasma profile. As shown in **Figure 6**, the fed-to-fasting transition evokes a significant rise in the abundance of key gluconeogenetic enzymes (GlcT, FBP1, PC, PEPCK) and drop in the abundance of key glycolytic enzymes (GK, PFK1, PFK2, FBP2, PK) in all zones. For two enzymes, the GlcT and the PEPCK, the zone-dependent protein differences become more pronounced compared to the fed state. By contrast, for the GK, FBP1, GSPP, and PK the zone-dependent protein differences became smaller.

The computed changes of enzyme profiles toward a more gluconeogenetic phenotype are accompanied by significant alterations of the intra-sinusoidal glucose gradient and the zone-dependent differences in the glucose exchange rate (**Figure 7**). Compared with the fed state, the porto-venous glucose difference becomes much larger in the fasted state (**Figure 7A**). The same holds for the glucose exchange rate (**Figure 7D**).

In agreement with experimental data (Babcock and Cardell, 1974), the glycogen stores are almost depleted after about 1 day of fasting when the levels of insulin and glucagon have adopted a new stable temporal profile. Notably, also for the fasted state, the computed average protein abundance ratios are in good agreement with experimental data which further substantiates the reliability of the model (see **Figure 5**).

Figure 8 illustrates the importance of dynamic zonation for the adaptation of the porto-venous glucose difference (AVGD) to a specific nutritional regime. Regulation of interconvertible enzymes by hormone-dependent phosphorylation alone, i.e., at fixed protein levels of the fed state (blue line), would result in an AVGD of about 3.5 mM for the typical range of portal glucose concentrations in the fasted state (red shaded area). Dynamic adaption of protein levels enlarges the AVGD to about 7 mM (red line) thus rendering the liver to a strong glucose producer in the fasted state.

Dynamic Metabolic Zonation of the Liver in Diabetes Type II ("Diabetic Liver")

Late diabetes type 2 is characterized by long persistence of high postprandial plasma glucose levels, reduced insulin levels (hypo-insulinemia) and elevated glucagon levels (hyper-glucagonemia). It is mainly the shift in the insulin/glucagon ratio that renders the liver to a glucose producer which on top of the insulin-resistant muscle and adipose tissue contributes to high plasma glucose levels. We tested whether our model can also correctly describe this metabolic abnormality and the observed changes of protein abundances in different zones. To this end, we used the glucose-hormone transfer function constructed for the diabetic case (see Bulik et al., 2016) to calculate the phosphorylation state of interconvertible enzymes and confronted the model over

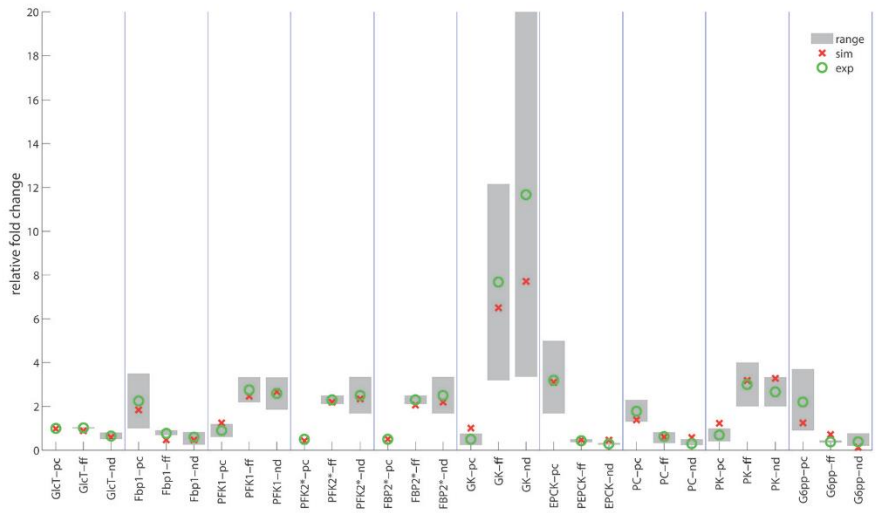

FIGURE 5 | Ratio of enzyme levels in hepatocytes. Red circles indicate the computed ratio of protein levels. Green circles and gray bars indicate the mean value and the range of variability of various experimentally determined ratios. First columns (pc): Portal-to-central ratios (= 24h-averaged protein levels between hepatocyte #1 and hepatocyte # 25) for the well-fed state of the rat. Experimental data were taken from (Sharma et al., 1964; Katz et al., 1977a,b; Trus et al., 1980; Jungermann and Katz, 1982, 1989; Probst et al., 1982; Teutsch and Lowry, 1982; Miethke et al., 1985; Quistorff, 1985; Wölfle and Jungermann, 1985; Morselt et al., 1987; Chen and Katz, 1988; Wals et al., 1988; Evans et al., 1989; Frederiks et al., 1991; Jones and Titheradge, 1996; Minchenko et al., 2003). Second columns (ff): Fed-to-fasted ratios of 24h- and zone-averaged mean enzyme levels. Experimental data taken from (Dipietro and Weinhouse, 1960; Wimhurst and Manchester, 1970b; Ballard and Hopgood, 1973; Bock et al., 1973; Zalitis and Pitot, 1979; Cladaras and Cottam, 1980; Neely et al., 1981; Bahnak and Gold, 1982; Van Schaftingen and Hers, 1983; Donofrio et al., 1984; Colosia et al., 1988; Crepin et al., 1988; Thorens et al., 1990; Giffin et al., 1993; Gannon and Nuttall, 1997). Third columns (nd): Normal-to-diabetic ratios of 24h- and zone-averaged mean enzyme levels. Experimental data taken from Dipietro and Weinhouse, 1960; Salas et al., 1963; Exton and Park, 1965; Wimhurst and Manchester, 1970a; Chang and Schneider, 1971; Dunaway et al., 1978; Weinberg and Utter, 1980; Neely et al., 1981; Donofrio et al., 1984; Miethke et al., 1985; Colosia et al., 1988; Crepin et al., 1988; Thorens et al., 1990; Miralpeix et al., 1992; Slieker et al., 1992; Gannon and Nuttall, 1997; Raju et al., 1999; Manna and Jain, 2012.

4 days repeatedly with a 24 h glucose profile of a diabetic rat until an almost stable 24 h pattern of protein abundances had established (**Figure 9**). As shown in **Figure 9D**, all hepatocytes work permanently as glucose producers, i.e., at all time points of the day the intra-sinusoidal glucose concentration increases along the portal-central axis (**Figure 9A**). The glycogen reserves are drastically diminished and the different time courses of glycogen emptying and filling between portal and central regions (see **Figure 2D**) are completely abolished. Taken together, the zonation of glucose metabolism in the diabetic liver bears a strong resemblance with that of the fasted liver. It is important to note that even in this pathophysiological case the computed average portal-to-central protein abundance ratios are in good agreement with experimental data (see **Figure 5**).

DISCUSSION

Metabolic Zonation of Hepatic Glucose Metabolism Is Driven by Concentration Gradients of Hormones and Metabolites

In this work we used a mathematical model to study the dynamic zonation of the hepatic glucose metabolism. To this end we extended our previously published multi-scale tissue model of the hepatic carbohydrate metabolism (Berndt et al., 2018) by rendering the protein levels of key regulatory enzymes of glycolysis and gluconeogenesis as dynamic model variables which are controlled by timely variable synthesis and degradation in dependence from the concentration of the four modulators glucose, insulin, glucagon and oxygen. The model correctly replicates experimentally determined protein levels in different zones of the liver acinus as well as the adaptation of the liver to a well-fed, fasted and diabetic state. From this we draw four main conclusions. (1) Zonation of the hepatic glucose metabolism is a necessary consequence of the fact that the expression of key regulatory enzymes is controlled by modulators that display a porto-central concentration gradient along the sinusoid. (2) Mechanisms controlling the adaptation of enzyme abundances to varying external conditions necessarily lead to the zonation of hepatic carbohydrate metabolism. (3) The four modulators considered in the model are sufficient to describe the dynamic zonation of the glucose metabolism of the a normal liver. (4) The use of phenomenological transfer functions which directly relate the protein turnover to known modulators of gene expression appears a promising modeling strategy to include variable protein levels in kinetic models in view of the fact that in a foreseeable future explicit kinetic modeling of complex gene-regulatory network is out of reach.

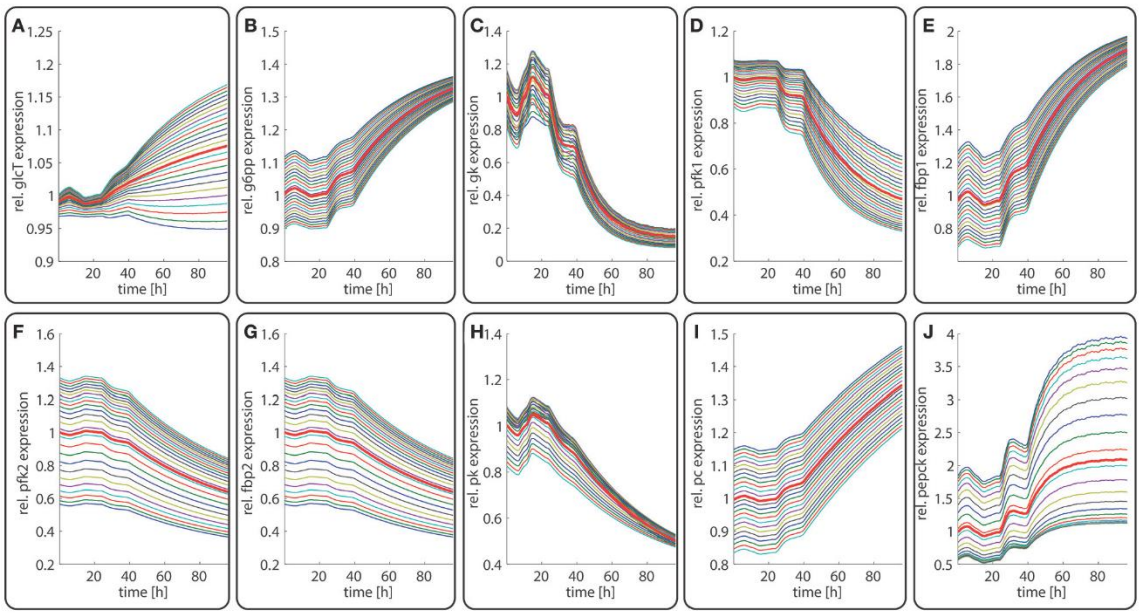

FIGURE 6 | Diurnal variations in the relative abundance of glycolytic and gluconeogenetic enzymes within hepatocytes along the porto-central axis during the transition from a fed state ($t = 0$–24 h) to a fasted state ($t > 24$ h). The curves illustrate the relative deviation of protein abundances from the overall spatial and 24 h mean (=24 h mean of the bold red curve). From the top to the bottom, the different curves refer to the spatial position of the hepatocyte counted from periportal to percentral. The bold red line refers to the average protein abundance across all cells. The vertical dotted line indicates onset of the starvation period. **(A)** GlcT, **(B)** G6PP, **(C)** GK, **(D)** PFK1, **(E)** FBPPFK1, **(F)** PFK2, **(G)** FBPPFK2, **(H)** PK, **(I)** PC, **(J)** PEPCK.

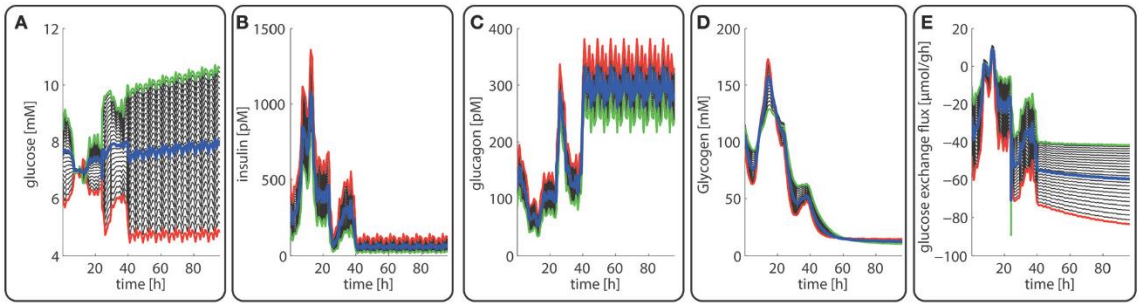

FIGURE 7 | Diurnal variations in the plasma levels of glucose **(A)**, insulin **(B)**, glucagon **(C)**, cellular glycogen **(D)** and the glucose exchange flux **(E)** in different zones along the porto-central axis during the transition from a well-fed state ($t = 0$–24 h) to a fasted state ($t > 24$ h) of the rate. The different curves refer to different spatial positions of hepatocytes, counted from periportal (red curve) to percentral (green curve). The bold blue line refers to the means values of the shown variables. Note that the red curves (= most portal cell) for the hormones and glucose are identical with their plasma profiles.

The Proposed Multi-Scale Model Encompasses All Levels of Metabolic Regulation

An important feature of the cellular metabolic network of the liver is the ability to adapt its functional output to varying external conditions such as changes in nutrient supply and varying hormone levels. These adaptive mechanisms operate at two different time scales. The short term adaptation occurs within seconds or minutes and is brought about by activity changes in the present metabolic enzymes by substrate availability, allosteric regulation and reversible phosphorylation. The second adaptive mechanism operates within hours or days and is brought about by changes in the enzyme abundances. It is already known for a long time that the total protein content

of liver enzymes may largely vary owing to enhanced protein degradation during fasting (providing glucogenic amino acids as substrate for gluconeogenesis) mediated by the hormone glucagon or enhanced protein synthesis by the hormone insulin (Hopgood et al., 1980). However, such general changes of the protein content do not tell anything about the changes in the abundance of individual enzymes, whose expression by insulin and glucagon differs profoundly. Therefore, it was necessary to develop empirical rate laws for the synthesis and degradation of individual enzymes. This phenomenological approach was chosen since currently biochemical information is insufficient to establish molecular-resolved kinetic models which include, for example, the interaction of transcription factors among each other and with specific DNA promotor regions, the processing of mRNA and the regulation of mRNA translation by micro RNAs and RNA-binding proteins. For example, PEPCK, probably the best-studied gluconeogenetic enzyme, is regulated by at least a dozen transcription factors with partially unknown interactions (Yang et al., 2009). Even if it was possible to explicitly model the mRNA transcription for individual enzymes, there is still a big gap in understanding post-transcriptional regulation and the processes of post-translational modification.

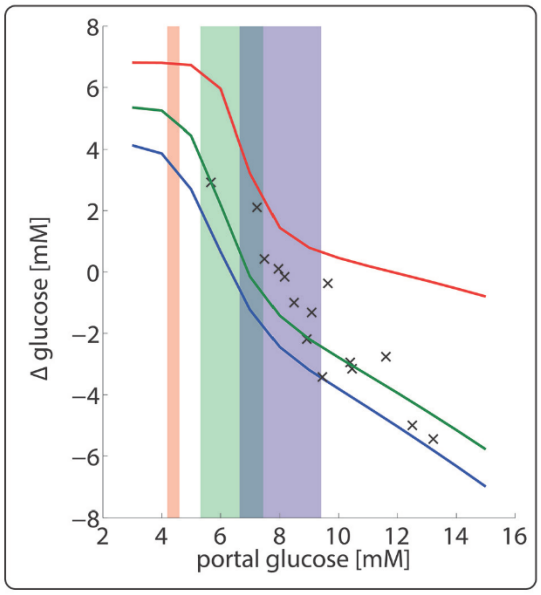

FIGURE 8 | Hepatic porto-venous glucose difference (AVGD) for the well-fed and fasted nutritional state. The daily variations of plasma glucose in the fasted, fed and well-fed state are indicated by the red-, green- and blue-shaded areas. The solid lines represent the AVGD if in the fasted state (red), fed state (green) and the well-fed state (blue). Crosses depict experimentally measured AVGD (Huang and Veech, 1988).

Metabolic Response of the Liver to Varying Nutritional Regimes

Our simulations suggest that in the presence of a constant daily nutritional regime the diurnal variation of enzyme abundances should be fairly moderate in the range of 10–20% around the mean. This is a lot less than daily variations in the abundance of the key regulatory enzyme of cholesterol synthesis, ßHMG-CoA reductase (Kirkpatrick et al., 1980), exhibiting a pronounced circadian rhythm or some enzymes of the amino acid metabolism as, for example, tyrosine transaminase the activity of which is almost four times as great several hours after nightfall as it is in the morning (Wurtman, 1974). In contrast, much larger changes of glycolytic and gluconeogenetic enzyme levels are elicited by a switch from well-fed to fasting conditions and vice versa. This metabolic adaptation occurs within a time span of several days (see **Figure 6**) and enables vertebrates to maintain the plasma glucose level in the absence of food. The slow change of enzyme concentration profiles implies that the capability of the fasted liver to clear a sudden excess of plasma glucose is diminished (impaired glucose tolerance) as the capacity of glycolytic enzymes and enzymes of the glycogen pathway a downregulated (Bulik et al., 2016). Intriguingly, there appears to be a striking similarity in the adaptive response of the liver to fasting conditions and diabetes type 2. In our modeling approach, this is mainly due to the fact that in both physiological settings the strong effect of insulin on the expression of glycolytic and gluconeogenetic

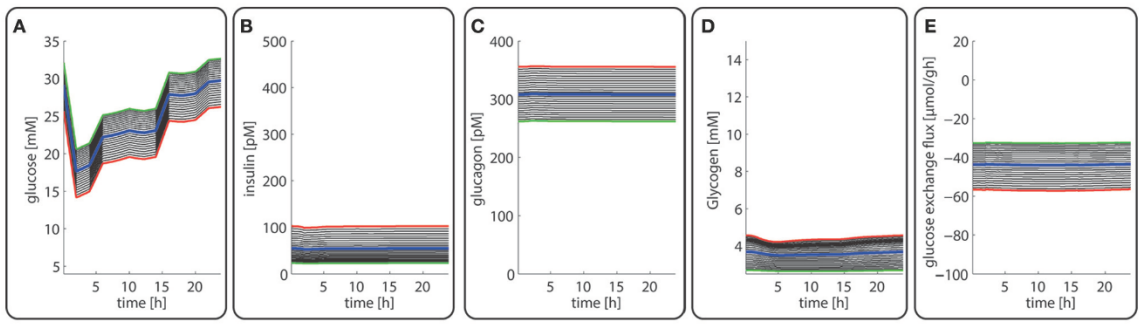

FIGURE 9 | Diurnal variations in the plasma levels of glucose **(A)**, insulin **(B)**, glucagon **(C)**, cellular glycogen **(D),** and the glucose exchange flux **(E)** in different zones along the porto-central axis of a diabetic rat.

enzymes is diminished whereas the effect of glucagon is more pronounced. As demonstrated in a previous model-based simulation study (König and Holzhütter, 2012), exposing the permanently glucose-releasing "starved" liver of the diabetic patient to a rigorous insulin treatment at persistently elevated glucagon level may increase the risk of severe hypoglycaemia. Thus, owing to the equally strong impact of both insulin and glucagon on the expression and phosphorylation state of liver enzymes, reconverting the "starved" liver of the diabetic patient into the normal metabolic phenotype requires the normalization of the plasma levels of both hormones.

Main Limitations of the Model and Outlook for Future Model Extensions

The used multiscale tissue model comprises a number of simplifications of the true anatomical structure of the liver which may impact on the simulated intra-sinusoidal concentration gradients of hormones and metabolites. For example, the blood flow rate within the pericentral zone of the sinusoid may vary if a sinusoid spreads out, forms anastomoses or merges with another sinusoid (Rappaport et al., 1954), anatomic peculiarities of liver parenchyma that are not yet considered in the STU model. Also, the number of periportal hepatocytes is higher (∼2–3-fold) compared to pericentral hepatocytes. Regarding the concentration gradient of oxygen, hormones and metabolites in the sinusoid it may be of relevance that the terminal branches of the hepatic artery rarely join with the portal vein already before the blood enters the sinusoids, as presumed in our model. In the vast majority the merger of arterial blood with blood from the portal vein, occurs a few cells downstream within the sinusoid (Ekataksin and Kaneda, 1999) resulting in a local increase of the concentration of oxygen concentration at this site. Despite these limitations, the model correctly describes glucose exchange rates, gradients and indicator dilution curves for a structurally normal liver (Berndt et al., 2018). Hence, the functional implications of the above limitations and other neglected aspects of the real topology of liver tissue remain unclear. Therefore, in future work we aim to embed our metabolic cell model in a 3-D reconstructions of a mouse lobule (Hoehme et al., 2017).

The rate laws presented in this paper are effective transfer functions describing directly the relation between modulators (nutrients and hormones) and the turnover rate of a protein. Usage of effective transfer function raises the question which properties of the underlying regulatory network have to be captured. Obviously, not all known modulators of protein synthesis and degradation have been considered in the model. Ground-breaking experiments pointed initially to the oxygen gradient as the most important driving force of metabolic zonation (Jungermann and Kietzmann, 1997, 2000). Later experiments with isolated hepatocytes incubated with varying concentrations of insulin or glucagon (Probst et al., 1982) revealed an important role of these hormones for the establishment of liver zonation. Meanwhile a lot more potential modulators of metabolic zonation have been described in the literature, among them Wnt/β-catenin pathway (Torre et al., 2010; Vasilj et al., 2012), MAPK/ERK pathway (Zeller et al., 2013), Hnf4-alpha (Colletti et al., 2009), or thyroid hormones (Weinberg and Utter, 1979). However, as demonstrated in this study, the dynamic zonation of the glucose metabolism can be well described in different physiological settings by taken into account only the four modulators oxygen, glucose, glucagon and insulin. The central role of oxygen, glucose, glucagon and insulin for the dynamic zonation of the glucose metabolism does not exclude that morphogens and growth factors may have an important role in the zonation of other metabolic subsystems (Gebhardt and Matz-Soja, 2014). For example, the expression of the glutamine synthetase is restricted to last few hepatocytes close to the venous pole. Complementary, the urea cycle enzyme carbamoylphosphate synthetase I (CPS I) is present in the periportal, intermediate, and the first few layers of the perivenous zone. It has been clearly demonstrated that Wnt/ß-catenin signaling pathway plays a central role in the stable maintenance of these peculiar zonation profiles (Burke et al., 2009).

CONCLUSION

In summary, we propose a self-consistent model of liver carbohydrate metabolism that consistently takes into account variable gene expression of metabolic enzymes, regulation of metabolic pathways, exchange of metabolites and hormones between the blood and hepatocytes and microperfusion of the liver. Once the input of hormones and nutrients to the periportal region the liver acinus is known, the model allows to compute the metabolic phenotype of individual hepatocytes along the porto-central axis. The local hormone and metabolite concentrations determine the phosphorylation state of the interconvertible enzymes, hormonal clearance rates and expression level of metabolic enzymes. The metabolic phenotype in turn determines the functional output (here: glucose exchange rate) of each hepatocyte and this way the venous glucose output of the acinus. Integration across a representative set of acini yields finally the total glucose output of the liver.

AUTHOR CONTRIBUTIONS

NB developed the concept, implemented the model, carried out the simulation, wrote the manuscript. H-GH developed the concept, advised the implementation of the model, wrote the manuscript.

FUNDING

NB was funded by the German Systems Biology Program "LiSyM," grant no. 31 L0057, sponsored by the German Federal Ministry of Education and Research (BMBF). The funders had no role in study design, data collection and analysis, decision to publish, or preparation of the manuscript.

SUPPLEMENTARY MATERIAL

The Supplementary Material for this article can be found online at: https://www.frontiersin.org/articles/10.3389/fphys.2018.01786/full#supplementary-material

REFERENCES

Allen, J. W., Khetani, S. R., and Bhatia, S. N. (2005). *In vitro* zonation and toxicity in a hepatocyte bioreactor. *Toxicol. Sci.* 84, 110–119. doi: 10.1093/toxsci/kfi052

Argaud, D., Zhang, Q., Pan, W., Maitra, S., Pilkis, S. J., and Lange, A. J. (1996). Regulation of rat liver glucose-6-phosphatase gene expression in different nutritional and hormonal states: gene structure and 5'-flanking sequence. *Diabetes* 45, 1563–1571. doi: 10.2337/diab.45.11.1563

Babcock, M. B., and Cardell, R. R. (1974). Hepatic glycogen patterns in fasted and fed rats. *Am. J. Anat.* 140, 299–337. doi: 10.1002/aja.1001400302

Bahnak, B. R., and Gold, A. H. (1982). Effects of alloxan diabetes on the turnover of rat liver glycogen synthase. Comparison with liver phosphorylase. *J. Biol. Chem.* 257, 8775–8780.

Balks, H. J., and Jungermann, K. (1984). Regulation of peripheral insulin/glucagon levels by rat liver. *Eur. J. Biochem.*141, 645–650. doi: 10.1111/j.1432-1033.1984.tb08240.x

Ballard, F. J., and Hopgood, M. F. (1973). Phosphopyruvate carboxylase induction by L-tryptophan. Effects on synthesis and degradation of the enzyme. *Biochem. J.* 136, 259–264. doi: 10.1042/bj1360259

Berndt, N., Horger, M. S., Bulik, S., and Holzhütter, H. G. (2018). A multiscale modelling approach to assess the impact of metabolic zonation and microperfusion on the hepatic carbohydrate metabolism. *PLoS Comput. Biol.* 14:e1006005. doi: 10.1371/journal.pcbi.1006005

Bock, K. W., Fröhling, W., and Remmer, H. (1973). Influence of fasting and hemin on microsomal cytochromes and enzymes. *Biochem. Pharmacol.* 22, 1557–1564. doi: 10.1016/0006-2952(73)90021-X

Braeuning, A., Ittrich, C., Köhle, C., Hailfinger, S., Bonin, M., Buchmann, A., et al. (2006). Differential gene expression in periportal and perivenous mouse hepatocytes. *FEBS J.* 273, 5051–5061. doi: 10.1111/j.1742-4658.2006.05503.x

Bulik, S., Holzhütter, H. G., and Berndt, N. (2016). The relative importance of kinetic mechanisms and variable enzyme abundances for the regulation of hepatic glucose metabolism-insights from mathematical modeling. *BMC Biol.* 14:15. doi: 10.1186/s12915-016-0237-6

Burke, Z. D., Reed, K. R., Phesse, T. J., Sansom, O. J., Clarke, A. R., and Tosh, D. (2009). Liver zonation occurs through a beta-catenin-dependent, c-Myc-independent mechanism. *Gastroenterology* 136, 2316–2324 e2311–2313. doi: 10.1053/j.gastro.2009.02.063

Chang, A. Y., and Schneider, D. I. (1971). Hepatic enzyme activities in streptozotocin-diabetic rats before and after insulin treatment. *Diabetes* 20, 71–77. doi: 10.2337/diab.20.2.71

Chen, K. S., and Katz, J. (1988). Zonation of glycogen and glucose syntheses, but not glycolysis, in rat liver. *Biochem. J.* 255, 99–104. doi: 10.1042/bj2550099

Christ, B., Nath, A., Bastian, H., and Jungermann, K. (1988). Regulation of the expression of the phosphoenolpyruvate carboxykinase gene in cultured rat hepatocytes by glucagon and insulin. *Eur. J. Biochem.* 178, 373–379. doi: 10.1111/j.1432-1033.1988.tb14460.x

Cladaras, C., and Cottam, G. L. (1980). Turnover of Liver Pyruvate-Kinase. *Arch. Biochem. Biophys.* 200, 426–433. doi: 10.1016/0003-9861(80)90373-2

Colletti, M., Cicchini, C., Conigliaro, A., Santangelo, L., Alonzi, T., Pasquini, E., et al. (2009). Convergence of Wnt signaling on the HNF4 alpha-driven transcription in controlling liver zonation. *Gastroenterology* 137, 660–672. doi: 10.1053/j.gastro.2009.05.038

Colosia, A. D., Marker, A. J., Lange, A. J., el-Maghrabi, M. R., Granner, D. K., Tauler, A., et al. (1988). Induction of rat liver 6-phosphofructo-2-kinase/fructose-2,6-bisphosphatase mRNA by refeeding and insulin. *J. Biol. Chem.* 263, 18669–18677.

Crepin, K. M., Darville, M. I., Hue, L., and Rousseau, G. G. (1988). Starvation or diabetes decreases the content but not the mRNA of 6-phosphofructo-2-kinase in rat liver. *Febs Lett.* 227, 136–140. doi: 10.1016/0014-5793(88)80884-6

Dice, J. F., and Goldberg, A. L. (1975). Statistical-analysis of relationship between degradative rates and molecular-weights of proteins. *Arch. Biochem. Biophys.* 170, 213–219. doi: 10.1016/0003-9861(75)90112-5

Dipietro, D. L., and Weinhouse, S. (1960). Hepatic glucokinase in the fed, fasted, and alloxan-diabetic rat. *J. Biol. Chem.* 235, 2542–2545.

Donofrio, J. C., Thompson, R. S., Reinhart, G. D., and Veneziale, C. M. (1984). Quantification of liver and kidney phosphofructokinase by radioimmunoassay in fed, starved and alloxan-diabetic rats. *Biochem. J.* 224, 541–547. doi: 10.1042/bj2240541

Dunaway, G. A., Leung, G. L., Thrasher, J. R., and Cooper, M. D. (1978). Turnover of hepatic phosphofructokinase in normal and diabetic rats-role of insulin and peptide stabilizing factor. *J. Biol. Chem.* 253, 7460–7463.

Dunaway, G. A., and Weber, G. (1974). Effects of hormonal and nutritional changes on rates of synthesis and degradation of hepatic phosphofructokinase isozymes. *Arch. Biochem. Biophys.* 162, 629–637. doi: 10.1016/0003-9861(74)90225-2

Ekataksin, W., and Kaneda, K. (1999). Liver microvascular architecture: an insight into the pathophysiology of portal hypertension. *Semin. Liver Dis.* 19, 359–382. doi: 10.1055/s-2007-1007126

el-Maghrabi, M. R., Lange, A. J., Kummel, L., and Pilkis, S. J. (1991). The rat fructose-1,6-bisphosphatase gene-structure and regulation of expression. *J. Biol. Chem.* 266, 2115–2120.

Evans, J. L., Quistorff, B., and Witters, L. A. (1989). Zonation of hepatic lipogenic enzymes identified by dual-digitonin-pulse perfusion. *Biochem. J.* 259, 821–829. doi: 10.1042/bj2590821

Exton, J. H., and Park, C. R. (1965). Control of gluconeogenesis in the perfused liver of normal and adrenalectomized rats. *J. Biol. Chem.* 240, 955–957.

Frederiks, W. M., Marx, F., and van Noorden, C. J. (1991). Homogeneous distribution of phosphofructokinase in the rat liver acinus: a quantitative histochemical study. *Hepatology* 14, 634–639. doi: 10.1002/hep.1840140410

Gabbay, R. A., Sutherland, C., Gnudi, L., Kahn, B. B., O'Brien, R. M., Granner, D. K., et al. (1996). Insulin regulation of phosphoenolpyruvate carboxykinase gene expression does not require activation of the Ras/mitogen-activated protein kinase signaling pathway. *J. Biol. Chem.* 271, 1890–1897. doi: 10.1074/jbc.271.4.1890

Gannon, M. C., and Nuttall, F. Q. (1997). Effect of feeding, fasting, and diabetes on liver glycogen synthase activity, protein, and mRNA in rats. *Diabetologia* 40, 758–763. doi: 10.1007/s001250050746

Gebhardt, R., and Matz-Soja, M. (2014). Liver zonation: novel aspects of its regulation and its impact on homeostasis. *World J. Gastroenterol.* 20, 8491–8504. doi: 10.3748/wjg.v20.i26.8491

Giffin, B. F., Drake, R. L., Morris, R. E., and Cardell, R. R. (1993). Hepatic lobular patterns of phosphoenolpyruvate carboxykinase, glycogen synthase, and glycogen phosphorylase in fasted and fed rats. *J. Histochem. Cytochem.* 41, 1849–1862. doi: 10.1177/41.12.8245433

Han, H. S., Kang, G., Kim, J. S., Choi, B. H., and Koo, S. H. (2016). Regulation of glucose metabolism from a liver-centric perspective. *Exp. Mol. Med.* 48:e218. doi: 10.1038/emm.2015.122

Hoehme, S., Friebel, A., Hammad, S., Drasdo, D., and Hengstler, J. G. (2017). Creation of three-dimensional liver tissue models from experimental images for systems medicine. *Methods Mol. Biol.* 1506, 319–362. doi: 10.1007/978-1-4939-6506-9_22

Hopgood, M. F., Ballard, F. J., Reshef, L., and Hanson, R. W. (1973). Synthesis and degradation of phosphoenolpyruvate carboxylase in rat-liver and adipose-tissue-changes during a starvation-refeeding cycle. *Biochem. J.* 134, 445–453. doi: 10.1042/bj1340445

Hopgood, M. F., Clark, M. G., and Ballard, F. J. (1980). Protein-degradation in hepatocyte monolayers-effects of glucagon, adenosine 3'-5'-cyclic monophosphate and insulin. *Biochem. J.* 186, 71–79. doi: 10.1042/bj1860071

Hopkirk, T. J., and Bloxham, D. P. (1979). Studies on the biosynthesis of hepatic pyruvate-kinase and its correlation with enhanced hepatic lipogenesis in meal-trained rats. *Biochem. J.* 182, 383–397. doi: 10.1042/bj1820383

Hopkirk, T. J., and Bloxham, D. P. (1980). Biosynthesis of rat-liver pyruvate-kinase-measurement of enzyme lifetime and the rate of synthesis at weaning. *Biochem. J.* 192, 507–516. doi: 10.1042/bj1920507

Huang, M. T., and Veech, R. L. (1988). Role of the direct and indirect pathways for glycogen synthesis in rat liver in the postprandial state. *J. Clin. Invest.* 81, 872–878. doi: 10.1172/JCI113397

Iynedjian, P. B., Jotterand, D., Nouspikel, T., Asfari, M., and Pilot, P. R. (1989). Transcriptional induction of glucokinase gene by insulin in cultured liver cells and its repression by the glucagon-cAMP system. *J. Biol. Chem.* 264, 21824–21829.

Jones, C. G., and Titheradge, M. A. (1996). Measurement of metabolic fluxes through pyruvate kinase, phosphoenolpyruvate carboxykinase, pyruvate dehydrogenase, and pyruvate carboxylase in hepatocytes of different acinar origin. *Arch. Biochem. Biophys.* 326, 202–206. doi: 10.1006/abbi.1996.0066

Jungermann, K., and Katz, N. (1982). Functional hepatocellular heterogeneity. *Hepatology* 2, 385–395. doi: 10.1002/hep.1840020316

Jungermann, K., and Katz, N. (1989). Functional specialization of different hepatocyte populations. *Physiol. Rev.* 69, 708–764. doi: 10.1152/physrev.1989.69.3.708

Jungermann, K., and Kietzmann, T. (1997). Role of oxygen in the zonation of carbohydrate metabolism and gene expression in liver. *Kidney Int.* 51, 402–412. doi: 10.1038/ki.1997.53

Jungermann, K., and Kietzmann, T. (2000). Oxygen: modulator of metabolic zonation and disease of the liver. *Hepatology* 31, 255–260. doi: 10.1002/hep.510310201

Katz, N., Teutsch, H. F., Jungermann, K., and Sasse, D. (1977a). Heterogeneous reciprocal localization of fructose-1,6-bisphosphatase and of glucokinase in microdissected periportal and perivenous rat-liver tissue. *FEBS Lett.* 83, 272–276. doi: 10.1016/0014-5793(77)81021-1

Katz, N., Teutsch, H. F., Sasse, D., and Jungermann, K. (1977b). Heterogeneous distribution of glucose-6-phosphatase in microdissected periportal and perivenous rat-liver tissue. *FEBS Lett.* 76, 226–230. doi: 10.1016/0014-5793(77)80157-9

Kietzmann, T., Cornesse, Y., Brechtel, K., Modaressi, S., and Jungermann, K. (2001). Perivenous expression of the mRNA of the three hypoxia-inducible factor alpha-subunits, HIF1alpha, HIF2alpha and HIF3alpha, in rat liver. *Biochem. J.* 354, 531–537. doi: 10.1042/bj3540531

Kietzmann, T., Roth, U., Freimann, S., and Jungermann, K. (1997). Arterial oxygen partial pressures reduce the insulin-dependent induction of the perivenously located glucokinase in rat hepatocyte cultures: mimicry of arterial oxygen pressures by H_2O_2. *Biochem. J.* 321(Pt 1),17–20.

Kirkpatrick, R. B., Robinson, S. F., and Killenberg, P. G. (1980). Diurnal-variation of rat-liver enzymes catalyzing bile-acid conjugation and sulfation. *Biochim. Biophys. Acta.* 620, 627–630. doi: 10.1016/0005-2760(80)90154-X

König, M., and Holzhütter, H. G. (2012). Kinetic modeling of human hepatic glucose metabolism in type 2 diabetes mellitus predicts higher risk of hypoglycemic events in rigorous insulin therapy. *J. Biol. Chem.* 287, 36978–36989. doi: 10.1074/jbc.M112.382069

La Fleur, S. E., Kalsbeek, A., Wortel, J., and Buijs, R. M. (1999). A suprachiasmatic nucleus generated rhythm in basal glucose concentrations. *J. Neuroendocrinol.* 11, 643–652. doi: 10.1046/j.1365-2826.1999.00373.x

Leskes, A., Siekevitz, P., and Palade, G. E. (1971). Differentiation of endoplasmic reticulum in hepatocytes : II. glucose-6-phosphatase in rough microsomes. *J. Cell Biol.* 49, 288–302. doi: 10.1083/jcb.49.2.288

Manna, P., and Jain, S. K. (2012). Decreased hepatic phosphatidylinositol-3,4,5-triphosphate (PIP3) levels and impaired glucose homeostasis in type 1 and type 2 diabetic rats. *Cell. Physiol. Biochem.* 30, 1363–1370. doi: 10.1159/000343325

Massillon, D. (2001). Regulation of the glucose-6-phosphatase gene by glucose occurs by transcriptional and post-transcriptional mechanisms-Differential effect of glucose and xylitol. *J. Biol. Chem.* 276, 4055–4062. doi: 10.1074/jbc.M007939200

Miethke, H., Wittig, B., Nath, A., Zierz, S., and Jungermann, K. (1985). Metabolic zonation in liver of diabetic rats. Zonal distribution of phosphoenolpyruvate carboxykinase, pyruvate kinase, glucose-6-phosphatase and succinate dehydrogenase. *Biol. Chem. Hoppe. Seyler.* 366, 493–501. doi: 10.1515/bchm3.1985.366.1.493

Minchenko, O., Opentanova, I., and Caro, J. (2003). Hypoxic regulation of the 6-phosphofructo-2-kinase/fructose-2,6-bisphosphatase gene family (PFKFB-1-4) expression *in vivo*. *FEBS Lett.* 554, 264–270. doi: 10.1016/S0014-5793(03)01179-7

Miralpeix, M., Carballo, E., Bartrons, R., Crepin, K., Hue, L., and Rousseau, G. G. (1992). Oral-administration of vanadate to diabetic rats restores liver 6-phosphofructo-2-kinase content and messenger-Rna. *Diabetologia* 35, 243–248. doi: 10.1007/BF00400924

Morselt, A. F., Frederiks, W. M., Copius Peereboom-Stegeman, J. H., and van Veen, H. A. (1987). Mechanism of damage to liver cells after chronic exposure to low doses of cadmium chloride. *Arch. Toxicol. Suppl.* 11, 213–215. doi: 10.1007/978-3-642-72558-6_34

Nauck, M., Wölfle, D., Katz, N., and Jungermann, K. (1981). Modulation of the glucagon-dependent induction of phosphoenolpyruvate carboxykinase and tyrosine aminotransferase by arterial and venous oxygen concentrations in hepatocyte cultures. *Eur. J. Biochem.* 119, 657–661. doi: 10.1111/j.1432-1033.1981.tb05658.x

Neely, P., El-Maghrabi, M. R., Pilkis, S. J., and Claus, T. H. (1981). Effect of diabetes, insulin, starvation, and refeeding on the level of rat hepatic fructose 2,6-bisphosphate. *Diabetes* 30, 1062–1064. doi: 10.2337/diab.30.12.1062

Noguchi, T., Inoue, H., and Tanaka, T. (1985). Transcriptional and post-transcriptional regulation of L-type pyruvate-kinase in diabetic rat-liver by insulin and dietary fructose. *J. Biol. Chem.* 260, 4393–4397.

Postic, C., Burcelin, R., Rencurel, F., Pegorier, J. P., Loizeau, M., Girard, J., et al. (1993). Evidence for a transient inhibitory effect of insulin on GLUT2 expression in the liver: studies *in vivo* and *in vitro*. *Biochem. J.* 293(Pt 1), 119–124.

Probst, I., Schwartz, P., and Jungermann, K. (1982). Induction in primary culture of gluconeogenic and glycolytic hepatocytes resembling periportal and perivenous cells. *Eur. J. Biochem.* 126, 271–278. doi: 10.1111/j.1432-1033.1982.tb06775.x

Quistorff, B. (1985). Gluconeogenesis in periportal and perivenous hepatocytes of rat liver, isolated by a new high-yield digitonin/collagenase perfusion technique. *Biochem. J.* 229, 221–226. doi: 10.1042/bj2290221

Raju, J., Gupta, D., Rao, A. R., and Baquer, N. Z. (1999). Effect of antidiabetic compounds on glyoxalase I activity in experimental diabetic rat liver. *Ind. J. Exp. Biol.* 37, 193–195.

Ramakrishnan, S. K., and Shah, Y. M. (2017). A central role for hypoxia-inducible factor (HIF)-2alpha in hepatic glucose homeostasis. *Nutr. Healthy Aging* 4, 207–216. doi: 10.3233/NHA-170022

Rappaport, A. M., Borowy, Z. J., Lougheed, W. M., and Lotto, W. N. (1954). Subdivision of hexagonal liver lobules into a structural and functional unit - role in hepatic physiology and pathology. *Anat. Rec.* 119, 11–33. doi: 10.1002/ar.1091190103

Rosa, J. L., Ventura, F., Tauler, A., and Bartrons, R. (1993). Regulation of hepatic 6-phosphofructo-2-kinase fructose 2,6-bisphosphatase gene-expression by glucagon. *J. Biol. Chem.* 268, 22540–22545.

Salas, M., Vinuela, E., and Sols, A. (1963). Insulin-dependent synthesis of liver glucokinase in the rat. *J. Biol. Chem.* 238, 3535–3538.

Schmucker, D. L., Mooney, J. S., and Jones, A. L. (1978). Stereological analysis of hepatic fine structure in the Fischer 344 rat. Influence of sublobular location and animal age. *J. Cell Biol.* 78, 319–337. doi: 10.1083/jcb.78.2.319

Sharma, C., Manjeshwar, R., and Weinhouse, S. (1964). Hormonal and dietary regulation of hepatic glucokinase. *Adv. Enzyme Regul.* 2, 189–200. doi: 10.1016/S0065-2571(64)80013-3

Sibrowski, W., Müller, M. J., and Seitz, H. J. (1981). Effect of different thyroid states on rat-liver glucokinase synthesis and degradation *Invivo*. *J. Biol. Chem.* 256, 9490–9494.

Sibrowski, W., Staegemann, U., and Seitz, H. J. (1982). Accelerated turnover of hepatic glucokinase in starved and streptozotocin-diabetic rat. *Eur. J. Biochem.* 127, 571–574. doi: 10.1111/j.1432-1033.1982.tb06910.x

Slieker, L. J., Sundell, K. L., Heath, W. F., Osborne, H. E., Bue, J., Manetta, J., et al. (1992). Glucose transporter levels in tissues of spontaneously diabetic Zucker fa/fa rat (ZDF/drt) and viable yellow mouse (Avy/a). *Diabetes* 41, 187–193. doi: 10.2337/diab.41.2.187

Teutsch, H. F., and Lowry, O. H. (1982). Sex specific regional differences in hepatic glucokinase activity. *Biochem. Biophys. Res. Commun.* 106, 533–538. doi: 10.1016/0006-291X(82)91143-3

Thorens, B., Flier, J. S., Lodish, H. F., and Kahn, B. B. (1990). Differential regulation of two glucose transporters in rat liver by fasting and refeeding and by diabetes and insulin treatment. *Diabetes* 39, 712–719. doi: 10.2337/diab.39.6.712

Torre, C., Perret, C., and Colnot, S. (2010). Molecular determinants of liver zonation. *Prog. Mol. Biol. Transl. Sci.* 97, 127–150. doi: 10.1016/B978-0-12-385233-5.00005-2

Trus, M., Zawalich, K., Gaynor, D., and Matschinsky, F. (1980). Hexokinase and glucokinase distribution in the liver lobule. *J. Histochem. Cytochem.* 28, 579–581. doi: 10.1177/28.6.7391551

Uyeda, K., and Repa, J. J. (2006). Carbohydrate response element binding protein, ChREBP, a transcription factor coupling hepatic glucose utilization and lipid synthesis. *Cell Metab.* 4, 107–110. doi: 10.1016/j.cmet.2006.06.008

Van Schaftingen, E., and Hers, H. G. (1983). The role of fructose 2,6-bisphosphate in the long-term control of phosphofructokinase in rat liver. *Biochem. Biophys. Res. Commun.* 113, 548–554. doi: 10.1016/0006-291X(83)91760-6

Vasilj, A., Gentzel, M., Ueberham, E., Gebhardt, R., and Shevchenko, A. (2012). Tissue proteomics by one-dimensional gel electrophoresis combined with label-free protein quantification. *J. Proteome Res.* 11, 3680–3689. doi: 10.1021/pr300147z

Wals, P. A., Palacin, M., and Katz, J. (1988). The zonation of liver and the distribution of fructose 2,6-bisphosphate in rat liver. *J. Biol. Chem.* 263, 4876–4881.

Weinberg, M. B., and Utter, M. F. (1979). Effect of thyroid-hormone on the turnover of rat-liver pyruvate-carboxylase and pyruvate-dehydrogenase. *J. Biol. Chem.* 254, 9492–9499.

Weinberg, M. B., and Utter, M. F. (1980). Effect of streptozotocin-induced diabetes mellitus on the turnover of rat liver pyruvate carboxylase and pyruvate dehydrogenase. *Biochem. J.* 188, 601–608. doi: 10.1042/bj1880601

Weinstein, S. P., O'Boyle, E., Fisher, M., and Haber, R. S. (1994). Regulation of GLUT2 glucose transporter expression in liver by thyroid hormone: evidence for hormonal regulation of the hepatic glucose transport system. *Endocrinology* 135, 649–654. doi: 10.1210/endo.135.2.8033812

Wimhurst, J. M., and Manchester, K. L. (1970a). A comparison of the effects of diabetes induced with either alloxan or streptozotocin and of starvation on the activities in rat liver of the key enzymes of gluconeogenesis. *Biochem. J.* 120, 95–103. doi: 10.1042/bj1200095

Wimhurst, J. M., and Manchester, K. L. (1970b). Suppression of pyruvate carboxylase by glucose in perfused rat liver. *Febs Lett.* 8, 91–94 doi: 10.1016/0014-5793(70)80232-0

Wölfle, D., and Jungermann, K. (1985). Long-term effects of physiological oxygen concentrations on glycolysis and gluconeogenesis in hepatocyte cultures. *Eur. J. Biochem.* 151, 299–303. doi: 10.1111/j.1432-1033.1985.tb09100.x

Wurtman, R. J. (1974). Daily rhythms in tyrosine-transaminase and other hepatic enzymes that metabolize amino-acids-mechanisms and possible consequences. *Life Sci.* 15, 827–847. doi: 10.1016/0024-3205(74)90001-0

Yang, J., Reshef, L., Cassuto, H., Aleman, G., and Hanson, R. W. (2009). Aspects of the control of phosphoenolpyruvate carboxykinase gene transcription. *J. Biol. Chem.* 284, 27031–27035. doi: 10.1074/jbc.R109.040535

Zalitis, J. G., and Pitot, H. C. (1979). Synthesis and degradation of rat-liver and kidney fructose bisphosphatase *Invivo. Arch. Biochem. Biophys.* 194, 620–631. doi: 10.1016/0003-9861(79)90657-X

Zeller, E., Hammer, K., Kirschnick, M., and Braeuning, A. (2013). Mechanisms of RAS/beta-catenin interactions. *Arch. Toxicol.* 87, 611–632. doi: 10.1007/s00204-013-1035-3

Conflict of Interest Statement: The authors declare that the research was conducted in the absence of any commercial or financial relationships that could be construed as a potential conflict of interest.

2.4 *A Unifying Mathematical Model of Lipid Droplet Metabolism* [42]

Dieses Kapitel basiert auf [42] (DOI: 10.1111/febs.14189).

Einleitung: Neben dem Fettgewebe hat auch die Leber die Fähigkeit, Fett in großen Mengen zu speichern. Sie nimmt Fettsäuren abhängig von deren Plasmakonzentration auf und speichert diese in Form von Triglyzeriden. Die Folge von langanhaltend hohen Fettsäurespiegeln im Plasma kann eine massive Einlagerung von Triglyzeriden in der Leber, die sogenannte Fettleber (Steatose), sein. Die nicht oder nur schwer wasserlöslichen Triglyzeride werden innerhalb von Hepatozyten in speziellen Organellen, den Lipidtropfen (*lipid droplets*) gespeichert. Sie sind umgeben von einer einzelnen Phospholipidschicht, die aufgrund ihrer Amphiphilie im Inneren eine hydrophobe Umgebung erzeugt, die das Speichern von hydrophoben Substanzen wie Triglyzeriden, Cholesterol und Cholesterinestern ermöglicht, und nach außen hydrophil ist und somit die Löslichkeit im wässrigen Zytosol der Zelle gewährleistet. Lipidtropfen unterliegen einer hohen Dynamik. Sie werden ständig neu gebildet, fusionieren untereinander zu größeren Tropfen, werden mit Triglyzeriden aufgefüllt und teilweise oder vollständig wiederabgebaut. Das in ihnen gespeicherte Fett wird für Energiegewinnung der Hepatozyten genutzt oder von der Leber in Form von Lipoproteinen (VLDL - *very low density lipoprotein*) für die systemische Versorgung abgegeben. Die Dynamik dieser Organellen wird von einer Reihe von regulatorischen Oberflächenproteinen (RSP – *regulatory surface proteins*) kontrolliert. Die bestuntersuchten RSP sind die sogenannten PAT-Proteine (*P*erilipin/*A*dipophilin/*T*IP47), denen eine entscheidende Rolle bei der Genese, dem Wachstum und dem Abbau der Lipidtropfen zukommt. In einer Vielzahl von Überexpressions- und Knockoutstudien wurde gezeigt, wie sehr die Menge der PAT-Proteine die Menge der gespeicherten Triglyzeride und die Größenverteilung der Lipidtropfen beeinflusst. Die Menge des gespeicherten Fettes hängt somit nicht nur vom Verhältnis von Angebot und Verbrauch ab, sondern auch von der Ausstattung des metabolischen Netzwerks und der Menge der RSP.

Fragestellung: Ziel dieser Arbeit war es, ein integratives Modell des hepatischen Lipidstoffwechsels zu erstellen, welches es ermöglicht, die molekularen Prozesse der Steatose-Entstehung besser zu verstehen.

Methode: Um die Rolle der RSP und den Einfluss der einzelnen metabolischen Prozesse, die an der Aufnahme, Speicherung und Verwertung von Fettsäuren in der Leber beteiligt sind, zu untersuchen, wurde ein kinetisches Modell des hepatischen Lipidmetabolismus unter Berücksichtigung des Lipidtropfenmetabolismus erstellt. Das Modell beinhaltet Aufnahme von Fettsäuren in die Leber, Veresterung zu Triglyzeriden, Aufnahme von Fettsäuren in Mitochondrien für die β-Oxidation, Bildung von Phospholipiden, Entstehung, Fusion und Abbau von Lipidtropfen sowie Bildung und Export von VLDL.

Ergebnis: Zuerst wurde untersucht, welche Prozesse auf die Fettakkumulation in der Leber den größten Einfluss haben. Es wurde gezeigt, dass die hepatische Fettspeicherung am empfindlichsten von der Fettsäureaufnahme sowie der Aktivitäten der Diacylglycerol-O-Acyltransferase 2 (DGAT2) und der Adipozyten-Triglyzerid-Lipase abhängt. Anschließend wurde mit dem Modell die Lipidtropfenverteilung in humanen Hepatomazellen nach Exposition mit freien Fettsäuren simuliert. Interessanter Weise führen bereits zufällige Schwankungen von 50% in der Aktivität der RSP zu einer großen Ungleichverteilung in der Fettspeicherung einzelner Zellen, die auf Organebene zu regionalen Unterschieden in der Fetteinlagerung von bis zu 500% führen würden. Das zeigt, dass die zelluläre Variabilität in der

Expression der metabolischen Enzyme und der RSP eine wichtige Determinante der hepatischen Fettakkumulation darstellt und deren Heterogenität erklären kann.

Diskussion: Die zentrale Frage war, welche Prozesse auf die Verfettung den größten Einfluss haben, wenn die Leber überschüssige Fettsäuren aus dem Plasma entfernen muss. Es konnten hier drei relevante Prozesse identifiziert werden. Einerseits werden durch Erhöhung der Transportkapazität mehr Fettsäuren aus dem Plasma aufgenommen, welche dann mittels Erhöhung der DGAT2-Aktivität vermehrt zu Triglyzeriden verestert werden, und schließlich wird durch Verminderung der Adipozyten-Triglyzerid-Lipase-Aktivität die Lipolyse bestehender Lipidtropfen unterbunden. Dabei ist es effizienter bestehende Lipidtropfen aufzufüllen, als neue anzulegen.

Eine andere wichtige Frage war, warum die Leberverfettung oftmals sehr heterogen verläuft. Leberzellen, die aus derselben Leber isoliert und unter identischen externen Bedingungen (Fettsäurekonzentration, Hormonkonzentration etc.) kultiviert wurden, weisen nach einiger Zeit sehr unterschiedliche Mengen an gespeicherten Fettsäuren auf [42, 55]. Tatsächlich konnten die unterschiedlichen Mengen an eingelagertem Fett in den Modellsimulationen reproduziert werden, wenn man eine zufällige Varianz in den Aktivitäten der Schlüsselenzyme mit dem Faktor zwei annimmt. Interessanterweise entspricht das den gemessenen Unterschieden in der Expression der RSP in den Leberzellen von Menschen mit verschiedenen Steatosegraden [56].

Um zu untersuchen, welche Rolle die simulierte Heterogenität in der Proteinexpression für die Fetteinlagerung einer normalen Leber spielt, wurde die gespeicherte Fettmenge für ein typisches Plasmaprofil an Glukose, Fettsäuren und Hormonen simuliert. Unter der Annahme, dass die Enzymaktivitäten zufällig mit einem Faktor von 1,5 variieren, ergibt das eine Heterogenität in der Menge des gespeicherten Fettes in der Leber von 300%. Besonders unter Fastenbedingungen, die durch einen erhöhten Plasmafettsäurespiegel gekennzeichnet sind, führt das dazu, dass bei etwa einem Viertel aller Fälle die Fetteinlagerung denen einer steatotischen Leber entspricht. Damit kann auch die räumliche Inhomogenität der Fettakkumulation bei der Steatose erklärt werden, wenn man davon ausgeht, dass ein bestimmtes Proteinprofil nicht nur für eine einzelne Zelle, sondern für ein Cluster von Zellen in einem gegebenen Gebiet gültig ist (z.B. in einer bestimmten Leberzone). Wenn das der Fall ist, ist zu erwarten, dass sich die unterschiedlichen Profile in der Fettakkumulation widerspiegeln und die Unterschiede zwischen verschiedenen Regionen deutlich sichtbar sind.

The FEBS Journal

FEBS PRESS science publishing by scientists

A unifying mathematical model of lipid droplet metabolism reveals key molecular players in the development of hepatic steatosis

Christin Wallstab[1], Dimitra Eleftheriadou[1], Theresa Schulz[2], Georg Damm[2,3], Daniel Seehofer[2,3], Jürgen Borlak[4], Hermann-Georg Holzhütter[1,†] and Nikolaus Berndt[1,†]

1 Institute of Biochemistry, Computational Systems Biochemistry Group, Charite – University Medicine Berlin, Germany
2 Clinic for General-, Visceral- and Transplantation Surgery, Charite – University Medicine Berlin, Germany
3 Department of Hepatobiliary Surgery and Visceral Transplantation, University of Leipzig, Germany
4 Centre for Pharmacology and Toxicology, Institute for Pharmaco- and Toxicogenomics, Hannover Medical School, Hannover, Germany

Keywords
hepatocytes; kinetic model; lipid droplets; PAT proteins; steatosis

Correspondence
H.-G. Holzhütter and N. Berndt, Charite – University Medicine Berlin, Institute of Biochemistry, Computational Systems Biochemistry Group, Charitéplatz 1, 10115 Berlin, Germany
Tel.: +49 30 450 528937
Tel: +49 30 450 528166 (HGH); +49 30 450 528466 (NB)
E-mails: hermann-georg.holzhuetter@charite.de (HGH); nikolaus.berndt@charite.de (NB)

†Shared senior authorship

(Received 12 January 2017, revised 2 June 2017, accepted 28 July 2017)

doi:10.1111/febs.14189

The liver responds to elevated plasma concentrations of free fatty acids (FFAs) with an enhanced uptake of FFAs and their esterification to triacylglycerol (TAG). On the long term, this may result in massive hepatic TAG accumulation called *steatosis hepatitis*. In hepatocytes, the poor water-soluble TAG is packed in specialized organelles: Lipid droplets (LDs) serving as transient cellular deposit and lipoproteins (LPs) transporting TAG and cholesterol esters to extra-hepatic tissues. The dynamics of these organelles is controlled by a variety of regulatory surface proteins (RSPs). Assembly and export of VLDLs are mainly regulated by the microsomal transfer protein (MTP) and apoprotein B100. Formation and lipolysis of LDs are regulated by several RSPs. The best studied regulators belong to the PAT (Perilipin/Adipophilin/TIP47) and CIDE families. Knockdown or overexpression of SRPs may significantly affect the total number and size distribution of LDs. Intriguingly, a large cell-to-cell heterogeneity with respect to the number and size of LDs has been found in various cell types including hepatocytes. These findings suggest that the extent of cellular lipid accumulation is determined not only by the imbalance between lipid supply and utilization but also by variations in the expression of RSPs and metabolic enzymes. To better understand the relative regulatory impact of individual processes involved in the cellular TAG turnover, we developed a comprehensive kinetic model encompassing the pathways of the fatty acid and triglyceride metabolism and the main molecular processes governing the dynamics of LDs. The model was parametrized such that a large number of experimental *in vitro* and *in vivo* findings are correctly recapitulated. A control analysis of the model revealed that variations in the activity of FFA uptake, diacylglycerol acyltransferase (DGAT) 2, and adipose triglyceride lipase (ATGL) have the strongest influence on the cellular TAG level. We used the model to simulate LD size distributions in human hepatoma cells and hepatocytes exposed to a

Abbreviations
ADRP, adipose differentiation-related protein; AGPAT, acylglycerolphosphate acyltransferase (EC 2.3.1.51); ATGL, adipocyte triglyceride lipase (EC 3.1.1.3); CPT1, carnitine palmitoyltransferase 1; DAG, diacylglycerol; DGAT1(2), diacylglycerol acyltransferase 1(2) (EC 2.3.1.20); FFA, free (nonesterified) fatty acids; FSP-27, Fat-specific protein 27; GLY3P, glycerol-3-phosphate; GPAT, glycerol-3-phosphate acyltransferase ((EC 2.3.1.15); HSL, hormone-sensitive lipase (EC 3.1.1.79); MAG, monoacylglycerol; MGL, monoglyceride lipase (EC 3.1.1.23); PAP, phosphatidic acid phosphatase (EC 3.1.3.4); PLIN1, perilipin 1; RSP, regulatory surface protein; TAG, triacylglycerol; TIP47 tail-interacting protein 47.

challenge with FFAs. A random fold change by a factor of about two in the activity of RSPs was sufficient to reproduce the large diversity of droplet size distributions observed in individual cells. Under the premise that the same extent of variability of RSPs holds for the intact organ, our model predicts variations in the TAG content of individual hepatocytes by a factor of about 3–6 depending on the nutritional regime. Taken together, our modeling approach integrates numerous experimental findings on individual processes in the cellular TAG metabolism and LD dynamics metabolism to a consistent state-of-the-art dynamic network model that can be used to study how changes in the external conditions or systemic parameters will affect the TAG content of hepatocytes.

Introduction

The liver possesses a high capacity to uptake free fatty acids (FFAs) from the plasma and to incorporate them into triacylglycerols (TAG), cholesterol esters, and membrane lipids. The water-insoluble TAGs are either packed into lipid droplets (LDs) serving as transient cellular lipid store or VLDL lipoproteins transporting lipids to extrahepatic tissues. LDs are cellular lipid storing and protein-decorated liposomes comprising a strikingly similar molecular architecture as plasma lipoproteins: A hydrophobic core mainly constituted by TAG and cholesterol ester (CE) molecules is surrounded by an unilamellar leaflet of phospholipids that is decorated by a large array of surface proteins [1]. LDs are the predominant organelle of adipocytes corresponding to the central function of adipose tissue as main TG storage of the body. LDs are highly dynamic organelles which are generated as small particles at the endoplasmic reticulum (ER), which may further grow by additional incorporation of lipid, fusion, or mutual lipid exchange and which may shrink during the hydrolysis of TAG and CE by specific lipases. The central function of LDs is to store TAG and CE if synthesis and/or uptake of FFAs and cholesterol (C) exceeds the cellular demand and to release these lipids in the opposite case. As saturated FFAs and free C are potentially cytotoxic, their conversion into nontoxic TG and CE and subsequent deposition in LDs are crucial for the maintenance of cell integrity. An overweening delivery of FFAs and/or C is commonly accompanied by an increase in the synthesis of TG and CE and thus in the number and size of LDs. This has been demonstrated in numerous *in vitro* experiments in which cells were incubated with high concentrations of free fatty acids [2–5]. On a whole-body scale, an imbalance between lipid synthesis and utilization results in an expansion of the visceral adipose tissue that may be accompanied by lipid accumulation in other organs like liver (hepatic steatosis), kidney, and pancreas.

Notably, the extent of lipid storage in LDs does not follow strictly the extent of fatty acid overload and displays remarkable cell-to-cell heterogeneity [6,7]. One possible reason might be variability in the expression of metabolic enzymes involved in lipid metabolism and of regulatory surface proteins (RSPs) controlling the formation, growth, and degradation of LDs. The best studied RSPs belong to the PAT (Perilipin/Adipophilin/TIP47) and CIDE (cell death–inducing DNA fragmentation factor 45-like effectors) protein families. Lack of RSPs required for the *de novo* synthesis of LDs or the overexpression of RSPs promoting the hydrolysis of LDs may both diminish the number and size of LDs. For example, inactivating in mice the Adfp gene coding for the PAT protein ADRP (perilipin 2) resulted in a 60% reduction in hepatic triglyceride. These animals were resistant to a diet-induced fatty liver, and the size distribution of LDs in hepatocytes was clearly shifted toward smaller particles [8]. In contrast, simultaneous down-regulation of the two PAT proteins ADRP and TIP47 in AML12 liver cells induced a marked increase in LD size and decrease in LD number [9]. These findings demonstrate that the relative abundance of RSPs has a large impact on the size distribution of LDs and hence on the size of the TG pool established in conditions of excessive lipid load. Another finding supporting this view is the observed transition from a large unilocular LD – a unique feature of the white adipocyte – to smaller multilocular LDs (as typically observed in brown adipocytes) when the CIDE-protein Fsp27 involved in the fusion of LDs was strongly downregulated [10].

Since the first description of lipid droplets [11], a rapidly increasing number of experimental studies have increased our knowledge on molecular mechanisms involved in the dynamics of LDs. However, a

computational model putting together this peace-wise knowledge into a consistent unifying framework is lacking so far. Here, we present a kinetic model that captures the triglyceride metabolism of animal cells and a multitude of molecular processes driving cellular LD dynamics. The model is generic in that it takes into account experimental findings obtained in different cell types from different species. However, parameterization of the model was performed to recapitulate experimental findings with rat hepatocytes. The model was validated by comparing computer simulations with a large set of independent experiments. Extensive model simulations were performed to evaluate how variations in the lipid load of hepatocytes and in the abundance of individual enzymes and regulatory proteins may influence the size distribution of LDs and thus the development of steatosis [12].

Results

Outline of the mathematical model

The metabolic module

The molecular processes included into the model are depicted in Fig. 1. In the following, numbers in brackets <> refer to the numbering of processes in Fig. 1. The model is composed of a metabolic module and a droplet/lipoprotein module. The metabolic module comprises the uptake of free fatty acids (FFA) from the blood plasma <1> where up to 7 FFAs are reversibly bound to albumin with different association constants. The model includes the passive diffusional uptake of FFAs and a carrier-mediated uptake of FFAs (mainly representing the transport protein CD36) that can be regulated by the amount of the carrier protein. FFAs are rapidly activated to acyl-CoA moieties by the enzyme fatty acyl-CoA synthetase <2>. Acyl-CoA can be taken up into mitochondria by the membrane carrier CPT-1 <3> where subsequent β-oxidation yields acetyl-CoA for the citric acid cycle. As CPT-1 is the rate limiting step in the degradation of FFAs, the activity of CPT-1 is taken as measure for the mitochondrial β-oxidation of acyl-CoA. Alternatively, acyl-CoA can be esterified with glycerol-3-phosphate to lysophosphatidic acid (LPA) and with LPA to phosphatidic acid (PA) <4>. Hydrolytic cleavage of the phosphate group from PA yields diacylglycerol (DAG) which can be converted to triacylglycerol (TAG) upon esterification with another acyl-CoA <6,7>. DAG can also be utilized for the synthesis of phospholipids <5>. There are two isoforms of the diacylglycerol acyltransferases, DGAT1 and DGAT2, catalyzing the last step in TAG synthesis. In the ER, they are both integral membrane-spanning proteins which are supposed to play distinct functional roles in different subdomains of the ER [13]. In the model, it is assumed that the TAG pool of the ER membrane synthesized by DGAT1 is used for *de novo* assembly of both LDs and VLDL lipoproteins <6>. The formation of VLDL lipoproteins is modeled as transfer of TAG synthesized by DGAT1 to apoprotein B100 (ApoB100) by the microsomal transfer protein (MTP). Availability of ApoB100 is controlled by insulin-dependent degradation. Synthesis of VLDL and release into the external space are modeled as a single step. DGAT2 interacts with nascent LDs and incorporates the synthesized TGA directly into these particles <8>.

The droplet/lipoprotein module

This module comprises central processes so far reported to control the dynamics of lipid droplets (LDs) and the export of the lipoprotein VLDL. In the model, the LDs are subdivided into $N_c = 30$ discrete size classes LD_i ($i = 1,\ldots N_c$) with radius $r_i = 0.1$ μm, i.e. the smallest LD has a radius of $r_1 = 0.1$ μm, the largest LD has a radius of $r_{30} = 3$ μm. Coating of LDs with SRPs has no effect on the size class. Nascent lipid droplets formed by *de novo* synthesis at the ER membrane belong to size class LD_1 and are not covered by RSPs. Each LD class is represented by the total amount of the lipid species L (L = TAG, DAG, MAG) contained in the LDs. The number of LDs in a given LD class LD_i is inferred from the volume $\Omega_i = (4/3)\pi\, r_i^3$ of a single LD and the total amount and volume of lipid species. Increase or decrease in the amount of any lipid species L_i in class LD_i is modeled as lipid transfer to the next higher or lower size class LD_{i+1} or LD_{i-1}, respectively (see paragraph below).

Further growth of LDs may proceed in different ways. LDs may reversibly bind to the ER membrane where they are filled with additional TAG synthesized by DGAT2 <8>. Binding to the ER membrane is facilitated in the presence of TIP47. As DGAT2 associates either with the ER membrane or with LDs, the filling rate in each class depends on LD numbers: The more LD are present in a given size class, the higher the fraction of DGAT2 involved in the TAG filling of that class and the lower the fraction of DGAT2 associated with the ER synthesizing TAG for LD formation. It is assumed that larger LDs are less likely to be associated with ER and being filled by DGAT2. On top of additional lipid loading at the ER, LDs may exchange their lipid content with each other whereby the larger particle successively absorbs the smaller one <10>. The

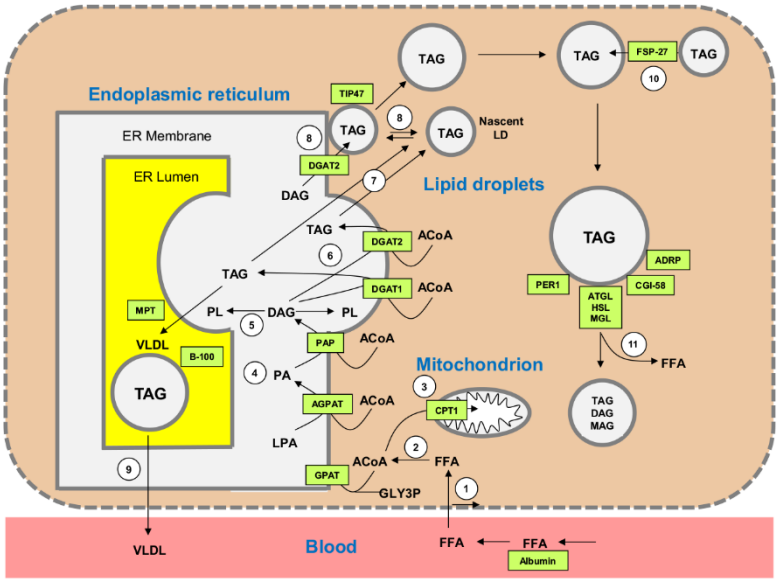

Fig. 1. Schematic representation of the processes included into the model. (1) Influx of free (nonesterified) fatty acids (FFAs) which in the plasma are in an equilibrium with albumin-bound fatty acids; (2) activation of FFAs with coenzyme A (CoA-SH) to acyl-CoA (ACoA); (3) uptake of acyl-CoA into mitochondria controlled by the carnitine palmitoyltransferase 1 (CPT1); (4) pathway of diacylglycerol (DAG) synthesis constituted by the following enzymatic steps: Synthesis of lysophosphatidic acid (LPA) from glycerol-3-phosphate (GLY3P) and acyl-CoA by the enzyme glycerol-3-phosphate acyltransferase (GPAT), synthesis of phosphatidic acid (PA) from LPA and acyl-CoA by the enzyme acylglycerolphosphate acyltransferase (AGPAT), dephosphorylation of PA to DAG and inorganic phosphate Pi by the enzyme phosphatidic acid phosphatase (PAP); (5) consumption of DAG for the synthesis of phospholipid (PL); (6) synthesis of triacylglycerol (TAG) by the enzymes diacylglycerol acyltransferase 1/2 (DAGT1/2). TAG synthesized by DGAT1 is used for the synthesis of the very-low-density lipoprotein (VLDL) and *de novo* synthesis of LDs. DGAT2 may localize either to the ER membrane contributing to the TAG pool used for the de novo synthesis of LDs or to LDs docked to the ER increasing their TAG content; (7) pinch-off of naked (protein-uncoated) LDs from the ER; (8) reversible docking of LDs coated with the tail-interacting protein 47 (TIP47) to the ER membrane and filling with TAG produced by DGAT2; (9) synthesis and export of the VLDL lipoprotein modeled as one overall process depending on the abundance of the microsomal transfer protein (MTP) and the apoprotein-B (apo-B); (10) TAG transfer between LDs upon fusion mediated by the regulatory surface protein FSP-27; (11) Successive lipolysis of LD-TAG: Hydrolysis of TAG to DAG and FFA by the enzyme adipocyte triglyceride lipase (ATGL) which is activated by the phosphorylated form of the protein CGI58, hydrolysis of DAG to monoacyl glycerol (MAG), and FFA by the enzyme hormone-sensitive lipase (HSL) which is directly activated by phosphorylation and also activated by the phosphorylated protein adipose differentiation-related protein (ADRP) and perilipin 1 (PLIN1) in dependence from the level of insulin and glucagon, hydrolysis of MAG to glycerol and FFA by the enzyme monoacylglycerol lipase. The reversible binding of the regulatory surface proteins TIP47, ADRP, PLIN1, CGI58, FSP27to LDs is not shown in this summarizing scheme. See the Data S1 for more details. Abbreviations: FFA, free (nonesterified) fatty acids, TAG, triacylglycerol DAG, diacylglycerol; MAG, monoacylglycerol; GLY3P, glycerol-3-phosphate; CPT1, carnitine palmitoyltransferase 1; GPAT, glycerol-3-phosphate acyltransferase ((EC 2.3.1.15); AGPAT, acylglycerolphosphate acyltransferase (EC 2.3.1.51); PAP, phosphatidic acid phosphatase (EC 3.1.3.4); DGAT1(2), diacylglycerol acyltransferase 1(2) (EC 2.3.1.20); ATGL, adipocyte triglyceride lipase (EC 3.1.1.3);HSL, hormone-sensitive lipase (EC 3.1.1.79); MGL, monoglyceride lipase (EC 3.1.1.23); TIP47, tail-interacting protein 47; ADRP, adipose differentiation-related protein; PLIN1, perilipin 1.

rate of lipid transfer depends on the size difference between LDs and on the diameter of the smaller LD and requires the presence of FSP27 on the surface of fusing particles [14].

The main process responsible for the shrinking of LDs is the removal of fatty acids from the lipid esters TAG, DAG, and MAG [11]. The lipase ATGL catalyzes preferentially the conversion of TAG to DAG. The enzyme has a steady basal rate but may increase its activity after co-localization with CGI-58 [15]. The hormone-sensitive lipase HSL is activated by hormone-dependent phosphorylation and preferentially hydrolyzes diacylglycerol (DAG). The last step resulting in the complete lipolysis of TAG is catalyzed by the monoglyceride lipase (MGL).

Regulatory surface proteins and LD-associated enzymes

Generation, growth, remodeling, and degradation of LDs are controlled by diverse RSPs and LD-associated

enzymes which may reversibly bind to the surface of LDs. Generally, the rate of each elementary step affecting the lipid content of a LD and thus its size depends on the abundance of specific RSPs and enzymes on the LD surface. The model includes reversible binding of the following RSPs to the surface of LDs: TIP47, ADRP, perilipin (PLIN) 1, CGI-58, FSP27, ATGL, and HSL (Fig. 2). Reversible binding of regulatory surface proteins to LDs is modeled as time-dependent change in the fractional surface area X_{LD} of a LD covered with protein X (X = ATGL, PLIN1, perilipin, TIP47):

$$\frac{\mathrm{d}X_{\mathrm{LD}}}{\mathrm{d}t} = k_{\mathrm{on}}(X)\ SF_n - k_{\mathrm{off}}(X)\ X_{\mathrm{LD}}$$

SF_n denotes the fractional free (unoccupied) surface area of the LDs. $k_{\mathrm{on}}(X)$ is an effective rate which depends on the total cytosolic pool of X. Accordingly, X_0 denotes the (dimensionless) relative cytosolic amount of protein species X which is put to unity in the reference case and to values < 1 or > 1 in model simulations of experiments where the expression rate of X was altered by knockdown or overexpression.

The classical PAT proteins TIP47, ADRP, perilipin (PLIN1) are treated as competitors for unoccupied regions on the LD surface. The association constants for the binding of PATs depend on the surface curvature of the LD and the fraction of unoccupied LD surface. CGI-58 is treated as co-regulator that is recruited to the LD surface by ADRP and PLIN1. Upon phosphorylation, CGI58 binds to ATGL and HSL, which both bind to the unoccupied LD surface. FSP27 is recruited to the LD surface in dependence on LD surface curvature. Figure 2 depicts the model-based computation of the relative occupancy of LDs with RSPs ad LD-associated enzymes as function of the LD size. The association constants of the RSPs have been estimated by adjusting models simulations to a large asset of independent experiments (see section model validation.

Dynamic changes in the amount and composition of LDs

Growth and shrinking of LDs due to changes of their lipid content are implemented as follows. Uptake of a given lipid amount $v_{\mathrm{TAG}}\ \Delta t = \Delta\ \mathrm{TAG} > 0$ into a LD owing to lipid (TAG) flow v within the time span Δt would actually increase the size of a LD (marked yellow in Fig. 3A). However, as the model works with a finite number of discrete size classes, this process is described by a reduction $\mathrm{LD}_n \rightarrow \mathrm{LD}_n(1 - \Delta\ \mathrm{LD}_n)$ in the number of LD class (n) and concomitant increase $\mathrm{LD}_{n+1} \rightarrow \mathrm{LD}_{n+1}(1 + \Delta\ \mathrm{LD}_n)$ of the number of LDs in the next-higher size class (n + 1). Note that this implementation entails that the count LD_n of LDs in size class (n) is not an integer but a real number. The increment $\Delta\ LD_n$ is put to $\Delta\ \mathrm{LD}_n = \Delta\ \mathrm{TAG}/(\mathrm{TAG}_{n+1} - \mathrm{TAG}_n)$ arguing that a LD of size class (n) is fully converted into a LD of size class (n + 1) if the lipid uptake equals the difference $\mathrm{TAG}_{n+1} - \mathrm{TAG}_n$ in the lipid content of the two particles. Accordingly, loss of a given lipid amount $\Delta TAG < 0$ is modeled by putting $\mathrm{LD}_n \rightarrow \mathrm{LD}_n\ (1 - \Delta\ \mathrm{LD}_n)$ and $LD_{n-1} \rightarrow LD_{n-1}\ (1 + \Delta\ LD_n)$ with $\Delta\ \mathrm{LD}_n = |\Delta\ \mathrm{TAG}|/(\mathrm{TAG}_n - \mathrm{TAG}_{n-1})$. Importantly, both uptake and release of TAG into or from LDs of size class (n) increases the total TAG content and thus LD numbers of the neighboring size classes (n + 1) or (n − 1) but diminishes the total TAG content and the number of LDs of size class (n).

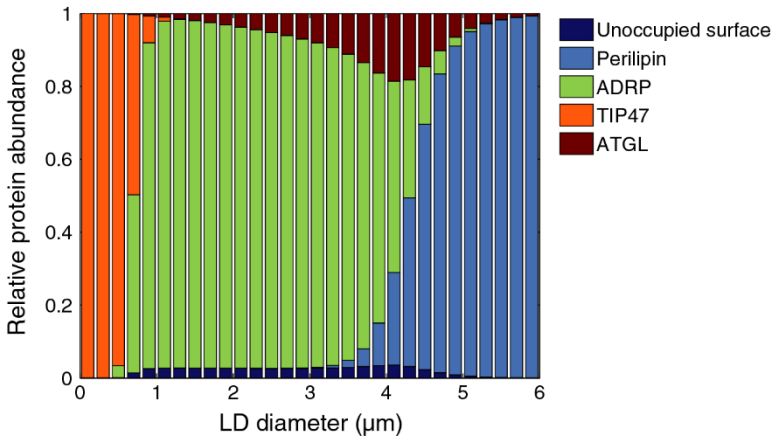

Fig. 2. Computed relative occupancy of LD surface by RSPs as function of LD size. The fractions refer to the RSP binding kinetics of the reference case (normal rat hepatocyte).

Hormonal control of lipid metabolism, LD degradation, and VLDL export

Our model contains regulatory proteins (HSL, CGI58, PLIN1) that are regulated by hormone-dependent reversible phosphorylation. Furthermore, ApoB100 degradation is insulin sensitive [16]. The relationship between the phosphorylation state of hormone-sensitive proteins and the plasma level of insulin and glucagon is described by a phenomenological signal function (see Data S3).

Model parameterization

For the metabolic enzymes of the model, available kinetic information was taken into account. The maximal enzyme activity (V_{max}) is a linear function of the protein abundance which may vary in different physiological states of the liver (e.g. steatosis). Therefore, numerical values of the V_{max} values had to be estimated from metabolic experiments where the uptake rate of free fatty acids, the synthesis of triglycerides, and the export of the lipoprotein VLDL have been measured in dependence of the external concentration of FFAs (Data S2). The rate equations for all processes of the model are given in Data S1. Steady-state metabolite concentrations and fluxes are listed in Data S4.

All computations were performed with MATLAB Release 2009a, The MathWorks, Inc. (Natick, MA, USA) using the ode15s integration routine.

For the rates of the processes involved in the generation and remodeling of LDs, the situation is less comfortable. Kinetic parameters for individual processes (e.g. TIP-47 dependent synthesis of nascent LDs as function of the TAG content of the ER and amount of TIP-47) are technically challenging and not available yet. Current knowledge in the field relies predominantly on transfection experiments where a specific regulatory protein was either disabled or overexpressed, and the accompanying changes of the TAG content, LD size distribution, and other functions of lipid metabolism were measured. Therefore, we varied the numerical values for the reaction rates and binding constants such that the final model parametrization enables simulations that were in good qualitative concordance with data from a larger number of independent knockdown and overexpression experiments carried out with liver tissue or hepatocytes.

Table 1 shows the results of experiments and of related model simulations where the abundance of individual regulatory proteins in the liver was either increased (liver-specific overexpression) or decreased (liver-specific knockdown). The simulations were carried out at steady state where all internal variables of the model do not show temporal variations as well as at nonstationary conditions. Steady state corresponds to the following two experimental conditions: (a) Hepatocytes in culture were exposed to a constant metabolic challenge (e.g. presence of FFAs in the external medium) for a time that was sufficiently long to reach a new stationary state, (b) Metabolic parameters (e.g. lipid droplet size distribution) were measured in livers or hepatocytes of transgenic laboratory animals with liver-specific knockout or overexpression of a distinct SRP. Nonstationary conditions are applicable if metabolic parameters (e.g. the activity of the β-oxidation pathway) have been measured during a short-time interval after onset of the perturbation (e.g. administration of radioactively labeled FFAs). Bold arrows in Table 1 indicate the direction of predicted and experimentally observed changes in central parameters of lipid and LD metabolism: Total TAG content of the cell, secretion rate of VLDL (=B-100 secretion), rate of mitochondrial fatty acid oxidation, rate of phospholipid synthesis (represented by the rate of the diacylglycerol choline phosphotransferase, DCPT) and

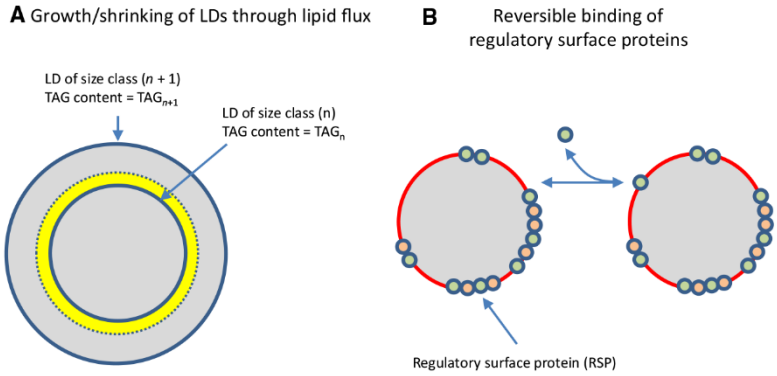

Fig. 3. Elementary process affecting the size distribution and protein composition of LDs.

Table 1. Predicted and observed changes of selected metabolic parameters at liver-specific inhibition or activation of regulatory surface proteins and metabolic enzymes. For each metabolic parameter, the symbols (arrows or circles) in the first column indicate the direction of the alteration predicted by the model: ⇧ up-regulation, ⇩ down-regulation, ○ no significant change, ⇨ right-shift of LD size distribution, ⇦ left-shift of LD size distribution. The symbols in the second column indicate the changes observed in the referenced experiment. Red symbols highlight a discrepancy between predicted and observed changes. Blue symbols indicate changes observed in nonhepatic cells.

Protein	Cellular TAG		VLDL secretion		β-oxidation		Phospholipid synthesis		LD size distribution	
DGAT1	⇧	⇧ [20] ⇧ [18]	⇧	⇧ [20] ○ [18]	⇩		⇩	⇩ [46]	⇦	⇦ [19]
DGAT1	⇩	⇩ [17,19] ⇧ [21]	⇩	⇩ [17]	○	○ [21]	⇧		⇨	⇨ [21] [19]
DGAT2	⇧	⇧ [20] ⇧ [18]	⇩	○ [20]	⇧	⇩ [22] ⇩ [21]	⇩		⇨	⇨ [12]
DGAT2	⇩	⇩ [22] ⇩ [17]	○	○ [21] ○ [17]	⇩	⇧ [22] ⇧ [21]	⇧	⇧ [21]	⇦	⇦ [21] [19]
MTP	⇧	⇩	⇧	⇧ [47]	⇩		⇩		⇨	
MTP	⇩	⇧ [48]	⇩	⇩ [49] ⇩ [50]	⇧		⇧	⇧ [48]	○	
ATGL	⇧	⇩ [51]	○	○ [52]	⇧	⇧ [51] ⇧ [52]	○		⇦	⇦ [53]
ATGL	⇩	⇧ [52]	○	○ [52]	⇩	⇩ [52]	○		⇨	
HSL	⇧	⇩ [51]	○	○ [51]	⇧	⇧ [51]	○		○	
HSL	⇩	⇧ [54]	○		⇩	⇩ [54] ○	○			⇨ [54]
CGI-58	⇩	⇧ [55]	○	○ [55]	○	⇩ [55]	○		○	○ [55]
FSP-27	⇩	⇩ [56]	⇧		○		⇩		⇦	⇦ [56]
ADFP	⇩	⇩ [9]	○		○				⇦	⇦ [57]
TIP-47	⇩	○ [9]							○	○ [9]

size distribution of LDs. Insignificant changes are symbolized by circles. If no data for liver cells but other cell types were available, we refer to such data by blue-colored symbols. Note that in some cases, the experimental findings are deviating. The only discrepancies between model simulations and experimental observations concern the impact of changes in the activity of DGAT1 on the TAG content and DGAT2 on β-oxidation. In contrast to the majority of experimental findings [17–20], our model predicts no significant change in the cellular TAG pool with changes in the activity of DGAT1. However, also an increase in cellular TAG content with decreased activity of DGAT1 has been observed in primary hepatocytes [21]. According to our model assumptions, DGAT1 and DGAT2 compete for a common DAG pool of the ER. Hence, an increased activity of DGAT1 reduces the level of DAG available to DGAT2 which fills up small LDs with TAG, thus promoting their growth. We speculate that adaptive/compensating changes in other protein levels might account for this discrepancy. Unlike experimental findings in [21,22], the model simulations predict an increase of β-oxidation at overexpressed DGAT2. According to the model simulations, the elevated TAG level at DGAT2 overexpression should be associated with a higher rate of lipolysis, thus increasing the cellular level of fatty acids and hence their supply to mitochondrial β-oxidation. A detailed description of all validation experiments listed in Table 1 is given in Data S2.

As example for the capability of the fully parametrized model to correctly recapitulate the outcome of 20 independent experiments (Data S2), Fig. 4 shows the results of a simulated overexpression and knockdown of the microsomal transfer protein (MTP). MTP overexpression redistributes TAG synthesized in the ER from *de novo* LD synthesis toward VLDL export. This results in an increased TAG export and diminished cellular TAG content. As the rate of TAG lipolysis depends on the number of LDs, the rate of TAG degradation and thus the availability of DAG for PL synthesis and β-oxidation of fatty acids are reduced. Analogously, MTP knockdown decreases TAG export, increases cellular TAG content, increases TAG turnover, and thereby leads to increased PL synthesis and β-oxidation.

Model applications

Control analysis: Quantification of pro-steatotic and anti-steatotic effects elicited by activation and inhibition of individual molecular processes

We used the model to assess how changes in the maximal activity of individual molecular processes included into the model influence the TAG content and LD size distribution at fixed external load with FFAs. To this end, the maximal activity of a single molecular process was increased and decreased by 10% and the stationary LD distribution was calculated at fixed external concentration of 0.5 mM FFAs. The result of this control analysis is shown in Fig. 5.

The model predicts that among all RSPs the largest influence is exerted by the ATGL. Uptake of FFAs is

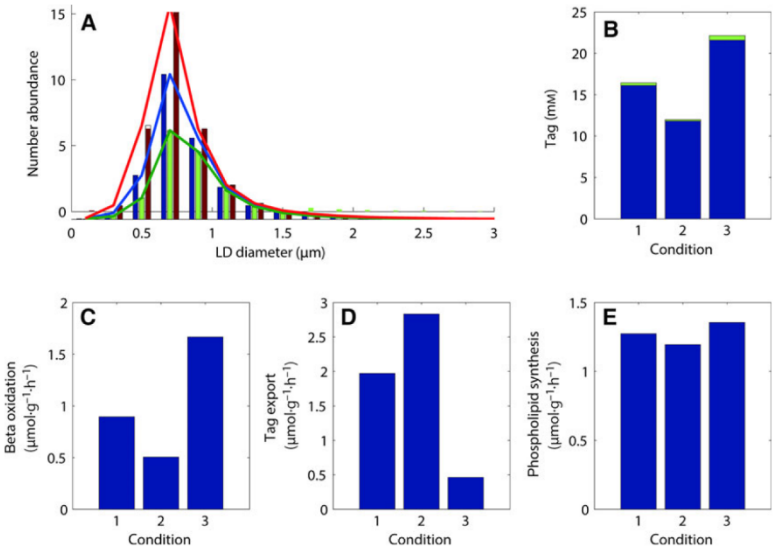

Fig. 4. Changes of selected metabolic parameters associated with overexpression or knockdown of microsomal transfer protein (MTP). (A) LD size distribution, (B) cellular TAG content, (C) rate of β-oxidation, (D) TAG export rate, (E) rate of phospholipid synthesis. Condition 1 – default MTP abundance (blue curve in A); Condition 2 – MTP overexpression: 10-fold increase of protein abundance (green curve in A); Condition 3 – MTP knockdown (10-fold reduction) of protein abundance (red curve in A).

an important controlling step, while the enzymes AGPAT and PAP of the TAG synthesizing pathway have little control contrary to DGAT1 and DGAT2 catalyzing the last reaction step and competing for the common precursor metabolite DAG with DCPT. The results of the control analysis are in concordance with several experimental findings. The expression of CD36, an important transporter of FFAs into the cell, is increased in animal models of NAFLD and in humans with NAFLD [23]. Liver ATGL expression was found to be decreased in hepatic steatosis patients [24]. Fsp27 is also highly expressed in the steatotic liver [25].

Changes of the lipid droplet size distribution in TAG accumulating PLC cells

Several studies have demonstrated that exposure of hepatocytes to high concentrations of free fatty acids in the medium leads to a rapid cellular accumulation of TAG within a few hours whereby the size of LDs increases. However, measurements of the dynamic changes in the LD size distributions during TAG accumulation are lacking so far. To fill this gap, we performed experiments with human hepatoma cells (PLC) which were incubated with a mixture of palmitate and oleate over 24 h and determined the LD size distribution at several time points (see Fig. 6).

Starting at about 6 h, the median of the LD size distribution exhibited a significant right-shift toward larger LDs with increasing incubation time. This right-shift, however, did not change the width of the distribution, indicating that the fraction of small LDs was reduced while the fraction of large LDs became larger with increasing lipid load. The shift from smaller toward larger LDs is physiologically plausible as the TAG content of a spherical LD particle with radius R is proportional to R^3. A large LD with radius $R = 2$ μm stores the same amount of TAG as 23 small LDs with radius $R = 0.7$ μm. Model simulations recapitulated the observed temporal changes in the shape of the LD size distribution up to the time point 6 h, but failed to reproduce the right-shift of the median, the extensive disappearance of small LDs and the long tail of the distribution toward larger LDs observed after 24 h. We suspected that changes of protein abundances may have occurred during the 24-h incubation accounting for the preferred formation of larger LDs. Indeed, hepatic lipid accumulation has been shown to be accompanied by significant alterations in the abundance of PAT and CIDE proteins [25–27], which are mainly mediated by the transcriptional factors PPARγ and CREBH. Reasoning that the most efficient way of hepatocytes to accommodate their TAG storage capacity to a higher TAG load can be brought about by changes in the expression levels of those proteins displaying the strongest pro-lipogenic effects, we included into the model a temporal change in the activities of the DGAT2 and FSP27 which according to the control analysis above turned out to have strong influence on LD size distribution. This model extension brought the simulated LD size distribution only slightly closer to the experimental data (blue curves in Fig. 6). Randomly varying the activity of other SRPs did not improve the situation. We, thus, suspected additional

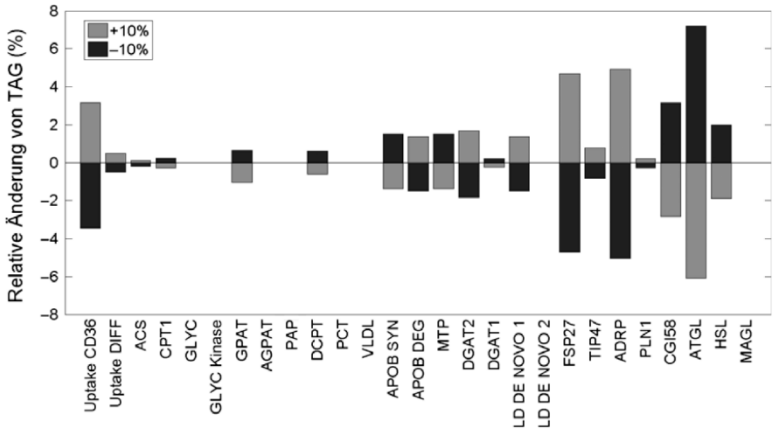

Fig. 5. Relative change of the cellular TAG level elicited by a change (±10%) of the maximal activity of the individual processes indicated at the bottom scale.

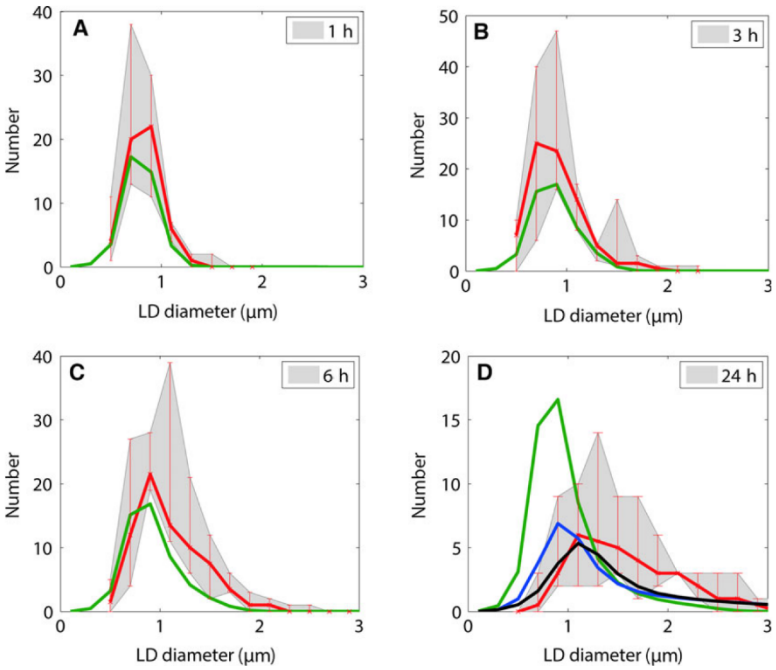

Fig. 6. Experimental and simulated LD size distributions in PLC cells. Cells were incubated with a 1:1 mixture of 0.5 mM palmitate/oleate for a time interval of 1 h, 3 h, 6 h, and 24 h. The number and size of LDs was analyzed in 73 different cells. Red curves: Median size distribution (red curves) and the 25% percentiles (gray-green areas) computed. Green curves: Simulated LD size distributions at default protein abundances. Blue curve: Simulated LD size distributions at 3-fold increase of DGAT2 activity and 3-fold increase of FSP27 activity between 6 h and 24 h. Black curve: Simulated LD size distributions at 3-fold increase of DGAT2 activity, 8-fold increase of FSP27 activity and modified DGAT2 filling kinetics (2-fold increase of the parameter r_ld-dgat2 restricting the size of LDs which can be effectively filled with TAG by DGAT2) during between 6 h and 24 h.

changes in at least one of the two alternative mechanisms in the model that may cause the disappearance of small LDs. Increase in LD site may result from either additional TAG loading to existing LDs by DGAT2 or transfer of TAG from smaller to larger LDS mediated by FSP27. As an increase of FSP27 has already turned out to be not sufficient to reproduce the observed LD size distribution at 24 h, we concluded that changes in the LD size preference of DGAT2 must have occurred during the 24 h FFA challenge. Indeed, increasing the model parameter r_ld-dgat2 that defines the largest size of LDs which can be effectively filled with TAG by DGAT2, we achieved a perfect match between observed and simulated LD size distributions at 24 h (black curves in Fig. 6). The kinetic model parameter r_ld-dgat2 aggregates a number of elementary steps involved in the recruitment of LDs to the ER membrane and the association of DGAT2 with docked LDs. Thus, it is difficult to provide a clear mechanistic explanation for the presumed change in the kinetics of LD expansion. Electron microscopic technique of freeze-fracture replica immune-gold labeling (FRIL) have provided evidence that expanding LDs are resident at

specialized domains of the ER where the membranes of the ER lie external to and follow the contour of the LD enclosing it like an egg-cup [28]. How these specific LD docking sites of the ER are formed and why they are capable of accommodating larger LDs under conditions of severe FFA challenge as suggested by our simulations remains to be clarified. Ultrastructural changes of the ER may play a role as overloading the ER of CHO cells by means of a palmitate-induced accelerated synthesis of neural lipids dramatically dilated the ER and impaired ER morphology within a few hours [29].

Heterogeneity of the lipid droplet size distribution in TAG accumulating human hepatocytes

In a second experiment, we exposed hepatocytes isolated from the same human liver to a FFA challenge for 24 h. Careful analysis of the number and size of LDs in 27 individual cells revealed largely deviating LD size distributions (see the example in Fig. 7A) pointing to considerable heterogeneity in the expression level of key regulatory proteins. The corresponding mean LD size distribution and the associated 25% percentiles are depicted in Fig. 7B. We used the model to figure out potential protein expression patterns that may account for the observed variability in LD size distributions. As the model has been parametrized for rat hepatocytes, it was necessary to calibrate some model parameters to recapitulate the median LD distribution observed after 24 h of FFA-induced TAG accumulation (black curve in Fig. 6D). Then, we randomly varied the abundance of (a) FFA uptake-CD36, (b) DGAT1, (c) DGAT2, (d) FSP27, (e) ADRP, and (f) ATGL that according to the control analysis should have the strongest impact on the LD size distribution. We fixed the maximal fold change in the expression of these proteins by a factor in a range between 1 (no change) and 5 and computed LD size distributions for 100 randomly generated protein abundance patterns. Next, we checked whether the computed LD size distribution belongs statistically to the ensemble of observed distributions. A simulated distribution was defined as 'hit' if the occupation of a predefined number of size classes remained within the range defined by the 25% percentiles of the experimental distribution. The number of size classes which had to fulfill this hit criterion was varied between 5 and 11

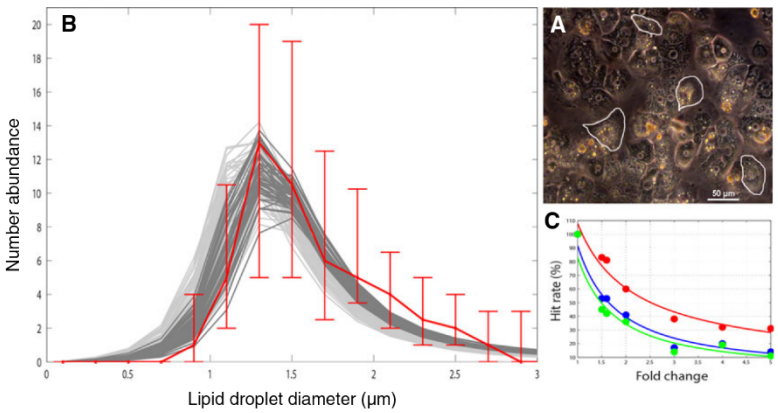

Fig. 7. Heterogeneity of TAG levels and LD size distributions in individual human hepatocytes. (A) Phase contrast light photomicrograph of confluent primary human hepatocytes revealing a large heterogeneity in the number of size of LDs of individual cells. Four individual hepatocytes are marked by red contours. The cells were incubated for 24 h with a 1:1 mixture of 0.5 mM palmitate/oleate. (B) Median LD size distribution (bold red curve) and ranges of variability (= 25% quantiles, i.e. 25% of values were below and above) obtained by averaging across the LD size distributions of 27 individual cells. In order to match the median size distribution some of the model parameters had to be changed by the following factors (in brackets) with respect to their values in the reference model for the rat hepatocyte: DAGT2 (10), FFA (10), r_d_dgat2 (0.5), ATGL (0.005), FSP27 (0.5). For the generation of random size distributions, the abundance of the following six key regulatory proteins (= influencing factors) was randomly varied by a factor of 2, 3, 4, and 5: (a) FFA uptake-CD36, (b) DGAT1, (c) DGAT2, (d) FSP27, (e) ADRP and (f) ATGL. Dark-gray curves mark simulated LD size distributions (about 50% of all curves) falling into the 11 variability ranges defined by the experimental data, curves violating the hit criterion are marked in light-gray. The thin dark-gray and light-gray curves refer to the 50% LD size distributions falling either into or outside the ranges of experimentally observed variability in the simulations carried out with a maximal random fold change by a factor of 1.5. (C) Fraction of simulated LD size distributions falling into 5 (red points), 8 (blue points) or 11 (= all) (green points) of the variability ranges defined by the 25% percentiles of the data at various maximal fold changes. A fold change by a factor of about 1.5 was sufficient to generate about 50% of statistically correct size distributions.

(= total number of size classes). We varied the allowed maximal random fold change of activities between 1 and 5 and checked the relative fraction of hits (Fig. 7C). This analysis revealed that depending on the number of size classes forced to meet the hit criterion, a modest random fold change by a factor of 1.4–1.9 (Fig. 7C) yielded a fraction of about 50% hits, i.e. was sufficient to account the broad scatter of experimental data. Fig 7B shows the set of randomly generated LD size distributions with a maximal gene expression fold change of 1.5 meeting the criterion that about 50% of curves are located with the 25% percentiles of all 11 size classes considered (dark-gray curves).

Taken together, the comparison of experimentally determined and simulated LD size distributions in two different types of liver cells strongly suggests that the extent of temporal TAG accumulation upon a FFA challenge depends sensitively upon adaptive gene expression of pro-lipogenic enzymes and RSPs.

Diurnal dynamics of lipid droplets

Based on our findings with isolated liver cells, we used the model to simulate changes in the TAG metabolism of the rat liver in response to diurnal variations of glucose, FFAs, insulin, and glucagon in the blood plasma (Fig. 8). The plasma profiles of hormones and metabolites for the fed and fasted rat were taken from our previous work [30] (Data S1). The randomly generated abundance profiles of the six key regulatory proteins explaining the variability of the LD size distribution in isolated human hepatocytes (see previous section) were used to generate LD size distributions at each hour of a 24-h time interval. For the fed rat, relative changes of the cellular TAG content of individual hepatocytes amount to about ± 15% with lowest and highest values at 0 h and 12 h. Cells with the lowest absolute TAG content of about 10 mM (dark-blue curves and columns in Fig. 8B,C) display a slightly larger diurnal variability than cells with the highest TAG content of about 20 mM (light-blue curves and columns).

In contrast, the relative TAG content in hepatocytes of the fasted rat (= 48 h starvation period) shows only small variations of few percent as the FFA plasma level and of glucagon in this conditions is constantly elevated. The absolute TAG levels may even reach values above 35 mM, i.e. under starvation conditions a significant portion of cells may already be assessed as being steatotic.

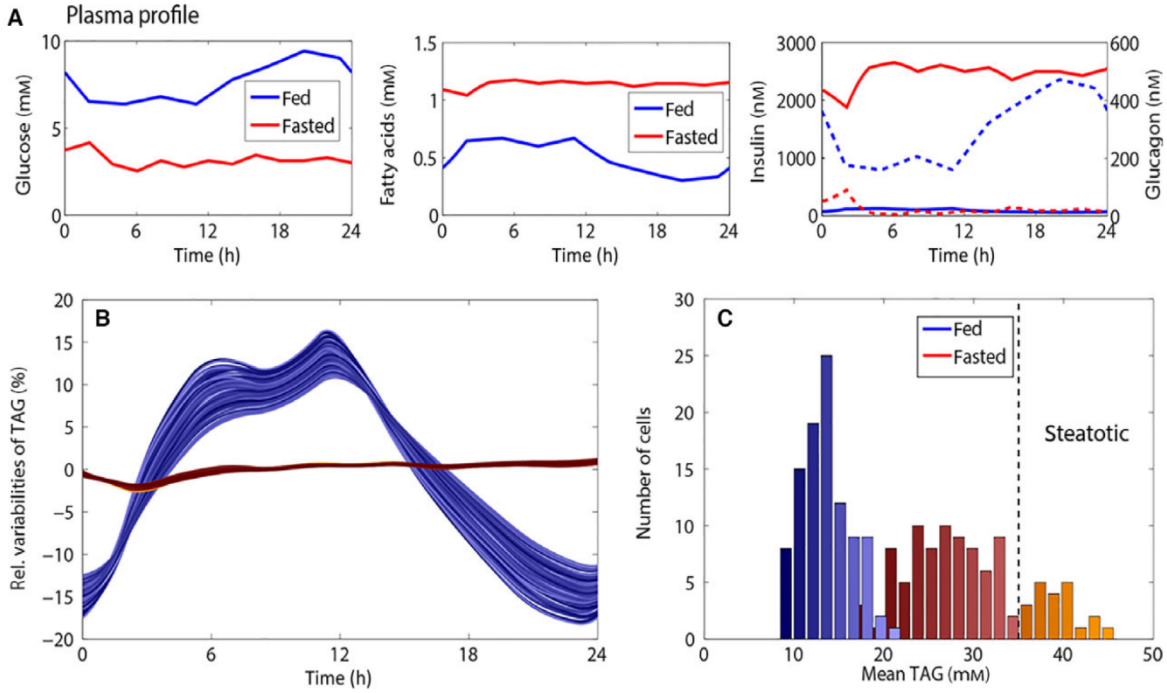

Fig. 8. Simulated diurnal TAG profile of rat hepatocytes *in vivo*. (A) 24 h concentration profiles of glucose, FFAs, insulin and glucagon (dotted lines) of the fed and fasted rat (see Data S3). (B) Relative variability of the cellular TAG content with respect to the 24 h mean. The curves were generated by randomly varying the activities of FFA uptake, CD36, DGAT1, DGAT2, FSP27, ADRP and ATGL at a maximal fold change of 1.5. Color depth decreases with increasing absolute TAG content shown in 7C. (C) Frequency distribution of the mean cellular TAG content (=24 h mean). Cells with TAG levels above 35 mM are designated as being steatotic (dashed line).

Discussion

The model – a unifying framework

Owing to the central role of the cellular TAG metabolism in obesity, hepatic steatosis, diabetes, and myopathies [31], ongoing intensive experimental research aims at the elucidation of molecular mechanisms controlling the cellular TAG level. Mathematical models of hepatic and systemic lipid metabolism may help to decipher key processes controlling the cellular TAG pool and hence suited as targets of medical drugs antagonizing the excessive TAG accumulation in the liver (steatosis). Pratt *et al.* [32] have developed a compartment model of systemic TAG turnover including in a phenomenological manner the synthesis and degradation of TAG in liver, skeletal muscle, and adipose tissue. But their model disregards the LD metabolism. Other models have focused on specific aspects of the assembly and plasma catabolism of VLDL, the central lipid exporter of the liver [33,34]. A mathematical model combining the hepatic metabolism of free fatty acids and TAG with the formation and degradation of LDs is lacking so far. Therefore, the aim of our work was to develop a unifying mathematical model that captures both the available information on the regulation of metabolic enzymes involved in TAG metabolism and the more qualitative findings on the cellular distribution and dynamics of LDs. We are fully aware that our model has to be regarded as an interim computational framework that will have to be extended and updated along with novel experimental findings. For example, some key players as the CIDE protein FSP27 have been identified quite recently and would have missed in a model that was developed 5 years earlier. The Arf1/COPI protein machinery, known for its role in vesicle trafficking, was recently shown to localize to cellular LDs to target specific TG-synthesis enzymes to LD surfaces [35]. The researchers admit that the mechanism of Arf1/COPI action is unclear thus complicating their incorporation into a mechanistic model. Moreover, the precise function of certain proteins like DGAT1 and DGAT2 still has to be resolved. In particular, our model neglects the spatial aspects of the lipid metabolism as, for example, the active microtubular transport of LDs [36] restricting their mutual interaction in space. As a general problem with all kinetic models of cellular reactions systems, many molecular items necessarily remain unnoticed. At best, their action is indirectly captured in the parametrization of the processes that are explicitly taken into account.

Despite these obvious and necessary limitations, the good concordance of model predictions with a large array of independent experimental findings (Table 1) confers a high degree of credibility to the model, thus making it a useful tool for the generation of hypothesis which may guide further experimentation.

Control analysis

One important conclusion derived from the comparison of model simulations with observed LD size distribution in TAG accumulating cells is that variations in the expression level of enzymes, and RSPs may play a decisive role in the short-term adaptation of liver cells to a FFA load. The control analysis reveals that the most efficient strategy of hepatocytes to convert external FFAs into cellular TAG consists in an increase of the FFA uptake, up-regulation of DGAT2 catalyzing the incorporation of activated FFAs into pre-existing LDs by esterification with DAG, and down-regulation of ATGL in order to prevent lipolysis of growing LDs. From this, it appears that adding TAG to already existing LDs is preferred against *de novo* synthesis of many nascent LDs to increase the TAG content above the normal. It is tempting to speculate that this is due to the fact that storage of TAG in larger LDs is economically favorable as it requires less phospholipids and RSPs compared to storing the same amount of TAG in small LDs. The pro-lipogenic changes of key regulatory proteins predicted by our model simulations are corroborated by studies demonstrating that hepatic lipid accumulation is accompanied by significant alterations in the abundance of PAT- and CIDE proteins [25–27] which are mainly mediated by the transcription factors PPARγ and CREBH.

Heterogeneity of LD size distribution *in vitro*

In agreement with previous findings [7], we observed a large heterogeneity of the TAG content and the LD size distribution in individual human hepatocytes isolated from the same liver and incubated with an excess of FFAs. This heterogeneity could be well reproduced in model simulations where the activity of key regulatory proteins was randomly sampled thus pointing to cell-to-cell differences in the gene expression (transcription or translation) of these proteins. Notably, only moderate variations by a factor of about two were sufficient to match the broad scatter of experimentally determined and simulated LD distributions. Such variability in the expression of PAT proteins has been indeed measured in specimens taken from normal

human livers and livers with varying degree of steatosis [27].

The source of variability of key regulatory proteins is not known yet. Earlier studies on single cells and population transcriptomics have revealed striking differences in global gene expression distributions [37] which, however, become largely reduced across cell ensembles [38]. On top of genetically determined 'noise', the activities of certain metabolic enzymes (e.g. glutamine synthetase) in hepatocytes display a zonal heterogeneity, i.e. their expression level depends on the spatial position of the cell along the sinusoid. It has been suggested that this zonation reflects differences in the plasma concentrations of metabolites (including oxygen) [39] and morphogens like β-catenin [40] between the periportal and perivenous region of the sinusoid. For example, β-catenin transgenic mice fed with a high-fed diet developed prominent perivenous steatosis. As the spatial origin of human hepatocytes used in our experiments is unknown, we cannot discriminate between the relative impact of these two possible sources of expression variability. Repetition of the experiment with cells stemming preferentially from either zone [41] could help to clarify this point.

Heterogeneity of LD size distribution *in vivo*

Under the assumption that a similar variability in the abundance of key regulatory proteins as estimated from the experiments with isolated cells also holds in the intact organ, we simulated the diurnal cellular TAG profile of rat hepatocytes in response to a typical plasma profile of glucose and FFAs. Modest random variations of key regulatory processes by a factor of 1.5 gave rise to changes by a factor of three in the TAG content of individual cells. Under starvation conditions characterized by a constantly elevated plasma level of FFAs, this implied that the TAG in about 25% of all simulated cells already reached concentration levels of 40 mM thus crossing the border line to steatosis. Whether this remarkable variability may account for the heterogeneous TAG distribution in steatotic livers depends upon the spatial distribution of heterogenous gene expression. If a specific expression profile holds for clusters of cells adjacent to each other (e.g. in a specific spatial zone of the lobule), one would expect significant variability if the TAG cells belonging to clusters with different expression profiles. The data from mouse liver sections in [7] do not support this view. If the expression heterogeneity occurs from cell to cell without any spatial bias, cell-to-cell variability in the TAG content would average out across a mesoscopic scale. Thus, further experimentation is required to further clarify how the individual risk for the development of a steatosis and the distribution of steatotic regions across the liver is determined by expression variability of key regulatory proteins of the TAG metabolism and LD dynamics. Single-cell transcriptomics [42] and (even better) single-cell proteomics of the respective proteins in cells taken from defined spatial regions of the liver could yield the necessary information.

Regarding the physiological significance of the large variability in the lipid storing capacity of individual cells deviating hypotheses have been expressed in the literature. Herms *et al.* [7] have argued that the existence of a subpopulation of cells that effectively collect and store lipids might be beneficial for the organ as a whole. They argue that a high-lipid subpopulation accumulates more LDs and hence more reactive oxygen species (ROS). This reduces the risk of lipotoxicity to the whole population. The overall lipid homeostasis should not be endangered since high-lipid cells can supply stored lipids to the other cells. However, excessive lipid storage is accompanied by an enlargement of cell size reducing the sinusoids radius and impairing hepatic microcirculation (regional hypoxia). It has been hypothesized that this may give rise to a vicious cycle (positive feedback) in that oxygen shortage reduces the usage of FFAs in β-oxidation, which favors the esterification of FFAs into the TAG pool and thus further enhances cell ballooning [43]. Another self-amplifying circuit resulting in heterogeneously distributed TAG clusters might be established by the enhanced local secretion of pro-inflammatory cytokines like TNF-α released from steatotic hepatocytes [44]. As TNF-α promotes TAG accumulation in hepatocytes [45], severely steatotic cells might induce enhanced TAG accumulation in neighboring cells.

Materials and methods

Materials

DMEM medium was purchased by GE Healthcare (Pasching, Austria). Supplements: fetal calf serum (FCS), Pen/Strep, HEPES, MEM NEAA, Pyruvate, L-glutamine, and PBS were purchased from Gibco (Paisley, UK). Dexamethasone was obtained from Merck (Fortecortin®, Darmstadt, Germany). Human insulin was purchased from Sanofi Aventis (Frankfurt am Main, Germany). All other chemicals were purchased from Sigma (Munich, Germany), if not stated differently. Rat-tail collagen was prepared in our laboratory according to the protocol established by Rajan *et al.* [58]. The hepatocyte culture medium was based on

DMEM, supplemented with 10% FCS, 1 mM L-glutamine, 32 $mU \cdot mL^{-1}$ insulin, 15 mM HEPES, 1% MEM NEAA (100x), 1 mM Pyruvate and 1 $\mu g \cdot mL^{-1}$ Fortecortin. The hepatocyte control medium based on DMEM supplemented with 5% FCS, 1 mM L-glutamine, 15 mM HEPES, 1% MEM NEAA (100x), and 1 mM Pyruvate.

PHH Isolation

The PHH was isolated from macroscopically healthy tissue that remained from resected human liver of patients with primary or secondary liver tumors or benign local liver diseases. Informed consent of the patients for the use of tissue for research purposes was obtained according to the ethical guidelines of the Charité – Universitätsmedizin Berlin. Cell isolation was performed using a two-step collagenase P perfusion technique [59,60]. Hepatocytes were seeded at a density of 1.0×105 cells$\cdot cm^{-2}$ in six-well-plates (BD Sciences, Franklin Lakes, NJ, USA) coated with rat-tail collagen. Cells were cultivated in hepatocyte culture medium for 12 h at 37°C in a humidified incubator at 5% CO_2. The morphologically of the cells was inspected daily by light microscopy. Cell culture medium was changed every day.

Steatosis induction

Steatosis was induced by cultivation of PHH in free fatty acids (FFA) containing medium for 5d. According to [61] the FFA mixture contains oleic and palmitic acid with a 2:1 ratio and a final concentration of 0.6 mM. After 12-h culture in hepatocyte culture medium, the cells were washed with PBS and medium was changed to control medium or to control medium containing FFA mixture and the cells were incubated for up to 5 days. During this time, medium of the hepatocyte culture was changed daily. After the medium exchange, the morphology and lipid accumulation were inspected using a Axiovert 135 microscope (Carl Zeiss AG, Oberkochen, Germany) and documented by taking pictures in 320-time magnification.

Human hepatoma cells (PLC)

The human hepatoma cell line PLC is an established cell line and is available through the American type culture collection (ATCC). The cell line was cultured in DMEM supplemented with 10% fetal calf serum, 1% glutamine, and 1% pen- strep at 37°C with 100% humidity and 5% CO_2. The cell culture media and reagents were purchased from Gibco, Big Cabin, OK, USA. The morphologically of the cells was inspected daily by phase contrast microscopy.

Cell treatment

At around 80% confluence, PLC cells were treated with 0.5 mM of an equimolar mixture of palmitic and oleic acid (PA/OA) for 1 h, 3 h, 6 h, and 24 h. The PPH was treated with 0.6 mM of 2:1 mixture of palmitic and oleic acid (PA/OA) for 23 h. The final DMSO concentration in control and PA/OA-treated cell cultures was 0.5% v/v. The culture medium was changed daily.

Quantification of lipid droplet distribution

After fatty acid incubation, cells were washed with 1x PBS twice. Finally the cells were suspended in 0.2 mM MDH and incubated at 37°C for 15 min in the dark. After staining, the cells were washed with 1x PBS thrice to remove excess stain and re-suspended in phenol red free media. The images were captured by phase contrast fluorescence microscopy at 40× using time-lapse z-stack (Nikon TiE) and further analyzed using the NIS elements software version 4.13 NIS (Nikon Corporation, Tokyo, Japan). The images were captured by light microscopy (Carl Zeiss) and the data were analyzed with NIS elements software.

Conclusion

Taken together, our modeling approach puts together numerous individual experimental findings on lipid and LD metabolism to a consistent mechanistic network. Based on this network model, we provide an estimation of the variability in the abundance of central enzymes and RSPs accounting for the observed intercellular heterogeneity of LD size distributions. We propose a mechanism according to which cells exposed to a FFA challenge may switch from the *de novo* synthesis of LDs to enforced lipid loading to already existing LDs. Finally, we provide an estimation of the variability of the cellular TAG content of the human liver *in vivo* and discuss possible implications of this heterogeneity for the development of hepatic steatosis as a self-amplifying process.

Author contributions

CW planned experiments, performed experiments, analyzed data, and developed the model. DE analyzed

data. TS planned experiments and performed experiments. GD planned experiments and performed experiments. DS planned experiments. JB planned experiments. HGH planned and developed the model and wrote the MS. NB developed the model and wrote the MS.

Acknowledgements

This work was supported by funding from the graduate school 'Computational Systems Biology' (GRK 1722) of the German Research Council and the Systems Biology Program 'LiSym' of the German Federal Ministry of Education and Research (BMBF) (grant no. 31L0057).

References

1 Carman GM (2012) Thematic minireview series on the lipid droplet, a dynamic organelle of biomedical and commercial importance. *J Biol Chem* **287**, 2272.
2 Krahmer N, Guo Y, Wilfling F, Hilger M, Lingrell S, Heger K, Newman HW, Schmidt-Supprian M, Vance DE, Mann M *et al.* (2011) Phosphatidylcholine synthesis for lipid droplet expansion is mediated by localized activation of CTP:phosphocholine cytidylyltransferase. *Cell Metab* **14**, 504–515.
3 Mei S, Ni HM, Manley S, Bockus A, Kassel KM, Luyendyk JP, Copple BL & Ding WX (2011) Differential roles of unsaturated and saturated fatty acids on autophagy and apoptosis in hepatocytes. *J Pharmacol Exp Ther* **339**, 487–498.
4 Rohwedder A, Zhang Q, Rudge SA & Wakelam MJ (2014) Lipid droplet formation in response to oleic acid in Huh-7 cells is mediated by the fatty acid receptor FFAR4. *J Cell Sci* **127**, 3104–3115.
5 Yao HR, Liu J, Plumeri D, Cao YB, He T, Lin L, Li Y, Jiang YY, Li J & Shang J (2011) Lipotoxicity in HepG2 cells triggered by free fatty acids. *Am J Transl Res* **3**, 284–291.
6 Gocze PM & Freeman DA (1994) Factors underlying the variability of lipid droplet fluorescence in MA-10 Leydig tumor cells. *Cytometry* **17**, 151–158.
7 Herms A, Bosch M, Ariotti N, Reddy BJ, Fajardo A, Fernandez-Vidal A, Alvarez-Guaita A, Fernandez-Rojo MA, Rentero C, Tebar F *et al.* (2013) Cell-to-cell heterogeneity in lipid droplets suggests a mechanism to reduce lipotoxicity. *Curr Biol* **23**, 1489–1496.
8 Chang BH, Li L, Paul A, Taniguchi S, Nannegari V, Heird WC & Chan L (2006) Protection against fatty liver but normal adipogenesis in mice lacking adipose differentiation-related protein. *Mol Cell Biol* **26**, 1063–1076.
9 Bell M, Wang H, Chen H, McLenithan JC, Gong DW, Yang RZ, Yu D, Fried SK, Quon MJ, Londos C *et al.* (2008) Consequences of lipid droplet coat protein downregulation in liver cells: abnormal lipid droplet metabolism and induction of insulin resistance. *Diabetes* **57**, 2037–2045.
10 Nishino N, Tamori Y, Tateya S, Kawaguchi T, Shibakusa T, Mizunoya W, Inoue K, Kitazawa R, Kitazawa S, Matsuki Y *et al.* (2008) FSP27 contributes to efficient energy storage in murine white adipocytes by promoting the formation of unilocular lipid droplets. *J Clin Investig* **118**, 2808–2821.
11 Wotton RM & Mosti ME (1955) The direct absorption of previously stained fat in droplet form by the myocardium of the cat. *Anat Rec* **122**, 39–47.
12 Stone SJ, Myers HM, Watkins SM, Brown BE, Feingold KR, Elias PM & Farese RV Jr (2004) Lipopenia and skin barrier abnormalities in DGAT2-deficient mice. *J Biol Chem* **279**, 11767–11776.
13 Yen CL, Stone SJ, Koliwad S, Harris C & Farese RV Jr (2008) Thematic review series: glycerolipids DGAT enzymes and triacylglycerol biosynthesis. *J Lipid Res* **49**, 2283–2301.
14 Gong J, Sun Z, Wu L, Xu W, Schieber N, Xu D, Shui G, Yang H, Parton RG & Li P (2011) Fsp27 promotes lipid droplet growth by lipid exchange and transfer at lipid droplet contact sites. *J Cell Biol* **195**, 953–963.
15 Lass A, Zimmermann R, Haemmerle G, Riederer M, Schoiswohl G, Schweiger M, Kienesberger P, Strauss JG, Gorkiewicz G & Zechner R (2006) Adipose triglyceride lipase-mediated lipolysis of cellular fat stores is activated by CGI-58 and defective in Chanarin-Dorfman Syndrome. *Cell Metab* **3**, 309–319.
16 Haas ME, Attie AD & Biddinger SB (2013) The regulation of ApoB metabolism by insulin. *Trends Endocrinol Metab* **24**, 391–397.
17 Liu Y, Millar JS, Cromley DA, Graham M, Crooke R, Billheimer JT & Rader DJ (2008) Knockdown of acyl-CoA:diacylglycerol acyltransferase 2 with antisense oligonucleotide reduces VLDL TG and ApoB secretion in mice. *Biochim Biophys Acta* **1781**, 97–104.
18 Millar JS, Stone SJ, Tietge UJ, Tow B, Billheimer JT, Wong JS, Hamilton RL, Farese RV Jr & Rader DJ (2006) Short-term overexpression of DGAT1 or DGAT2 increases hepatic triglyceride but not VLDL triglyceride or apoB production. *J Lipid Res* **47**, 2297–2305.
19 Wilfling F, Wang H, Haas JT, Krahmer N, Gould TJ, Uchida A, Cheng JX, Graham M, Christiano R, Frohlich F *et al.* (2013) Triacylglycerol synthesis enzymes mediate lipid droplet growth by relocalizing from the ER to lipid droplets. *Dev Cell* **24**, 384–399.
20 Yamazaki T, Sasaki E, Kakinuma C, Yano T, Miura S & Ezaki O (2005) Increased very low density lipoprotein secretion and gonadal fat mass in mice

overexpressing liver DGAT1. *J Biol Chem* **280**, 21506–21514.
21 Li C, Li L, Lian J, Watts R, Nelson R, Goodwin B & Lehner R (2015) Roles of Acyl-CoA: diacylglycerol acyltransferases 1 and 2 in triacylglycerol synthesis and secretion in primary hepatocytes. *Arterioscler Thromb Vasc Biol* **35**, 1080–1091.
22 Choi CS, Savage DB, Kulkarni A, Yu XX, Liu ZX, Morino K, Kim S, Distefano A, Samuel VT, Neschen S *et al.* (2007) Suppression of diacylglycerol acyltransferase-2 (DGAT2), but not DGAT1, with antisense oligonucleotides reverses diet-induced hepatic steatosis and insulin resistance. *J Biol Chem* **282**, 22678–22688.
23 Mitsuyoshi H, Yasui K, Harano Y, Endo M, Tsuji K, Minami M, Itoh Y, Okanoue T & Yoshikawa T (2009) Analysis of hepatic genes involved in the metabolism of fatty acids and iron in nonalcoholic fatty liver disease. *Hepatol Res* **39**, 366–373.
24 Kato M, Higuchi N & Enjoji M (2008) Reduced hepatic expression of adipose tissue triglyceride lipase and CGI-58 may contribute to the development of non-alcoholic fatty liver disease in patients with insulin resistance. *Scand J Gastroenterol* **43**, 1018–1019.
25 Xu X, Park JG, So JS & Lee AH (2015) Transcriptional activation of Fsp27 by the liver-enriched transcription factor CREBH promotes lipid droplet growth and hepatic steatosis. *Hepatology* **61**, 857–869.
26 Okumura T (2011) Role of lipid droplet proteins in liver steatosis. *J Physiol Biochem* **67**, 629–636.
27 Straub BK, Stoeffel P, Heid H, Zimbelmann R & Schirmacher P (2008) Differential pattern of lipid droplet-associated proteins and de novo perilipin expression in hepatocyte steatogenesis. *Hepatology* **47**, 1936–1946.
28 Robenek H, Buers I, Hofnagel O, Robenek MJ, Troyer D & Severs NJ (2009) Compartmentalization of proteins in lipid droplet biogenesis. *Biochim Biophys Acta* **1791**, 408–418.
29 Borradaile NM, Han X, Harp JD, Gale SE, Ory DS & Schaffer JE (2006) Disruption of endoplasmic reticulum structure and integrity in lipotoxic cell death. *J Lipid Res* **47**, 2726–2737.
30 Bulik S, Holzhutter HG & Berndt N (2016) The relative importance of kinetic mechanisms and variable enzyme abundances for the regulation of hepatic glucose metabolism–insights from mathematical modeling. *BMC Biol* **14**, 15.
31 Greenberg AS, Coleman RA, Kraemer FB, McManaman JL, Obin MS, Puri V, Yan QW, Miyoshi H & Mashek DG (2011) The role of lipid droplets in metabolic disease in rodents and humans. *J Clin Investig* **121**, 2102–2110.
32 Pratt AC, Wattis JA & Salter AM (2015) Mathematical modelling of hepatic lipid metabolism. *Math Biosci* **262**, 167–181.
33 Adiels M, Packard C, Caslake MJ, Stewart P, Soro A, Westerbacka J, Wennberg B, Olofsson SO, Taskinen MR & Boren J (2005) A new combined multicompartmental model for apolipoprotein B-100 and triglyceride metabolism in VLDL subfractions. *J Lipid Res* **46**, 58–67.
34 Shorten PR & Upreti GC (2005) A mathematical model of fatty acid metabolism and VLDL assembly in human liver. *Biochim Biophys Acta* **1736**, 94–108.
35 Wilfling F, Thiam AR, Olarte MJ, Wang J, Beck R, Gould TJ, Allgeyer ES, Pincet F, Bewersdorf J, Farese RV Jr *et al.* (2014) Arf1/COPI machinery acts directly on lipid droplets and enables their connection to the ER for protein targeting. *eLife* **3**, e01607.
36 Welte MA, Gross SP, Postner M, Block SM & Wieschaus EF (1998) Developmental regulation of vesicle transport in Drosophila embryos: forces and kinetics. *Cell* **92**, 547–557.
37 Elowitz MB, Levine AJ, Siggia ED & Swain PS (2002) Stochastic gene expression in a single cell. *Science* **297**, 1183–1186.
38 Piras V & Selvarajoo K (2015) The reduction of gene expression variability from single cells to populations follows simple statistical laws. *Genomics* **105**, 137–144.
39 Jungermann K & Kietzmann T (2000) Oxygen: modulator of metabolic zonation and disease of the liver. *Hepatology* **31**, 255–260.
40 Behari J, Li H, Liu S, Stefanovic-Racic M, Alonso L, O'Donnell CP, Shiva S, Singamsetty S, Watanabe Y, Singh VP *et al.* (2014) Beta-catenin links hepatic metabolic zonation with lipid metabolism and diet-induced obesity in mice. *Am J Pathol* **184**, 3284–3298.
41 Lindros KO & Penttila KE (1985) Digitonin-collagenase perfusion for efficient separation of periportal or perivenous hepatocytes. *Biochem J* **228**, 757–760.
42 Halpern KB, Shenhav R, Matcovitch-Natan O, Toth B, Lemze D, Golan M, Massasa EE, Baydatch S, Landen S, Moor AE, Brandis A *et al.* (2017) Single-cell spatial reconstruction reveals global division of labour in the mammalian liver. *Nature* **542**, 352–356.
43 Schleicher J, Guthke R, Dahmen U, Dirsch O, Holzhuetter HG & Schuster S (2014) A theoretical study of lipid accumulation in the liver-implications for nonalcoholic fatty liver disease. *Biochim Biophys Acta* **1841**, 62–69.
44 Pan X, Wang P, Luo J, Wang Z, Song Y, Ye J & Hou X (2015) Adipogenic changes of hepatocytes in a high-fat diet-induced fatty liver mice model and non-alcoholic fatty liver disease patients. *Endocrine* **48**, 834–847.
45 Endo M, Masaki T, Seike M & Yoshimatsu H (2007) TNF-alpha induces hepatic steatosis in mice by enhancing gene expression of sterol regulatory element binding protein-1c (SREBP-1c). *Exp Biol Med* **232**, 614–621.

46 Bagnato C & Igal RA (2003) Overexpression of diacylglycerol acyltransferase-1 reduces phospholipid synthesis, proliferation, and invasiveness in simian virus 40-transformed human lung fibroblasts. *J Biol Chem* **278**, 52203–52211.
47 Tietge UJ, Bakillah A, Maugeais C, Tsukamoto K, Hussain M & Rader DJ (1999) Hepatic overexpression of microsomal triglyceride transfer protein (MTP) results in increased in vivo secretion of VLDL triglycerides and apolipoprotein B. *J Lipid Res* **40**, 2134–2139.
48 Hebbachi A & Gibbons GF (1999) Inactivation of microsomal triglyceride transfer protein impairs the normal redistribution but not the turnover of newly synthesized glycerolipid in the cytosol, endoplasmic reticulum and Golgi of primary rat hepatocytes. *Biochim Biophys Acta* **1441**, 36–50.
49 Minehira K, Young SG, Villanueva CJ, Yetukuri L, Oresic M, Hellerstein MK, Farese RV Jr, Horton JD, Preitner F, Thorens B *et al.* (2008) Blocking VLDL secretion causes hepatic steatosis but does not affect peripheral lipid stores or insulin sensitivity in mice. *J Lipid Res* **49**, 2038–2044.
50 Raabe M, Veniant MM, Sullivan MA, Zlot CH, Bjorkegren J, Nielsen LB, Wong JS, Hamilton RL & Young SG (1999) Analysis of the role of microsomal triglyceride transfer protein in the liver of tissue-specific knockout mice. *J Clin Investig* **103**, 1287–1298.
51 Reid BN, Ables GP, Otlivanchik OA, Schoiswohl G, Zechner R, Blaner WS, Goldberg IJ, Schwabe RF, Chua SC Jr & Huang LS (2008) Hepatic overexpression of hormone-sensitive lipase and adipose triglyceride lipase promotes fatty acid oxidation, stimulates direct release of free fatty acids, and ameliorates steatosis. *J Biol Chem* **283**, 13087–13099.
52 Ong KT, Mashek MT, Bu SY, Greenberg AS & Mashek DG (2011) Adipose triglyceride lipase is a major hepatic lipase that regulates triacylglycerol turnover and fatty acid signaling and partitioning. *Hepatology* **53**, 116–126.
53 Smirnova E, Goldberg EB, Makarova KS, Lin L, Brown WJ & Jackson CL (2006) ATGL has a key role in lipid droplet/adiposome degradation in mammalian cells. *EMBO Rep* **7**, 106–113.
54 Wu JW, Wang SP, Alvarez F, Casavant S, Gauthier N, Abed L, Soni KG, Yang G & Mitchell GA (2011) Deficiency of liver adipose triglyceride lipase in mice causes progressive hepatic steatosis. *Hepatology* **54**, 122–132.
55 Guo F, Ma Y, Kadegowda AK, Betters JL, Xie P, Liu G, Liu X, Miao H, Ou J, Su X *et al.* (2013) Deficiency of liver Comparative Gene Identification-58 causes steatohepatitis and fibrosis in mice. *J Lipid Res* **54**, 2109–2120.
56 Zhou L, Park SY, Xu L, Xia X, Ye J, Su L, Jeong KH, Hur JH, Oh H, Tamori Y *et al.* (2015) Insulin resistance and white adipose tissue inflammation are uncoupled in energetically challenged Fsp27-deficient mice. *Nat Commun* **6**, 5949.
57 Najt CP, Senthivinayagam S, Aljazi MB, Fader KA, Olenic SD, Brock JR, Lydic TA, Jones AD & Atshaves BP (2016) Liver-specific loss of Perilipin 2 alleviates diet-induced hepatic steatosis, inflammation, and fibrosis. *Am J Physiol Gastrointest Liver Physiol* **310**, G726–G738.
58 Rajan N, Habermehl J, Cote MF, Doillon CJ & Mantovani D (2006) Preparation of ready-to-use, storable and reconstituted type I collagen from rat tail tendon for tissue engineering applications. *Nat Protoc* **1**, 2753–2758.
59 Pfeiffer E, Kegel V, Zeilinger K, Hengstler JG, Nussler AK, Seehofer D & Damm G (2015) Featured Article: Isolation, characterization, and cultivation of human hepatocytes and non-parenchymal liver cells. *Exp Biol Med (Maywood)* **240**, 645–656.
60 Kegel V, Deharde D, Pfeiffer E, Zeilinger K, Seehofer D & Damm G (2016) Protocol for Isolation of Primary Human Hepatocytes and Corresponding Major Populations of Non-parenchymal Liver Cells. *J Vis Exp* e53069.
61 Gomez-Lechon MJ, Donato MT, Martinez-Romero A, Jimenez N, Castell JV & O'Connor JE (2007) A human hepatocellular in vitro model to investigate steatosis. *Chem Biol Interact* **165**, 106–116.

Supporting information

Additional Supporting Information may be found online in the supporting information tab for this article:

Data S1. Rate Equations and kinetic parameters.
Data S2. Model fitting to experiments (parametrization).
Data S3. Plasma profiles of metabolites and hormones.
Data S4. Metabolite concentrations and fluxes.

2.5 *HEPATOKIN1 is a biochemistry-based model of liver metabolism for applications in medicine and pharmacology* [43]

Dieses Kapitel basiert auf [43] (DOI: 10.1038/s41467-018-04720-9).

Einleitung: Die Leber ist eines der stoffwechselaktivsten Organe des Körpers. Sie nimmt eine zentrale Rolle in der Verwertung von Zuckern, Fetten und Aminosäuren ein. Wie in 2.2-2.4 gezeigt, sorgt sie durch koordiniertes Umschalten zwischen Glykolyse und Glykoneogenese sowie Glykogensynthese und Glykogenabbau dafür, dass sich der Glukosespiegel in engen Grenzen bewegt. Im Kohlenhydratstoffwechsel ist sie außerdem verantwortlich für die Metabolisierung anderer Zucker wie Galaktose und Fruktose. Im Fettstoffwechsel nimmt die Leber die Rolle einer Schaltzentrale zwischen den Organen ein. Sie nimmt Fettsäuren vom Fettgewebe aus der Blutbahn auf und synthetisiert daraus Triglyzeride. Sie synthetisiert Fettsäuren und Cholesterol, die entweder in Lipidtropfen gespeichert oder als VLDL für die systemische Versorgung exportiert werden. In Zeiten der Nahrungskarenz wandelt die Leber Fettsäuren in Ketonkörper um. Im Aminosäurestoffwechsel des Körpers ist sie wesentlich mitverantwortlich für die Aminosäurezusammensetzung des Blutes und die Entgiftung von Ammoniak in Form von Harnstoff oder Glutamin. Zusätzlich ist die Leber für die Entsorgung von Xenobiotika und die Entgiftung von Alkohol zuständig. Alle diese verschiedenen metabolischen Funktionen müssen zeitgleich und unter sehr verschiedenen metabolischen Bedingungen realisiert werden. Folgerichtig ist die Leber eines der energieintensivsten Organe des Körpers und verbraucht ca. 10-20% des systemischen Sauerstoffs. Die gleichzeitige Regulation aller dieser Stoffwechselwege erfordert ein gut koordiniertes System von Enzymen.

Fragestellung: Ziel dieser Arbeit war es, ein molekular aufgelöstes Modell des hepatischen Zentralstoffwechsels zu erstellen, das die funktionelle Interpretation von Proteomdaten hinsichtlich verschiedener Leberfunktionen ermöglicht.

Methode: Es wurde ein molekular aufgelöstes kinetisches Modell des hepatischen Zentralstoffwechsels erstellt. Das Modell beinhaltet Stoffwechselwege der Glykolyse, Glykoneogenese, Glykogenaufbau und -abbau, Fruktosemetabolismus, Galaktosemetabolismus, oxidativen und nicht-oxidativen Pentosephosphatweg, Fettsäureaufnahme und -synthese, Triglyzeridsynthese, Synthese und Abbau von Lipidtropfen, Synthese und Abgabe von VLDL, Zitratzyklus, Atmungskette, oxidative Phosphorylierung, β-Oxidatition, Ketonkörpersynthese, Alanin-, Serin-, Glutamat- und Glutaminstoffwechsel, Harnstoffbildung sowie Alkoholmetabolismus.

Resultat: Das Modell wurde auf eine Reihe verschiedener Fragestellungen aus dem Bereich der Grundlagenforschung, Ernährungswissenschaften, Medizin und Pharmakologie angewendet. Es wurde untersucht, welchen Einfluss die einzelnen Enzyme und ihre jeweiligen kinetischen Parameter auf die verschiedenen Leberfunktionen haben, welche Auswirkung Alkoholkonsum auf den metabolischen Zustand der Leber hat und wie das Medikament Valproat den Leberstoffwechsel beeinflusst. Die funktionellen Konsequenzen von Genmutationen wurden am Beispiel verschiedener Mutationen von Enzymen des Galaktosestoffwechsels (Galaktosämien) untersucht. Von besonderer Bedeutung ist die Möglichkeit, mit dem Modell Proteinprofile funktionell zu interpretieren. So wurden am Beispiel von humanen HCC und Leberadenomen die metabolischen Veränderungen im Tumor untersucht.

Diskussion: Ein zentrales Ziel der Systembiologie ist es, das Verhalten eines Systems aus dem Eigenschaften und Wechselwirkungen seiner molekularen Konstituenten abzuleiten. Dieses Ziel wird bei der Modellierung metabolischer Systeme lediglich von kinetischen Modellen erreicht, dem Goldstandard der metabolischen Modellierung. Bisher waren kinetische Modelle auf kleine Subsysteme wie die Glykolyse beschränkt. Diese Arbeit präsentiert ein kinetisches Modell des zentralen Lebermetabolismus, das die wichtigsten Stoffwechselwege inklusive Energie-, Kohlenhydrat-, Fett- und Aminosäurestoffwechsel molekular aufgelöst abbildet und damit zum ersten Mal ein großskaliges metabolisches Netzwerk kinetisch beschreibt. Das Modell berücksichtigt dabei die Regulation der metabolischen Enzyme durch Substratverfügbarkeit, allosterische Regulation und Interkonversion (hormonelle Regulation).

Ziel dieser Arbeit war die Etablierung eines Systems, dass eine funktionale Interpretation von Proteindaten ermöglicht und es erlaubt, den metabolischen Zustand der Leber abhängig von internen und externen Bedingungen zu evaluieren. Neben der Beantwortung verschiedener medizinischer und Grundlagen-orientierter Fragestellungen war ein Hauptanliegen dieser Arbeit zu zeigen, dass es möglich ist, ein großes kinetisches Modell auf Basis von gemessenen Enzymdaten zu erstellen. Durch Vergleich von simulierten Metabolitkonzentrationen und Austauschflüssen mit experimentellen Daten unter verschiedensten physiologischen Bedingungen wird dabei insbesondere gezeigt, dass *in vitro*-bestimmte Enzymkinetiken geeignet sind, die tatsächlichen Zustände in Zellen adäquat abzubilden.

Der unmittelbare Mehrwert dieser Modellsimulationen liegt darin, dass alle Metaboliten und Flüsse des metabolischen Systems gleichzeitig berechnet werden können. Damit steht dem Anwender ein kompletteres Bild zur Verfügung, als es experimentell zu erreichen wäre, aber experimentell überprüft werden kann. Außerdem ist es möglich, die funktionellen Auswirkungen hypothetischer Veränderungen in den äußeren und inneren Bedingungen zu untersuchen.

nature COMMUNICATIONS

ARTICLE

DOI: 10.1038/s41467-018-04720-9 OPEN

HEPATOKIN1 is a biochemistry-based model of liver metabolism for applications in medicine and pharmacology

Nikolaus Berndt[1], Sascha Bulik[1,2], Iwona Wallach[1], Tilo Wünsch[3], Matthias König[4], Martin Stockmann[2], David Meierhofer[5] & Hermann-Georg Holzhütter[1]

The epidemic increase of non-alcoholic fatty liver diseases (NAFLD) requires a deeper understanding of the regulatory circuits controlling the response of liver metabolism to nutritional challenges, medical drugs, and genetic enzyme variants. As in vivo studies of human liver metabolism are encumbered with serious ethical and technical issues, we developed a comprehensive biochemistry-based kinetic model of the central liver metabolism including the regulation of enzyme activities by their reactants, allosteric effectors, and hormone-dependent phosphorylation. The utility of the model for basic research and applications in medicine and pharmacology is illustrated by simulating diurnal variations of the metabolic state of the liver at various perturbations caused by nutritional challenges (alcohol), drugs (valproate), and inherited enzyme disorders (galactosemia). Using proteomics data to scale maximal enzyme activities, the model is used to highlight differences in the metabolic functions of normal hepatocytes and malignant liver cells (adenoma and hepatocellular carcinoma).

[1] Institute of Biochemistry Computational Systems Biochemistry Group, Charité – Universitätsmedizin Berlin, Charitéplatz, 110117 Berlin, Germany. [2] German Federal Institute for Risk Assessment Max-Dohrn-Straße 8-10, 10589 Berlin, Germany. [3] Department of General, Visceral and Transplantation Surgery Augustenburger Platz, Charité – Universitätsmedizin Berlin - Campus Virchow-Klinikum, 113353 Berlin, Germany. [4] Institute for Biology, Institute for Theoretical Biology, Humboldt-University Berlin, Invalidenstraße 43, Haus, 410115 Berlin, Germany. [5] Max Planck Institute of Molecular Genetics/Mass Spectroscopy, Ihnestraße 63-73, 14195 Berlin, Germany. Correspondence and requests for materials should be addressed to H.-G.H. (email: hergo@charite.de)

Inferring the response of a biological system to external or internal perturbations from the properties and interactions of its constituting molecules is a central goal of systems biology[1]. With regard to metabolic systems, reaching this goal requires the establishment of mathematical models enabling the computation of metabolite concentrations and fluxes at given external conditions (nutrients and hormones), gene expression level of metabolic enzymes, and the systems history (e.g., current filling of nutrient stores).

Chemical reactions and mass transport are the basic processes in a metabolic network. They are catalyzed by specific enzymes and transport proteins that are regulated in multiple ways by their immediate ligands, allosteric effectors, hormone-dependent reversible phosphorylation, and variable gene expression. Often, a single specific regulatory enzyme feature is key for the regulation of a complete metabolic pathway. For example, the strongest regulator of the mitochondrial fatty acid transporter, carnitine palmitoyltransferase (CPT), is the competitive inhibitor malonyl-CoA. Decrease of malonyl-CoA concentration during the overnight fast is lifesaving because activation of CPT enables the enhanced oxidation of fatty acids to acetyl CoA and hence the formation of glucose-sparing ketone bodies in the liver[2]. This example underlines the importance of biochemistry-based kinetic models that incorporate such important regulatory features of enzymes.

The strong medical interest in a better understanding of the molecular processes underlying the regulation of liver metabolism arises from the fact that an ongoing metabolic imbalance of the organ, e.g., due to excessive intake of drugs, alcohol or fructose, may result in an abnormal accumulation of lipids (steatosis) thereby increasing the risk of developing serious liver diseases such as hepatitis, cirrhosis, and cancer[3]. Aiming at the in vivo assessment of liver metabolism, we developed a kinetic multi-pathway model of hepatocytes with hitherto unprecedented scope and level of detail. The model includes the regulation of enzyme activities by allosteric effectors, hormone-dependent reversible phosphorylation, and variable protein abundances. For each enzyme, rate equations have been developed that take into account the enzyme's kinetic and regulatory features as revealed and quantified by means of in vitro assays. In the following, we give an overview of the model while referring the interested reader to the extensive Supplementary material containing all technical details. We focus in the main text on simulations of the dynamic metabolic output of the liver at different plasma profiles of metabolites and hormones. Using quantitative proteomics data for the scaling of maximal enzyme activities, the model opens the goal for a quantitative functional interpretation of gene expression changes. We applied this approach to reveal the patient-specific metabolic profile of adenoma and HCC. In summary, our model provides a powerful tool for computational studies of liver metabolism in health and disease.

Results

Model description. The metabolic part of the kinetic model comprises the major cellular metabolic pathways of cellular carbohydrate, lipid, and amino acid metabolism of hepatocytes (see Fig. 1). The model also contains key electrophysiological processes at the inner mitochondrial membrane, including the membrane transport of various ions, the mitochondrial membrane potential, and the generation and utilization of the proton-motive force. The time-dependent variations of model variables (=concentration of metabolites and ions) are governed by first-order differential equations. Time-variations of small ions were modeled by kinetic equations of the Goldman–Hodgkin–Katz type as used in our previous work[4]. The rate laws for enzymes and membrane transporters were either taken from the literature or constructed on the basis of published experimental data. The mathematical form of the kinetic rate laws for enzymes and membrane transporters was dictated by the reaction mechanism and taken from enzymological in vitro studies, preferably for the liver of the rat or, and if not available, in the order mice → human → bovine → dog. The same ranking of species was applied for the retrieval of numerical values for the kinetic parameters. For every kinetic parameter we cite one experimental reference. If several numerical values for the same kinetic parameter and the same species were reported, we used one representative value that fits with the majority of the reported values and that—whenever possible—was taken from an enzyme assay that reported consistent values for other kinetic parameters. Mathematical terms in the rate law related to allosteric enzyme effectors, which are not included in the model were neglected. Their average contribution is indirectly contained in the fitted V_{max} values. More than 90% of the parametric model input holds for the rat liver. Supplementary Note 1 contains all kinetic equations and model parameters sorted by individual pathways. All model simulations were performed using MATLAB, Release R2011b, The MathWorks, Inc., Natick, Massachusetts, United States.

The regulation of key reaction steps in mutually opposing pathways (e.g., glycolysis and gluconeogenesis, lipid synthesis, and lipolysis) by hormone-sensitive reversible enzyme phosphorylation represents an important regulatory principle to control the direction of the net flux[5]. The signaling part of the model comprises the insulin and glucagon dependent regulation of key regulatory enzymes by reversible phosphorylation. The rate laws for these enzymes take into account that the phosphorylated and de-phosphorylated states of the enzyme possess differing maximal activities and kinetic properties. As in our previous work[6], we used phenomenological mathematical functions to relate the enzyme's phosphorylation state to the plasma concentrations of glucose (Supplementary Note 2)

The model boundaries are given by the metabolite and hormone concentrations in the extracellular space. The flux through reactions not considered in the model were put to zero, i.e., carbon influx into and efflux from the modeled metabolic subsystem is exclusively mediated by the exchange fluxes through the plasma membrane.

Model calibration. Except for the V_{max} values, which may vary owing to variable gene expression, the numerical values for all other model parameters were taken from reported kinetic studies of the isolated enzyme. The V_{max} values (Supplementary Table 1) were estimated by fitting the model to 585 measurements of exchange fluxes and internal metabolites obtained in 25 different experiments carried out with perfused livers or isolated hepatocytes, covering a broad range of 21 important liver functions (Supplementary Note 3). A description of each simulated experiment, its physiological relevance, the initial conditions of the simulation, and a comparative plot of measured and simulated data is given in the Supplementary Note 3. For each of the 585 model simulations, we forced the concentration values of 170 internal metabolites to remain within the concentration ranges defined on the basis of in vivo and in vitro measurements (see Supplementary Data 1 and Supplementary Fig. 1). For more details of the parameter fitting procedure see Methods.

An illustrative example of a calibration simulation is shown in Fig. 2 depicting the relationship between the partial oxygen pressure (pO_2) and selected model variables. Under normoxic conditions, ATP is almost exclusively generated by oxidative

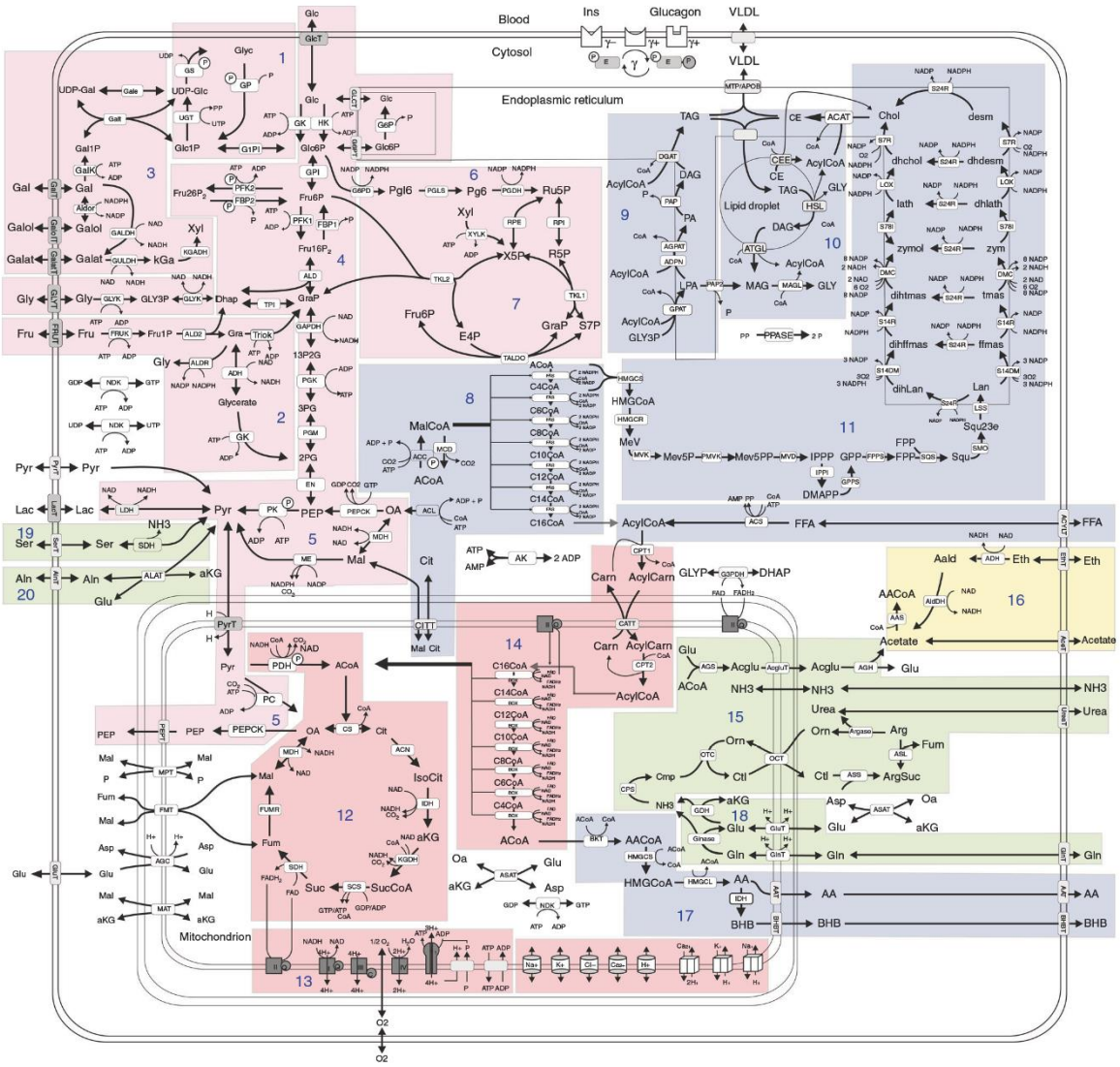

Fig. 1 Reaction scheme of the metabolic sub-model. Reactions and transport processes between compartments are symbolized by arrows. Single pathways as defined in biochemical text books are numbered and highlighted by different coloring: (1) glycogen metabolism, (2) fructose metabolism, (3) galactose metabolism, (4) glycolysis, (5) gluconeogenesis, (6) oxidative pentose phosphate pathway, (7) non-oxidative pentose phosphate pathway, (8) fatty acid synthesis, (9) triglyceride synthesis, (10) synthesis and degradation of lipid droplets and synthesis of VLDL lipoprotein, (11) cholesterol synthesis, (12) tricarbonic acid (TCA) cycle, (13) respiratory chain & oxidative phosphorylation, (14) β-oxidation of fatty acids, (15) urea cycle, (16) ethanol metabolism, (17) ketone body synthesis, (18) ammonia formation, (19) serine utilization, and (20) alanine utilization. Small cylinders and cubes symbolize ion channels and ion transporters. Double-arrows indicate reversible reactions, which may proceed in both directions according to the value of the thermodynamic equilibrium constant and cellular concentrations of their reactants. Reactions are labeled by the short names of the catalyzing enzyme or membrane transporter given in the small boxes attached to the reactions arrow. Metabolites are denoted by their short names. Full names and kinetic rate laws of reaction rates are outlined in Supplementary Note 1. The full names of metabolites and a comparison of experimentally determined and calculated cellular metabolite concentrations is given in Supplementary Data 1

phosphorylation. If the external O_2 level drops below critical levels of about 15 mmHg, the cellular O_2 level becomes too low to saturate complex IV of the respiratory chain, which decreases the flow of electrons, the proton-motive force, and thus the rate of oxidative phosphorylation. The fall of ATP blocks ATP-dependent reaction steps in anabolic metabolic pathways, such as gluconeogenesis and urea synthesis. Therefore, these two cardinal anabolic functions of the liver become severely restricted.

Inspection of the transition from the normoxic to the hypoxic state elicited by a sudden drop of oxygen allows to trace back the causal chain of molecular events underlying the relationship between falling O_2 levels and reduced rates of hepatic glucose and

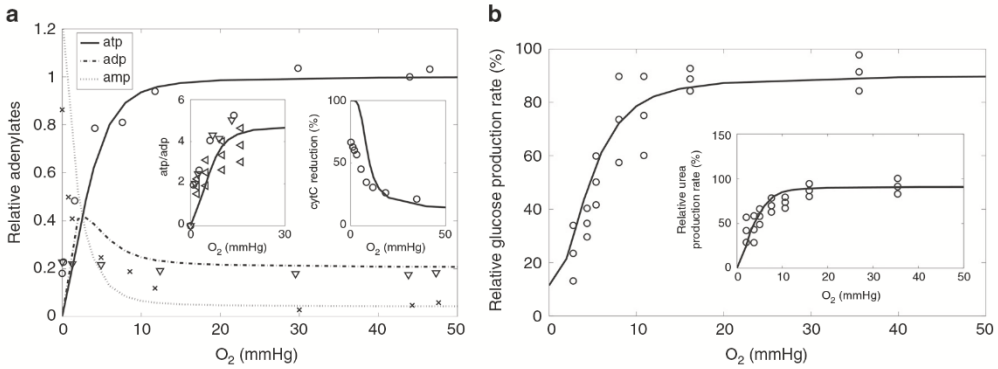

Fig. 2 Effect of hypoxia on selected model variables. **a** Adenine nucleotides ATP, ADP, and AMP. Small insertions: ATP/ADP ratio and reductions state of cytochrome c. **b** Relative production rates of glucose and urea (small insertion). Discrete symbols refer to experimental data from various publications. For details see Supplementary Note 3

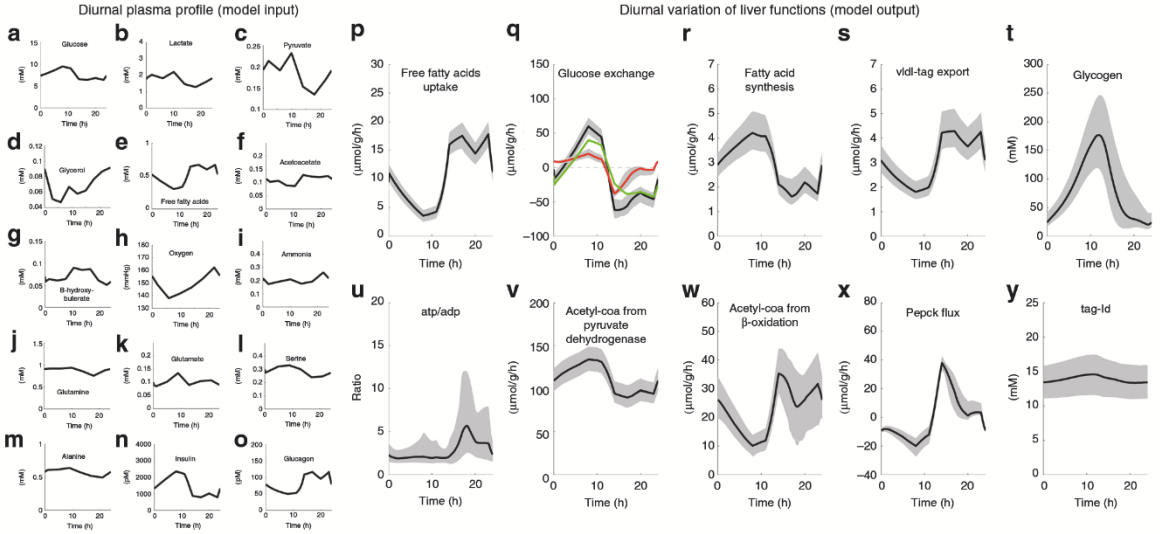

Fig. 3 Simulated diurnal changes of selected metabolic functions of a normal rat liver. Left panels: 24 h plasma profile of hormones and metabolites of an ad libitum fed rat serving as model input. **a** glucose, **b** lactate, **c** pyruvate, **d** glycerol, **e** free fatty acids, **f** acetoacetate, **g** β-hydroxy butyrate, **h** oxygen, **i** ammonia, **j** glutamine, **k** glutamate, **l** serine, **m** alanine, **n** insulin, **o** glucagon. Right panels: Simulated diurnal profile of 10 selected metabolic functions (=model output). **p** uptake of free fatty acids, **q** glucose exchange, **r** fatty acid synthesis, **s** triglyceride export by VLDL, **t** glycogen content, **u** ATP/ADP ratio, **v** rate of pyruvate dehydrogenase (=entry of glucose carbons into the citric acid cycle), **w** rate of β-oxidation (=entry of fatty acid carbons into the citric acid cycle), **x** rate of PEPCK, **y** triglyceride content. The green and red curves in **q** represent the rate of glycolysis/gluconeogenesis and glycogen synthesis/degradation (=flux through the phosphoglucomutase). Note that negative exchange fluxes indicate net release from the liver to the plasma. Gray areas around the solid curves encompass 95% of values obtained in 100 recurrent simulations where the V_{max} value of each enzyme was randomly sampled from an interval between 90 and 110% of the reference value

urea production. The experimentally observed deviation in the cytochrome c reduction state from the expected thermodynamic equilibrium at low O_2 levels points to electron acceptors outside the respiratory chain not considered by the model[7].

Assessment of liver metabolism in vivo. The metabolic state of the liver is mainly dictated by the plasma concentrations of metabolites and hormones, which are continuously changing depending on various factors such as the individual time regime of eating and fasting, the amount and composition of the food, physical activity or presence of systemic diseases like diabetes. Our model offers the possibility to simulate these scenarios in a quantitative manner by using the plasma profile of metabolites and hormones as model input. Fig. 3. shows the simulated diurnal variation of some key metabolic functions for a normal liver (see Supplementary Fig. 2 for a larger set of 24 functions). The effect of inter-individual variability of protein abundances on the shape of the simulated trajectories was taken into account by Monte–Carlo sampling, where the V_{max} values of all enzymes were randomly varied by ±10% in correspondence with reported average inter-individual variation of 19% of the liver proteome[8].

During the day and free access to nutrients, the liver takes up glucose (Fig. 3q), and stores it in glycogen (peaking around 10 h)

(Fig. 3t). Removal of excess carbohydrates from the plasma is a vital liver function preventing violent oscillations in circulating glucose after feeding. If, for example, 100 g of glucose were delivered in its entirety into the extracellular fluid, plasma glucose levels would rise by 37 mmol/l, whereas the measured rise is rarely more than 10% of this[9]. During the night, i.e., without intake of carbohydrates but ongoing glucose consumption (predominantly by the brain), the liver stabilizes the plasma glucose level by the export of glucose. Glucose release is accompanied by a significant drop of the hepatic glycogen reserve by about 80% and an increase of the rate of gluconeogenesis (cf. red and green curves in Fig. 3q)[10]. The hepatic uptake rate of fatty acids follows the plasma level of fatty acids (Fig. 3p and Fig. 3e)[11]. Owing to the inhibitory effect of insulin on Apo-B, the export rate of triglycerides to extra-hepatic organs contained in very low density lipoprotein (VLDL) is low if the glucose and insulin plasma levels are high and vice versa[12].

Of notice, endogenous de novo synthesis of fatty acids is inversely regulated against the import of fatty acids and the export of VLDL (Fig. 3r, p, s). This is mainly accomplished by regulation of the acetyl-CoA carboxylase by allosteric effectors (e.g., fatty acids) and reversible phosphorylation[13]. Contrary to the fast glycogen stores, hepatic triglyceride stores serve as long-term fuel reserve and are almost unaffected during a normal diurnal feeding cycle (Fig. 3y)[14].

Notably, the model allows to monitor intracellular metabolic changes, which are hardly accessible to direct experimentation. For example, the model predicts diurnal changes of the ATP/ADP ratio by a factor of about two. The relative share of glucose and fatty acids in the oxidative ATP production of the liver (quantified by the ratio of fluxes through the pyruvate dehydrogenase and β-oxidation both yielding Acetyl-CoA) varies between 13:1 (at 10 h) and 2:1 (at 15 h), reflecting the adaptation in fuel preference over the day. Counterintuitively, the energetically most comfortable situation with a ratio ATP:ADP ≈ 6 is reached when the uptake of fatty acids and their relative share in oxidative ATP production is highest corresponding to times when the energetic demand for VLDL synthesis and gluconeogenesis peaks. Importantly, the 24 h concentration changes of all internal metabolites remained within experimentally overserved concentration ranges (see Supplementary Data 1 and Supplementary Fig. 1).

Sensitivity analysis of the model. We performed a sensitivity analysis of our model to figure out those parameters, which upon changes of their numerical value have a large impact on the computed network states and thus deserve special care in the model parametrization procedure.

The sensitivity of stationary network states to changes of enzyme parameters was evaluated by means of π-elasticity coefficients, local response coefficients and global response coefficients (defined in Methods). As reference state we have chosen the steady-state that is adopted if the concentrations of all external metabolites are put to their 24 h mean values. All sensitivity measures are given in the Supplementary Data 4.

The distribution of π-elasticity coefficients (EC), quantifying the regulatory importance of an enzyme, reveals a balance between activating and inhibitory regulatory effects (Fig. 4a). Inspecting the occurrence of the four different parameter categories (see Table 1) reveals that large negative ECs are mainly accounted for by parameters of the category "*N*", which determine the deviation of the rate law from a hyperbolic shape (e.g., the exponent $n > 1$ in a Hill equation). The large group of parameters with EC = 1 is constituted by the V_{max} values, which commonly occur as pre-factor of the rate law. The balanced share of the category "KM" in the fraction of positive and negative ECs is due to the fact that increasing the Km value of a reaction substrate lowers the affinity and thus the reaction rate whereas increasing the Km value of a product (of a reversible reaction) has the opposite effect.

Infinitesimal response coefficients ($\widetilde{R}$) of all model parameters were computed with respect to 24 metabolic functions. For the statistical evaluation we recorded all parameters and associated metabolic functions meeting the condition $|\widetilde{R}| \geq R^*$ putting the threshold R^* to 0.1, 0.5, and 1.0, respectively. 181 (=17.4%), 79 (=7.6%), and 33 (=3.1%) parameters affected at least one metabolic function (see Fig. 4b). Interestingly, there are some parameters with a strong impact on multiple metabolic functions (see Supplementary Fig. 5). Parameters affecting at least three different metabolic functions with $|\widetilde{R}| \geq 1$ are shown in Fig. 4d. They belong to processes located at the core of oxidative phosphorylation (F0F1-ATPase, complex I of the respiratory chain and mitochondrial uncoupling) or enzymes of the glycolytic pathway (glucokinase and phosphofructokinase 1).

Finite response coefficients (R) may differ from the infinitesimal ones owing to the non-linearity of rate laws. We calculated response coefficients for a finite parameter change by 50% and repeated the analysis shown in Fig. 4a, b (see Supplementary Figs. 3 and 4). A comparison with infinitesimal response coefficients (see Fig. 4c) shows, that the infinitesimal response coefficients have indeed the tendency to underestimate the system's response to finite parameter changes.

Dynamic control analysis of liver metabolism. The abundance of metabolic enzymes can be altered by regulated changes of protein expression and degradation, but also by chemical modifications (i.e., adduct formation with acetaldehyde) or inhibition by medical drugs. To check the functional consequences of such changes of enzyme abundances, we performed a dynamic metabolic control analysis (MCA), which differs from conventional MCA in that changes of the time course of model variables rather than changes of steady-state values are being calculated in response to a small perturbation of model parameters. To this end, we diminished the maximal activity of each of the 221 enzymes by 10% and computed the mean effect of this partial inhibition on the 24 h profile of 24 metabolic functions. This analysis revealed large differences in the capacity of individual enzymes to control metabolic functions by changes of their protein abundance (see Fig. 5). About 30% of all enzymes catalysing reactions that are close to the thermodynamic equilibrium have virtually no impact on the metabolic response of the liver. By contrast, about 10% of all enzymes exert significant control of more than a single metabolic function. As expected, inhibition of components of mitochondrial oxidative phosphorylation (e.g., reactions #38,39) influences almost all metabolic functions owing to the central function of ATP. But also less prominent reactions as the uptake of alanine (reaction #141) or the degradation of apoprotein B (reaction #156) have control over several metabolic functions. This kind of analysis can be used to identify potential targets for the treatment of hepatic diseases like steatosis. Such targets are indicated by red scores in column 17 of Fig. 5. Among the top-ranking putative anti-steatotic enzymes are GPAT (glycerol-P acyl transferase), mitochondrial uncoupling protein UCP or ACC1/2 (acetyl-CoA carboxylase), which are all discussed in the literature as potential targets for anti-steatotic drugs[15].

Acute response of liver metabolism to a bolus of ethanol. This example was chosen to illustrate how the model can be used to check the feasibility of hypotheses about the molecular basis of physiological or pathophysiological phenomena, in this case the

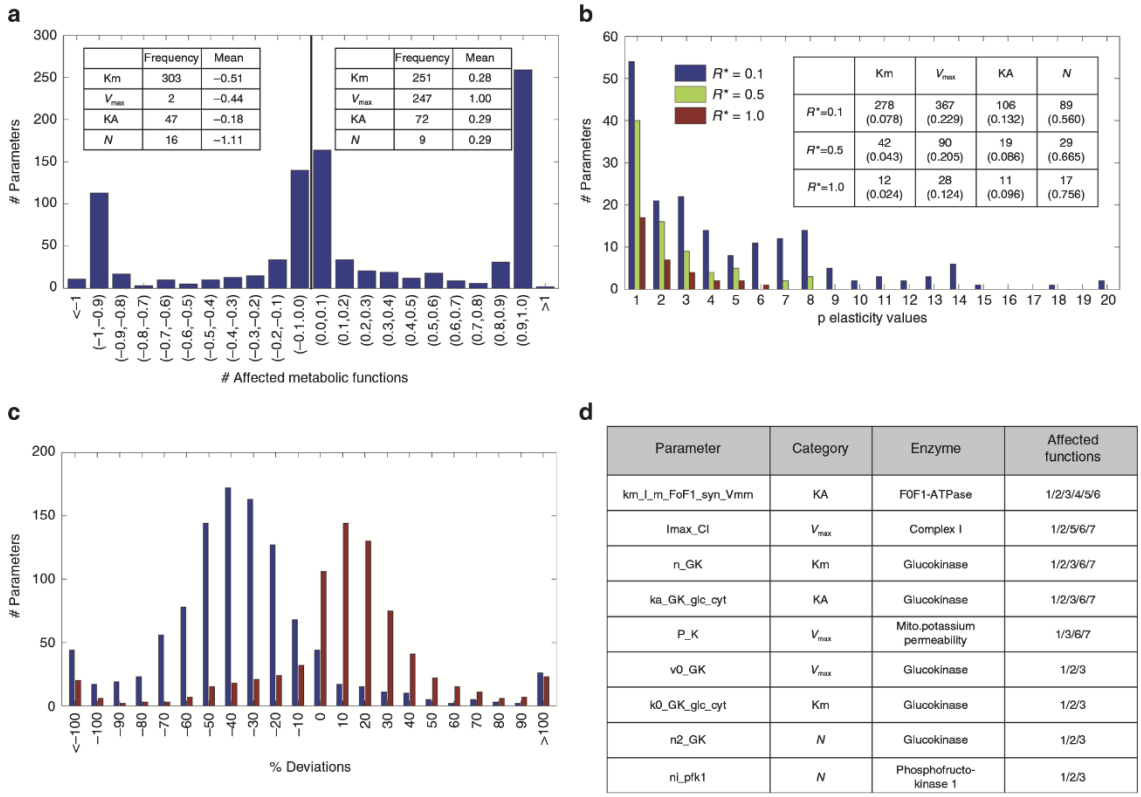

Fig. 4 Parameter sensitivity analysis. **a** Distribution of π-elasticity coefficients (see equation (3) in Methods) and the relative occurrence of the four different parameter categories (see Table 1) and the category mean within the group of parameters with negative and positive ECs. Note that the total number of ECs (947) is smaller than the total number of parameters because in the reference state some reactions are not operative (e.g., fructose metabolism). **b** Frequency of parameters (*y*-axis) affecting a given number of metabolic functions (*x*-axis) with an infinitesimal response coefficient that is larger than the threshold value R^* (0.1, 0.5, and 1.0). The inserted Table shows the absolute and relative frequencies (in brackets) of parameter categories. The relative frequency is given by the absolute frequency divided by the total frequency (see Table 1). **c** Relative differences $D = 100\ \frac{\tilde{R}-R}{R}$ between infinitesimal response coefficients (with $R > 0.1$) and finite response coefficients computed for a 50% parameter change. Blue bars: 50% parameter reduction ($p \to p/2$). Red bars: 50% parameter increase ($p \to 1.5p$). **d** List of parameters affecting at least three different metabolic functions with an infinitesimal response coefficients $R \geq 1.0$. Numbering of metabolic functions: (1) glucose exchange rate, (2) lactate exchange rate, (3) pyruvate exchange rate, (4) glycerol exchange rate, (5) fatty acid uptake rate, (6) acetoacetate secretion rate, (7) β-hydroxybuterate secretion rate, (8) oxygen uptake rate, (9) ammonia uptake rate, (10) glutamine exchange rate, (11) glutamate exchange rate, (12) serine exchange rate, (13) alanine exchange rate, (14) urea secretion rate, (15) acetate exchange rate, (16) VLDL secretion rate, (17) glycogen storage, (18) cellular triglyceride concentration, (19) cholesterol synthesis lrate, (20) fatty acid synthesis rate, (21) mitochondrial membrane potential, (22) ATP/ADP ratio, (23) NAD/NADH ratio (cytosolic), and (24) NADP/NADPH ratio (cytosolic)

Table 1 Model statistics

Model item	Number	Model item	Number
Enzymes & transporters	209	Kinetic parameters (total)	1040
- Catalyzing a single reaction	189	Parameters of type "KM" affinity constants of reactants	604
- Catalyzing several reactions	20	Parameters of type "KA" affinity constants of allosteric effectors	139
Compartments	4	Parameters of type "VMAX" maximal activities	272[a]
Metabolites	274	Parameters of type "N" parameters determining the deviation from a hyperbolic rate law	27
Exchange fluxes with plasma	21		

[a]Note that there are more parameters of type "VMAX" than enzymes/transporters because 20 enzymes catalyze more than a single reaction

interrelation between alcohol drinking and development of a fatty liver. The main detoxification route of alcohol comprises the subsequent action of the enzymes alcohol dehydrogenase (ADH) and acetaldehyde dehydrogenase (ALDH) converting ethanol to acetate via the intermediate acetaldehyde (pathway #16, Fig. 1). Both reactions reduce NAD^+ to NADH. It is commonly argued that inhibition of fatty acid β-oxidation due to the lowered NAD^+/NADH ratio and the elevated de novo synthesis of fatty acids

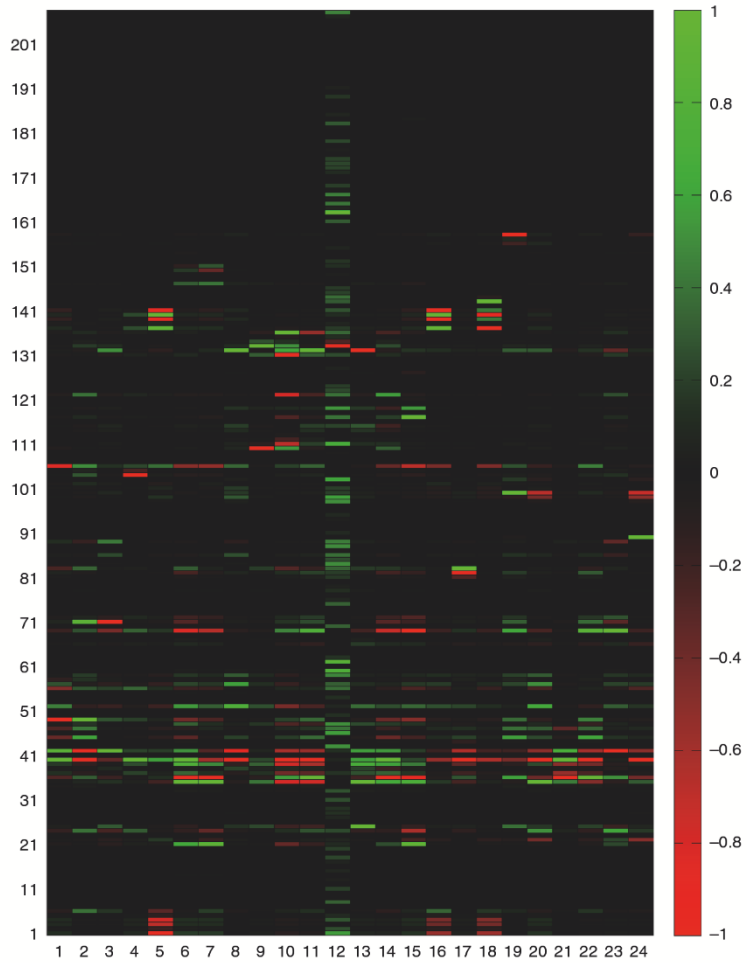

Fig. 5 Dynamic control of 24 different metabolic functions. The maximal activity of each enzyme model was reduced by 10% and the resulting changes of the diurnal time-courses of 24 selected metabolic functions were quantified by means of the time-averaged response coefficient (defined by equation (6) in Methods). To quantify the relative impact of individual enzymes, the maximal positive and negative values means of the time-averaged response coefficients (Supplementary Data 2) were normalized to the range [−1, +1]. Numbering of metabolic functions: (1) glucose exchange rate, (2) lactate exchange rate, (3) pyruvate exchange rate, (4) glycerol exchange rate, (5) fatty acid uptake rate, (6) acetoacetate secretion rate, (7) β-hydroxybuterate secretion rate, (8) oxygen uptake rate, (9) ammonia uptake rate, (10) glutamine exchange rate, (11) glutamate exchange rate, (12) serine exchange rate, (13) alanine exchange rate (14) urea secretion rate; (15) acetate exchange rate, (16) VLDL secretion rate, (17) glycogen storage, (18) cellular triglyceride concentration, (19) cholesterol synthesis rate, (20) fatty acid synthesis rate, (21) mitochondrial membrane potential, (22) ATP/ADP ratio, (23) NAD/NADH ratio (cytosolic), (24) NADP/NADPH ratio (cytosolic)

from massively formed acetate are the key factors contributing to the development of a fatty liver (see e.g.,[16]). We used our model to check the soundness of this reasoning by simulating the effect of a single bolus of ethanol added to the standard plasma profile (see Fig. 6). A steep rise of the plasma alcohol level occurred if the ethanol infusion rate approached 100 µM/g/h (red curves) indicating saturation of ADH. The alcohol challenge induced a transient increase of the cellular triglyceride content (Fig. 6d) that was paralleled by an increased release of and lactate into the plasma (Fig. 6b). However, up to high plasma peak values of 38 mM (corresponding to 1.75 per mille) these transient alterations disappeared within a few hours after cessation of the ethanol bolus. The simulations reveal that lowered ratios of NAD^+/NADH and pyruvate/lactate decrease the availability of pyruvate for the carboxylation to oxaloacetate and thus diminish the formation of citrate by the citrate synthase. Hence, there is no significant citrate-dependent activation of the acetyl-CoA synthetase catalyzing the rate-limiting step of fatty acid synthesis. Notably, these model-based findings are in concordance with early experiments of Guynn[17] who observed a decrease of malonyl-CoA, citrate, and the activity of the acetyl-CoA carboxylase in response to acute ethanol administration. Hence, long-term changes in the expression of lipogenic enzymes remains the likely mechanism accounting for the development of an alcoholic fatty liver. Indeed, the transient increase of the toxic intermediate acetaldehyde (Fig. 6c) can activate the pro-lipogenic transcription factor SREB-1[18] and inhibit the transcription factor PPAR-α controlling the expression of enzymes involved in the β-oxidation of fatty acids[19].

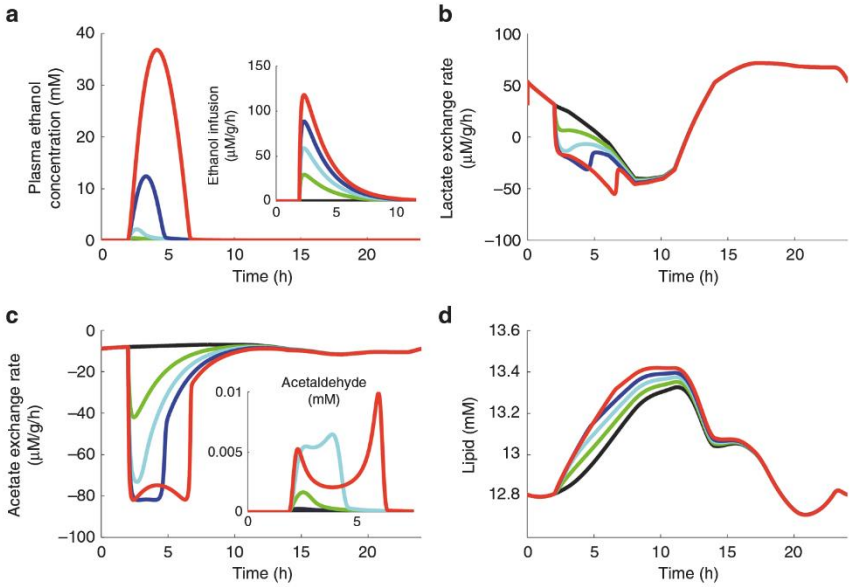

Fig. 6 Response of liver metabolism to an alcohol challenge. **a** Plasma profile of ethanol at three different alcohol infusion profiles depicted in the small insertion. **b** Lactate exchange flux. **c** Acetate exchange flux. The profile of the toxic intermediate acetaldehyde is depicted in the small insertion. Note that the inhibition of the alcohol dehydrogenase at high ethanol concentrations accounts for the delayed steep rise of acetaldehyde if ethanol has already dropped to low level. **d** Triglyceride content. Whereas the plasma level of ethanol was normalized at times 5–7 h, the cellular increase of triglyceride persisted about 4 h up to time point $T = 11$ h

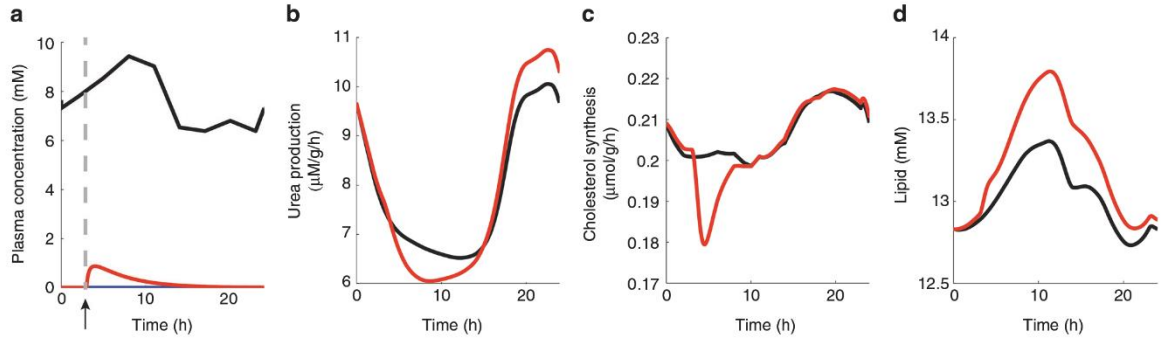

Fig. 7 Metabolic effects of a single dose of valproate. **a** 24 h plasma glucose profile of the rat (black curve) and plasma profile of VPA after a bolus given at $t = 2$ h (red curve) adopted from[38] as the detoxification of VPA by the microsomal CYP system is not part of the model. **b** Urea production rate. **c** Synthesis rate of cholesterol. **d** Cellular triglyceride content. Black curves refer to the reference case in the absence of VPA

Drug-induced steatosis by valproate. An important application of the model consists in the quantitative investigation of metabolic changes elicited by medical drugs or toxins acting on specific metabolic enzymes. We have chosen the anticonvulsive drug valproic acid (VPA) as example. Clinical experience with VPA therapy has shown a number of fatal cases of hyperammonemia[20] and excessive triglyceride accumulation[21]. These adverse effects can be attributed to the VPA-dependent inhibition of two key enzymatic steps. Being chemically an analog of a medium-chain fatty acid, VPA is activated to valproyl-CoA thus sequestering CoA and acting as competitive inhibitor of the carnitin-palmitoyl-transferase 1 (CPT1)[22]. VPA also inhibits the N-acetyl-glutamate synthetase (AGS) and thus the formation of acetyl glutamate, a strong activator of the urea cycle[23]. The interactions of VPA with CPT1 and AGS have been kinetically characterized and thus could be included in the model in detail. Fig. 7 shows the diurnal metabolic profile of selected metabolic functions in response to a single dose of VPA. At elevated plasma levels of VPA, the synthesis of urea is reduced (mean rate within 2–12 h = 7.87 μmol/g/h vs. 8.21 μmol/g/h for the reference case). However, across 1 day, the mean urea production rate is not significantly altered (9.56 vs. 9.44 μmol/g/h). In contrast, the triglyceride content is increased during the whole time span of VPA metabolization. Intriguingly, the simulation predicts a reduced synthesis rate of cholesterol. Such a cholesterol-depleting effect of VPA in the liver has not been reported so far but may account for a statistically significant drop of total serum cholesterol in epileptic outpatients on anticonvulsant monotherapy with VPA[24].

Assessing the severity of inherited metabolic disorders. The model offers the possibility to assess the severity of a hereditary

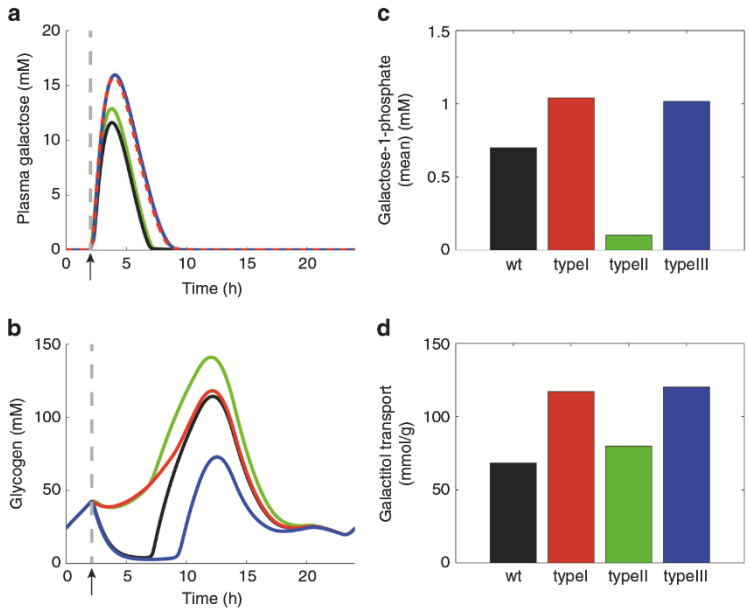

Fig. 8 Dynamic changes in hepatic galactose metabolism. Rate equations for the enzymes of the Leloir pathway and kinetic parameters of the deficient enzymes (type I: GALT-red curves; type II: GALK-green curves; type III: GALE-blue curves) are given in Supplementary Note 4. The simulations were performed by starting at time $T = 2$ h the influx of galactose to the normal plasma. The influx was modeled by a phenomenological function taking into account the time delay between oral galactose intake and galactose appearance in the plasma. **a** Plasma profiles of galactose. **b** Cellular glycogen content. **c** Mean cellular Gal1P. **d** Mean galactitol transport rate

metabolic liver disease just knowing the altered kinetic properties of the defective enzyme. In this example, we focus on galactosemia, a rare genetic metabolic disorder that is caused by a deficiency of one of the three enzymes GALK, GALT, and GALE (cf. pathway #3, Fig. 1), which together constitute the so-called Leloir pathway converting galactose to UDP-glucose. Galactose can also be reduced to galactitol by the NADPH-dependent aldose reductase. Galactitol is an osmotically active compound that is considered a major factor in cataract formation if produced excessively. Finally, galactose can be oxidized to galactonate by the NAD-dependent galactose dehydrogenase. Galactonate is either released into the plasma or further metabolized to xylulose.

The clinical manifestations of each enzyme deficiency differ markedly. Patients with GALK deficiency (type II galactosemia) may present cataracts only. In contrast, GALT deficiency (type I classical galactosemia) is potentially lethal and demonstrates long-term, organ-specific complications[25]. While the molecular mechanisms underlying the pathogenesis of Type I galactosemia are still poorly understood, it is generally accepted that the intermediate galactose-1-phosphate (Gal1P) is the toxic metabolite responsible for the galactosemia phenotype.

Fig. 8 shows simulated temporal changes of the hepatic galactose metabolism elicited by a galactose challenge of a normal subject and of three patients suffering from galactosemia of type I, II, or III, respectively. Taking the area under the curves (AUC) of gal1P and galactitol as risk markers for systemic clinical complications and cataract, respectively, (Fig. 8c, d) the patient with GALT deficiency has by far the highest risk of systemic complications and an equally high risk of cataract than the patient with GALK deficiency. It has to be noted that this is a computational case study of individual patients. Note that kinetic alterations of genetic GALE variants are a continuum entailing a large scatter in the severity of galactosemia III[26].

Metabolic phenotyping of liver tumors. The gene expression profile of a tumor typically deviates strongly from that of the corresponding normal tissue[27] but the functional implications of these deviations remain often elusive. The model offers the opportunity to unravel the functional implications of changes in the protein abundance of metabolic enzymes in patient-specific liver tumors. To this end, we used the ratio of protein abundances of enzymes measured in the tumor cell and the normal hepatocyte by quantitative proteomics (Supplementary Data 3) to scale the corresponding ratio of V_{max}-values. As an example, Fig. 9 shows diurnal variations of selected metabolic functions of an adenoma and two hepatocellular carcinoma (HCC) resected from the liver of three individual patients (Supplementary Note 5). The simulations reveal remarkable differences between the metabolic profiles of the adenoma and the two HCC. Although the two HCC both display all metabolic features of the Warburg effect as a high rate of glucose consumption and lactate formation, depleted glycogen stores, reduced oxygen uptake, and lowered ATP/ADP ratio, the adenoma shows an almost normal glucose metabolism but severe alterations in the lipid metabolism (e.g., lowered rates of fatty acid uptake and TAG synthesis). The oxidative phosphorylation capacity is reduced in the two HCC but increased in the adenoma. Comparing the metabolic profiles of the two HCC, there is a high similarity with respect to the glucose and energy metabolism but remarkable heterogeneity in the lipid and amino acid/nitrogen metabolism. For example, the uptake rates of glutamine, an important tumor substrate with several pleiotropic effects[28], differ by a factor of about five. Taken together, this pilot study points to the existence of a unique, patient-specific metabolic profile of tumors despite some basic metabolic communalities (e.g., Warburg effect in the two HCC).

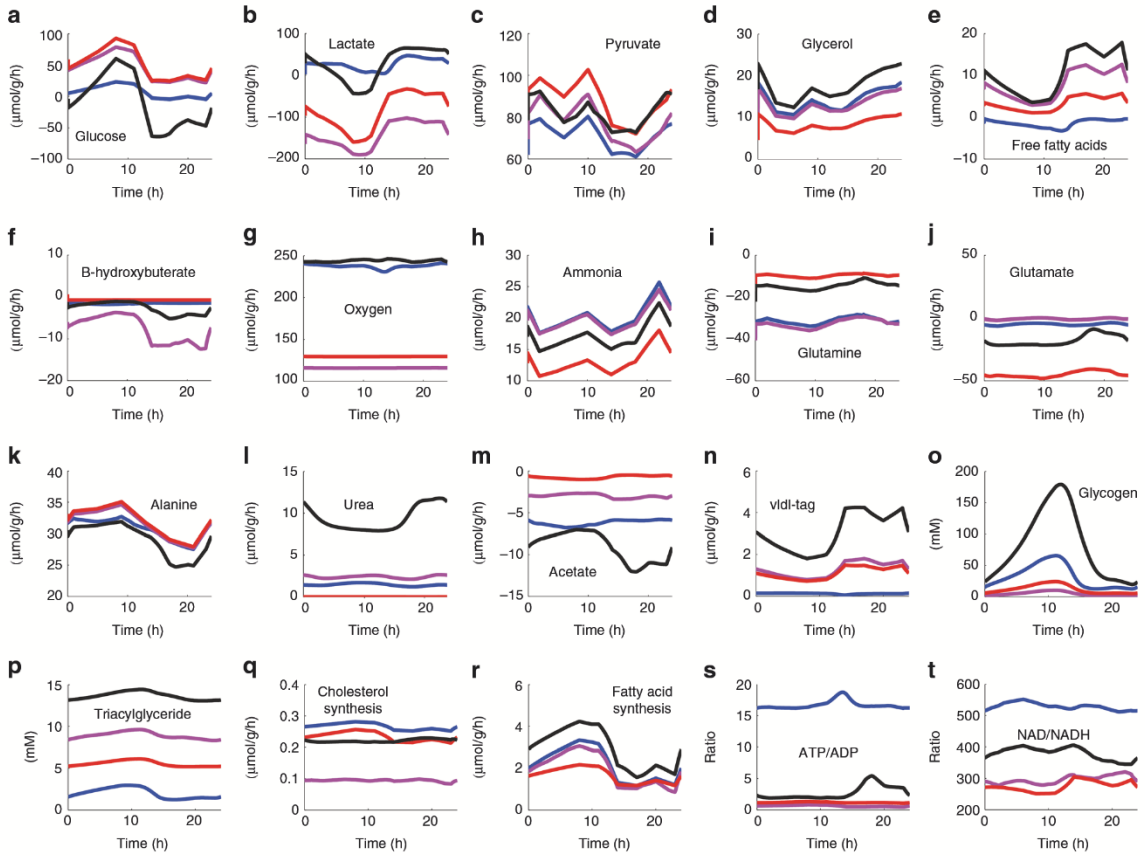

Fig. 9 Metabolic profiling of liver tumors. Black lines: Normal hepatocyte. Red lines: T1 HCC, Pink lines: T3a HCC. Blue lines: Adenoma. The tumor tissues were obtained from three different patients and the proteome was determined by shot-gun proteomics. Relative protein abundances were used to scale maximal enzyme activities (Supplementary Data 3). The diurnal metabolite-hormone profile used as model input was the same as in Fig. 2. **a** glucose exchange rate, **b** lactate exchange rate, **c** glycogen content, **d** pyruvate exchange rate, **e** glycerol exchange rate, **f** oxygen uptake rate, **g** ATP/ADP ratio, **h** NAD/NADH ratio (cytosol); **i** acetate exchange rate, **j** free fatty acid exchange rate, **k** TAG content, **l** β-hydroxybutyrate exchange rate, **m** cholesterol synthesis, **n** fatty acid synthesis rate, **o** TAG export by VLDL, **p** ammonia exchange rate, **q** glutamine exchange rate, **r** glutamate exchange rate, **s** alanine exchange rate, **t** urea synthesis rate

Discussion

Our work was inspired by both medical and methodological challenges. The bio-medical challenge was to establish a modeling platform that enables in silico studies of the response of the liver metabolism to variations of the external and internal conditions.

In order to illustrate the utility of the model for basic research and a variety of medical applications, we simulated temporal variations in the metabolic state of the liver in response to diurnal changes in the plasma profile of metabolites and hormones at normal conditions, nutritional challenges, drugs with metabolic side effects, enzymopathies, and altered gene expression profiles in liver tumors. The value of such model simulations consists in the ability to monitor simultaneously a large array of metabolites and fluxes in vivo. This is an exquisite situation, which can hardly be achieved in experiments because of ethical, technical, and economical restrictions. Hypotheses on molecular mechanisms underlying the system's behavior are commonly based on a restricted set of experimental observations of system variables and parameters. The presented model provides a means to check the feasibility of such hypothesis by filling the observational gaps by computation. The simulation of metabolic effects elicited by an alcohol bolus may serve as example for such model-based hypothesis testing. Our simulations demonstrate the capability of liver metabolism to rapidly return to the normal state even after pronounced ethanol challenges, thus excluding alcohol-induced steatosis to result merely from metabolic dysregulation.

Applying the model to physiological or pathological states of the liver deviating from the reference state for a longer time period, adaptive alterations of enzyme abundances have to be taken into account. Hitherto, mechanistic models of the cellular protein turnover including the regulation of gene expression and proteolysis are not available yet. As an appropriate substitute, one may take advantage of the ongoing progress in quantitative proteomics by using experimentally determined changes of protein abundances to scale the maximal activities of enzymes and membrane transporters[6]. We used this approach to study the functional implications of altered enzyme levels in liver tumors. Our preliminary results suggest the existence of patient-specific metabolic profiles, which eventually may help to optimize individualized drug therapies. This computational approach may serve as an example for a proteome-based metabolic profiling of other liver diseases, such as liver steatosis, liver fibrosis, or liver cirrhosis.

The methodological challenge was to provide a paradigm for the feasibility of a large-scale kinetic modeling approach that takes into account the biochemistry of the system. Most common in the modeling of large metabolic networks is the application of constraint-based optimization methods, also known as flux-balance analysis (FBA)[29]. The applicability of this approach is restricted to the calculation of stationary flux distributions, which are obtained by optimizing a plausible objective function that relates basic cellular functions as, for example, the production rate of biomass or energy, to the fluxes through the constituting biochemical reactions. Additionally, upper flux constraints have to be imposed to assure a finite solution of the optimization problem. See ref.[30] for a review of the genome-wide metabolic flux distributions for various cell types based on constraint-based methods. For a more detailed review on current activities aiming at the development of mathematical whole-cell models we refer the reader to the report of the 2015 Whole-Cell Modeling Summer School[31].

Another modeling approach to large systems consists in the constructions of phenomenological kinetic models, where the need for detailed enzyme characterization is bypassed by using simplified rate laws, e.g., of the mass-action type or lin-log type. Such rate laws have fewer free scalable parameters that can be conveniently estimated by the ensemble modeling methods[32]. But naturally, this comes at the price of limited predictive power and ability to incorporate biochemical information. FBA models lack time responses and metabolite concentrations, while simplified rate laws lack the possibility to incorporate changes in kinetic parameters (as in inherited genetic diseases), enzyme isoforms (e.g., in cancer cells), and allosteric regulation.

The limitations of the above modeling techniques can be overcome by kinetic models resting at the principles of chemical kinetics and thermodynamics and including all (for the purpose of the model) relevant molecular details of enzyme regulation[33]. Hitherto, the development and validation of such biochemistry-based kinetic models has been limited to small metabolic subsystems comprising 10–30 reactions (see e.g., the model repositories[34,35]). Frequently quoted arguments for such a long standstill in the development of larger kinetic models are the lack of kinetic information on metabolic enzymes for most cell types and the general perception that data from enzymatic assays do not reflect the in vivo situation. The latter argument must be doubted by noting that all well-validated and often cited fit-for-purpose kinetic models of small metabolic systems—from the Heinrich-Rapoport models of red cell metabolism[36] to the model of the mammalian methionine cycle[37]—are ultimately based on in vitro enzyme parameters. There is simply no better information source for enzyme regulation than in vitro assays. Taking into account species-specific differences in kinetic constants and critically checking the plausibility of reported values by biochemical arguments (e.g., thermodynamic feasibility) may considerably reduce the degree of uncertainty in the choice of kinetic parameters. At the end, the decisive argument for the validity of the chosen numerical values of enzymatic parameters is the correct functioning of the network under a multitude of physiological conditions.

Finally, we want to emphasize that the development of a kinetic metabolic model of this complexity and detail was possible because metabolism is the by far best investigated cellular subsystem and, therefore, better accessible to mechanistic mathematical modeling than signaling or gene-regulatory networks. Our research was inspired by the vision that in the end all this information on individual enzymes can be brought together in large dynamic network models.

Methods

Model calibration. We used a constraint optimization procedure to estimate numerical values for the V_{max} values of all enzymes. For each of the 585 model simulations, we forced the concentration values of 170 internal metabolites M_i ($i = 1,\ldots,170$) to remain within the concentration ranges $\left[M_i^{\min}, M_i^{\max}\right]$ defined on the basis of in vivo and in vitro measurements (see Supplementary Data 1). This condition was implemented by introducing a penalty function $H(M_i)$ punishing calculated metabolite concentration falling out of the expected range:

$$H(M_i) = \begin{cases} \left(M_i - M_i^{\max}\right)^2 & \text{if } M_i > M_i^{\max} \\ \left(M_i^{\min} - M_i\right)^2 & \text{if } M_i < M_i^{\min} \\ 0 & \text{else} \end{cases} \quad (1)$$

With this setting, the constrained optimization problem can be converted into an unconstrained optimization problem:

$$F = \sum_{\alpha=1}^{21}\left[\left(\frac{1}{y_\alpha^{\exp}}\right)^2 \sum_{i=1}^{N_\alpha}\left(y_{\alpha i}^{\exp} - y_{\alpha i}^{\mathrm{mod}}\right)^2 + \left(\frac{1}{\bar{M}^{\exp}}\right)^2 \sum_{i=1}^{N_\alpha}\left(\sum_{j=1}^{M} H\left(M_{\alpha ij}\right)\right)\right] \rightarrow \text{MINIMUM} \quad (2)$$

where the mean value of the observed variable in experiment (α), $\bar{y}_\alpha^{\exp} = (1/N_\alpha)\sum_{i=1}^{N_\alpha} y_{\alpha i}$, and the mean concentration value of all metabolites, $\bar{M}^{\exp}$ ($\bar{M}^{\exp}$ =1.48 mM), were used to deal with dimensionless variables and to properly scale the relative contributions of the two additive terms.

Statistical measures. For the sensitivity and control analysis of the model we used the following measures:

(i) The π-elasticity coefficient, which is defined as partial derivative of the rate v of the isolated enzyme, i.e., at fixed values $\{E\}_0$ of the enzyme's effectors as reactants, allosteric effectors, and hormones with respect to an (infinitesimal) small perturbation of the parameter p,

$$\pi = \frac{p}{v}\frac{\partial v}{\partial p}\bigg|_{\{E_0\}} \quad (3)$$

(ii) The response coefficient, which is defined as change of the steady-state value of an arbitrary model variable Y_i (e.g., metabolite concentration, reaction rate, and membrane potential) caused by a change of model parameter p_j,

$$R_{ij} = \frac{p_j}{\Delta p_j}\frac{\Delta Y_i}{Y_i} = \frac{1}{\lambda - 1}\left(\frac{Y_i(\lambda p)}{Y_i(p)} - 1\right) \quad (4)$$

whereby the second term on the right-hand side of relation (2) holds if the parameter change is expressed as λ-fold change of the initial parameter value, $p_j \rightarrow \lambda p_j$.

In the control theory of metabolism it is common to study the response of the system to infinitesimal parameter changes,

$$\tilde{R}_{ij} = \lim_{\Delta p_j \to 0}\frac{p_j}{\Delta p_j}\frac{\Delta Y_i}{Y_i} = \lim_{\lambda \to 1}\frac{1}{\lambda - 1}\left(\frac{Y_i(\lambda p)}{Y_i(p)} - 1\right) = \frac{p_j}{Y_i}\frac{\partial Y_i}{\partial p_j} \quad (5)$$

We will refer to R_{ij} and $\tilde{R}_{ij}$ as finite and infinitesimal response coefficients.

(iii) For the sensitivity analysis of non-stationary states, we defined the time-averaged response coefficient

$$\langle R\rangle_T = \frac{\int_0^T \left|Y_{\mathrm{pert}} - Y_{\mathrm{ref}}\right| \mathrm{d}t}{\int_0^T \left|Y_{\mathrm{ref}}\right| \mathrm{d}t} \quad (6)$$

where Y_{ref} and Y_{pert} denote the time-dependent changes of model variable Y in the absence (ref) and presence (pert) of a perturbation and T is the time interval of interest.

Code availability. An executable SBML file of the model is available from the authors on request.

Data availability. All data and public data sources used for the development, calibration, and exemplary model simulations are contained in the supplementary information.

Received: 1 August 2017 Accepted: 14 May 2018
Published online: 19 June 2018

References

1. Kirschner, M. W. The meaning of systems biology. *Cell* **121**, 503–504 (2005).
2. Foster, D. W. Malonyl-CoA: the regulator of fatty acid synthesis and oxidation. *J. Clin. Invest.* **122**, 1958–1959 (2012).
3. Morgan, B. Fatty liver disease: the liver labyrinth. *Nature* **516**, S8–S9 (2014).
4. Berndt, N., Kann, O. & Holzhütter, H. G. Physiology-based kinetic modeling of neuronal energy metabolism unravels the molecular basis of NAD(P)H fluorescence transients. *J. Cereb. Blood Flow. Metab.* **35**, 1494–1506 (2015).
5. König, M., Bulik, S. & Holzhütter, H. G. Quantifying the contribution of the liver to glucose homeostasis: a detailed kinetic model of human hepatic glucose metabolism. *PLoS Comput. Biol.* **8**, e1002577 (2012).
6. Bulik, S., Holzhütter, H. G. & Berndt, N. The relative importance of kinetic mechanisms and variable enzyme abundances for the regulation of hepatic glucose metabolism—insights from mathematical modeling. *BMC Biol.* **14**, 15 (2016).
7. Giorgio, M. et al. Electron transfer between cytochrome c and p66Shc generates reactive oxygen species that trigger mitochondrial apoptosis. *Cell* **122**, 221–233 (2005).
8. Zhang, X. et al. Proteomic analysis of individual variation in normal livers of human beings using difference gel electrophoresis. *Proteomics* **6**, 5260–5268 (2006).
9. Alberti K. G. M. M., Johnston D. G., Piniewska-Hulas M. & Whittaker J. Disturbances of metabolic homeostasis in liver disease. *Acta Med. Port.* **3**, 35–47 (1981).
10. Rothman, D. L., Magnusson, I., Katz, L. D., Shulman, R. G. & Shulman, G. I. Quantitation of hepatic glycogenolysis and gluconeogenesis in fasting humans with 13C NMR. *Science* **254**, 573–576 (1991).
11. Bradbury, M. W. Lipid metabolism and liver inflammation. I. Hepatic fatty acid uptake: possible role in steatosis. *Am. J. Physiol. Gastrointest. Liver Physiol.* **290**, G194–G198 (2006).
12. Marrino, P., Gavish, D., Shafrir, E. & Eisenberg, S. Diurnal variations of plasma lipids, tissue and plasma lipoprotein lipase, and VLDL secretion rates in the rat. A model for studies of VLDL metabolism. *Biochim. Biophys. Acta* **920**, 277–284 (1987).
13. Volpe, J. J. & Vagelos, P. R. Mechanisms and regulation of biosynthesis of saturated fatty acids. *Physiol. Rev.* **56**, 339–417 (1976).
14. Rosenfeld, B. & Lang, J. M. Diurnal changes in liver and plasma lipids of choline-deficient rats. *J. Lipid Res.* **7**, 10–16 (1966).
15. Anderson, N. & Borlak, J. Molecular mechanisms and therapeutic targets in steatosis and steatohepatitis. *Pharmacol. Rev.* **60**, 311–357 (2008).
16. Rasineni, K. & Casey, C. A. Molecular mechanism of alcoholic fatty liver. *Indian J. Pharmacol.* **44**, 299–303 (2012).
17. Guynn, R. W., Veloso, D., Harris, R. L., Lawson, J. W. & Veech, R. L. Ethanol administration and the relationship of malonyl-coenzyme A concentrations to the rate of fatty acid synthesis in rat liver. *Biochem. J.* **136**, 639–647 (1973).
18. You, M., Fischer, M., Deeg, M. A. & Crabb, D. W. Ethanol induces fatty acid synthesis pathways by activation of sterol regulatory element-binding protein (SREBP). *J. Biol. Chem.* **277**, 29342–29347 (2002).
19. Nanji, A. A., Dannenberg, A. J., Jokelainen, K. & Bass, N. M. Alcoholic liver injury in the rat is associated with reduced expression of peroxisome proliferator-alpha (PPARalpha)-regulated genes and is ameliorated by PPARalpha activation. *J. Pharmacol. Exp. Ther.* **310**, 417–424 (2004).
20. Verrotti, A., Trotta, D., Morgese, G. & Chiarelli, F. Valproate-induced hyperammonemic encephalopathy. *Metab. Brain. Dis.* **17**, 367–373 (2002).
21. Becker, C. M. & Harris, R. A. Influence of valproic acid on hepatic carbohydrate and lipid metabolism. *Arch. Biochem. Biophys.* **223**, 381–392 (1983).
22. Aires, C. C. et al. Inhibition of hepatic carnitine palmitoyl-transferase I (CPT IA) by valproyl-CoA as a possible mechanism of valproate-induced steatosis. *Biochem. Pharmacol.* **79**, 792–799 (2010).
23. Hjelm, M., Oberholzer, V., Seakins, J., Thomas, S. & Kay, J. D. Valproate inhibition of urea synthesis. *Lancet* **1**, 923–924 (1987).
24. Nikolaos, T. et al. The effect of long-term antiepileptic treatment on serum cholesterol (TC, HDL, LDL) and triglyceride levels in adult epileptic patients on monotherapy. *Med. Sci. Monit.* **10**, MT50–MT52 (2004).
25. Lai, K., Elsas, L. J. & Wierenga, K. J. Galactose toxicity in animals. *IUBMB Life* **61**, 1063–1074 (2009).
26. Timson, D. J. The structural and molecular biology of type III galactosemia. *IUBMB Life* **58**, 83–89 (2006).
27. Xu, K. et al. A comparative analysis of gene-expression data of multiple cancer types. *PLoS ONE* **5**, e13696 (2010).
28. Shanware, N. P., Mullen, A. R., DeBerardinis, R. J. & Abraham, R. T. Glutamine: pleiotropic roles in tumor growth and stress resistance. *J. Mol. Med (Berl.)* **89**, 229–236 (2011).
29. Orth, J. D., Thiele, I. & Palsson, B. O. What is flux balance analysis? *Nat. Biotechnol.* **28**, 245–248 (2010).
30. Bordbar, A., Monk, J. M., King, Z. A. & Palsson, B. O. Constraint-based models predict metabolic and associated cellular functions. *Nat. Rev. Genet.* **15**, 107–120 (2014).
31. Waltemath, D. et al. Toward community standards and software for whole-cell modeling. *IEEE T Bio-Med Eng.* **63**, 2007–2014 (2016).
32. Tan, Y. & Liao, J. C. Metabolic ensemble modeling for strain engineers. *Biotechnol. J.* **7**, 343–353 (2012).
33. Cornish-Bowden, A. Putting the systems back into systems biology. *Perspect. Biol. Med.* **49**, 475–489 (2006).
34. Chelliah, V., Laibe, C. & Le Novere, N. BioModels Database: a repository of mathematical models of biological processes. *Methods Mol. Biol.* **1021**, 189–199 (2013).
35. van Gend, C., Conradie, R., du Preez, F. B. & Snoep, J. L. Data and model integration using JWS Online. *Silico Biol.* **7**, S27–S35 (2007).
36. Rapoport, T. A., Heinrich, R. & Rapoport, S. M. Regulatory principles of glycolysis in erythrocytes invivo and invitro—minimal comprehensive model describing steady states, quasi-steady states and time-dependent processes. *Biochem. J.* **154**, 449–469 (1976).
37. Saa, P. A. & Nielsen, L. K. Construction of feasible and accurate kinetic models of metabolism: a Bayesian approach. *Sci. Rep.* **6**, 29635 (2016).
38. Marahatta, A., Bhandary, B., Jeong, S. K., Kim, H. R. & Chae, H. J. Soybean greatly reduces valproic acid plasma concentrations: a food-drug interaction study. *Sci. Rep.* **4**, 4362 (2014).

Acknowledgement

This work was funded by the German Systems Biology Programs "Virtual Liver", grant no. 0315741,"LiSyM", grant no. 31L0057 and 031L0058, the e:Bio (Module I) project "HepatomaSys", grant no.0316172A, all sponsored by the German Federal Ministry of Education and Research (BMBF), and the Max Planck Society.

Author contributions

N.B. and H.-G.H. designed and guided the project and have written the manuscript. N.B. and S.B. have implemented the model. T.W. and M.S. provided the tumor samples and clinical data. D.M. performed the proteomics. M.K. contributed to the development of the signaling module and design of the figures. I.W. supported the literature search for kinetic data and revised the manuscript.

Additional information

Supplementary Information accompanies this paper at https://doi.org/10.1038/s41467-018-04720-9.

Competing interests: The authors declare no competing interests.

Reprints and permission information is available online at http://npg.nature.com/reprintsandpermissions/

Publisher's note: Springer Nature remains neutral with regard to jurisdictional claims in published maps and institutional affiliations.

3. Diskussion

3.1 Modellierung: System im Detail verstehen

Eine wichtige Aufgabe der Modellierung ist es, aus der Fülle der verfügbaren Informationen die relevanten herauszufiltern und in einem konsistenten Modell zu verarbeiten. Dabei ist es sowohl wichtig, möglichst viele verschiedene Fälle richtig zu beschreiben, als auch die verarbeiteten Informationen und Ergebnisse verständlich zu machen. Es ist die Aufgabe von Modellen, vereinfachte und verständliche Repräsentationen der Wirklichkeit zu konstruieren, mit denen man trotzdem möglichst viele vorhandenen Daten adäquat beschreiben kann. Im zweiten Schritt ermöglichen Modelle dann die Vorhersage noch nicht gemachter Experimente auf der einen Seite und das Auffüllen von experimentellen Lücken auf der anderen Seite. Ihre Kraft beziehen Modelle also vor allem aus ihrer Fähigkeit, unser Wissen zu ordnen und erfassbar zu machen, allerdings immer unter dem Vorbehalt ihrer Gültigkeit. In welchen Fällen ein Modell gültig ist und zu unserem Verständnis beiträgt, zeigt sich allerdings nur an der Übereinstimmung der Vorhersagen mit dem Experiment. Daher gilt zwar der Satz „Ein Modell ist solange richtig, bis es sich als falsch herausstellt.“, aber ein Modell gewinnt vor allem dadurch Kraft, dass es viele verschiede Situationen richtig beschreibt und damit Ordnungsprinzipien richtig erfasst. Man darf Modellierung deshalb auch nicht mit dem Fitten von mathematischen Funktionen an experimentelle Daten verwechseln, da dieser Art der Modellierung jedwede Erklärungskraft fehlt. Sie ist auf die Deskription und Interpolation von Daten zurückgeworfen. Normalerweise wird bei der Modellierung von großen metabolischen Netzwerken auf die Erstellung eines stöchiometrischen Netzwerks zurückgegriffen, dass benutzt wird, um unter vorgegebenen Zwangsbedingungen und Optimierungskriterien metabolische Flüsse auszurechnen (FBA-Methode). Diese Art der Modellierung hat allerdings sehr starke Begrenzungen. Erstens gibt es keine Regulation der Flüsse, da Metabolit-konzentrationen gar nicht betrachtet werden. Zweitens gilt die zugrundeliegende Flussbilanz an den Knoten nur im stationären Zustand. Daher sind keine dynamischen Simulationen möglich. Drittens basieren die Zielfunktionen, die die Zwangsbedingungen definieren, weniger auf harten biologischen Faktoren als auf der Ingeniosität des Modellierers. Beispielsweise sind die Optimierung der Biomasse und die Minimierung der internen Flüsse des Netzwerks gern genutzte Kriterien. Wie sich die Biomasse allerdings zusammensetzt, ist willkürlich, und für die Annahme, dass die Flüsse innerhalb eines metabolischen Systems minimal sind, gibt es keinen belastbaren Beweis. Im Gegenteil haben wir bereits im hepatischen Glukosestoffwechsel mehrere Substratzyklen aufgezeigt, die aufgrund der verschiedenen potentiellen Funktionen (Glykolyse vs. Glukoneogenese) gar nicht zu vermeiden sind. Schuetz et al. zeigten sehr schön, dass vermeintliche Optimierungskriterien der Realität nicht standhalten und dass man eine gewichtete Kombination von Optimierungskriterien braucht, um die experimentellen Daten richtig zu beschreiben [57]. Die Gewichtung ist dabei allerdings von den Daten abhängig, so dass ein zugrundeliegendes allgemeines Kriterium schlichtweg nicht identifiziert werden konnte. Zusätzlich müssen außerdem noch ähnlich willkürliche obere Grenzen für die Flüsse gesetzt werden, um sicherzustellen, dass das zugrundeliegende Optimierungsproblem eine finite Lösung hat.

Andere Modellierungsansätze konstruieren große metabolische Netzwerke, in denen statt realistischer Enzymkinetiken vereinfachte Kinetiken benutzt werden (z.B. lineare oder lin-log-Kinetiken). Diese Ratengleichungen zeichnen sich durch wenige Parameter aus, die oftmals über statistische Methoden bestimmt werden [58]. Die methodische Einfachheit hat allerdings

den Preis, dass diese Kinetiken die Regulation der Enzyme nicht oder nur unzureichend abbilden. Vor allem sind sie nicht in der Lage, bekanntes biochemisches Wissen über Affinitäten und allosterische Regulatoren abzubilden. Damit fehlen die Feedback- und Feedforward-Regulationen, ohne die der Stoffwechsel nicht zu verstehen ist. Ebenfalls können sie funktionale Beeinträchtigungen aufgrund von Isoformänderungen und Mutationen (z.B. bei vererbbaren Krankheiten oder bei Tumoren) nicht abbilden, deren Grundlage ja gerade Veränderungen in den kinetischen Parametern von Enzymen sind.

Kinetische Modelle haben diese Einschränkung nicht, benötigen dafür aber sehr viel mehr Informationen. Neben dem Wissen über die kinetischen Regulationsmechanismen braucht man Informationen über die Thermodynamik (Gleichgewichtskonstanten der einzelnen Reaktionen) und natürlich die kinetischen Parameter für jedes Enzym.

> *„Daher waren kinetische Modelle bisher auf kleine Netzwerke mit weniger als 30 Reaktionen beschränkt. Der lange Stillstand in der Entwicklung von großen kinetischen Modellen wird oftmals damit begründet, dass es nicht genug Informationen über die kinetischen Eigenschaften von Enzyme gäbe und diese nicht verlässlich die in vivo-Situation widerspiegelten, da sie in vitro erhoben worden wären. Dass die zweite Aussage nicht notwendigerweise richtig ist, wird allerdings bereits bei kleinen kinetischen Modellen deutlich, die ebenfalls mit in vitro-Daten parametrisiert wurden und sehr gut die in vivo-Situation abbilden (z. B. das Rapoportmodell der Erythrozyten [59]). Es gibt letztendlich keine bessere Methode, um kinetische Eigenschaften von Enzymen zu bestimmen. Wie bei allen experimentellen Daten müssen aber natürlich auch diese auf Plausibilität überprüft werden, z.B. durch Vergleich verschiedener Gruppen und Organismen, Abgleich mit Konzentrationen der beteiligten Metabolite und Einfluss auf das Netzwerkverhalten. Mit diesen Mitteln kann man mögliche Unsicherheiten in den kinetischen Parametern sehr gut eingrenzen. Am Ende ist das überzeugendste Argument für die Richtigkeit großer kinetischer Netzwerke des Metabolismus allerdings die korrekte funktionelle Beschreibung von vielen verschiedenen physiologischen und pathologischen Situationen.“* (Übersetzung durch den Autor aus [43])

Die hier vorgestellten Modelle benutzen in erster Linie Methoden der kinetischen Modellierung, welche die regulatorischen Eigenschaften der das Netzwerk konstituierenden Enzyme und Transporter detailliert berücksichtigt und somit quantitative Vorhersagen des Systemverhaltens ermöglichen. Das Ziel ist es Modelle zu etablieren, die eine funktionale Interpretation von Proteindaten ermöglichen und es erlauben, metabolische Zustände der Leber abhängig von internen und externen Bedingungen zu berechnen. Letztendlich ist die Entwicklung solcher Modelle aber abhängig von den verfügbaren Informationen. Der Stoffwechsel ist mit Abstand das bestuntersuchteste System und damit einer mathematischen Beschreibung viel zugänglicher als z.B. die Genregulation. Dass Generationen von Biochemikern jahrzehntelange fast jedes metabolische Enzym charakterisiert haben, ist die Voraussetzung für ein solches Unterfangen.

Wie die zur Verfügung stehenden Informationen die Art der Modellierung beeinflussen, lässt sich anhand der hier vorgestellten Modelle sehr gut illustrieren. Besonders in dem selbstkonsistenten Modell des Glukosestoffwechsels [41] werden für die einzelnen Module sehr unterschiedliche Modellansätze benutzt. Während das metabolische Modell des Glukosestoffwechsels auf sehr vielen einzelnen Beobachtungen beruht (jeder kinetische Parameter einer Enzymkinetik sowie die Enzymkinetik selber entspricht oftmals einer Vielzahl von Experimenten) und eine hohe Erklärungskraft besitzt (korrekte Vorhersage von Metabolit-

konzentrationen und Austauschflüssen unter verschiedenen Bedingungen), sind andere Teile dieses Modells, wie die Relation zwischen Blutzucker und Plasmahormonspiegel oder die Relation zwischen Plasmahormonspiegel und Phosphorylierungsgrad der interkonvertierbaren Enzyme, lediglich Fitfunktionen. Diese geben zwar gemessene Zusammenhänge richtig wieder, haben aber keinerlei erklärende Kraft. Sie können z.B. nicht auf Werte extrapoliert werden, die jenseits der Messwerte liegen. Daher ist es immer wichtig, sich klar zu machen, welchen Gültigkeitsbereich die verschiedenen Modellteile haben.

> *„Da unser heutiges biochemisches Wissen nicht ausreicht, um ein molekular aufgelöstes kinetisches Netzwerk des Proteinstoffwechsels zu entwickeln, haben wir für diesen Teil ebenfalls einen phänomenologischen Ansatz gewählt. Während prinzipiell viele Schritte der Proteinsynthese bekannt sind, bleibt deren Regulation weitgehend unverstanden. Es ist beispielsweise unklar, wie verschiedene Transkriptionsfaktoren untereinander oder mit spezifischen DNA-bindenden Promoterregionen interagieren. Gleiches gilt etwa für das Prozessieren von mRNA oder der Regulation der mRNA-Translation durch Mikro-RNAs und RNA-bindende Proteine. Die Expression der PEPCK, eines der bestuntersuchten glukoneogenetischen Enzyme, wird z.B. von mindestens einem Dutzend Transkriptionfaktoren mit unbekannter Wechselwirkung kontrolliert [60]. Selbst wenn es möglich wäre, die mRNA-Transkription für einzelne Enzyme zu modellieren, wären wir immer noch nicht in der Lage, die Transkriptionsprofile in Proteinprofile zu übersetzen, da unser Verständnis der posttranskriptionalen Regulation und der Prozesse der posttranslationalen Modifikation sehr lückenhaft ist.“* (Übersetzung durch den Autor aus [41])

Obwohl auch die Gleichungen für die Proteinsynthese und den Proteinabbau in diesem Modell effektive Transferfunktionen sind, die den Zusammenhang zwischen Effektoren (Nährstoffe und Hormone) und den Synthese- und Abbauraten der Proteine darstellen, beschreibt das Modell sehr gut die metabolische Adaptation des hepatischen Glukosestoffwechsels mit den vier Modulatoren Glukose, Insulin, Glukagon und Sauerstoff beim Übergang von wohlgenährt zu gefastet und bei der diabetischen Adaptation. Das schließt natürlich nicht aus, dass andere Effektoren wie Morphogene und Wachstumsfaktoren eine wichtige Rolle in der Zonierung spielen. Es weist aber darauf hin, dass sie bei den hier betrachteten Veränderungen einen Hintergrund bilden, der sich selbst nicht wesentlich verändert und dadurch zumindest für den Glukosestoffwechsel nicht regulativ ist. Das muss aber nicht für andere metabolische Subsysteme gelten [61]. So findet man beispielsweise die Glutaminsynthetase nur in den periznetralen Hepatozyten, während die Carbamoylphosphat-Synthetase I, das Schlüsselenzym der Harnstoffsynthese, auf die periportale Zone beschränkt ist. Hauptverantwortlich dafür ist der Wnt/ß-Catenin-Signalweg [62] (siehe [41]).

Wie die Qualität der vorhandenen Daten die Modellqualität bestimmt, sieht man sehr gut beim Vergleich des kinetischen Modells des Glukosestoffwechsels [39] mit dem kinetischen Modell des Lipidmetbolismus [42]. Im Vergleich zu den metabolischen Enzymen des Glukosestoffwechsels ist unser Wissen über die Regulation der beteiligten Enzyme des Fettstoffwechsels und insbesondere der Lipidtropfen eher gering. Beispielsweise sind die Unterschiede in der kinetischen Regulation der beiden Isoformen der Diacylglycerol-O-Acyltransferasen DGAT1 und DGAT2, die den finalen Schritt der Triglyzeridsynthese katalysieren, nicht bekannt und kinetische Eigenschaften der RSP fehlen völlig. Daher müssen die regulativen Eigenschaften aus dem Systemverhalten geschätzt werden, weshalb dieses Modell eher vorläufigen Charakter hat und im Lichte neuerer Erkenntnisse erweitert und verfeinert werden muss. Trotzdem liefern die Modellsimulationen eine sehr gute Überein-

stimmung mit einer großen Anzahl von unabhängigen experimentellen Beobachtungen. Außerdem kann das Modell zur Generierung von Hypothesen genutzt werden, die dann experimentell überprüft werden können.

Die Regulation metabolischer Systeme geschieht auf verschiedenen Ebenen. Neben der Langzeitregulation, die auf Ebene der Proteinmengen stattfindet, gibt es noch die Kurzzeitregulation, die die Effizienz der vorhandenen Proteine steuert. Die Kurzzeitregulation lässt sich in kinetische, allosterische und hormonelle Regulation durch Interkonversion (generell Regulation durch chemische Modifikation) unterteilen. Die Langzeitregulation beruht dagegen größtenteils auf Proteinsynthese und -abbau. Während die Kurzzeitregulation für verschiede Enzyme sehr gut erforscht ist, sind die Prinzipien der Langzeitregulation zwar bekannt, ihre Ausgestaltung für die einzelnen Enzyme aber weitgehend unerforscht. Trotzdem erfährt die Langzeitregulation in Form der Genexpression die größte Aufmerksamkeit, was wohl an der Erwartung liegt, durch statistische Analyse von Omikdaten die fehlenden Informationen überflüssig zu machen. Obwohl es offensichtlich ist, dass Enzymmengen einen großen Einfluss auf die metabolische Leistung eines Systems haben, ist die ausschließliche Konzentration darauf, wie es z.B. in der Flussbilanzanalyse oder der Pathway-Enrichment-Analyse gemacht wird, äußerst fragwürdig. Grundsätzlich bestimmt die Menge eines Enzyms die metabolische Kapazität der von ihm katalysierten Reaktionen. Wieviel Fluss von einer Reaktion aber tatsächlich getragen wird, hängt vom Verhältnis des zur Verfügung stehenden Substrats und den kinetischen Eigenschaften des Enzyms ab. Das Gleiche gilt für Kofaktoren und allosterische Regulatoren. Da die Konzentration der Metabolite aber von dem gesamten metabolischen System abhängt, ist die Regulation der einzelnen Flüsse nur aufgrund der Menge der sie tragenden Enzyme gar nicht zu verstehen. Vielmehr ist eine ganzheitliche Systembetrachtung unter Berücksichtigung der regulativen Enzymeigenschaften, der Proteinmengen, der Metabolite und der äußeren Bedingungen notwendig. Noch weniger nachvollziehbar ist die weitverbreitete Fokussierung auf Genexpressionsprofile, da unser derzeitiges Verständnis, wie sich diese Profile in funktionelle Proteinmengen übersetzen lassen, wie oben erörtert, äußerst beschränkt ist und sie bestenfalls die Proteinsynthese beschreiben.

Unsere Analysen [39, 43] zeigen, dass es nicht ohne weiteres möglich ist, eine Hierarchie unter den verschiedenen Regulationsebenen auszumachen. Ob die Kurzzeitregulation oder die Langzeitregulation wichtiger ist, hängt vom betrachteten Enzym und vom metabolischen Zustand ab. Sogar ob ein Enzym überhaupt regulatorisch wichtig ist, ändert sich bei verschiedenen Bedingungen. Gleiches gilt für die verschiedenen Ebenen der Kurzzeitregulation und für die Frage, ob die Proteinsynthese wichtiger ist als der Proteinabbau [39, 41]. Für die hier untersuchten Systeme der Leber gilt allerdings, dass es nicht ratsam ist, bestimmte Regulationsebenen einfach auszublenden.

Neben der Regulation des Stoffwechsels auf zellulärem Level gibt es noch Regulationsmechanismen, die auf Gewebeebene (und/oder Systemebene) operieren. Dies geschieht hauptsächlich durch Kontrolle der lokalen Nährstoff- und Hormonkonzentrationen durch die Gewebeumgebung. Wir konnten zeigen [40, 41], wie groß der Einfluss der metabolischen Zonierung auf die Funktionalität der Leber ist. Die Zonierung ist das Resultat der variablen Umgebung innerhalb eines Sinusoids [41], die ihrerseits nicht unabhängig vom lokalen Metabolismus ist. Da die Metabolite selbst die Genexpression der metabolischen Enzyme maßgeblich beeinflussen, ergibt sich daraus ein enger Zusammenhang zwischen Leberfunktion, Leberstruktur und Genexpression. Im Kohlenhydratstoffwechsel der Leber erkennt

man das sehr gut daran, dass der metbolische Phänotyp von gefasteten Hepatozyten denen von diabetischen Hepatozyten und Hepatozyten in der periportalen Zone der Leber ähnelt, während gut genährte Hepatozyten metabolische Ähnlichkeiten mit perizentralen Hepatozyten auffweisen. Die zugrunde liegenden molekularen Mechnismen, die wesentlich auf den Hormonen Glukagon und Insulin beruhen, sind ausführlich in [41] beschrieben. Die Hormone sind auch ein gutes Beispiel dafür, dass die Kurzzeit- und Langzeitregulation oft zwei Seiten derselben Medaille sind. Während Insulin im allgemenein den Proteingehalt der Leber erhöht [63] (und Glukagon ihn vermindert), kann die Abhängigkeit der Menge einzelner Proteine von Insulin und Glukagon sehr unterschiedlich sein. Die Kurzzeitregulation durch Insulin besteht in der direkten Aktivierung von Enzymen der Glykolyse und Inaktivierung von Enzymen der Glukonegenese [40]. Gleichzeitig aktiviert Insulin auch die Genexpression der glykolytischen Enzyme, während es die Expression von glukoneogenetischen Enzymen hemmt [41]. Gleiches gilt für die Glukagon-induzierte Hemmung der Glykolyse und Aktivierung der Glukoneogense. Grundsätzilch ergibt es Sinn anzunehmen, dass Kurzzeitregulation und Langzeitregulation Hand in Hand gehen. Daraus folgt, dass es einen starken intrinsischen Zusammenhang zwischen Langzeit- und Kurzzeitregulation gibt, der außerdem eng mit der strukturellen Organisation verbunden ist und diese sowohl mitbestimmt als auch von ihr abhängt. Statt einer Hirachie der Regulationsebenen ist also das Bild eines komplexen Regelkreises angebracht. Genau wie bei der kineitschen Regulation müssen diese Regelkreise allerdings für jedes Enzym einzeln anlysiert werden.

Die enge Verknüpfung von Gewebestruktur und metabolischer Regulation hat auch unmittelbar praktische Folgen für den Leberstoffwechsel. So kann zum Beispiel der Ort und die Art der Fettakkumulation in der Leber als diagnostischer Parameter verwendet werden, aus dem sich auf strukturelle und metabolische Besonderheiten der betroffenen Gebiete schließen lässt [64-66]. Ob es einen funktionellen Mehrwert solcher Heterogenitäten gibt oder ob sie lediglich Folge zufälliger Varianzen auf struktureller und metabolischer Ebene mit negativen Konsequenzen sind, ist unklar. Einerseits könnte beispielsweise die Akkumulation von Fett in ausgewählten Zellen andere Zellen vor Fettüberladung und damit einhergehender Lipotoxizität schützen [55], andererseits führt die Verfettung von Zellen zu deren Anschwellen (*ballooning*), wodurch die umgebenden Gefäße komprimiert werden, was zu einer lokalen Minderperfusion führt [67]. Die daraus resultierende Hypoxie würde wiederum die Oxidation von Fettsäuren erschweren, was wiederum die Fettakkumulation und den Ballooning-Effekt verstärken würde. Unstrittig ist jedoch, dass verfettete Hepatozyten vermehrt pro-inflammatorische Zytokine wie TNF-α sezernieren [68], die ihrerseits die Fettspeicherung [69] begünstigen und zu Firbose- und Zirrhosebildung beitragen (siehe [42]).

3.2 Klinischer Nutzen der Modelle

Die hier vorgestellten Modelle eröffnen eine weite Palette an Möglichkeiten für die klinische Nutzung, indem sie die Untersuchung zentraler metabolischer Funktionen der Leber ermöglichen.

Der Hauptnutzen für die Medizin besteht in der Anwendung der hier vorgestellten Modelle auf (patho)physiologische Situationen wie Fasten, Diabetes, Steatose, Entzündung, Zirrhose, Fibrose und HCC (einige dieser Anwendungen wurden bereits exemplarisch in den vorgelegten Arbeiten behandelt). Diese Erkrankungen zeichnen sich durch simultane Veränderungen in den Proteinmengen und den strukturellen Parametern aus. Grundsätzlich werden Ver-

änderungen in den Proteinmengen immer dann wichtig, wenn sich die betrachteten Zustände über längere Zeiträume von denen einer normalen gesunden Leber unterscheiden.

Da es bisher nicht möglich ist, Veränderungen in den Proteinmengen dynamisch zu beschreiben, ist man darauf angewiesen, experimentell bestimmte Proteinmengen für die Skalierung der Modelle zu benutzen. Das ist machbar, da durch massenspektrometrische Analyse von Leberbiopsien patientenspezifische Proteindaten zur Verfügung stehen, die mittels der vorgestellten Modelle funktionell interpretiert werden können. Die Stärke der Modelle ist dabei ihre Fähigkeit, die kinetische Regulation mit der Netzwerktopologie zu verknüpfen und damit auch Proteinprofile, bei denen innerhalb eines Stoffwechselweges manche Proteine herauf- und andere herunterreguliert sind, verstanden werden können. Das Verständnis der teils scheinbar widersprüchlichen Befunde und die Einschätzung der regulatorischen Bedeutung der einzelnen Proteine können nur gelingen, wenn die Regulation der Enzyme explizit berücksichtigt wird [39]. Durch die Parametrisierung der verschiedenen Modelle anhand Proteomdaten aus Leberproben können individualisierte Modellvarianten erzeugt werden, die eine Bestimmung des funktionellen Zustands einzelner Patientenlebern ermöglichen.

Mit Methoden wie der metabolischen Kontrollanalyse kann der Einfluss einzelner enzymkinetischer Parameter auf ausgesuchte Leberfunktionen analysiert werden. Das ist hilfreich, um geeignete Ziele für eine pharmakologische Intervention zu definieren, die einerseits essentielle Leberfunktionen nicht zu stark in Mitleidenschaft zieht und andererseits selektiv auf das erkrankte Gewebe wirkt. Insbesondere bei bekannten molekularen Wirkmechanismen von Medikamenten kann deren Einfluss auf die Leberfunktion simuliert und sowohl Dosis-Wirkungskurven als auch Effektivität hinsichtlich der angestrebten Behandlung und möglicher Nebenwirkungen untersucht werden. Dieses Vorgehen haben wir am Beispiel von Valproat illustriert [43]. Es könnten aber auch andere Medikamente wie Statine (Inhibitoren der Cholesterolsynthese) oder Metformin (Medikament zur Behandlung von Diabetes und bei Tumoren) damit evaluiert werden.

Die Erstellung patientenspezifischer Modellvarianten zur funktionellen Bewertung von proteomischen Veränderungen in pathologischen Gewebe wurde ebenfalls in [43] am Beispiel von drei humanen HCCs gezeigt. Durch Kombination der Methoden konnten wir zeigen, dass Veränderungen im Metabolismus zu einer selektiven Anfälligkeit des Tumors für Medikamente (Metformin) führen können, die direkt auf den Stoffwechsel wirken (Manuskript in Vorbereitung). Zukünftig könnten solche Analysen zu einer zielgerichteten und individualisierten Behandlung von Tumoren führen.

Durch Berücksichtigung der Zusammenhänge zwischen strukturellen und nicht-invasiven bildgebenden Parametern [70, 71] und durch Einbeziehung von Gewebeparametern im Modell können auch Daten aus bildgebenden Verfahren wie CT oder Elastographie funktionell ausgewertet werden. Wir konnten zeigen, wie sich aus CT-basierten Perfusionsmessungen individuelle Leberfunktiogramme erstellen lassen [40]. In der gleichen Arbeit wurde gezeigt, wie bedeutsam die strukturellen Eigenschaften der Leber für ihre metabolische Leistung ist. Daher ist zu erwarten, dass die strukturellen Veränderungen bei Steatose, Steatohepatitis, Fibrose und Zirrhose [72, 73] ebenfalls einen starken Einfluss auf die Leberfunktion haben werden. Der nächste Schritt wird nun darin bestehen, das vorgestellte Funktiogramm auf Patienten mit Leberpathologien anzuwenden und diese funktionale Auswertung mit anderen nicht-invasiven Methoden wie z.B. der Elastographie zu vergleichen und zu kombinieren.

„Aus biologischer Sicht ermöglicht das Verständnis der regulatorischen Bedeutung der einzelnen Enzyme und ihrer verschiedenen Regulationsebenen eine zielgerichtete Medikamentenentwicklung. Beispielsweise übt das bifunktionale Enzym PFK2/FBP2 nur sehr wenig Kontrolle auf den stationären Glukosefluss in der Leber aus. Daher werden auch Medikamente, die dieses Enzym nicht-kompetitiv hemmen, nur sehr wenig Einfluss auf den Glukosestoffwechsel haben. Im Gegensatz dazu hätten Medikamente, die nur auf die phosphorylierte oder die dephosphorylierte Form (als nur auf PFK2 oder FBP2) wirken, einen sehr starken Einfluss auf den hepatischen Glukosefluss. Das kann beispielsweise bei der Behandlung von Diabetes oder Tumoren nützlich sein, wo die Phosphatase TIGAR, die den Abbau von Fruktose-2,6-bisphophat katalysiert, wie eine selektive FBP2-Überexpression wirkt." (Übersetzung durch den Autor aus [39])

3.3 Nutzen für die Grundlagenwissenschaft

Eine Stärke der hier vorgestellten Modelle besteht in ihrer Fähigkeit, verschiedene experimentelle Daten (enzymatische Charakterisierungen, Proteomik, Metabolomik, Flussmessungen) gemeinsam in einen einheitlichen Rahmen zu integrieren. Das ermöglicht die Bewertung von Einzelbefunden in einem gemeinschaftlichen Kontext. Die Frage, ob ein Befund richtig und plausibel ist, wird damit erweitert zu der Frage, ob ein Befund mit anderen (möglicherweise gesicherteren) Befunden übereinstimmt. Beispielsweise wird bei der Bewertung der Richtigkeit eines enzymkinetischen Parameters oftmals angeführt, dass bereits die Art und Weise, wie er erhoben wurde (*in vitro*, isoliertes Enzym, Mediumzusammensetzung, Temperatur, pH-Wert etc.), daran zweifeln lässt, dass er überhaupt die Verhältnisse in einer lebenden Zelle abbildet. Mithilfe der Modelle kann nun die Frage nach der Genauigkeit eines einzelnen Wertes dahingehend uminterpretiert werden, ob der in Frage stehende Wert sich sinnvoll in das bestehende System von Enzymparametern einfügt. Dabei ist plötzlich ebenso wichtig, welchen Wert andere kinetische Parameter des Enzyms haben, wie sich diese Werte zu den Metabolitkonzentrationen verhalten, wie sich andere Enzyme im selben und in angrenzenden Stoffwechselwegen verhalten usw. Man kann die Modelle zusätzlich dazu benutzen, die Stabilität von metabolischen Systemen gegenüber Änderungen in den kinetischen Parametern untersuchen.

Mit Hilfe der metabolischen Kontrollanalyse ist die Identifizierung derjenigen Enzyme und Parameter möglich, die einen großen Einfluss auf das Systemverhalten haben. Um zu korrekten Vorhersagen zu kommen und das metabolische System richtig zu beschreiben, ist daher die korrekte Abbildung dieser Enzyme besonders wichtig. Es wurde gezeigt [74], dass die Qualität kinetischer Modelle davon abhängt, ob die ratenlimiterenden Enzyme richtig dargestellt werden. Im Gegensatz dazu können schnelle Gleichgewichtsprozesse mit vereinfachten Kinetiken beschrieben werden, da der genaue Wert der kinetischen Konstanten nicht entscheidend ist (der Wert der Gleichgewichtskonstanten aber sehr wohl). Ofen bleibt jedoch, wie man die entscheidenden Prozesse identifiziert, und genau diese Funktion erfüllen die hier vorgestellten Modelle. Grundsätzlich wird statt anekdotischer Einordnung ein unbestechlicher mathematischer Rahmen geschaffen, der Widersprüche sofort aufdeckt. Damit Lücken aufgedeckt werden können, ist auch die ständige Konfrontation dieser Modelle mit neuen Daten und Anwendungsgebieten so wichtig. Der Anspruch ist es, Modelle zu generieren, die eine Vielzahl von Situationen abbilden und eben gerade nicht nur einzelne Experimente beschreiben.

Umgekehrt basieren Hypothesen über molekulare Mechanismen bei Veränderungen im Systemverhalten oftmals auf wenigen isolierten Beobachtungen. Mit den hier vorgestellten Modellen kann man die Plausibilität solcher Hypothesen bewerten, indem man Lücken in den experimentellen Beobachtungen durch Simulationen ergänzt. Dadurch kann ein viel komplexeres Bild erzeugt werden, dass entweder zu Widersprüchen führt und damit die Ausgangshypothese falsifiziert oder überprüfbare Vorhersagen liefert, die dann experimentell bestätigt werden können.

Als Beispiel kann der metabolische Effekt von Alkohol auf die Leber dienen. Unsere Simulationen zeigen klar, dass die Leber nach Alkoholaufnahme innerhalb kurzer Zeit in ihren ungestörten Zustand zurückkehrt [43]. Das lässt darauf schließen, dass Alkohol-induzierte Lebersteatosen nicht das Ergebnis einer kurzzeitigen metabolischen Entgleisung sind, sondern andere Mechanismen wie eine veränderte Genexpression eine entscheidende Rolle spielen müssen. Um den Alkohlmetbolismus adäquat beschreiben zu können, mussten wir außerdem einen neuen regulatorischen Term für die Alkoholdehydrogenase postulieren [43], der dann experiemtell am aufgereinigten Enzym bestätigt werden konnte (nicht publizierte Daten).

Ein weiteres Beispiel ist die regulative Bedeutung von Enzymen des Glukosestoffwechsels. In [39] wurde argumentiert, dass Modellvorhersagen über die regulatorische Bedeutung einzelner Enzyme dadurch überprüft werden können, dass man nach Veränderungen in Enzymeigenschaften sucht, die etwa bei bekannten Mutationen oder durch pharmakologische Intervention (Inhibitoren oder Aktivatoren) auftreten, und die simulierten Änderungen imitiert und dann überprüft, ob die vorhergesagten Veränderungen mit beobachteten Veränderungen der Plasmametabolite übereinstimmen. Durch Simulation verschiedener Umgebungsbedingungen, hier wohlgenährt und gefastet, konnte gezeigt werden, dass die regulative Bedeutung der verschiedenen Enzyme vom Ernährungszustand abhängt, was unterschiedliche experimentelle Befunde über die Wichtigkeit verschiedener Enzyme erklärt. Daran erkennt man auch eine weitere Stärke der Modellierung: Man kann sehr viel mehr virtuelle Experimente durchführen als reale und dabei eine Vielzahl von metabolischen Funktionen und Parameter gleichzeitig berechnen. Die Anzahl der simulierbaren Flüsse und Metabolitkonzentrationen übersteigt bei weitem die messbaren Größen und liefert somit ein sehr viel vollständigeres Bild, das experimentell nicht zu erreichen ist aber punktuell überprüft werden kann. Daneben kann man auch die funktionellen Konsequenzen von hypothetischen Veränderungen in den äußeren und inneren Bedingungen untersuchen. All das versetzt den Anwender in eine äußerst komfortable Situation, bei der technische, ethische und finanzielle Erwägungen, die bei experimentellen Untersuchungen oftmals die entscheidenden Hemmnisse darstellen, entfallen [43].

3.4 Ausblick

In dieser Arbeit wurde eine Reihe von Modellen des Leberstoffwechsels vorgestellt, die eine Simulation der Lebereaktion auf unterschiedlichste Stimuli wie variable Ernährungsprofile, Medikamente, Gendefekte und veränderte Genexpression ermöglichen. Um den Nutzen dieser Modelle sowohl für die Klinik als auch für die Grundlagenforschung zu illustrieren, haben wir die Modelle auf verschiedene Fragestellungen aus der Medizin, Genetik und Ernährungswissenschaft angewendet [39-43].

Wie in der Einleitung beschrieben, bleibt das Übersetzen von histologischen und nicht-invasiv-gewonnen Daten in ein Funktiogramm der Leber ein ungelöstes Problem der modernen Diagnostik. Das hier vorgestellte Gewebemodell der Leber [40] ermöglicht es nun aber, aus strukturellen Parametern (wie sie aus Leberbiopsien gewonnen werden können) zusammen mit regionalen Perfusionsmessungen der Leber (wie man sie beispielsweise aus einem Perfusions-CT bekommt) und patientenspezifischen Proteomikdaten eine Gesamtleber-funktion zu berechnen. Durch Kombination dieser Modelle mit modernen nicht-invasiven Methoden der Bildgebung wie der Elastographie, die für die Abbildung von strukturellen Veränderungen geeignet ist, könnte es in Zukunft gelingen Leberfunktionen besser einzu-schätzen.

Zum Schluss ist noch anzumerken, dass die Leber metabolisch gesehen das kompetenteste und komplexeste Organ ist. Die hier vorgestellten Modelle können demnach als Machbarkeits-beweis und Blaupause für andere Organe wie Hirn oder Herz dienen.

4. Zusammenfassung

Wir haben hier eine Reihe von Arbeiten zum Metabolismus der Leber präsentiert [39-43], die verschiedene Aspekte der Regulation des Leberstoffwechsels abbilden. Das bestuntersuchte Subsystem ist sicherlich der Glukosestoffwechsel, der die Aufnahme und Abgabe von Glukose (Glykolyse/Glukoneogenese) sowie den Aufbau und Abbau der hepatischen Glykogenreserve beschreibt. Drei Arbeiten entwickeln ein komplexes Bild der Regulation dieses Stoffwechsel-weges. Die erste Arbeit beschäftigt sich mit der Kurzzeitregulation unter Berücksichtigung der kinetischen, der allosterischen und der hormonellen Regulation [39]. Die zweite Arbeit [40] bettet dieses kinetische Modell des hepatischen Glukosestoffwechsels in ein Gewebemodell der Leber ein, das ihre strukturellen und morphologischen Besonderheiten sowie den Blutfluss und die metabolische Zonierung der Leber berücksichtigt. Die dritte Arbeit [41] erweitert dieses Bild um ein Modell des Proteinabbaus und der Proteinsynthese aufgrund von Hormon- und Nährstoffgradienten innerhalb der Leber bei verschiedenen (patho)physiologischen Zuständen. Dadurch wird zusätzlich die Langzeitadaptation der Leber mittels Genexpression beschrieben. Die vierte Arbeit [42] entwickelt ein Modell des Fettstoffwechsels der Leber mit Fokus auf den Lipidtropfenmetabolismus mit dem Ziel die molekularen Mechanismen der Leberverfettung besser zu verstehen. Schlussendlich präsentiert die fünfte Arbeit Heptaokin1, das erste molekular aufgelöste kinetische Modell des Zentralstoffwechsels der Leber [43].

5. Literaturverzeichnis

1. Kirschner, M.W., *The meaning of systems biology.* Cell, 2005. **121**(4): p. 503-504.
2. Horsthemke, B., *A critical view on transgenerational epigenetic inheritance in humans.* Nat Commun, 2018. **9**(1): p. 2973.
3. McGivan, J., et al., *Rat liver glutaminase. Regulation by reversible interaction with the mitochondrial membrane.* Eur J Biochem, 1985. **148**(2): p. 323-7.
4. Jin, L., et al., *Role of glucokinase in the subcellular localization of glucokinase regulatory protein.* Int J Mol Sci, 2015. **16**(4): p. 7377-93.
5. Kagimoto, T. and K. Uyeda, *Hormone-stimulated phosphorylation of liver phosphofructokinase in vivo.* J Biol Chem, 1979. **254**(13): p. 5584-7.
6. Agius, L. and M. Peak, *Intracellular binding of glucokinase in hepatocytes and translocation by glucose, fructose and insulin.* Biochem J, 1993. **296 (Pt 3)**: p. 785-96.
7. Dzeja, P. and A. Terzic, *Adenylate kinase and AMP signaling networks: metabolic monitoring, signal communication and body energy sensing.* Int J Mol Sci, 2009. **10**(4): p. 1729-72.
8. Viollet, B., et al., *Activation of AMP-activated protein kinase in the liver: a new strategy for the management of metabolic hepatic disorders.* J Physiol, 2006. **574**(Pt 1): p. 41-53.
9. Horike, N., et al., *AMP-activated protein kinase activation increases phosphorylation of glycogen synthase kinase 3beta and thereby reduces cAMP-responsive element transcriptional activity and phosphoenolpyruvate carboxykinase C gene expression in the liver.* J Biol Chem, 2008. **283**(49): p. 33902-10.
10. Van Schaftingen, E., et al., *Control of liver 6-phosphofructokinase by fructose 2,6-bisphosphate and other effectors.* Proc Natl Acad Sci U S A, 1981. **78**(6): p. 3483-6.
11. Reinhart, G.D. and H.A. Lardy, *Rat liver phosphofructokinase: kinetic activity under near-physiological conditions.* Biochemistry, 1980. **19**(7): p. 1477-84.
12. Hue, L. and M.H. Rider, *Role of fructose 2,6-bisphosphate in the control of glycolysis in mammalian tissues.* Biochem J, 1987. **245**(2): p. 313-24.
13. Mitchell, P., *Chemiosmotic coupling in oxidative and photosynthetic phosphorylation.* Biol Rev Camb Philos Soc, 1966. **41**(3): p. 445-502.
14. Graham, J.W., et al., *Glycolytic enzymes associate dynamically with mitochondria in response to respiratory demand and support substrate channeling.* Plant Cell, 2007. **19**(11): p. 3723-38.
15. Wallimann, T., et al., *Intracellular compartmentation, structure and function of creatine kinase isoenzymes in tissues with high and fluctuating energy demands: the 'phosphocreatine circuit' for cellular energy homeostasis.* Biochem J, 1992. **281 (Pt 1)**: p. 21-40.
16. Berndt, N. and H.G. Holzhutter, *Mathematical Modeling of Cellular Metabolism.* Recent Results Cancer Res, 2016. **207**: p. 221-32.
17. Braet, F. and E. Wisse, *Structural and functional aspects of liver sinusoidal endothelial cell fenestrae: a review.* Comp Hepatol, 2002. **1**(1): p. 1.
18. Jungermann, K. and N. Katz, *Functional specialization of different hepatocyte populations.* Physiol Rev, 1989. **69**(3): p. 708-64.
19. Jungermann, K. and N. Katz, *Functional hepatocellular heterogeneity.* Hepatology, 1982. **2**(3): p. 385-95.
20. Jungermann, K., *Zonation of metabolism and gene expression in liver.* Histochem Cell Biol, 1995. **103**(2): p. 81-91.
21. Yeh, M.M. and E.M. Brunt, *Pathological features of fatty liver disease.* Gastroenterology, 2014. **147**(4): p. 754-64.
22. Ovchinsky, N. and J.E. Lavine, *A critical appraisal of advances in pediatric nonalcoholic Fatty liver disease.* Semin Liver Dis, 2012. **32**(4): p. 317-24.
23. Dietrich, P. and C. Hellerbrand, *Non-alcoholic fatty liver disease, obesity and the metabolic syndrome.* Best Pract Res Clin Gastroenterol, 2014. **28**(4): p. 637-53.
24. Lonardo, A., et al., *Nonalcoholic fatty liver disease: a precursor of the metabolic syndrome.* Dig Liver Dis, 2015. **47**(3): p. 181-90.

25. Bussler, S., et al., *Novel Insights in the Metabolic Syndrome in Childhood and Adolescence.* Horm Res Paediatr, 2017. **88**(3-4): p. 181-193.
26. Kaur, J., *A comprehensive review on metabolic syndrome.* Cardiol Res Pract, 2014. **2014**: p. 943162.
27. Schwimmer, J.B., et al., *Prevalence of fatty liver in children and adolescents.* Pediatrics, 2006. **118**(4): p. 1388-93.
28. Charlton, M.R., et al., *Frequency and outcomes of liver transplantation for nonalcoholic steatohepatitis in the United States.* Gastroenterology, 2011. **141**(4): p. 1249-53.
29. Kleiner, D.E., et al., *Design and validation of a histological scoring system for nonalcoholic fatty liver disease.* Hepatology, 2005. **41**(6): p. 1313-21.
30. Everson, G.T., et al., *The spectrum of hepatic functional impairment in compensated chronic hepatitis C: results from the Hepatitis C Anti-viral Long-term Treatment against Cirrhosis Trial.* Aliment Pharmacol Ther, 2008. **27**(9): p. 798-809.
31. Dyson, J.K., Q.M. Anstee, and S. McPherson, *Non-alcoholic fatty liver disease: a practical approach to treatment.* Frontline Gastroenterol, 2014. **5**(4): p. 277-286.
32. Wiegand, S., et al., *Obese boys at increased risk for nonalcoholic liver disease: evaluation of 16,390 overweight or obese children and adolescents.* Int J Obes (Lond), 2010. **34**(10): p. 1468-74.
33. Wong, V.W., et al., *Disease progression of non-alcoholic fatty liver disease: a prospective study with paired liver biopsies at 3 years.* Gut, 2010. **59**(7): p. 969-74.
34. Weiss, J., M. Rau, and A. Geier, *Non-alcoholic fatty liver disease: epidemiology, clinical course, investigation, and treatment.* Dtsch Arztebl Int, 2014. **111**(26): p. 447-52.
35. Tilg, H. and A.R. Moschen, *Evolving therapies for non-alcoholic steatohepatitis.* Expert Opin Drug Discov, 2014. **9**(6): p. 687-96.
36. Gille, C., et al., *HepatoNet1: a comprehensive metabolic reconstruction of the human hepatocyte for the analysis of liver physiology.* Mol Syst Biol, 2010. **6**: p. 411.
37. Schwendel, A., et al., *Models for the regulation of purine metabolism in rat hepatocytes: evaluation of tracer kinetic experiments.* Am J Physiol, 1997. **273**(1 Pt 1): p. G239-46.
38. Krauss, M., et al., *Integrating cellular metabolism into a multiscale whole-body model.* PLoS Comput Biol, 2012. **8**(10): p. e1002750.
39. Bulik, S., H.G. Holzhutter, and N. Berndt, *The relative importance of kinetic mechanisms and variable enzyme abundances for the regulation of hepatic glucose metabolism--insights from mathematical modeling.* BMC Biol, 2016. **14**: p. 15.
40. Berndt, N., et al., *A multiscale modelling approach to assess the impact of metabolic zonation and microperfusion on the hepatic carbohydrate metabolism.* PLoS Comput Biol, 2018. **14**(2): p. e1006005.
41. Berndt, N. and H.-G. Holzhütter, *Dynamic Metabolic Zonation of the Hepatic Glucose Metabolism Is Accomplished by Sinusoidal Plasma Gradients of Nutrients and Hormones.* Frontiers in Physiology, 2018. **9**(1786).
42. Wallstab, C., et al., *A unifying mathematical model of lipid droplet metabolism reveals key molecular players in the development of hepatic steatosis.* FEBS J, 2017. **284**(19): p. 3245-3261.
43. Berndt, N., et al., *HEPATOKIN1 is a biochemistry-based model of liver metabolism for applications in medicine and pharmacology.* Nat Commun, 2018. **9**(1): p. 2386.
44. Allen, J.W., S.R. Khetani, and S.N. Bhatia, *In vitro zonation and toxicity in a hepatocyte bioreactor.* Toxicol Sci, 2005. **84**(1): p. 110-9.
45. Jungermann, K. and T. Kietzmann, *Oxygen: modulator of metabolic zonation and disease of the liver.* Hepatology, 2000. **31**(2): p. 255-60.
46. Probst, I., P. Schwartz, and K. Jungermann, *Induction in primary culture of 'gluconeogenic' and 'glycolytic' hepatocytes resembling periportal and perivenous cells.* Eur J Biochem, 1982. **126**(2): p. 271-8.

47. Kietzmann, T. and K. Jungermann, *Modulation by oxygen of zonal gene expression in liver studied in primary rat hepatocyte cultures.* Cell Biol Toxicol, 1997. **13**(4-5): p. 243-55.
48. Jungermann, K. and T. Kietzmann, *Role of oxygen in the zonation of carbohydrate metabolism and gene expression in liver.* Kidney Int, 1997. **51**(2): p. 402-12.
49. Torre, C., C. Perret, and S. Colnot, *Molecular determinants of liver zonation.* Prog Mol Biol Transl Sci, 2010. **97**: p. 127-50.
50. Zeller, E., et al., *Mechanisms of RAS/beta-catenin interactions.* Arch Toxicol, 2013. **87**(4): p. 611-32.
51. Colletti, M., et al., *Convergence of Wnt signaling on the HNF4alpha-driven transcription in controlling liver zonation.* Gastroenterology, 2009. **137**(2): p. 660-72.
52. Weinberg, M.B. and M.F. Utter, *Effect of thyroid hormone on the turnover of rat liver pyruvate carboxylase and pyruvate dehydrogenase.* J Biol Chem, 1979. **254**(19): p. 9492-9.
53. Kirkpatrick, R.B., S.F. Robinson, and P.G. Killenberg, *Diurnal-Variation of Rat-Liver Enzymes Catalyzing Bile-Acid Conjugation and Sulfation.* Biochimica Et Biophysica Acta, 1980. **620**(3): p. 627-630.
54. Wurtman, R.J., *Daily Rhythms in Tyrosine-Transaminase and Other Hepatic Enzymes That Metabolize Amino-Acids - Mechanisms and Possible Consequences.* Life Sciences, 1974. **15**(5): p. 827-847.
55. Herms, A., et al., *Cell-to-cell heterogeneity in lipid droplets suggests a mechanism to reduce lipotoxicity.* Curr Biol, 2013. **23**(15): p. 1489-96.
56. Straub, B.K., et al., *Differential pattern of lipid droplet-associated proteins and de novo perilipin expression in hepatocyte steatogenesis.* Hepatology, 2008. **47**(6): p. 1936-46.
57. Schuetz, R., et al., *Multidimensional Optimality of Microbial Metabolism.* Science, 2012. **336**(6081): p. 601-604.
58. Tan, Y. and J.C. Liao, *Metabolic ensemble modeling for strain engineers.* Biotechnol J, 2012. **7**(3): p. 343-53.
59. Rapoport, T.A., R. Heinrich, and S.M. Rapoport, *The regulatory principles of glycolysis in erythrocytes in vivo and in vitro. A minimal comprehensive model describing steady states, quasi-steady states and time-dependent processes.* Biochem J, 1976. **154**(2): p. 449-69.
60. Yang, J., et al., *Aspects of the control of phosphoenolpyruvate carboxykinase gene transcription.* J Biol Chem, 2009. **284**(40): p. 27031-5.
61. Gebhardt, R. and M. Matz-Soja, *Liver zonation: Novel aspects of its regulation and its impact on homeostasis.* World Journal of Gastroenterology, 2014. **20**(26): p. 8491-8504.
62. Burke, Z.D., et al., *Liver Zonation Occurs Through a beta-Catenin-Dependent, c-Myc-Independent Mechanism.* Gastroenterology, 2009. **136**(7): p. 2316-2324.
63. Hopgood, M.F., M.G. Clark, and F.J. Ballard, *Protein degradation in hepatocyte monolayers. Effects of glucagon, adenosine 3':5'-cyclic monophosphate and insulin.* Biochem J, 1980. **186**(1): p. 71-9.
64. Decarie, P.O., et al., *Fatty liver deposition and sparing: a pictorial review.* Insights Imaging, 2011. **2**(5): p. 533-538.
65. Hamer, O.W., et al., *Fatty liver: imaging patterns and pitfalls.* Radiographics, 2006. **26**(6): p. 1637-53.
66. Tandra, S., et al., *Presence and significance of microvesicular steatosis in nonalcoholic fatty liver disease.* J Hepatol, 2011. **55**(3): p. 654-659.
67. Schleicher, J., et al., *A theoretical study of lipid accumulation in the liver-implications for nonalcoholic fatty liver disease.* Biochimica Et Biophysica Acta-Molecular and Cell Biology of Lipids, 2014. **1841**(1): p. 62-69.
68. Pan, X., et al., *Adipogenic changes of hepatocytes in a high-fat diet-induced fatty liver mice model and non-alcoholic fatty liver disease patients.* Endocrine, 2015. **48**(3): p. 834-47.
69. Endo, M., et al., *TNF-alpha induces hepatic steatosis in mice by enhancing gene expression of sterol regulatory element binding protein-1c (SREBP-1c).* Exp Biol Med (Maywood), 2007. **232**(5): p. 614-21.

70. Hudert, C.A., et al., *US Time-Harmonic Elastography: Detection of Liver Fibrosis in Adolescents with Extreme Obesity with Nonalcoholic Fatty Liver Disease.* Radiology, 2018. **288**(1): p. 99-106.
71. Reiter, R., et al., *Wideband MRE and static mechanical indentation of human liver specimen: sensitivity of viscoelastic constants to the alteration of tissue structure in hepatic fibrosis.* J Biomech, 2014. **47**(7): p. 1665-74.
72. Peeters, G., et al., *A multilevel modeling framework to study hepatic perfusion characteristics in case of liver cirrhosis.* J Biomech Eng, 2015. **137**(5): p. 051007.
73. Debbaut, C., et al., *Perfusion characteristics of the human hepatic microcirculation based on three-dimensional reconstructions and computational fluid dynamic analysis.* J Biomech Eng, 2012. **134**(1): p. 011003.
74. Bulik, S., et al., *Kinetic hybrid models composed of mechanistic and simplified enzymatic rate laws--a promising method for speeding up the kinetic modelling of complex metabolic networks.* FEBS J, 2009. **276**(2): p. 410-24.

Danksagung

In erster Linie danke ich Prof. Dr. Hermann-Georg Holzhütter für seine stets unterstützende, kritische und dennoch aufgeschlossene Art, den kontroversen und immer auf Wahrheitsfindung angelegten wissenschaftlichen Austausch sowie die stetige Ermunterung, eigene Forschungsinteressen und Herangehensweisen umzusetzen. Eine offenere, wissenschaftlichere und menschlichere Umgebung ist kaum vorstellbar.

Weiter gilt mein Dank meinen Kollaborationspartnern für die Bereitstellung der experimentellen Daten und den wissenschaftlichen Austausch.

Zuletzt danke ich meinen Kollegen Sascha Bulik, Johannes Eckstein und Iwona Wallach für allerlei technische, moralische und fachliche Unterstützung.

Erklärung

§ 4 Abs. 3 (k) der HabOMed der Charité

Hiermit erkläre ich, dass

- weder früher noch gleichzeitig ein Habilitationsverfahren durchgeführt oder angemeldet wurde,
- die vorgelegte Habilitationsschrift ohne fremde Hilfe verfasst, die beschriebenen Ergebnisse selbst gewonnen sowie die verwendeten Hilfsmittel, die Zusammenarbeit mit anderen Wissenschaftlern/Wissenschaftlerinnen und mit technischen Hilfskräften sowie die verwendete Literatur vollständig in der Habilitationsschrift angegeben wurden,
- mir die geltende Habilitationsordnung bekannt ist.

Ich erkläre ferner, dass mir die Satzung der Charité – Universitätsmedizin Berlin zur Sicherung Guter Wissenschaftlicher Praxis bekannt ist und ich mich zur Einhaltung dieser Satzung verpflichte.

15.05.2019

……. ……

Datum Unterschrift